

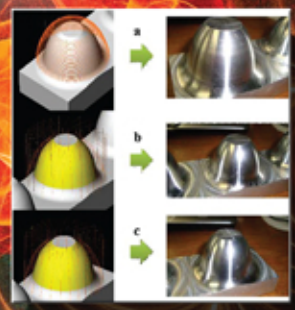
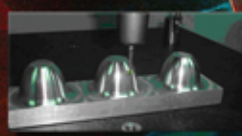
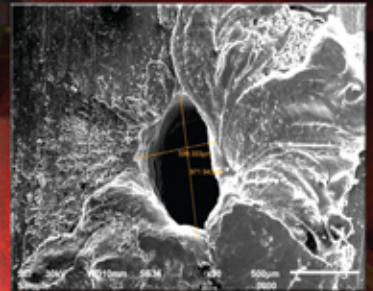


Materials and Manufacturing Technology
J. Paulo Davim (Series Editor)

Manufacturing Engineering

New Research

J. Paulo Davim
Editor



NOVA

MATERIALS AND MANUFACTURING TECHNOLOGY

MANUFACTURING ENGINEERING

NEW RESEARCH

No part of this digital document may be reproduced, stored in a retrieval system or transmitted in any form or by any means. The publisher has taken reasonable care in the preparation of this digital document, but makes no expressed or implied warranty of any kind and assumes no responsibility for any errors or omissions. No liability is assumed for incidental or consequential damages in connection with or arising out of information contained herein. This digital document is sold with the clear understanding that the publisher is not engaged in rendering legal, medical or any other professional services.

MATERIALS AND MANUFACTURING TECHNOLOGY

J. PAULO DAVIM - SERIES EDITOR –

UNIVERSITY OF AVEIRO, PORTUGAL

Drilling of Composite Materials

J. Paulo Davim (Editor)

2009. ISBN: 978-1-60741-163-5

(Hardcover)

Metal Cutting: Research Advances

J. Paulo Davim (Editor)

2010. ISBN: 978-1-60876-207-1

(Hardcover)

Micro and Nanomanufacturing Research

J. Paulo Davim (Editor)

2010. ISBN: 978-1-61668-488-4

(Hardcover)

Tribology of Composite Materials

J. Paulo Davim (Editor)

2010. ISBN: 978-1-61668-319-1

(Hardcover)

Artificial Intelligence in Manufacturing Research

J. Paulo Davim (Editor)

2010. ISBN: 978-1-60876-214-9

(Hardcover)

Tribology Research Advances

J. Paulo Davim (Editor)

2011 - 1st Quarter.

ISBN: 978-1-60692-885-1

(Hardcover)

Manufacturing Technology Research. Volume 1

*J. Paulo Davim and Mark. J. Jackson
(Editors)*

2011 - 1st quarter.

ISBN: 978-1-61122-001-8

(Hardcover)

Manufacturing Technology Research. Volume 2

*J. Paulo Davim and Mark. J. Jackson
(Editors)*

2011. ISBN: 978-1-61324-950-5

(Hardcover)

Biomedical Tribology

J. Paulo Davim (Editor)

2011. ISBN: 978-1-61470-056-2

(Hardcover)

Medical Device Manufacturing

*Mark J. Jackson and J. Paulo Davim
(Editors)*

2012-March.

ISBN: 978-1-61209-715-2

(Hardcover)

Metal Matrix Composites

J. Paulo Davim (Editor)

2012. ISBN: 978-1-61209-771-8

(Hardcover)

**Micro and Nanomanufacturing
Research**

J. Paulo Davim (Editor)

2012 1st Quarter.

ISBN: 978-1-61942-003-8

(Softcover)

Tribology of Composite Materials

J. Paulo Davim (Editor)

2012-July. ISBN: 978-1-62100-999-3

(Softcover)

Wood and Wood Products

J. Paulo Davim (Editor)

2012. ISBN: 978-1-62081-973-9

(Softcover)

**Artificial Intelligence in
Manufacturing Research**

J. Paulo Davim (Editor)

2013. ISBN: 978-1-62618-557-9

(Softcover)

**Machining: Operations, Technology
and Management**

J. Paulo Davim (Editor)

2013. ISBN: 978-1-62100-579-7

(Hardcover)

**Manufacturing Engineering:
New Research**

J. Paulo Davim (Editor)

2015 - 1st Quarter.

ISBN: 978-1-63463-378-9

(Hardcover)

MATERIALS AND MANUFACTURING TECHNOLOGY

MANUFACTURING ENGINEERING

NEW RESEARCH

J. PAULO DAVIM

EDITOR

The logo for Nova Publishers features the word "nova" in a bold, lowercase serif font. The letter "o" is replaced by a stylized globe showing the Americas. To the left of the "nova" text is a decorative graphic of a semi-circle of dots of varying sizes, creating a sense of motion or a signal. Below "nova" is the word "publishers" in a smaller, lowercase serif font. At the bottom of the logo is the text "New York" in an italicized serif font.
nova
publishers
New York

Copyright © 2015 by Nova Science Publishers, Inc.

All rights reserved. No part of this book may be reproduced, stored in a retrieval system or transmitted in any form or by any means: electronic, electrostatic, magnetic, tape, mechanical photocopying, recording or otherwise without the written permission of the Publisher.

For permission to use material from this book please contact us:
nova.main@novapublishers.com

NOTICE TO THE READER

The Publisher has taken reasonable care in the preparation of this book, but makes no expressed or implied warranty of any kind and assumes no responsibility for any errors or omissions. No liability is assumed for incidental or consequential damages in connection with or arising out of information contained in this book. The Publisher shall not be liable for any special, consequential, or exemplary damages resulting, in whole or in part, from the readers' use of, or reliance upon, this material. Any parts of this book based on government reports are so indicated and copyright is claimed for those parts to the extent applicable to compilations of such works.

Independent verification should be sought for any data, advice or recommendations contained in this book. In addition, no responsibility is assumed by the publisher for any injury and/or damage to persons or property arising from any methods, products, instructions, ideas or otherwise contained in this publication.

This publication is designed to provide accurate and authoritative information with regard to the subject matter covered herein. It is sold with the clear understanding that the Publisher is not engaged in rendering legal or any other professional services. If legal or any other expert assistance is required, the services of a competent person should be sought. FROM A DECLARATION OF PARTICIPANTS JOINTLY ADOPTED BY A COMMITTEE OF THE AMERICAN BAR ASSOCIATION AND A COMMITTEE OF PUBLISHERS.

Additional color graphics may be available in the e-book version of this book.

Library of Congress Cataloging-in-Publication Data

Manufacturing Engineering: New Research / [edited by] J. Paulo Davim (Department of Mechanical Engineering, University of Aveiro Campus Santiago Aveiro, Portugal).

pages cm. -- (Materials and manufacturing technology)

Includes bibliographical references and index.

ISBN: ; 9: /3/85685/5; 8/5 (eBook)

1. Production engineering. I. Davim, J. Paulo, editor.

TS176.M359 2014

670--dc23

2014041001

Published by Nova Science Publishers, Inc. † New York

CONTENTS

Preface		ix
Research and Review Studies		xiii
Chapter 1	Development of House of Quality in the Context of Advanced Remanufacturing System <i>S. Vinodh and K. J. Manjunatheshwara</i>	1
Chapter 2	Jigless Manufacturing of Aerospace Structural Assemblies <i>JJV. Jeyasingh, K. Santhosh Kumar, Shibu Gopinath and Koshy M George</i>	11
Chapter 3	Manufacturing of Polymer Nano Composites <i>Sridharan Veerapuram and Muthukrishnan Nambi</i>	23
Chapter 4	Optimal Control of Drilling Process for Hole Making in Fiber Reinforced Plastics: A Review <i>Amrinder Pal Singh, Kishore Debnath, Manu Sharma and Inderdeep Singh</i>	33
Chapter 5	Quality in the Machining: Characteristics and Techniques to Obtain Good Results <i>C. H. Lauro, L. C. Brandão, S. M. Ribeiro Filho and J. P. Davim</i>	51
Chapter 6	A Comparison of Milling Cutting Path Strategies for Aluminium 6262-T6 Alloys Fabrication <i>W. O. Leite, J. C. Campos Rubio, J. Tejero, F. Mata and I. Hanafi</i>	77
Chapter 7	Application of Fuzzy Logic in Modeling and Optimization of Surface Roughness in Turning <i>Arup Kumar Nandi</i>	91
Chapter 8	Perspective of Wire Electrical Discharge Machining: A Review <i>S. K. Garg, A. Manna and Ajai Jain</i>	129

Chapter 9	Experimental Analysis of Die Sinking EDM Process on AISI P 20 Tool Steel Using Response Surface Methodology <i>G. K. Bose and K. K. Mahapatra</i>	163
Chapter 10	Ytterbium Fiber Laser Machining of AA6061 Matrix and Al/Al ₂ O ₃ -MMC <i>Alakesh Manna</i>	189
Chapter 11	Laser Transformation Hardening of Steel <i>Karupuudaiyar Ramaraj Balasubramanian, Purushothaman Dinesh Babu and Gengusamynaidu Buvanashakaran</i>	213
Chapter 12	Material Joining Process of Non-Ferrous Metals <i>N. Muthukrishnan and V. Gurusamy</i>	241
Index		257

PREFACE

Currently, manufacturing engineering assumes a great importance to industrialized countries (G7) and countries with emerging economies (BRICS). Manufacturing engineering is a discipline of engineering dealing with “*different manufacturing practices and the research and development of systems, processes, machines, tools and equipment*”. Manufacturing engineering is important to several advanced industries such as automotive, aeronautic, aerospace, alternative energy, moulds and dies, biomedical, etc. This book aims to provide the research and review studies on manufacturing engineering.

Chapter 1 – Remanufacturing system is considered to be unstable and inefficient compared to manufacturing. Advanced manufacturing systems use a number of quality tools in order to improve their performance. Hence in order to improve remanufacturing system it is advisable to use similar tools in the context of remanufacturing. This study analyses the wastes generated during remanufacturing activities and prominent tools which can be used in reducing such wastes. Also, the prioritisation of tools must be done in order to achieve better results in the context of advanced remanufacturing systems. The practical validity of the approach has been tested in a manufacturing scenario.

Chapter 2 – Jigless Assembly is a new manufacturing concept in structural assemblies and is gaining attention in aerospace industry because of specific advantages over the Jig aided assembly. Aerospace manufacturing industry practices the most advanced technologies for machining, welding, assembly and inspection processes. The demand for introducing newer technologies is ever increasing. The mechanical structures of a Re-usable Launch Vehicles resembles an airplane and the design of Components and Assemblies are almost similar. The quality of the airframe structure is assessed by the degree of closeness of the assembly to the design in terms of its dimensions and geometrical parameters. Airframe assembly process plays a major role in flight performance. A detailed study is carried out to simplify the assembly tooling design by way of transferring the tooling functions to the components itself. The tooling design approach and the case study results are presented in this chapter.

Chapter 3 – Polymer nano composites are offering best alternative for conventional metals in various fields of engineering. They deliver exceptional mechanical, electrical and thermal properties. Modification of filling of matrix with nano sized particles of metals and non metals is an ever promising task. Effective utilization of properties of nano fillers can be achieved only by homogenous dispersion in matrix. This is ensured by better interfacial adhesion of filler and matrix. Functionalization of filler and addition of surfactants has been

the route to good level of dispersion. Many techniques are available to disperse filler particles in matrix. Calendaring has been very effective in achieving this task. In-situ polymerization gives better dispersion when compared to other mechanical and acoustic techniques. Modified matrix is used to manufacture composites by different methods. Hand lay-up has been widely used in academia for research projects. Pultrusion has been used for manufacturing long composites of various cross sections including channels. Filament winding is used for fabricating cylindrical vessels. Use of natural fibres as reinforcement in composites has been extensive since recent past. The surface of natural fibres has to be modified in order to achieve better bonding between fibre and matrix. Alkali treatment has been widely used, which is easy and effective. Study of mechanical, electrical and thermal behaviour of composites is very interesting and promising for researchers.

Chapter 4 – Damage caused during drilling in fiber reinforced plastics (FRP's) is an important research area for materials industry. Delamination is a critical form of damage as it leads to very high rates of rejected drilled parts. Delamination majorly depends on the thrust force and torque generated during drilling in FRP's. Both thrust force and torque are functions of the feed rate during drilling process. Models of drilling in different materials available in literature, have either modeled thrust force with feed rate or torque with feed rate. To control the damage due to delamination, control of both thrust force and torque is required. Thrust force and torque models with feed rate can be clubbed in state space to form a combined thrust force and torque model with feed rate. This model can be controlled by using an optimal controller. The optimal controller provides the user with a control effort handle to assign weightage to control effort being exerted for controlling thrust force or torque according to requirements.

Chapter 5 – To obtain great results in the machining of new materials, the manufacture industry required development of tools and techniques. Enhanced knowledge of these tools and techniques can offer a decreasing of cost, time, and risk to operator. This chapter debates the quality of the machined surface, the aspects and characteristics to analyse the desired quality. Furthermore, it presents some developments (tool and techniques) applied in the machining process to obtain the quality of surface.

Chapter 6 – This chapter presents a comparison of milling cutting path strategies for Aluminium 6262-T6. To search for more efficient cutting path strategies for machined parts, an interactive process planning and analyzing method is introduced. Several rigid combinations of machining parameters are examined based on the evaluation of surface finish, thickness accuracy and machining time in the visual charts. In order to obtain the best cutting path strategy, CAM software have been used to utilize the cutting path for machining Aluminium alloy parts into CNC end milling machine. The resulting of cutting path strategies is solved by experimental method. From the experiment, it was found that the circular path strategy provided 17% less time, fewer errors, and worse accuracy. The Z level from bottom to top strategy had lowers circularity and better accuracy compared to Z level from top to bottom.

Chapter 7 – This chapter presents the application of fuzzy logic in modeling and optimization of surface roughness of hard materials through a machining process, turning. Modeling of surface roughness in turning process presented in this chapter uses TSK-type fuzzy logic rule followed by a genetic algorithm (GA) is used to optimise the critical machining parameters based on the developed model. In order to construct the optimal

knowledge base of the fuzzy model, the genetic linear regression approach is adopted which introduces the multiple regression in the framework of a GA.

Chapter 8 – This chapter presents the detail of various process parameters of WEDM and their effect on machining performance characteristics. It presents the review of the various modeling method used to optimize the WEDM process parameters and performance of WEDM for conventional tool and die materials, Metal matrix composites (MMC) and ceramics. The final part of the chapter presented the future scope of WEDM.

Chapter 9 – Electric Discharge Machining (EDM) is one of the most widely used non-traditional machining processes for machining intricate shapes in high strength electro-conductive materials by spark erosion. EDM has penetrated the commercial manufacturing field and has seen through technological development in various directions. The present study is focusing on the electric discharge machining (EDM) of AISI P – 20 tool steel for finding out the effect of machining parameters such as discharge gap current (GI), pulse on time (POT), pulse off time (POF) and spark gap (SG) on performance responses like Material removal rate (MRR), Surface Roughness (Ra) & Overcut (OC) using Square-shaped Cu tool with Lateral flushing. A well-designed experimental scheme is used to reduce the total number of experiments. The experiment is conducted with the L27 orthogonal array based on the Taguchi method and significant process parameters are identified using Analysis of Variance (ANOVA). It is found that MRR and Ra are significantly affected by gap current and pulse on time respectively. Whereas overcut is affected only by gap current. These experimental data are investigated using Response Surface Methodology (RSM) for effect of four EDM parameters on the responses. Response surfaces are considered to explore the importance of the variables and their levels so as to optimize the responses. Finally multi-response optimization is conceded out by means of overlaid contour plots and desirability functions.

Chapter 10 – This chapter presents some specific investigated results acquired during Ytterbium fiber laser machining of AA6061-Matrix and Al/Al₂O₃-MMC. Some important features of laser beam machining process are also explained in the chapter. The effects of the Ytterbium fiber laser machining parameters such as laser power, modulation frequency, gas pressure, wait time, pulse width on the machining performance criteria e.g., metal removal rate and tapering phenomena have been analyzed through various graphs and reported in the chapter. From machining of AA6061-Matrix results, it is clear that the material removal rate (MRR) increases radically with increase in laser power specifically ranges from 300 to 400 watts. MRR also increases with increase in modulation frequency ranges from 500 to 800 Hz. But during machining of Al/Al₂O₃-MMC, it is found that the MRR increases with increase in laser power ranges from 400 to 1000 watts. Drilled hole deviation and taper increase with increase in modulation frequency ranges from 600 to 1000 Hz. However, optimization of Ytterbium fiber laser machining parameters can be effectively minimized the taper.

Chapter 11 – Lasers have been used in several ways to transform the properties of surfaces, particularly the surfaces of metals. Most often, the intention of the processing is to harden the surface to provide a better wear resistance and fatigue life. This process is termed as transformation hardening, is applicable to certain types of steel and cast iron. Steels and cast irons are particularly good candidates for transformation hardening. Laser surface transformation hardening, commonly known as heat treating, makes use of the rapid heating and cooling rates produced on metal surfaces exposed to scanning laser beams. The process has unique advantages, particularly when used to enhance surface properties in local areas

without affecting other areas of the component surface. Surface mechanical properties (hardness, abrasion, resistance, etc.) and chemical properties, (corrosion resistance, etc.) can often be greatly enhanced through the metallurgical reactions produced during these heating and cooling cycles. This chapter will describe the use of lasers and laser parameters to harden the surface of steels through rapid heating and quenching of a surface layer and the change take place in surface properties after hardening.

Chapter 12 – Nonferrous metals are non-iron-based metals such as aluminum and aluminum alloys, copper and copper alloys, nickel and nickel alloys, titanium and titanium alloys, and magnesium and magnesium alloys. Today, nonferrous metals are used in various welding constructions for various industrial applications. However, their weld ability is fairly different from that of steel, due to specific physical and metallurgical characteristics. Therefore, the welding procedure for nonferrous metals should be systematically examined taking into account the intrinsic characteristics of the particular nonferrous metal to be welded, in order to obtain sound weldments. The main requirement for safe commercial joining processes, particularly in the light-gauge area or low melting point materials or non-ferrous metals like Magnesium, Aluminum, Nickel, titanium etc., requires welding processes with maximum process stability and adjustable, reduced heat input. The problem associated with the non-ferrous materials are low melting point, low vaporization point, distortion during welding, spatter problems etc., However, new applications in particular require a high deposition rate and precise deposition of the wire electrode. Unsurprisingly, the requirement for minimal spatter has now become a demand for virtually no spatter. Arc welding now meets these requirements, even in the lower power end, to an extent that has never been seen before. There is a requirement of new approach, which incorporates welding current polarity changing and reversal of the wire movement into process control, that must offers a greater degree of freedom, with the result that these demands can be met in full. This chapter focuses on the welding of aluminum, aluminum alloys, copper, copper alloys, nickel, magnesium and magnesium alloys, nickel alloys that are used more extensively for industrial applications.

RESEARCH AND REVIEW STUDIES

Chapter 1

DEVELOPMENT OF HOUSE OF QUALITY IN THE CONTEXT OF ADVANCED REMANUFACTURING SYSTEM

S. Vinodh^{1,} and K. J. Manjunatheshwara^{1,*}*

¹Department of Production Engineering, National Institute of Technology,
Tiruchirappalli, India

ABSTRACT

Remanufacturing system is considered to be unstable and inefficient compared to manufacturing. Advanced manufacturing systems use a number of quality tools in order to improve their performance. Hence in order to improve remanufacturing system it is advisable to use similar tools in the context of remanufacturing. This study analyses the wastes generated during remanufacturing activities and prominent tools which can be used in reducing such wastes. Also, the prioritisation of tools must be done in order to achieve better results in the context of advanced remanufacturing systems. The practical validity of the approach has been tested in a manufacturing scenario.

Keywords: House of Quality; Advanced remanufacturing tools; Material recovery; Sustainability

NOTATIONS

a_j Row vector denoting absolute weights corresponding to advanced remanufacturing tools ($j = 1 \dots m$)

* E-mail: vinodh_sekar82@yahoo.com, vinodh@nitt.edu.

* E-mail: manjunatheshwara@yahoo.co.in.

- R_{ij} Square matrix where weights are assigned to relate elimination of wastes and advanced remanufacturing tools ($i=1 \dots n, j=1 \dots m$)
- c_i Column vector of importance potential in facilitating elimination of wastes ($i=1 \dots n$)
- m Number of advanced remanufacturing tools
- n Number of wastes to be eliminated
- b_j Row vector of relative weights for advanced remanufacturing tools ($j=1 \dots m$)
- d_i Column vector of absolute weights for elimination of wastes ($i=1 \dots n$)

INTRODUCTION

Remanufacturing is a material recovery option which is considered to be superior when compared to other available options of material recovery. It is a process of restoring the used products to useful life. Remanufacturing follows a series of steps starting with inspection of the returned core. The inspected product is disassembled, cleaned, defective components are repaired or replaced, and reassembly is done. A final inspection ensures the product ready for usage.

Organisations requiring their products to be remanufactured must redesign their products considering disassembly aspects. Process modifications are also done to facilitate remanufacturing. These alterations facilitate remanufacturing but do not improve operating efficiency. Remanufacturing system is considered to be inefficient and unstable when compared to manufacturing. This is because the incoming cores and demand for remanufacturing products are uncertain. Hence product lead time and operating costs of remanufacturing are high. There exists a need to improve remanufacturing operations.

Improvement in efficiency of manufacturing systems is achieved by quality tools. This idea can be used in achieving efficient remanufacturing system. The contemporary manufacturing organisations use a number of proficient quality tools which are proven to be beneficial in improving productivity; reduction of costs, product development time, production lead time; and improving quality. The contribution of the chapter is that it presents an approach for prioritizing wastes and remanufacturing tools in the context of advanced manufacturing systems.

This chapter presents a case analysis being conducted in a pump manufacturing organisation where the wastes generated during remanufacturing activities are identified and a control matrix is prepared in order to prioritise the quality tools that help to achieve better results.

LITERATURE REVIEW

The literature has been reviewed in the context of applications of HoQ in advanced manufacturing systems. Temponi et al. (1999) developed a fuzzy logic based HoQ to understand vague customer requirements, for better communication among team members and for easy representation of requirements. An inference scheme was developed as a validation technique. Olhager and West (2002) applied Quality Function Deployment (QFD) in a real time case study at a firm to deploy manufacturing flexibility at various hierarchical

levels while considering market requirements. The study also discussed the pros and cons of application of QFD in enhancing manufacturing flexibility.

Kaebnick et al. (2003) understood the importance of sustainability in product design and development. They developed Environmentally Concious Quality Function Deployment (ECQFD) to transform enviromental requirements into Engineering Characteristics for design. A sustainable trade-off model was created followed by a simplified Life Cycle Assessment (LCA), a decision model for making End of Life (EoL) decision was created.

Akao and Mazur (2003) understood the importance of Qulaity QFD in various sectors and functions. They conducted detailed literature survey of QFD and its applications. The authors identified best practices in QFD and future directions.

Silva et al. (2004) integrated QFD and Value Analysis (VA) tools which served as a decision making tool. The proposed methodology was capable of making cost considerations in product development. The study was conducted based on a survey among young males' sport bicycle requirements.

Sakao (2007) used an eco-design method which integrated tools like LCA, QFDE (QFD for environment) and Theory of Inventive Problem Solving (TRIZ). The author used QFDE which is an extension of QFD for identifying the required quality characteristics of components based on Voice of Customers (VOC) and Voice of the Environment (VOE). The identified product characteristics helped in product design and development. The author conducted a case study to validate the findings.

Utne (2008) applied QFD integrated with Life Cycle Cost (LCC) and Life Cycle Assessment (LCA) to evaluate environmental effects and costs involved in the system development process. The study was conducted to handle sustainability issues in Norwegian fisheries. The customers' requirements were transformed into system requirements at every stage of life cycle.

Oke et al. (2009) identified that few components of automobile really serve customers comfort while using an automobile. Based on the identified customer needs, the authors developed an optimal design which served waste reduction. The authors integrated QFD and VA tools for the purpose.

Vinodh and Chintha (2010) used fuzzy QFD for enabling sustainability in a manufacturing organisation. The authors developed two HoQs between sustainable performance measures and sustainable attributes; and between sustainable attributes and sustainable enablers. The authors proposed improvements in environmental, economical and social sustainability aspects of the product.

Vinodh and Rathod (2010) applied QFDE in a rotary switch manufacturing organisation. The authors carried out the study in four phases. Phase I and II involved identification of rotary switch parts that contribute in enhancing environmental conciousness. The next two phases of QFDE involved evaluation of effect of design improvement carried out to achieve the required environmental attributes. The authors conclude that using QFDE at early stages of product development will be beneficial.

Lin et al. (2010) studied interdependence relations among Environmental Production Requirements (EPRs) aspects and Sustainable Production Indicators (SPIs) criteria using fuzzy QFD.

The authors determined 'Whats' and 'Hows' for solving environmental practices problem. Since the data were imprecise, Fuzzy QFD and ANP were used to solve the relationship.

Vinodh et al. (2011) used QFD in eco-function matrix integrated VSM. The authors conducted a study to achieve sustainability in manufacturing firm by implementing lean tools and techniques. A current state map was created using VSM and QFD was applied to prioritise wastes to be eliminated and also to find appropriate waste elimination techniques for eliminating the identified wastes.

Rathod et al. (2011) integrated environmentally conscious QFD (ECQFD) with Life Cycle Assessment (LCA) to develop environmentally conscious products. The study ensured sustainable product development. The tool was used in End-of-Life decision making of the components.

Mohanraj et al. (2011) employed QFD in a lean manufacturing environment for prioritisation of wastes and to identify suitable tools to eliminate them. The authors integrated QFD with VSM and were successful in test implementing the approach in an Indian pump manufacturing organisation.

Vinodh and Srikrishna (2012) developed a fuzzy logic based Eco-QFD that integrated ecological considerations with cost, quality and customer needs. The framework enabled prioritisation of technical attributes and environmental concerns with which limiting the utilisation of resources was possible.

Prasad and Chakraborty (2013) used a QFD based approach for material selection. Prior to this study material selection decision was done using mathematical approaches which used subjective judgements. The authors used a software prototype to automate this decision making process. This approach proved to provide accurate results as derived by the past researchers.

Dursun and Karsak (2013) developed a methodology in which fuzzy multi-criteria decision making approach integrated with QFD was used for supplier selection process. The authors identified required characteristics of products acquired from suppliers. The identified attributes were used to find supplier assessment criteria. The suppliers were assessed based on the criteria. Two interrelated HoQ matrices were used for evaluating suppliers.

From the remanufacturing perspective a resourceful idea of matrix development has been done. Sundin and Bras (2005) developed a RemPro-matrix in their study of product remanufacturing in functional sales. The authors identified the necessary product properties at different stages of remanufacturing. They derived relations among product properties and remanufacturing stages. The identified product properties were taken as design considerations. This study extends the idea of RemPro-matrix proposed by Sundin and Bras (2005) to prioritize wastes and advanced remanufacturing tools.

METHODOLOGY

House of Quality (HoQ) is developed in order to translate voice of customers into technical descriptors (Planning matrix), determined technical descriptors are in turn used to find product properties (Design matrix), and product properties are translated into process steps (Operating matrix) and finally operational steps are identified using process steps (Control matrix). A series of matrix relationships does the complex task of capturing customer requirements. In this manner, manufacturing organisations reap benefits by producing products that exactly reflect the customer needs.

Development of HoQ involves formation of a team from different departments such as marketing, design, quality, finance and production. Communication among team members is an important aspect. The key matrices will be developed in-line with prioritisation mechanism.

Since operational steps (usage of tools) is to be derived using identified wastes which are to be eliminated, a control matrix is prepared which defines major wastes to be eliminated and prominent tools to eliminate them. The steps necessary for building HoQ are as follows:

Step 1 – A cross functional team (CFT) involving members from all departments is formed. The team should be aware of benefits that can be achieved by developing HoQ. Inter disciplinary team members ensured the needs of every function being satisfied.

Step 2 – The team identifies factors affecting remanufacturing efficiency and identifies wastes involved in remanufacturing activities that cause remanufacturing system to be inefficient.

Step 3 – The team studied the usage of tools and list prominent tools that can be used in the context of remanufacturing system.

Step 4 – The team discusses the importance of tools over elimination of wastes and quantifies the relationship between elimination of wastes and tools that facilitate elimination of wastes.

Step 5 – Correlation between tools would be understood in order to identify other tools which can be prerequisite for implementing prioritised tools.

Step 6 – Absolute weights of wastes are computed using importance potential and remanufacturing propensity. Absolute weights and relative weights of advanced remanufacturing tools are calculated and quality tools are prioritized based on the scores.

The elements of HoQ of advanced remanufacturing system are as follows:

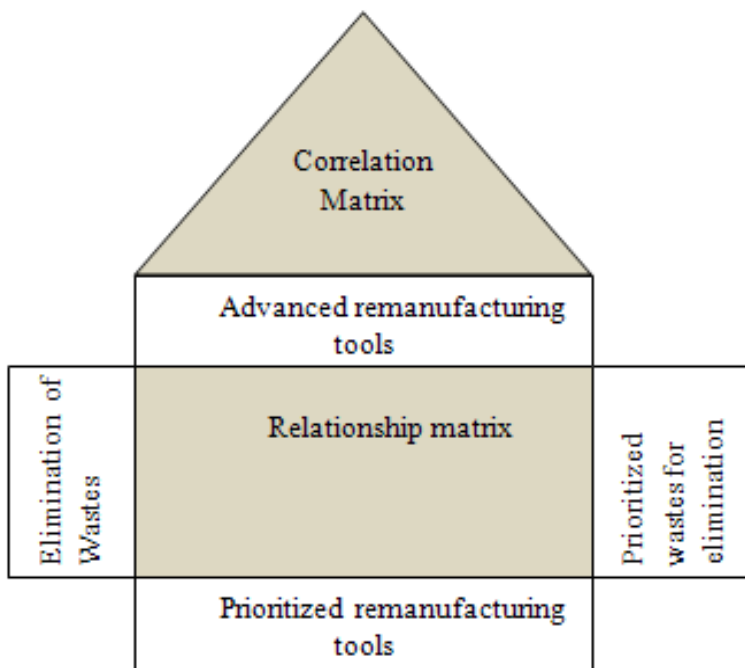


Figure 1. Elements of HoQ in the context of remanufacturing.

CASE STUDY

A pump manufacturing organisation was chosen for the study. The organisation had implemented a wide variety of quality tools. Remanufacturing is still in the developmental stage and hence invention of strategies to enhance remanufacturing proficiency was a challenge before the organisation. The study induced the idea of advanced remanufacturing system where appropriate tools are used for improving remanufacturing proficiency of the organisation.

As an initial step to the approach, a cross functional team was formed. The team identified problems in remanufacturing and wastes generated in the process of remanufacturing. The team suggested tools that can be used for bringing improvements in the system. The identified tools also included certain remanufacturing tools. The tools were termed as advanced remanufacturing tools.

House of Quality (HoQ) of advanced remanufacturing systems is a control matrix which relates seven wastes identified in the context of remanufacturing and advanced remanufacturing tools that can be implemented in operational steps to eliminate the wastes.

The wastes such as overproduction, over processing, waiting, inventory, transport, defects and motion were considered.

The advanced remanufacturing tools identified by the cross functional team were 7S, Value Stream Mapping (VSM), Kaizen, Kanban, Design for Manufacturing and Assembly (DFMA) and End-of-Life (EoL) decision making. Tools like Kanban and Kaizen were already in use to ensure efficient manufacturing in the firm. Other tools were chosen based on the remanufacturing requirements.

7S is an advanced remanufacturing tool which considers environmental aspects in the traditional 5S concept. 7S helps the organization to enhance environmental performance while also reducing wastes and thus increasing the productivity.

VSM can be used for mapping the process to understand the material and information flow; to identify wastes and also measures to eliminate wastes. The elimination of wastes facilitates streamlining of process thus enabling single piece flow.

Kaizen can be an effective tool which helps to bring about incremental changes in the process. The non-conformities to quality are identified and measures to be taken are listed and the workforce is involved to bring about the changes in incremental steps.

Kanban can be used for inventory control, which facilitates the movement of right materials to the right areas at right time. Unnecessary piling up of stock is avoided and thus reducing the cost involved.

DFMA is an important tool in the context of remanufacturing since disassembly is a major process step affecting the remanufacturing duration. Efforts are to be made at the design stage to facilitate remanufacturing.

EoL decision making is a strategy making tool which considers profitability of the action taken on returned cores. Thus EoL decision making helps the industrial practitioners to identify the remanufacturing potentiality of a returned product.

Elimination of identified wastes are placed row wise. The identified advanced remanufacturing tools are placed column-wise. The relationship between remanufacturing tools and elimination of wastes is depicted using symbols: Weak (Δ), Medium (\circ) and Strong (\bullet) with rating 1, 3 and 9 respectively. Correlation within advanced remanufacturing tools in

the study include Strong positive (●), Positive (○), Negative (X) and Strong negative (◇) relationship symbols with rating +9, +3, -3 and -9 respectively.

The importance potential is rated using 1-10 scale (1- least important and 10 - most important), and remanufacturing propensity is rated using similar 1-10 scale (1- least potential for remanufacturing and 10 – highest potential for advanced remanufacturing).

The equations used for computing absolute weight and relative weight in prioritizing remanufacturing tools are presented as follows:

$$a_j = \sum_{i=1, j=1}^{n, m} R_{ij} c_i$$

where, a_j is row vector denoting absolute weights corresponding to advanced remanufacturing tools ($j = 1 \dots m$); R_{ij} is a square matrix where weights are assigned to relate elimination of wastes and advanced remanufacturing tools ($i=1 \dots n, j=1 \dots m$); c_i is a column vector of importance potential in facilitating elimination of wastes ($i=1 \dots n$); m , number of advanced remanufacturing tools; and n , number of wastes to be eliminated.

The relative weight of j th advanced remanufacturing tool is determined by replacing the importance potential in the previous equation with absolute weight for prioritization of elimination of wastes.

Elimination of Wastes	Advanced remanufacturing tools						Importance to Customer	Remanufacturing Propensity	Absolute Weight
	7S	VSM	Kaizen	Kanban	DFMA	EoL Decision Making			
Elimination of Overproduction	○		○	●			5	5	25
Elimination of Overprocessing	○	●	●	○			5	5	25
Elimination of Waiting	○	●	○	○			7	7	49
Elimination of Inventory	△	●	○	●		○	10	10	100
Elimination of Transport	○	●	●	○			5	5	25
Elimination of Defects	△	○	○	△	●	○	7	7	49
Elimination of Motion		●	○	○	●		5	5	25
Absolute Weight	83	309	252	193	63	51			
Relative Weight	521	2163	1194	1546	666	447			

Figure 2. HoQ of advanced remanufacturing system.

$$b_j = \sum_{i=1, j=1}^{n, m} R_{ij} d_i$$

where b_j , row vector of relative weights for advanced remanufacturing tools ($j=1\dots m$); d_i = column vector of absolute weights for elimination of wastes ($i=1\dots n$). HoQ pertaining to this study is shown in Figure 2.

RESULTS AND DISCUSSIONS

From the computations carried out, prioritization of wastes based on absolute weights was done. Inventory with highest absolute weight of 100, Defects and Waiting with 49 scores each were the most important wastes to be eliminated for remanufacturing improvement.

Relative weights of tools Value Stream Mapping, Kanban and Kaizen were found to be 2163, 1546 and 1194 respectively which were higher than the relative weights of tools 7S, DFMA and EoL decision making. Thus the team emerged out with important tools that facilitate improvement in functioning of remanufacturing system.

Value Stream Mapping (VSM), Kanban and Kaizen were proved to be significant in elimination of prioritised wastes such as inventory, defects and waiting.

The correlation matrix also showed that mutual relation among identified tools and tools having significant relation with 7S, and hence 7S was also considered to be prerequisite for the implementation of identified tools.

The members of Cross Functional Team decided over areas where these tools can be implemented to eliminate wastes and transform the remanufacturing system to a beneficial one.

MANAGERIAL IMPLICATIONS

The cross-functional team was exposed to the principles of extending HoQ in the context of advanced manufacturing systems. The team were exposed to seven types of wastes, need for elimination, and appropriate techniques required for eliminating those wastes. Then the team executed the steps of HoQ in succession towards prioritization of wastes and techniques. Then the practical feasibility of deploying waste elimination techniques was deliberated by the team. The management also decided over providing the required training to the workforce in order to make them adapt to the operational advancements.

CONCLUSION

This article presented an approach of HoQ encompassed with prioritisation mechanisms in the context of advanced remanufacturing system. The prioritisation of wastes for elimination and identification advanced remanufacturing tools helped practitioners in effective decision making. This study also provided practical insights on deploying HoQ

concept in the context of remanufacturing to enable modern managers to make appropriate decisions.

REFERENCES

- Akao, Y., Glenn H. Mazur, (2003). The leading edge in QFD: past, present and future. *International Journal of Quality and Reliability Management*, Vol. 20, No. 1, 20 – 35.
- Dursun, M., and Karsak, E. E. (2013). A QFD-based fuzzy MCDM approach for supplier selection. *Applied Mathematical Modelling*, Vol. 37, No. 8, 5864-5875.
- Fábio Luís Ramos da Silva, Katia Lucchesi Cavalca, Franco Giuseppe Dedini, (2004). Combined application of QFD and VA tools in the product design process. *International Journal of Quality and Reliability Management*, Vol. 21, No. 2, 231 – 252.
- Jan Olhager, B. Martin West, (2002). The house of flexibility: using the QFD approach to deploy manufacturing flexibility. *International Journal of Operations and Production Management*, Vol. 22, No. 1, 50 – 79.
- Kaebernick, H., Kara, S., and Sun, M. (2003). Sustainable product development and manufacturing by considering environmental requirements. *Robotics and Computer-Integrated Manufacturing*, Vol. 19, No. 6, 461-468.
- Lin, Y., Cheng, H. P., Tseng, M. L., and Tsai, J. C. (2010). Using QFD and ANP to analyze the environmental production requirements in linguistic preferences. *Expert Systems with Applications*, Vol. 37, No. 3, 2186-2196.
- Mohanraj, R., Sakthivel, M., and Vinodh, S. (2011). QFD integrated value stream mapping: an enabler of lean manufacturing. *International Journal of Productivity and Quality Management*, Vol. 7, No. 4, 501-522.
- Oke, S. A., Onabajo, O. A., Oyekeye, M. O., and Oluwo, A. (2009). Application of QFD and VA tools in the design of an automobile. *International Journal of Productivity and Quality Management*, Vol. 4, No. 5, 525-548.
- Prasad, K., and Chakraborty, S. (2013). A quality function deployment-based model for materials selection. *Materials and Design*, Vol. 49, 525-535.
- Rathod, G., Vinodh, S., and Madhyasta, U. R. (2011). Integration of ECQFD and LCA for enabling sustainable product design in an electric vehicle manufacturing organisation. *International Journal of Sustainable Engineering*, Vol. 4, No. 3, 202-214.
- Sakao, T. (2007). A QFD-centred design methodology for environmentally conscious product design. *International Journal of Production Research*, Vol. 45, No. 18-19, 4143-4162.
- Sundin, E., and Bras, B. (2005). Making functional sales environmentally and economically beneficial through product remanufacturing. *Journal of Cleaner Production*, Vol. 13, No. 9, 913-925.
- Temponi, C., Yen, J., and Amos Tiao, W. (1999). House of quality: A fuzzy logic-based requirements analysis. *European Journal of Operational Research*, Vol. 117, No. 2, 340-354.
- Utne, I. B. (2009). Improving the environmental performance of the fishing fleet by use of Quality Function Deployment (QFD). *Journal of Cleaner Production*, Vol. 17, No. 8, 724-731.

- Vinodh, S., and Chintha, S. K. (2011). Application of fuzzy QFD for enabling sustainability. *International Journal of Sustainable Engineering*, Vol. 4, No. 4, 313-322.
- Vinodh, S., and Rathod, G. (2010). Application of QFD for enabling environmentally conscious design in an Indian rotary switch manufacturing organisation. *International Journal of Sustainable Engineering*, Vol. 3, No. 2, 95-105.
- Vinodh, S., and Srikrishna, J. (2012). Application of fuzzy logic-based Eco-QFD for a disconnecting switch. *International Journal of Sustainable Engineering*, Vol. 5, No. 2, 109-119.
- Vinodh, S., Arvind, K. R., and Somanaathan, M. (2011). Tools and techniques for enabling sustainability through lean initiatives. *Clean Technologies and Environmental Policy*, Vol. 13, No. 3, 469-479.

Chapter 2

JIGLESS MANUFACTURING OF AEROSPACE STRUCTURAL ASSEMBLIES

***JJV. Jeyasingh*, K. Santhosh Kumar, Shibu Gopinath
and Koshy M George***

Materials and Mechanical Entity, Vikram Sarabhai Space Centre
Thiruvananthapuram, Kerala, India

ABSTRACT

Jigless Assembly is a new manufacturing concept in structural assemblies and is gaining attention in aerospace industry because of specific advantages over the Jig aided assembly. Aerospace manufacturing industry practices the most advanced technologies for machining, welding, assembly and inspection processes. The demand for introducing newer technologies is ever increasing. The mechanical structures of a Re-usable Launch Vehicles resembles an airplane and the design of Components and Assemblies are almost similar. The quality of the airframe structure is assessed by the degree of closeness of the assembly to the design in terms of its dimensions and geometrical parameters. Airframe assembly process plays a major role in flight performance. A detailed study is carried out to simplify the assembly tooling design by way of transferring the tooling functions to the components itself. The tooling design approach and the case study results are presented in this chapter.

Keywords: Jigless, Jigless Manufacturing, Assembly Jig, Jigs & Fixtures, Assembly Process, DFA (Design for Assembly)

1. INTRODUCTION

The aircraft industry is a high precision and low volume production industry where the assembly of an aero-structure is carried out using specially designed jigs which conforms to

*Corresponding author: E-mail: jeswin_jeyasingh@yahoo.com, Tel No:(+91)0471-2563579, Fax: (+91)0471-2562152.

the final shape of the product within specified tolerances. An aero structure is unique in shape for which the product specific jigs are used nowadays. These jigs contribute to the accuracy of the final product assembly. Hence the product specific jigs are to be made with high accuracy guaranteeing consistency and quality. Product specific jigs are having disadvantages like high cost, limited interchangeability, longer lead time, maintenance requirements, storage space and high expenditure of labour [1].

The Indian Space Research expands to the next generation of launch vehicles with the advanced technologies, viz. Re-usable launch vehicles. The Re-usable launch vehicle resembles an aircraft like winged structure. The structures of this kind are expected to have dimensions and its related geometrical parameters exactly as per the design to ensure the desired flight performance. In launch vehicle system, the reliability of the structure must be doubly ensured which has a direct impact on the structures. The stringent requirement of dimensional accuracy is imparted in the realization of components and structural assembly to form the complete airframe structure. The aerospace manufacturing practices the most advanced technologies for machining, assembly and inspection etc. with the advent of modern computer based systems.

It is a well known fact that no component can be manufactured exactly to the design dimensions with zero deviations. There is always a deviation from the mean value of the dimension. To control these deviations to the minimum level, tolerancing methodology is practiced. These components are positioned and assembled accurately to form the airframe structure. Accuracy of the structural assembly is contributed by the method of assembly process and the accuracy of individual components in which the former is dominant. Assembly tooling has evolved over many decades, from simple fixtures to the specific tooling concept for the modern aircraft systems. This applies to the launch vehicle airframes also. The requirement of high performance demands for closer tolerances in terms of geometry as well as dimensions which calls for evolving newer tooling concepts.

The design iterations of an aerospace structure or component is never a stopping process whose designs are improved frequently. The jigs constructed for specific type of products can be modified only to a little extent without sacrificing the accuracy for the updations happening in the components. Hence the interchangeability is limited in these jigs. The revised tooling needs to be reconstructed over a period of time which is similar to constructing a new setup. Obviously, the realisation time of jigs will be more for making these high accuracy jigs. Hence to overcome the above limitations, new concepts in tooling are being tried. One such concept is the Jigless Assembly for manufacturing of large aerospace structures.

2. OBJECTIVE OF THE STUDY

Jigless Manufacturing otherwise called as the Jigless Aerospace Manufacturing (JAM) is aimed at reducing or eliminating the need for product specific jigs during the manufacturing process. This concept is introduced in design, manufacture and inspection of an airframe structure integrating the advanced technological developments in 3D Geometric Modeling, CNC Machining, Assembly and Inspection. With the need for improving the manufacturing

process of an airframe structural assembly and to introduce the Jigless Assembly approach, the following objectives are drawn:

- Feasibility study of implementing the JAM concept in the assembly process of the Tail and Wing structures of airframe.
- Possibility of transferring the tooling functions from assembly jigs to the existing component configuration without compromising the design intents.
- Selection of appropriate geometry features enabling the arrest of degrees of freedom (DOF) during the assembly process.
- Design of simple generalized jigs enabling the JAM concept for the Tail and Wing structures and propose optimized assembly sequence.
- Analyze the effect of introducing the JAM concept.

3. MANUFACTURE OF AN AIRFRAME STRUCTURE ADOPTING JAM CONCEPT

Jig is a workpiece locating and holding device which positions and guides or controls the tools for mechanical operations. The geometrical and dimensional accuracy requirements of the structure are governed by the accuracy of assembly jigs. Airframe assemblies are realized by the accurate machining of the components and precise assembly using jigs. The accuracy of the assembly directly plays a major role in the flight performance. An aerospace jig and its product assembly operations go hand in hand. The latter is the user technology while the former is the enabling technology. Currently, the assembly of an aero-structure is carried out using uniquely designed product specific assembly jigs that ensures the design requirements in the final assembly. The newer concepts are based on the accurate part location and support during product build which are more advantageous in terms of ensuring consistency, accuracy and quality. A move towards minimizing or eliminating the product specific tooling by the application and integration of relevant technologies and methodologies is the latest trend in the tooling area [2]. One such concept is the ‘Jigless Manufacturing’ which offers significant benefits. The jigless manufacture does not mean that it is fixtureless as simple fixtures are still needed to hold and support parts during the assembly operations whose intent is to make these fixtures generic. An important requirement for the success of this technology is the introduction of measurement (or inspection) systems into a real time control loop. A measurement is the link between the design and the manufacture. The basic requirements of measurement are online operation, rapid measurement, low latency, high reliability and a data link to the 3D CAD design. Use of today’s advanced 3-dimensional digital mock-up coupled with the inspection and automation technologies enable the success of the Jigless manufacturing methodology. The potential gains of this new approach are:

- Minimizing the product specific jigs, fixtures and tooling
- Simple design
- Improvement in quality
- Large cost savings
- Significant lead time reduction.

3.1. Design Approach for the Assembly Jigs Enabling Jigless Assembly

Jigless Assembly means, an assembly without the use of jigs which indirectly means that parts are to be manufactured to sufficient accuracy to ensure correct assembly. Also, the jigless assembly is not necessarily fixtureless [or tool less] assembly. Jigs cannot be completely eliminated and are needed for basic referencing, location and component support. Components can be designed in such a way that it can have the geometric features which permits its assembly with bare minimum requirement of jigs and fixtures. Three major areas of study and research towards the attainment of the jigless assembly are design, assembly processes, feature based methods and tolerance representation [2].

3.2. Design for Function (X) [DF-X]

“Design for function (DFX)” is an improved concept where the function mentioned can be manufacturing, aesthetics, assembly, disposal, service, etc.. The design for function aims at bringing together all downstream functions in the product conceptualization (or design) stage itself. It aims at optimizing the product design to result in lesser lead time and lower product cost [3].

3.3. Design for Manufacturing (DFM)

Design for manufacturing in simple terms is the process of designing products considering the manufacturing aspects also. DFM is currently a commonly used jargon in industries. Even though the concept of DFM originated in the 18th century with the introduction of the concept of interchangeable parts by LeBlanc, it took years to gain wide popularity. Design for Manufacturing includes a detailed method study, process optimization and the breakdown of process into different material options for the product, tools, setups, etc. These factors are compared on a scale of cycle-time and cost. The optimal combination of these factors is chosen.

3.4. Design for Assembly (DFA)

As a subset of DFM, the design for assembly considers the assembly aspects (or easiness) of the product while designing the product. In a wider perspective, it is a tool through which the multi-functionality is assigned to individual components of the product, wherever possible. Multi-functionality of parts leads to a less number of parts in the assembly which directly increases the ease of assembly. Some of the guidelines to implement DFA in the components are: design for parts handling, avoiding asymmetry, maximizing asymmetry if asymmetry is unavoidable, avoiding tangling, design for insertion and fastening, providing generous tolerances, guides and tapers to aid the assembly, minimizing the number of fasteners and the use of standard fasteners, etc..

4. RESULTS & DISCUSSION

4.1. Case Study 1: Jigless Manufacture of Tail Assembly

4.1.1. Tail Structural Assembly

Tails are the structures of the launch vehicle meant for yaw control. There are two Tails, one at the right side and the other at the left side of the fuselage. They are connected to the Fuselage with proper interfaces to handle the load transfer and geometry requirements. The tail structure consists of torsion box sub assembly, leading edge, trailing edge and the skin panels as shown in Figure 1. The torsion box sub assembly consists of spars and ribs made of Aluminium alloy material. The spars have 'I' cross section connected by four 'Z' sectioned ribs.

Two 'C' section ribs are used to connect the spars at the top and the bottom side. The location and position of the individual elements determine the geometry and overall accuracy of the Tail structure.

4.1.2. Conventional Assembly jig for Tail Structure

There are two conventional assembly jigs designed and realized to facilitate the assembly of ribs, spars and skin panels for Tail (LH) & Tail (RH) as shown in Figure 3a. The assembly jig is first calibrated and the reference for components is derived using locally machined pads on the jigs. The assembly procedure for the assembly of components is framed to have “hinder free” assembly with intermediate inspection stages. As per the pre-defined assembly sequence, the components are assembled utilizing the locators, supports and clamps provided in the jig to ensure their position and orientation which are confirmed through inspection. This procedure of the assembly results in more manual effort and the overall cost increases due to more number of references, jig elements, complex inspection methodology and time and less accessibility to achieve the required geometry. To overcome the above difficulties and to improve the quality, the JAM approach is introduced in the structural assembly of aerospace structures.



Figure 1. Tail Structure of Airframe.

4.1.3. Design of JAM Enabled Jig for the Assembly of Tail Structure

To enable the jigless manufacture, an attempt is made to re-design the configuration of the structural parts without affecting their original design intent. Towards this, the feature based approach is adopted to modify the interface design of the mating components [4]. A careful analysis on the selection of mating features between the components is carried out considering the design requirements such as stiffness, load transfer, failure mode, manufacturability, accuracy and precision achievability, etc.

By adopting the 3D digital mock-up approach, these features are individually fitted on to the components and checked for assembly easiness, degrees of freedom for assembly, manufacturing feasibility, design performance, inspection feasibility, etc.. Different types of features are considered for the study and are ranked based on the above parameters for selection and implementation. Latches are mostly of protrusion type features which helps the components to locate and catch mostly female parts to hold the protrusion in position. There is no restriction for using these two features separately in components. Their functionality can be combined and even a new feature can be developed simulating the function of both latch and catch. Outcome of the geometric feature analysis suggests the ‘protrusion with hole’ feature in spars to act as a self locating and positioning feature to hold ribs. Similarly the ‘hole’ feature is found suitable in ribs for arresting DOF. The modified interface design of spars and ribs are shown in Figure 2. Implementation of the precise self locating features reduces the number of locators for positioning the ribs and spars. This modification demands change in the manufacturing methodology and its parameters for the realization of components [5-7].

This enables the reduction in number of locators which leads to a simplified assembly and inspection procedures. 3D digital simulation is carried out for the modified assembly procedure to assess the assembly sequence, orientation of assembly considering the accessibility, time required for assembly, etc.

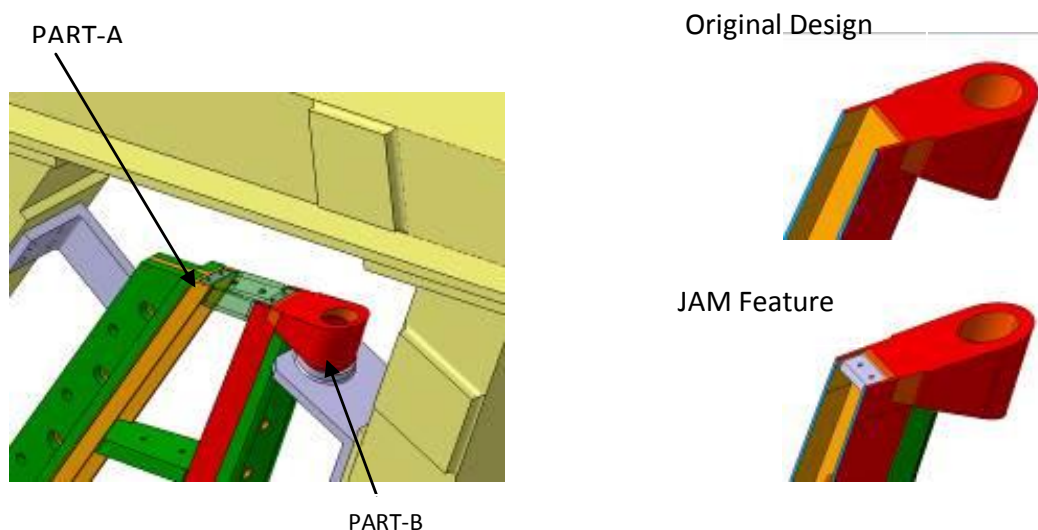


Figure 2. Self locating and Positioning feature added in Part A & B.

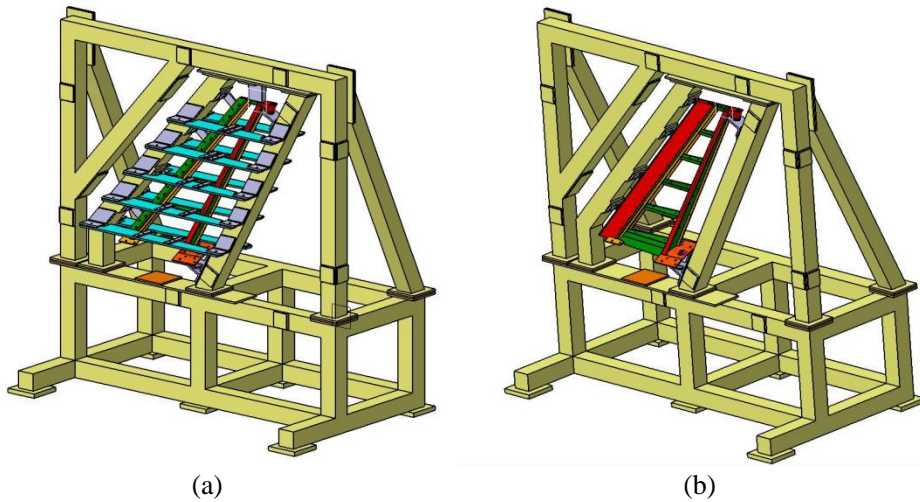


Figure 3. (a) Conventional Jig for Tail Assembly (b) Jigless enabled Jig for Tail Assembly.

4.1.4. Benefits of the Jigless Assembly in Tail Structure

The implementation of the jigless concept in the component design and the related modifications in the assembly methods has benefited in various facets like design, manufacturing, assembly and inspection. The modern inspection instrument like laser tracker which is based on non-contact inspection technology is used for inspecting the location and position of components. The Laser Tracker requires interference free access to the components and its references which are ensured by reduction in the number of jig elements enabling the implementation of the jigless manufacturing concept. Figure 3a & 3b shows the variation on the designs of the jigless enabled jig with respect to the conventional jig for the tail structure which infers on the improvement in productivity.

Table-1 below shows the simplicity obtained by enabling the Jigless concept in the existing conventional Tail Assembly Jig without compromising quality.

Table 1. Comparison of jig design and assembly process parameters for Vertical Tail Conventional Jig & Jigless enabled Jig

Jig Description	Conventional Assembly Jig	Jigless enabled Assembly Jig
No. of Locators	28	7
No. of Contour Plates	10	0
No. of Facing Plates	10	0
Assembly Time (Simulated)	67 Hrs. 30 Mins.	25 Hrs.
Part Machining	Simple	Slightly difficult
Accuracy	More in Jig	More in Parts
Accessibility	Difficult	Easy
Inspection Accuracy	Less	More
No. of Jigs	Two	One
Frequency of Jig Calibration	More	Less

4.2. Case Study 2: Jigless Manufacture of Wing Assembly

4.2.1. Wing Structure of Airframe

There are two Wing structures connected to the fuselage structure of the vehicle, one at the right side and the other at the left side. Wings are meant for pitch control of the vehicle and plays a major role in ascent and descent phases of the flight along with Control Surfaces. Wing is a built-up structure consisting of components like Spars, Ribs & Panels. The Front Spar and the Rear Spar are connected by four Ribs. The geometry of all the components are complex in nature with three dimensional aerofoil profiles and are made up of Aluminium Alloy material. The joint configuration at the spar-rib connections is complex which adds more difficulty in the manufacturing of the components as well as its assembly. The profiled skin panels are used to cover the wing internals.



Figure 4. Wing structure of airframe.

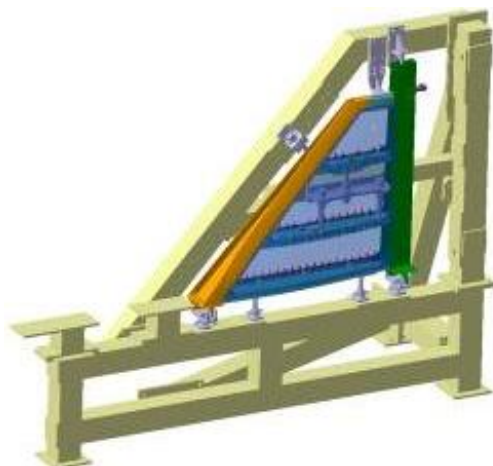


Figure 5. Design of conventional Wing Assembly jig.

4.2.2. Conventional Assembly Jig for the Wing Structure

The configuration of the wing structure is complex with more number of geometric features embedded in the structural components compared to the Tail structure. The assembly methodology adopted for wing structure is similar to that of the Tail structure. There are two assembly jigs, one for the left wing and the other for the right wing designed and manufactured adopting the conventional approach to facilitate the assembly of wing components. The method of deriving reference is from the machined pads mounted on to the jig structure and the ICY media for the wing - fuselage interface. The ICY media is used to locate and position the front and the rear spar to start the wing assembly process. The present design of components allows the ribs to lap just below the locating pads of spars. Hence self location is not possible for these components which requires precise fastening. This leads to the assembly constraints at the spar-rib interface at the front and rear locations which requires special tools for fastening. Figure 5 shows the design or construction of a conventional wing assembly jig.

4.2.3. Design of JAM Enabled Jig for Assembly of Wing Structure

The Wing components have a highly complex profiled geometry with lots of other geometrical features embedded in it to take care of the functional and structural design requirements. A detailed analysis on the joint configuration of the components at the mating interfaces indicates the need for the design of different type of locators, supports and clamps on the conventional jig. the assembly difficulties, constraints and special tool requirements are studied and analysed.

Feature modifications at the component's mating interfaces are carried out and analysed for the transfer of the tooling functions such as location, position, orientation and support from the assembly jig to the wing components. Changes in the design of interface geometric features of the components are introduced after ranking different types of features with respect to the original design requirements of the components considering the manufacturability, accuracy, inspectability and accessibility.

The modified configuration of the rib extensions as a self locating feature for assembling at the top of the locating pad of spar instead of bottom side is shown in Figure 6. Two holes are introduced on either side of the Ribs. One is identified as a dowel hole and the other as normal. The dowel holes can be placed in such a way that they are diagonally opposite in the Rib. Corresponding holes are introduced in Spar locations. The alternate holes are identified as dowel holes for positioning the consecutive ribs. Dowel pins inserted during the assembly ensures the location of ribs, front spar and rear spar together within the tolerance band of dowel pins. The Jigless enabled design of wing jig is shown in Figure 6b.

4.2.4. Benefits of the Jigless Assembly in Wing Structure

The design of jigless enabled assembly jig for the wing structure becomes very simple when the tooling functions are transferred to the individual component design. This results in less number of jig elements. The assembly process becomes easy and more accessibility exists for the components during assembly. The total number of locators are reduced to four by eliminating six locators. Thus the lead time and cost for the manufacture of assembly jig is considerably reduced. This has resulted in overall improvement of the assembly process in

terms of inspection efforts, accuracy and consistency of the structure. Figure 7 shows the design variation between the conventional jig and the jigless enabled assembly jig.

Table-2 shows the simplicity obtained by enabling the Jigless concept in the existing conventional Wing Assembly Jig without compromising quality.

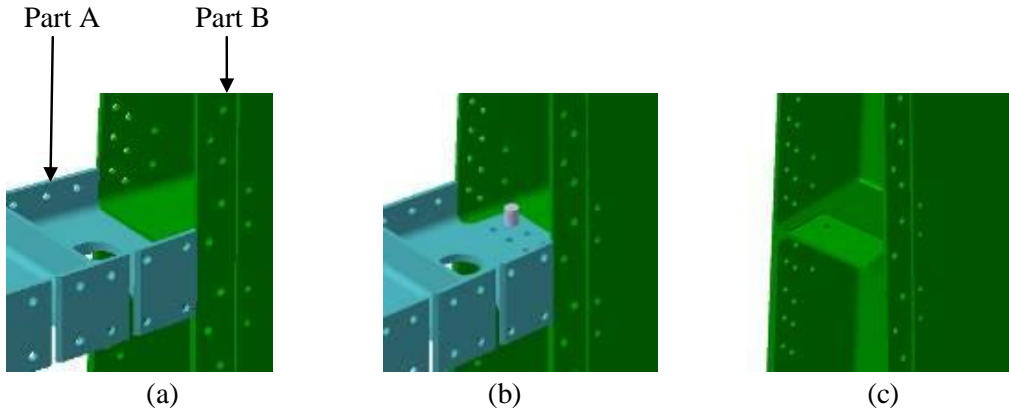


Figure 6. (a) Existing interface of Part A & B (b) Modified interface of Part A & B enabling JAM (c) Part B with JAM Feature.

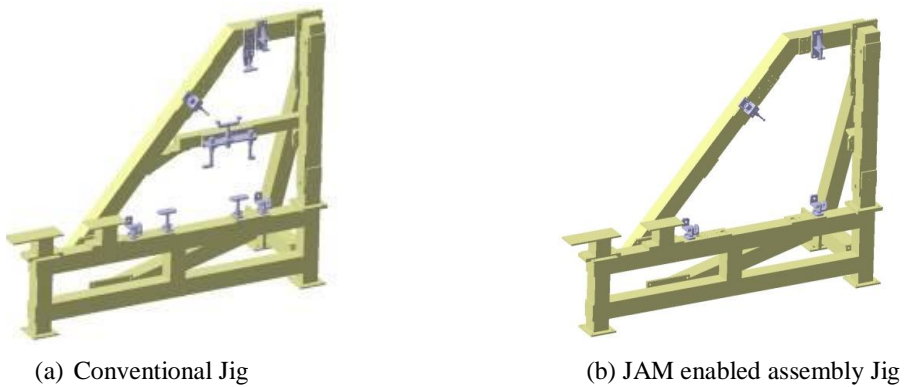


Figure 7. Design variation between the Conventional jig and Jigless enabled assembly Jig.

Table 2. Comparison of jig design and assembly process parameters for Wing conventional Jig & Jigless enabled Jig

Jig Description	Conventional Assembly Jig	Jigless enabled Assembly Jig
No of Locators	10	4
No of Support Beams	1	0
Accuracy	More in Jig	More in Parts
Accessibility	Difficult	Easy
Inspection Accuracy	Less	More
No of Jigs	Two	One
Frequency of Calibration	More	Less

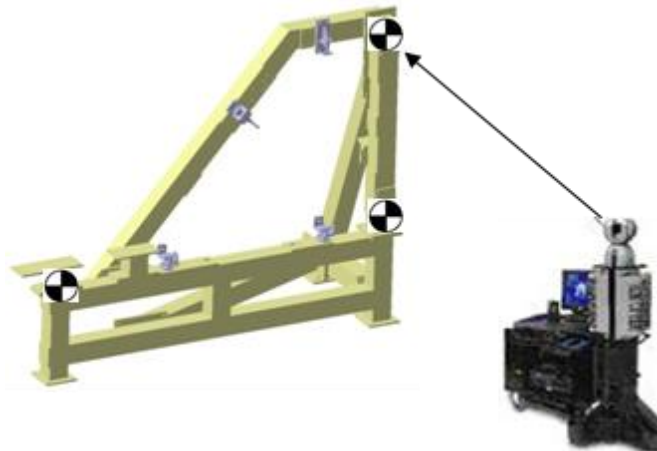


Figure 8. Inspection setup for Wing Assembly jig.

5. INSPECTION OF JIGLESS ASSEMBLY

Every aspects of the jigless manufacturing concept is based on 3D-CAD models which are used for the manufacture and assembly of components. The conventional inspection practice for the assembly is carried out as a stage operation after completion of the assembly and as checkpoints during the assembly process. This practice is totally improved by the introduction of jigless concept which enables real-time and closed loop control inspection of components in the assembly based on 3D-CAD model data. Hence the inspection of components is parallel to the assembly realization which increases the productivity and quality of the hardware. The inspection methodology using advanced inspection instruments viz. laser tracker based on non-contact inspection is felt very much useful in stacking the components to the exact position. The quality of inspection by a laser tracker is further enhanced by reduction in the number of assembly elements. A typical inspection setup of wing assembly is shown in Figure 8. The datum targets are established in the assembly jig which are used for setting up of the jig locators and assembly of structural components.

CONCLUSION

Studies have been carried out for the manufacture of large airframe structural assemblies of Re-usable Launch vehicle using conventional jig as well as the JAM enabled jig. The possible benefits observed from the case studies of two airframe structures in respect to the parameters related to jig design, jig manufacture and product assembly processes are presented here. The present study reveals that the implementation of the JAM concept in the manufacture of aerospace structures leads to a considerable reduction in lead time and cost for the design and realisation of assembly jigs, reduction in product assembly time, effort and improvement in quality. The effective integration of 3D geometric modelling strategies, CAM based on 3D models, automation and non-contact based inspection methodologies are very important to achieve good results. The level of accuracy and quality is determined by the

CAM techniques adopted at the component level itself which is higher in today's manufacturing trends. This new practice eliminates the requirement of frequent calibration of jigs incurring more cost and time thus leading to about 50% reduction in inspection and assembly procedures.

REFERENCES

- [1] Boothroyd. G. (1994). "Product design for manufacture and assembly", *Computer Aided Design*, 26(7), 505-520.
- [2] Soe,Naing. (2004). "Feature based design for Jigless assembly", Ph.D *Thesis*.
- [3] Andreasen, M. M., Ler, S., Lund, T.&Swift, K. G. (1988). "Design for assembly". 2nd ed. Bedford, UK: IFS.
- [4] Goodrich. (2001). "GRIDLOCK technology", Goodrich Aerostructures Group.
- [5] Deepu Krishnan, SandeepVerma, Shashank Saxena, Vinu Paul & Jeyasingh, J. J. V. (2007). "Jigless Assembly - a new concept in Aerospace Manufacturing", *Proceedings of National Aerospace Manufacturing Seminar*, 343-352.
- [6] Shashank, Saxena K.,Santhosh Kumar, Jeyasingh, J. J. V., Kothandaraman, G. & Sinha, P. P. (2009). "Jigless Assembly- A Case Study" *Proceedings of National Aerospace Manufacturing Seminar*, 139-150.
- [7] Shashank, Saxena, K., Santhosh Kumar, Jeyasingh, J. J. V., Shibu, Gopinath & Koshy M. George. (2013). "Studies on Jigless Manufacturing of Aerospace structural assemblies", 2nd International Conference on Advanced Manufacturing and Automation, 643-648.
- [8] Allen, A. J. & Swift, K. G. (1990). "Manufacturing process selection and costing", *Proceedings of Institution of Mechanical Engineers*, Vol. 23, 143-148.

Chapter 3

MANUFACTURING OF POLYMER NANO COMPOSITES

*Sridharan Veerapuram and Muthukrishnan Nambi**

Nano Materials Research Cell, Department of Mechanical Engineering,
Sri Venkateswara College of Engineering, Irungattukottai,
Tamilnadu, India

ABSTRACT

Polymer nano composites are offering best alternative for conventional metals in various fields of engineering. They deliver exceptional mechanical, electrical and thermal properties. Modification of filling of matrix with nano sized particles of metals and non metals is an ever promising task. Effective utilization of properties of nano fillers can be achieved only by homogenous dispersion in matrix. This is ensured by better interfacial adhesion of filler and matrix. Functionalization of filler and addition of surfactants has been the route to good level of dispersion. Many techniques are available to disperse filler particles in matrix. Calendaring has been very effective in achieving this task. In-situ polymerization gives better dispersion when compared to other mechanical and acoustic techniques. Modified matrix is used to manufacture composites by different methods. Hand lay-up has been widely used in academia for research projects. Pultrusion has been used for manufacturing long composites of various cross sections including channels. Filament winding is used for fabricating cylindrical vessels. Use of natural fibres as reinforcement in composites has been extensive since recent past. The surface of natural fibres has to be modified in order to achieve better bonding between fibre and matrix. Alkali treatment has been widely used, which is easy and effective. Study of mechanical, electrical and thermal behaviour of composites is very interesting and promising for researchers.

Keywords: Polymer, nano composites, filler, functionalization, manufacturing

* E-mail: mk@svce.ac.in.

INTRODUCTION

Composites are materials manufactured by combining materials with different properties. They have widely replaced conventional metals in almost all engineering applications like aerospace parts, automotive body, sports car, tennis racket, cycle frame etc. Passenger flights, holiday cruise ships, yachts etc. are widely using polymer based composites for structural parts. Composite materials have the ease to be manufactured in various shapes and contours. The high strength to weight ratio offered by these materials is the major advantage over metal counterparts. In order to improve strength of polymer materials, various synthetic fibres were used to reinforce it. The fibres include glass, carbon, Kevlar etc. Now a day's natural fibres from jute, sisal, hemp, kenaf, banana, agave, bamboo etc. are widely used as reinforcement in composites. In order to enhance the performance of these composites, modified matrices have been used. The modification is mainly done with nano sized particles of carbon, silica and metals. These particles are called as nano fillers. To incorporate nano fillers into matrix effectively, various techniques have been followed. Carbon nano tubes (CNTs) has been the most widely used nano. Addition of nano fillers in the matrix has enhanced the mechanical properties of composites. Such a composite is termed as polymer nano composite. Manufacturing polymer nano composites has been very challenging and difficult. The enhancement in properties of nano composites mainly depend on the level of dispersion of nano fillers in the matrix, which requires specific instruments. The level of dispersion should be monitored during manufacturing nano composites. Polymer nano composites have been reported to have increased mechanical, thermal and electrical properties. The effective loading required to achieve such enhancement has also been very less. Due to this, polymer nano composites have received more attention in research and development.

Various nano fillers are being used these days, in which carbon based fillers have been predominant. Carbon Nano Tubes (CNT) has been the epicentre of research on polymer nano composites during the last two decades. Other nano fillers that have been used include graphene, carbon nano fibres, metal nano particles of titanium, chromium etc. Nano silica is another filler material that has been widely used.

In this chapter, manufacturing of polymer nano composites and other associated topics are briefly discussed.

NANO FILLERS

Nano fillers are particles of different material in nano ($\times 10^{-9}$ m) size. Nano particles are prepared by different methods. Carbon nano particles like CNT, graphene, fibres, fullerenes are synthesised by arc discharge, laser ablation, chemical vapour deposition, rapid thermal expansion and exfoliation of graphite. CNTs are available as single walled, double walled or multi walled. These are long cylinders of bonded carbon atoms. The length and diameter of these CNTs can be varied during synthesis. Graphene is available as single layered or multi layered flakes. Each sheet of graphene is one carbon atom thick. Metal and ceramic nano particles are prepared by repeated breaking down of metals using mechanical force, like in a ball mill. Almost all nano fillers are commercially available at various sizes according to the requirement. They are either available as dry powders or suspended in a liquid medium.

In this chapter, manufacturing of polymer nano composites with carbon nano fillers has been discussed. For metal and ceramic based fillers, suitable literature is suggested.

FUNCTIONALIZATION OF NANO PARTICLES

Enhancement in properties due to nano fillers is best achieved only when there is uniform dispersion of them in the matrix. Proper dispersion ensures efficient transfer of load in nano composites. The nano fillers due to their large surface area tend to agglomerate during dispersion process. In order to overcome this problem, many attempts have been made to uniformly disperse the nano fillers and at the same time prevent re-agglomeration. The process of changing the surface of nano fillers, to enhance bonding, is called functionalization. It is done either by chemical (covalent) or physical (non-covalent) method. Due to functionalization, higher stability of dispersion is achieved, as it prevents re-agglomeration and enhances coupling of filler particles with the matrix.

Chemical functionalization is the process of modifying the wall or surface of nano filler using a suitable chemical for providing covalent bonding between filler and polymer matrix.

CNTs have been chemically functionalized by many techniques such as fluorination, acid treatment, amine group etc. These active groups can be introduced directly on filler surface (direct functionalization) or on the defect sites present (defect functionalization).

Direct functionalization involves attaching chemical elements on the surface wall. The fluorination process is one of the direct functionalization techniques, in which CNTs are treated with fluorine at higher temperatures. This attaches fluorine on CNTs with a weak C-F bond, which can be successfully replaced by amino, alkyl or hydroxyl groups. In similar way, carbene, nitride, chlorine, bromine has also been attached to side walls of CNTs. In defect site functionalization, oxidising agents such as strong acids like nitric acid and sulphuric acid have been used. These add carboxylic groups on the side wall. Chemicals like hydrogen peroxide have also been used along with nitric acid to attach hydroxyl groups. Such functionalization has improved the dispersion in solvents and polymer matrix. Acid treated CNTs have shown greater stability in water, which can be used to process homogenous dispersion in water soluble matrices. As a result a good bonding is achieved between matrix and filler that enhancement in mechanical and electrical properties.

Defect functionalization is a method of transforming defect site like open ends holes on wall, irregularity on the hexagon carbon ring etc. These defects are filled with carboxylic or hydroxyl groups. Various agents used such process include strong acids, their combinations, potassium permanganate, ozone etc. These are active functional groups that enhance solubility in various solvents. Due to functionalization, hydrophobic surface is transformed into hydrophilic. This ensures strong interfacial bond with polymer matrix, which allows polymer nano composites to possess high mechanical and electrical properties.

Graphene differs from CNTs in its structure. Unlike CNTs, graphene is flat and has a single layer of carbon atoms, packed in a honeycomb lattice. Chemical or covalent functionalization of graphene is a preferred method, as it facilitates dispersion and prevents re-agglomeration. Various agents used to modify graphene include organic amines, alkyl lithium reagents, and isocyanides and diisocyanate compounds. The surface of graphene is modified with carboxyl and hydroxyl groups.

Physical functionalization or non-covalent functionalization is the process of modifying the surface of filler by polymer wrapping or using surfactant substitution.

CNTs are suspended in the presence of polymer, which leads to wrapping of polymer molecules on CNT surface to form a complex. This is achieved by Van der Waals interaction and π - π stacking of CNTs. Surfactants are compounds that get adsorbed to the surface and make them soluble in various solvents. Sodium dodecyl sulphate, Sodium dodecyl benzene sulphonate, Tween 20, Tween 80, Triton X 100, Sodium cholate hydrate, Sodium deoxycholate are some of the surfactants used in various studies. The adsorption of surfactant on CNT surface reduces the surface tension and thereby reducing its ability to re-agglomerate. Different types of surfactants have been used in many studies, which include non-ionic, anionic and cationic surfactants. Non-ionic surfactants have been used for water-soluble polymers and cationic surfactants are used for other polymers. An optimum CNT-to-surfactant ratio has to be maintained, as lower or higher ratios have been reported to have reduced the dispersion level.

Graphene has been functionalized by coating reduced graphite oxide nano platelets with an amphiphilic polymer. By using 7, 7, 8, 8-tetracyanoquinodimethane (TCNQ) anion as stabilizer, water soluble and organic solvent soluble graphene sheets have been prepared. Pyrene derivatives and sulfonated polyaniline have also been used to functionalize graphene sheets by non-covalent method angle X-ray scattering (SAXS), scanning electron microscopy (SEM), and transmission electron microscopy (TEM). The level of dispersion of nano filler and matrix has to be reported while studying nano composites.

MANUFACTURING OF POLYMER NANO COMPOSITES

Dispersion Techniques

In order to fully utilize the properties of nano fillers, they have to be dispersed uniformly into the polymer matrix. There are two types of polymers available, thermo set and thermoplastic. Thermosetting polymers are available in the form of resin, with a range of viscosity, while thermoplastics are available in solid form as pellets or granules.

Sonication is the process of agitating the contents using high frequency ultrasonic waves and cavitations produced by a transducer. These waves create, grow and implode a bubble in the liquid, which results in mixing. Sonication should be done in intervals, as it causes raise in temperature of the contents. Sonication is done by either using a probe or water bath. Probe sonication is a high power or strong sonication and bath type is mild. The probe tip delivers high energy density in smaller volume. Sonication power plays a vital role in keeping the nano fillers in its original size. High-power sonication for longer time reduces the filler size, which results in reduced enhancement of properties in nano composites. For instance aspect ratio of CNTs, nano fibres and flake size of graphene are reported to have been reduced due to prolonged sonication. It is better to find out suitable sonication power and time for the type of nano fillers used. On the other hand bath sonication has been widely used as it is cheap and affordable. Bath sonication is advantageous because in probe sonication nano fillers tend to agglomerate near the tip of the probe. It is less effective when compared to probe sonication, but produce less detrimental effect on nano fillers.

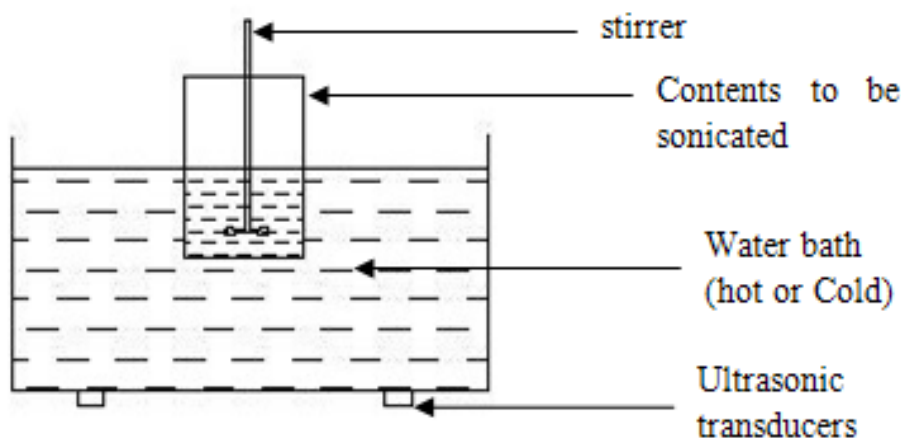


Figure 1. schematic representation of sonication combined with stirring.

Stirring is mixing of contents by application of mechanical force using an over head or a magnetic stirrer, by creating a vortex in the centre. In over head stirrer, the blade portion is immersed in the liquid and rotation is given through a motor. The blades should be properly designed as mixing of the contents is desired and not emulsification. Specially designed rotor blades are available in the market at a lower price to achieve required mixing. The speeds of the blades are set at a level, suitable for nano filler mixing. Many composites are prepared by rigorous mixing at high speeds.

Magnetic stirring involves mixing the contents by rotation of magnetic pellets by an electrically controlled rotating metal shaft that is attracted to magnet. The rotation on the shaft is transferred to the contents of the beaker through the pellets. Magnetic stirring is limited with respect to maximum achievable speed.

Calendaring is the process of employing shear force created by rollers to mix viscous polymers. Commonly a three-roll mill is employed. The 3-roll mills are named as feed, centre and apron rollers. These rollers create local high shear force, which is responsible for dispersion. The gap is reduced progressively and the contents are passed through these rollers several times. The gap and relative velocity between rollers can be adjusted to achieve required level of dispersion. Machines capable of maintaining a smaller gap of 5 micron are available in the market. By setting the speed and gap at optimal level, high shear force and short residence time can be offered to the contents. This greatly helps in reducing the damage caused to the nano fillers.

Polyester, vinyl ester, phenolic and epoxy grade resins are modified using above techniques. Using one of the above dispersion methods, nano fillers are dispersed in polymer matrix. Based on the observation it is suggested to use combination of stirring and sonication in a cycle or calendaring for effective dispersion in thermo set polymer matrix. Sonication can be carried out in an ice cold bath to overcome the effects of overheating. The contents are then transferred to a mould and nano composites are prepared. Often this is used to cast composite laminates.

Melt blending is a widely used process for modifying thermoplastic polymer matrix. It involves melting of pellets or granules of plastic to form a high viscous medium. The nano fillers are dispersed by application of high shear force. Twin screw extruder, high shear

mixer, dispersion kneader are few equipments used. In this, twin screw extruder is most widely used and has been effective. It consists of two co-rotating or counter rotating screws inside a barrel, which has different heating zones. The temperature is set according to the plastic used. The screws could be conical or cylindrical in shape. The polymer and the fillers are compounded in between screws and barrel under temperature, closer to the melt temperature of the plastic. The extrudate is generally passed through a die and water cooled before being passed through a pelletizer, where it is cut into pellets. If the die is replaced by a water cooled roller, sheets can be directly processed. The temperature and shear force are critical factors. Higher temperatures may reduce the viscosity of the plastic but will deteriorate the intrinsic property of nano filler. High shear force will ensure better dispersion but may lead to fragmentation of nano particles. Optimized temperature and shear force are key factors for a better performing nano composite. Poly ethylene, poly propylene, poly carbonate etc. are successfully compounded with nano fillers using this technique. Thermoplastic polymers are available as granules or powder i.e., in solid form. The monomers have weak bond, which can be broken down by application of heat. These polymers can be reformed any number of time. Nano fillers are dispersed in this matrix mainly by shear force.

Ball milling is another method used to mix matrix and filler material. It grinds the materials into fine powder. The contents to be mixed are put inside a jar with spherical balls of varying diameter. The material used for the jar and balls possess high strength. Generally ceramics, tungsten carbide are used. These jars are clamped on a platform rotated by planetary gears. As a result, high order dispersion is achieved. All thermoplastics and cryogenically cooled thermo set plastics are processed in this method.

Modified polymer matrix pellets or powder are formed as sheets using a compression moulding machine and used for preparing nano composites.

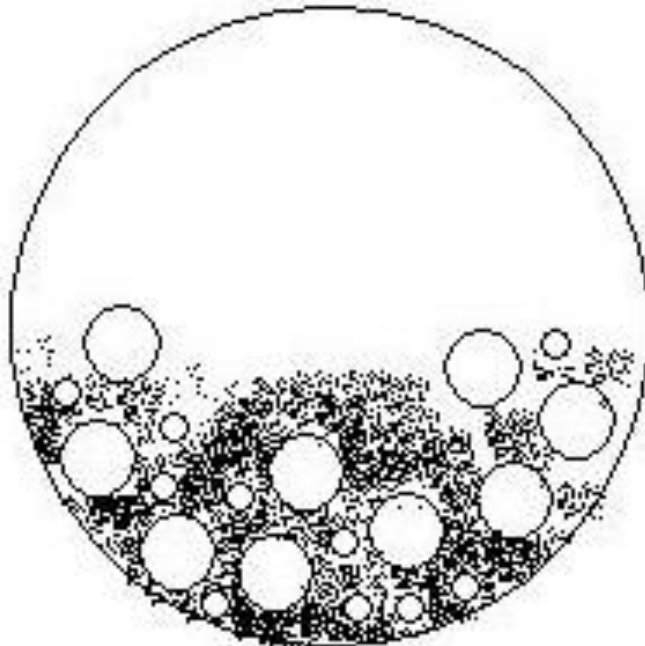


Figure 2. schematic of Ball milling process to mix plastic and filler.

In Situ Polymerization

This process is effective for all types of polymers, especially for the types that cannot be processed as stated above. Nano fillers are first dispersed in a suitable solvent. Acetone, ethanol, methanol, dichloride benzene, dimethyl formamide, methyl pyrrolidone are some of the widely used solvents. Note that acetone was widely used for CNT dispersion process and has been reported to have the least negative influence compared with other solvents such as ethanol and dimethyl formamide (DMF).

Nano particles tend to agglomerate due to large surface areas, especially carbon nano particles. So the particles should be de-aggregated or uniformly dispersed. This is followed by mixing of monomer. The contents are mixed and re dispersed well. Once required level of dispersion is achieved, the solvent is removed by application of heat, preferably in a hot water bath. A suitable hardener or initiator is added and polymerization is initialized. The contents are transferred to a mould and required nano composite is manufactured.

It is an efficient method to achieve uniform dispersion even at high loading of nano fillers. This method allows grafting or binding of polymer molecules on the surface of nano filler. In-situ polymerization has given the highest level of dispersion, when compared to any other technique.

MANUFACTURING METHODS

Composites are manufactured by various methods. Hand layup, filament winding, pultrusion, extrusion etc. are few of the widely used techniques. Composites contain two main ingredients, the fibre and the matrix. Fibre is majorly the load bearing member and matrix keeps them in its place. The percentage of these members in a composite depends on their nature and application. Generally 60% volume of matrix and 40% volume of fibre can be used, with or without filler, to start to know about composite preparation.

Hand lay-up is a technique which is used mostly in preparing laminates. Composite contains alternate layers of matrix and fibre, stacked to required height. In hand lay technique, calculated quantity of resin and fibre used. The following tools may be required. a base plate, separator film, mould, pot, brush, roller and top plate. Upon base plate mould with separator film is placed. Separator could be a film of deboning spray of non-sticky polymer like Teflon. Inside the mould, a layer of resin is coated first followed by fibre. The fibre could be unidirectional, bidirectional, inclined or woven mat. It is then rolled using a roller gently. This ensures removal of entrapped air bubbles and uniform deposition of matrix under the fibre. This sequence is followed until required height is reached. This top plate with separator is then placed to cover the contents. The whole stack is kept under load using a compression moulding machine. The authors used around 2.5 MPa load for 24 hours to manufacture epoxy based composites. The laminates thus produced are kept in hot air oven to remove any stresses induced. This is the most convenient technique to use. The pot time of resin should be known during layup. Otherwise resin will solidify in the pot.

Filament winding is used to manufacture shells, tubes, shafts, tanks etc. The fibre is wetted with matrix and wrapped on a mandrel. It is rotated at an optimal speed using a motor. This draws the fibre continuously. The resin coated fibre is passed through a carriage. The

speed of carriage and mandrel determines and length and pattern of the winding. Various angles of roving are can be achieved using this technique. Mandrel can be fixed and carriage can be traversed to obtain desired pattern or vice versa. Wind angle from 0° to 90° is possible. Generally a helical winding of fibre is achieved.

Pultrusion is a method to produce long composite of any cross section. Continuous strands of roving are pulled to a die of required pattern. On its way, the roving's are wetted in resin bath and passed under roller to remove extra resin. It is then pulled through die. On the other side of die, it is cut using a saw to achieve required size. Using this technique, long flat sheets, tubes, beams and sections can be manufactured.

Extrusion is used to produce composite with discontinuous fibres. This is similar to normal metal extrusion process and can be used for thermoplastic polymer composites. Twin screw extrusion is most widely used, which employs heat in the barrel to soften the plastic and mix with fibres. It is then forced through a die and cooled afterwards.

Fibres are the elastic member of the composite. They are classified as synthetic and natural. The synthetic fibres can be used as received. They are hydrophilic fibres. Natural fibres on the contrary are hydrophobic in nature. The surface of these fibres is too modified before employing as reinforcement. Many treatments are done to impart hydrophilic nature to natural fibres; these include washing with distilled water, mild detergent, alkali treatment, bleaching using hydrogen peroxide etc. Alkali treatment is widely used has been effective in improving bonding between matrix and fibre. It involves usage of an alkali, generally sodium hydroxide. 5 – 10 % NaOH solution is prepared and the fibres, washed with distilled water and dried, are kept soaked for approximately 2 hours. They are then taken out and washed with distilled water to remove any excess alkali. It is dried in room temperature for about two days and in a hot air oven for 2 – 3 hours. This process is referred as mercerization process.

APPLICATIONS OF NANO COMPOSITES

Due to its enhanced properties, nano composites are replacing conventional metals in various fields of application. These are low density materials with high mechanical and impact strength. It possess good strength-to-weight ratio, which makes it an immediate choice in various fields. The main application of carbon particles filled nano composites is in the field of electronics. Conducting polymers are being widely used in making electronic boards. These composites are even used in solar power cells. High end sports equipment such as bikes, rackets, base ball bats, sports helmet etc. are made using nano composites. Further developments in the field of nano particle synthesis may bring down their cost, which will see their usage growing exponentially.

CONCLUSION

An overview of polymer nano composites has been provided. A lot of work has been carried out in preparing a composite that would best utilize the potential of nano particles. The most important factor in obtaining a good nano composite is the level of dispersion. Various mechanical and acoustical techniques are being used to disperse filler particles in

matrix. Functionalization has been reported as the efficient way to achieve homogenous dispersion, which can be done as covalent or non-covalent way. Calendaring method has been reported to offer high dispersion. Melt blending is seen as an efficient way to large scale production. Recently, in-situ polymerization is showing fine level of dispersion and has been widely used these days. The performance of composite is directly related to the finesse in processing. In-situ polymerization technique has given maximum enhancement of mechanical properties. Electrical conductivity of polymer nano composites, even at low loading of carbon nano particles, is another advantage. Nano composites have shown more thermal stability than normal composites. Overall performance improvement has been achieved by using nano fillers. This makes polymer nano composites ideal for structural and functional applications in various fields of engineering.

REFERENCES

- Ahmad, M. Bin et al., 2011. Comparison of In Situ Polymerization and Solution-Dispersion Techniques in the Preparation of Polyimide / Montmorillonite (MMT). *Nanocomposites*, 0067, pp.6040–6050.
- Albuquerque, A. C. De et al., 2000. Effect of wettability and ageing conditions on the physical and mechanical properties of uniaxially oriented jute-roving-reinforced polyester composites. *Composites Science and Technology*, 60 (2000) 833-844.
- Aziz, S. et al., 2005. Modified polyester resins for natural fibre composites. *Composites Science and Technology*, 65(3-4), pp.525–535.
- Bernal, M. M., Hernandez, M. and Verdejo, R., 2013. Comparison of filler percolation and mechanical properties in graphene and carbon nanotubes filled epoxy nanocomposites. *European Polymer Journal*, 49(6), pp.1347–1353.
- Fiedler, B. et al., 2006. Fundamental aspects of nano-reinforced composites. *Composites Science and Technology*, 66(16), pp.3115–3125.
- Gkikas, G., Barkoula, N.-M. and Paipetis, a. S., 2012. Effect of dispersion conditions on the thermo-mechanical and toughness properties of multi walled carbon nanotubes-reinforced epoxy. *Composites Part B: Engineering*, 43(6), pp.2697–2705.
- Gojny, F. et al., 2005. Influence of different carbon nanotubes on the mechanical properties of epoxy matrix composites – A comparative study. *Composites Science and Technology*, 65(15-16), pp.2300–2313.
- Gojny, F. H. et al., 2004. Carbon nanotube-reinforced epoxy-composites: enhanced stiffness and fracture toughness at low nanotube content. *Composites Science and Technology*, 64(15), pp.2363–2371.
- Gojny, F. H. and Schulte, K., 2004. Functionalisation effect on the thermo-mechanical behaviour of multi-wall carbon nanotube/epoxy-composites. *Composites Science and Technology*, 64(15), pp.2303–2308.
- Hernández, M. et al., 2012. Overall performance of natural rubber/graphene nanocomposites. *Composites Science and Technology*, 73, pp.40–46.
- Kuilla, T. et al., 2010. Recent advances in graphene based polymer composites. *Progress in Polymer Science*, 35(11), pp.1350–1375.

- Ma, P.-C. et al., 2010. Dispersion and functionalization of carbon nanotubes for polymer-based nanocomposites: A review. *Composites Part A: Applied Science and Manufacturing*, 41(10), pp.1345–1367.
- Moazzami Gudarzi, M., 2012. Enhancement of dispersion and bonding of graphene-polymer through wet transfer of functionalized graphene oxide. *Express Polymer Letters*, 6(12), pp.1017–1031.
- Park, J.-M. et al., 2012. Optimum dispersion conditions and interfacial modification of carbon fiber and CNT–phenolic composites by atmospheric pressure plasma treatment. *Composites Part B: Engineering*, 43(5), pp.2272–2278.
- Paul, D. R. and Robeson, L. M., 2008. Polymer nanotechnology: Nanocomposites. *Polymer*, 49(15), pp.3187–3204.
- Pötschke, P. et al., 2005. Melt Mixing as Method to Disperse Carbon Nanotubes into Thermoplastic Polymers. *Fullerenes, Nanotubes and Carbon Nanostructures*, 13(sup1.), pp.211–224.
- Rastogi, R. et al., 2008. Comparative study of carbon nanotube dispersion using surfactants. *Journal of colloid and interface science*, 328(2), pp.421–8.
- Seyhan, A. T. et al., 2007. Critical aspects related to processing of carbon nanotube/unsaturated thermoset polyester nanocomposites. *European Polymer Journal*, 43(2), pp.374–379.
- Thostenson, E. T., Ziaee, S. and Chou, T.-W., 2009. Processing and electrical properties of carbon nanotube/vinyl ester nanocomposites. *Composites Science and Technology*, 69(6), pp.801–804.
- Velde, K. Van De and Kiekens, P., 2001. Thermoplastic pultrusion of natural fibre reinforced composites. 54.
- Wichmann, M. H. G. et al., 2006. Glass-fibre-reinforced composites with enhanced mechanical and electrical properties – Benefits and limitations of a nanoparticle modified matrix. *Engineering Fracture Mechanics*, 73(16), pp.2346–2359.

Chapter 4

**OPTIMAL CONTROL OF DRILLING PROCESS
FOR HOLE MAKING IN FIBER REINFORCED
PLASTICS: A REVIEW**

*Amrinder Pal Singh¹, Kishore Debnath², Manu Sharma¹
and Inderdeep Singh^{2*}*

¹Mechanical Engineering, University Institute of Engineering and Technology,
Panjab University, Chandigarh, India

²Department of Mechanical and Industrial Engineering,
Indian Institute of Technology Roorkee, Uttarakhand, India

ABSTRACT

Damage caused during drilling in fiber reinforced plastics (FRP's) is an important research area for materials industry. Delamination is a critical form of damage as it leads to very high rates of rejected drilled parts. Delamination majorly depends on the thrust force and torque generated during drilling in FRP's. Both thrust force and torque are functions of the feed rate during drilling process. Models of drilling in different materials available in literature, have either modeled thrust force with feed rate or torque with feed rate. To control the damage due to delamination, control of both thrust force and torque is required. Thrust force and torque models with feed rate can be clubbed in state space to form a combined thrust force and torque model with feed rate. This model can be controlled by using an optimal controller. The optimal controller provides the user with a control effort handle to assign weightage to control effort being exerted for controlling thrust force or torque according to requirements.

Keywords: Fiber reinforced plastics (FRPs), drilling, forces, delamination, modeling, control

* Corresponding author, E-mail: dr.inderdeep@gmail.com

1. INTRODUCTION

Properties like high specific strength, high stiffness in one direction, combination of high strength and toughness with light weight etc. are not available when using conventional materials. Modern day challenges urge unconventional combinations of properties that can be met using composite laminates [1]. Composite materials offer number of advantages in terms of high strength-to-weight ratio, high stiffness-to-weight ratio, good chemical and corrosion resistance, better impact characteristics, excellent mechanical properties and above all greater design flexibility [2,3]. FRP's have been found better for applications in aerospace, automotive, sports-goods, marine and medical industries [4,5].

Processing of composite materials into final products can be carried out using primary and secondary manufacturing processes. Primary manufacturing processes involve conversion of raw materials into simpler shapes which can further be processed using secondary manufacturing processes involving machining as per requirements of the design of product. Hand lay-up, compression molding, pultrusion and filament winding are some of the well-established primary manufacturing processes commonly used for FRP's [6]. To obtain complex shaped products, simple shapes obtained from primary manufacturing processes are assembled using secondary manufacturing processes. Drilling is a very commonly used secondary process e.g., assembly of a small aircraft using composite laminate parts, requires about 100000 holes for joining together different parts [7,8]. Delamination during drilling causes damage and adversely affects the surface finish and strength of composite laminate thereby leading to rejection [9,10].

2. DRILLING IN FRP'S

Drilling in composite laminates is different as compared to the drilling in conventional materials as drill has to pass alternatively through soft plastic (matrix) and hard fiber (reinforcement). Both these phases in a composite laminate possess different properties than each other. This diversity amongst constituents of composite laminates makes material removal mechanism complex due to drill alternatively cutting through soft and hard part in layers. Further during drilling in composite laminates, matrix phase and fiber reinforcement do not equally share the load [10,11]. This leads to damage around the hole during drilling. It spoils surface finish of drilled hole and also deteriorates strength of the composite laminate [12]. Many researchers have modeled this damage and characterized it [13-16]. Delamination, fiber pull-out, micro cracking, matrix burning, chipping and spalling are some common types of damage occurring in composite laminates [17]. Damage due to delamination is most important as during assembly of a typical aircraft delamination due to drilling leads to as high as 60% rejection of composite parts [18,19]. The two mechanisms causing delamination during drilling in FRP's are peel-up at drill entry and push-down at the exit of drill [20,7].

Feed rate and cutting speed are the two operating parameters that can be easily controlled during drilling operation [10]. Both the parameters should be optimized to drill damage free holes [21]. Damage caused by delamination occurring in composite laminate mainly depends on feed-rate during the drilling process [22-24,16]. When the composite laminate is drilled using high feed rates, failure is mainly caused due to damage caused due to impact [25]. Feed

rate is considered as most critical parameter influencing damage in the form of delamination around drilled hole in composite laminate. Therefore, it becomes pertinent to select such a feed rate that avoids this damage [26-31]. Size of delamination zone around the hole depends upon thrust force acting during drilling [6,32,33]. Researchers have found that delamination does not occur during drilling in a composite laminate, if thrust force acting during the drilling process is kept below a critical value [4]. It can be concluded that, it is not only the thrust force that causes the damage due to delamination, torque also plays very important role [34,35]. Torque is also dependent upon the feed-rate like thrust force during drilling in composite laminates [6,32].

3. MODELING OF DRILLING

Cutting force acting on composite laminate while drilling causes delamination damage. It produces a peeling force in the axial direction through slope of flute in drill. This peeling force is a function of drill geometry and friction forces. There is a critical value of thrust force for the composite laminate being drilled. If, the thrust force during drilling is kept below this critical value, no delamination occurs. This critical thrust force was modeled acting as a point load and distributed load at center of the circular composite plate based on linear elastic fracture mechanics (LEFM) theory [4,7,36]. The critical thrust force causing delamination at different ply-locations was modeled based on the lamination analysis of stiffness matrices of the FRP [37].

Artificial neural network (ANN) was used to model thrust force and torque as function of feed rate [38-40]. Delamination in carbon fiber reinforced plastics (CFRP) was estimated as a function of spindle speed, feed rate, drill diameter, drill geometry and point angle by using multi-layer feed-forward ANN [19,41]. Fuzzy logic was implemented to model dynamics of drilling in carbon fiber reinforced plastic by dividing the drilling process in three sub-models at entrance, middle and exit of composite. Autoregressive-moving-average (ARMA) linear equation was used to develop a relation of thrust force and feed rate. Fuzzy model was trained using the experimental data-sets using a gradient descent algorithm to simulate the thrust force during drilling. A second order reference thrust force model with a critical damping ratio ($\xi = 1$) was then used in fuzzy controller for controlled drilling [42]. Neural network was also used to model residual tensile strength caused by drilling in composite laminates [43].

Damage can be modeled using models of thrust force and torque identified through experiments [44]. While drilling, thrust force and torque varies with feed rate. Mathematical model in the form of first order transfer function was developed between thrust force and feed rate during drilling in steel and aluminium [45]. Similarly, thrust force and feed rate during drilling in cast iron was modeled as a third order system with delay [46,47]. Second order discretized model between thrust force and feed rate was developed for drilling of composite laminates [48]. It is very difficult to accurately measure the cutting torque during drilling. The accuracy also depends upon the capability, location and fixing of the torque sensor. Therefore requirement of torque sensor was eliminated by using a disturbance observer. This disturbance observer was subsequently used to model cutting torque during drilling in S45C carbon steel [49]. Drilling dynamics were captured by a third order model relating torque to

feed rate during drilling in AISI 1020 hot rolled steel and AISI 1045 steel [50,51]. Third order transfer function of thrust force with feed rate and torque with feed rate during drilling in glass fiber reinforced plastics was identified through drilling experiments [52-54].

4. CONTROL OF DRILLING

In situations where mathematical equations are difficult to obtain, artificial techniques like neural network, fuzzy logic etc. has been found to be convenient methods for control of drilling. Neural network was used to model the drilling process and thereafter the controlled feed rate was obtained using a neural controller so as to achieve desired thrust force. Output from the neural identifier was used to train the neural-controller with inputs as previous feed rate and thrust force error. Critical thrust force model developed using LEFM approach was used to provide reference thrust force for the controller [7,38]. In another neural network based controller, reference thrust force, previous feed rate and current thrust force was taken as input. The controller gave controlled feed rate as output to control thrust force during drilling [39]. Fuzzy controller worked in three steps namely fuzzification, inference and de-fuzzification. Second order system with critical damping ratio ($\xi = 1$) was used to provide reference thrust force to the fuzzy controller during drilling. The trained ARMA model was used to obtain the fuzzy rules for tracking given reference by the fuzzy controller [42].

Thrust force was controlled by using a Proportional-Integral (PI) controller. The proportional gain helped in quick tracking of reference by the controller whereas the integral gain ensured no offset error. The performance of this controller was found out to be good for constant process-gain, but in situations where the process gain varies like drilling in composite laminates, PI controller performance was found to be deteriorating [48]. Similarly PI control and pole-placement technique was used to control the torque. The parameters of the PI controller were calculated using classical Ziegler-Nichols method [50]. Thrust force was controlled using PID controller. The parameters of the PID controller were computed using classical Ziegler-Nichols method [55]. Overshoot was minimized with the help of proportional gain using classic root-locus method [46]. The cutting torque was controlled to prevent drill damage using a PID controller and proportional gain tuning was done using root locus method [51]. Input to the PID controller was error between a reference torque and actual torque [49]. Third order model of thrust force with feed rate/torque with feed rate identified for drilling in glass fiber reinforced plastics was controlled using PID controller. The gains of PID controller were computed using Ziegler-Nichols method. The controller was tested for tracking a given reference trajectory of thrust force/torque [52-54].

The process gain which may vary during drilling in composite laminates was identified in real time using recursive least squares with exponential forgetting [56]. The thrust force acting during drilling was then predicted based on this identified process gain. Error between reference thrust force and predicted thrust force was minimized by using controlled feed rate $u(k)$ [57].

$$u(k) = \hat{u}(k|k) = \left[F_r(k + \lambda_2|k) - \sum_{i=1}^{n_a} e_i^{(\lambda_2)} F_f(k + 1 - i) - \sum_{i=2}^{n_b} g_i^{(\lambda_2)} u(k + 1 - i - n_k) - \sum_{i=0}^{n_k-1} g_i^{(\lambda_2-i)} u(k + i - n_k) \right] / h^{(\lambda_2)}$$

where, $F_r(k + \lambda_2|k)$ was reference thrust force obtained from delamination free force reference [48].

First order non-linear relation between thrust force and feed rate was used to model the drilling process. The varying gain was taken as non-linear function of feed rate. Thrust force was controlled by using an adaptive control law given as:

$$u(k) = u(k - 1) + \{P(q^{-1})r(k + 1) - R(q^{-1})F(k)\}/b_1$$

where, u was control input (feed rate) to the controller, q^{-1} was delay operator, $P(q^{-1})$ represented closed loop poles defining desired regulation characteristics, r was command signal, F was measured force signal, $R(q^{-1}) = r_0 + r_1q^{-1} + r_2q^{-2} + \dots$ and b_1 varied as a function of cutting stiffness of material [45].

Drilling in a composite laminate was divided into number of stages along its thickness. Intelligent supervisory controller was designed to monitor the thrust force acting during these stages for subsequent control. A strategy for each stage was then prepared with the objective to minimize damage during drilling by controlling thrust force and torque. Reference thrust force and torque used for controller was [58]:

$$F = K_1(ud)^{1-a} + K_2d^2$$

$$T = K_3u^{1-a}d^{2-a}$$

where, F was thrust force in N, T was torque in N-m, a, K_1, K_2, K_3 were constants, d was drill diameter and u was taken as feed rate in mm/rev. [59].

5. OPTIMAL CONTROL

Researchers have made attempts to model the drilling process of different materials using analytical techniques, neural networks, fuzzy logic and transfer function models. Some works model thrust force while others model torque with feed rate to capture the drilling dynamics. These models have been controlled by using neural controllers, fuzzy controllers, PI and PID controllers. Damage due to delamination caused by drilling of composite laminates can be prevented if both thrust force and torque are controlled simultaneously using controlled feed rate. There is no research available in literature wherein simultaneous control has been demonstrated. Therefore, present work explains in detail control of both thrust force and torque simultaneously by assigning relative weightage. The optimal controller can track any given reference trajectory by minimizing the error between actual signal and reference signal and gives corresponding optimal feed rate values for damage free drilling.

5.1. Combined Thrust Force and Torque Model

Third order transfer function between thrust force and feed rate as identified by drilling in GFRP composite laminate giving step feed rate input is:

$$\frac{F}{u} = \frac{1.1884}{0.0000052581s^3 + 0.000015565s^2 + 0.4172s + 1} \quad (1)$$

This transfer function can be conveniently converted into following form in continuous state space:

$$\text{State equation} \quad \dot{X}(t) = A_c X(t) + B_c u(t)$$

where, $A_c = (n \times n)$ is system state matrix, $X = (n \times 1)$ is state variable vector, $B_c = (n \times r)$ is input (actuator location) control matrix and $u = (r \times 1)$ is input vector in continuous time. The identified thrust force model (equation 1) upon conversion into first order differential equations becomes [52,53]:

$$\begin{bmatrix} \dot{F} \\ \ddot{F} \\ \dddot{F} \end{bmatrix} = \begin{bmatrix} 0 & 1 & 0 \\ 0 & 0 & 1 \\ -190180 & -79351 & -2.9601 \end{bmatrix} \begin{bmatrix} F \\ \dot{F} \\ \ddot{F} \end{bmatrix} + \begin{bmatrix} 0 \\ 0 \\ 226010 \end{bmatrix} u(t) \quad (2)$$

Similarly third order transfer function between torque model and feed rate as identified by drilling in GFRP composite laminate giving step feed rate input is represented as:

$$\frac{T}{u} = \frac{3.2421}{0.000032769s^3 + 0.000046272s^2 + 0.9302s + 1} \quad (3)$$

Torque model (equation 3) upon conversion into state space becomes [54]:

$$\begin{bmatrix} \dot{T} \\ \ddot{T} \\ \dddot{T} \end{bmatrix} = \begin{bmatrix} 0 & 1 & 0 \\ 0 & 0 & 1 \\ -30517 & -28385 & -1.4121 \end{bmatrix} \begin{bmatrix} T \\ \dot{T} \\ \ddot{T} \end{bmatrix} + \begin{bmatrix} 0 \\ 0 \\ 98938 \end{bmatrix} u(t) \quad (4)$$

Combined state-space model representing thrust force and torque with feed rate is formulated by combining the two systems as shown in equation (2) and equation (4) as [60]:

$$\begin{bmatrix} \dot{F} \\ \ddot{F} \\ \dddot{F} \\ \dot{T} \\ \ddot{T} \\ \dddot{T} \end{bmatrix} = \begin{bmatrix} 0 & 1 & 0 & 0 & 0 & 0 \\ 0 & 0 & 1 & 0 & 0 & 0 \\ -190180 & -79351 & -2.9601 & 0 & 0 & 0 \\ 0 & 0 & 0 & 0 & 1 & 0 \\ 0 & 0 & 0 & 0 & 0 & 1 \\ 0 & 0 & 0 & -30517 & -28385 & -1.4121 \end{bmatrix} \begin{bmatrix} F \\ \dot{F} \\ \ddot{F} \\ T \\ \dot{T} \\ \ddot{T} \end{bmatrix} + \begin{bmatrix} 0 \\ 0 \\ 226010 \\ 0 \\ 0 \\ 98938 \end{bmatrix} u(t) \quad (5)$$

5.2. Solution of Non-Homogenous Equation

Complete solution of the following non-homogenous equation in presence of input $u(t)$ is obtained as:

$$\dot{X}(t) = A_c X(t) + B_c u(t)$$

$$\dot{X}(t) - A_c X(t) = B_c u(t)$$

Multiplying both sides with $e^{-A_c t}$

$$e^{-A_c t} [\dot{X}(t) - A_c X(t)] = e^{-A_c t} B_c u(t) \quad (6)$$

The derivative of $e^{-A_c t} X(t)$ is obtained as:

$$\frac{d}{dt} [e^{-A_c t} X(t)] = e^{-A_c t} \frac{d}{dt} (X(t)) + \frac{d}{dt} (e^{-A_c t}) X(t) = e^{-A_c t} \dot{X}(t) - e^{-A_c t} A_c X(t)$$

$$\frac{d}{dt} [e^{-A_c t} X(t)] = e^{-A_c t} [\dot{X}(t) - A_c X(t)]$$

Putting it in equation (6) yields:

$$\frac{d}{dt} [e^{-A_c t} X(t)] = e^{-A_c t} B_c u(t)$$

Integrating both sides with respect to t between limits t_0 and t :

$$\int_{t_0}^t \frac{d}{dt} [e^{-A_c t} X(t)] = \int_{t_0}^t e^{-A_c t} B_c u(t) dt$$

$$e^{-A_c t} X(t) - e^{-A_c t_0} X(t_0) = \int_{t_0}^t e^{-A_c t} B_c u(t) dt$$

Multiplying both sides with $e^{A_c t}$:

$$X(t) = e^{A_c(t-t_0)} X(t_0) + \int_{t_0}^t e^{A_c(t-t_0)} B_c u(t) dt \quad (7)$$

This solution (equation 7) of the non-homogenous equation describes change of state relative to initial condition $X(t_0)$ and input $u(t)$.

5.3. Converting Continuous Model in to Discrete

Input to A/D convertor is a continuous time function $f(k)$, $t \geq 0$ and output consists of sequence of real numbers $f(k)$, $k = 0, 1, 2, \dots$ with the following relation:

$$f(k) = f(t = kT); kT \leq t < (k + 1)T$$

where, T is the time interval between samples.

Zero order hold of the continuous input, $u(t) = u(kT)$; $kT \leq t < (k + 1)T$; $k = 0, 1, 2, \dots$

The solution of the non-homogenous shown in equation (7) can be converted to discrete form

$$X(t) = e^{A_c(t-kT)} X(kT) + \left[\int_{kT}^t e^{A_c(t-t_0)} B_c dt \right] u(kT); kT \leq t < (k + 1)T \quad (8)$$

In response to input feed rate $u(kT)$, the state (thrust force and or torque) settles to value $X((k+1)T)$ prior to application of input $u((k+1)T)$.

$$X((k+1)T) = e^{A_c T} X(kT) + \left[\int_{kT}^{(k+1)T} e^{A_c[(k+1)T-t_0]} B_c dt \right] u(kT)$$

$$X((k+1)T) = AX(kT) + Bu(kT)$$

where, $A = e^{A_c T}$ is system state matrix in discrete form and $B = \int_{kT}^{(k+1)T} e^{A_c[(k+1)T-t_0]} B_c dt$ is input control matrix in discrete form.

5.4. Discrete-Time Linear Quadratic Tracking

$$\text{State equation in discrete form, } X(k+1) = AX(k) + Bu(k) \quad (9)$$

$$\text{The output equation is, } Y(k) = CX(k) \quad (10)$$

where, $Y(k)$ is $(m \times 1)$ output vector and C is $(m \times n)$ output matrix. The initial condition is given as $X(k_0)$ is initial thrust force and torque which set at zero as there is no thrust force and torque initially acting on composite laminate. The final condition $X(k_f)$ is free with k_f fixed. It is required to make the error $e(k)$ between actual thrust force and torque and reference thrust force and torque as small as possible with minimum control effort so that the output $Y(k)$ tracks the desired output $Z(k)$ [61-63].

Let $Z(k) = (m \times 1)$ desired output vector specifying reference thrust force or/and torque to prevent delamination.

$$\text{Error vector, } e(k) = Y(k) - Z(k) \quad (11)$$

$$\text{Put } Y(k) = CX(k) \text{ in equation (11), } e(k) = CX(k) - Z(k) \quad (12)$$

The chosen performance index is a quadratic cost functional involving square or quadratic of error, and/or control:

$$J = \left(\frac{1}{2} e'(k_f) F e(k_f) \right) + \frac{1}{2} \sum_{k=k_0}^{k_f-1} [e'(k) Q e(k) + u'(k) R u(k)]$$

$$J = \left(\frac{1}{2} [CX(k_f) - Z(k_f)]' F [CX(k_f) - Z(k_f)] \right) + \frac{1}{2} \sum_{k=k_0}^{k_f-1} \{ [CX(k) - Z(k)]' Q [CX(k) - Z(k)] + u'(k) R u(k) \} \quad (13)$$

In this k_f is specified which is time taken for drilling, while $X(k_f)$ is not specified (free final state system).

Where, $F = (m \times m)$ is the symmetric positive semi-definite matrix. It is terminal cost weighted matrix to ensure that the error $e(k)$ in equation (12) at k_f is as small as possible.

$Q = (m \times m)$ is the symmetric positive definite matrix. It is an error weighted matrix to keep error small. Here weightage can be assigned to thrust force (at element 1, 1) or torque (at element 4, 4) depending upon the requirements of tracking.

$R = (r \times r)$ is the symmetric positive definite matrix. It is a control weighted matrix; quadratic nature of control cost expression indicates that one has to pay higher cost for large control effort.

Define the Hamiltonian \mathcal{H}^* (also called the Pontryagin \mathcal{H} function) at the optimal condition as:

$$\mathcal{H}^*(x^*(k), u^*(k), \lambda^*(k+1)) = V(x^*(k), u^*(k), k) + \lambda^{*\prime}(k+1)f(x^*(k), u^*(k), k)$$

where, λ is Lagrange multiplying vector also called co-state vector, chosen arbitrarily in such a way that coefficient of dependent variation $\delta X(k_f)$ vanishes in the general boundary condition introduced later [62].

$$\mathcal{H} = \frac{1}{2} \sum_{k=k_0}^{k_f-1} \{ [CX(k) - Z(k)]' Q [CX(k) - Z(k)] + u'(k) R u(k) \} + \lambda^{*\prime}(k+1) [AX(k) + Bu(k)] \quad (14)$$

The state is given in terms of the Hamiltonian as:

$$X^*(k+1) = \frac{\partial \mathcal{H}}{\partial \lambda^{*(k+1)}} = \frac{\partial}{\partial \lambda^{*(k+1)}} (\lambda'(K+1)AX(k) + \lambda'(K+1)Bu^*(k))$$

$$\frac{\partial}{\partial X} (X'AX) = AX + A'X$$

$$X^*(k+1) = AX^*(k) + Bu^*(k) \quad (15)$$

Using the Hamiltonian (equation 14) optimal co-state equation representing constraint relation becomes:

$$\begin{aligned} \lambda^*(k) &= \frac{\partial \mathcal{H}}{\partial X^*(k)} = \frac{\partial}{\partial X^*(k)} \left\{ \frac{1}{2} [CX(k) - Z(k)]' Q [CX(k) - Z(k)] + \lambda^{*\prime}(k+1) AX(k) \right\} \\ &= \frac{\partial}{\partial X^*(k)} \left[\frac{1}{2} (X'(k)C'QCX(k) - X'(k)C'QZ(k) - Z'(k)QCX(k) + Z'(k)QZ(k)) \right] + \\ &\frac{\partial}{\partial X^*(k)} [\lambda^{*\prime}(k+1)AX(k)] \\ &= \frac{1}{2} [C'QCX(k) + C'Q'CX(k) - C'QZ(k) - C'Q'Z(k)] + [A'\lambda^*(k+1)] \end{aligned}$$

As Q is symmetric matrix so $Q' = Q$

Optimal co-state equation is:

$$\lambda^*(k) = [C'QCX^*(k) - C'QZ(k)] + [A'\lambda^*(k+1)] \quad (16)$$

For simplicity let us define:

$$E = BR^{-1}B'$$

$$V = C'QC$$

$$W = C'Q$$

Hence optimal co-state equation becomes:

$$\lambda^*(k) = VX^*(k) - WZ(k) + A'\lambda^*(k+1) \quad (17)$$

The control equation giving optimization of performance index with respect to control $u(k)$ as obtained from the Hamiltonian:

$$\frac{\partial \mathcal{H}}{\partial u^*(k)} = 0 \xrightarrow{\text{yields}} \frac{1}{2} \frac{\partial}{\partial u^*(k)} [u'(k)Ru(k)] + \frac{\partial}{\partial u^*(k)} [\lambda'(k+1)Bu(k)] = 0$$

$$\frac{1}{2} [Ru(k) + R'u(k)] + [B'\lambda(k+1)] = 0$$

$$\frac{\partial}{\partial X} (X'AX) = AX + A'X$$

$$\frac{\partial}{\partial Y} (X'AY) = A'X$$

$$\frac{\partial}{\partial Y} (Y'AX) = AX$$

As R being symmetric so $R = R'$

$$\frac{1}{2} [Ru(k) + Ru(k)] + [B'\lambda(k+1)] = 0$$

$$[Ru(k)] + [B'\lambda(k+1)] = 0$$

$$[Ru(k)] = -[B'\lambda(k+1)]$$

Multiplying both sides by R^{-1}

$$[RR^{-1}u(k)] = -[R^{-1}B'\lambda(k+1)]$$

From which we have open-loop optimal control as a function of co-state in the following form:

$$u^*(k) = -[R^{-1}B'\lambda^*(k+1)] \quad (18)$$

Since the second partial of \mathcal{H} in equation (13) with respect to $u^*(k)$ is just R and R is chosen to be positive definite (ensures invertibility) hence it will minimize the cost functional [62].

Inserting the optimal control value in state and co-state equation yields:

$$X^*(k+1) = AX^*(k) - BR^{-1}B'\lambda^*(k+1)$$

$$X^*(k+1) = AX^*(k) - E\lambda^*(k+1) \quad (19)$$

$$\lambda^*(k) = VX^*(k) + A'\lambda^*(k+1) - WZ(k)$$

Combining the state and co-state equations, we obtain the Hamiltonian canonical system as:

$$\begin{bmatrix} X^*(k+1) \\ \lambda^*(k) \end{bmatrix} = \begin{bmatrix} A & -E \\ V & A' \end{bmatrix} \begin{bmatrix} X^*(k) \\ \lambda^*(k+1) \end{bmatrix} + \begin{bmatrix} 0 \\ -W \end{bmatrix} Z(k) \quad (20)$$

The state and co-state system is not symmetrical in the sense that $X^*(k+1)$ and $\lambda^*(k)$ are related in terms of $X^*(k)$ and $\lambda^*(k+1)$ and also non-homogenous due $Z(k)$ the forcing function.

The boundary conditions for these state and co-state equations are given by initial condition on the state as:

$$X(k_0) = 0$$

After applying Euler-Lagrange equation to the Lagrangian, generalized boundary condition, at the optimal condition in terms of Hamiltonian is

$$\left[\mathcal{H}^* + \left(\frac{\partial S(X^*(k), k)}{\partial k} \right) \right]_{k_f} \delta k_f + \left[\left(\frac{\partial S(X^*(k), k)}{\partial X^*(k)} \right) - \lambda^*(k) \right]_{k_f}' \delta X(k_f) = 0$$

For free final state system (in which k_f is fixed and state $X(k_f)$ free) δk_f becomes zero, the final boundary condition on the co-state is given by:

$$\left[-\lambda^*(k) + \left(\frac{\partial S(X^*(k), k)}{\partial X^*(k)} \right) \right]_{k_f}' \delta X(k_f) = 0$$

where, S equals the entire terminal cost term in the cost functional (equation 13). Here, for the present system in which $X(k_f)$ is not specified, $\delta X(k_f)$ becomes arbitrary. Hence the co-efficient of $\delta X(k_f)$ becomes zero, that is:

$$\left[-\lambda(k) + \left(\frac{\partial S(X(k), k)}{\partial X(k)} \right) \right]_{k_f} = 0$$

$$\lambda(k_f) = \left(\frac{\partial S(X(k_f), k_f)}{\partial X(k_f)} \right) = \frac{\partial \left[\frac{1}{2} e'(k_f) F e(k_f) \right]}{\partial X(k_f)}$$

$$\begin{aligned}
&= \frac{\partial}{\partial X(k_f)} \left\{ \frac{1}{2} [CX(k_f) - Z(k_f)]' F [CX(k_f) - Z(k_f)] \right\} \\
&= \\
&\frac{\partial}{\partial X(k_f)} \left\{ \frac{1}{2} [X'(k_f)C'FCX(k_f) - X'(k_f)C'FZ(k_f) - Z'(k_f)FCX(k_f) + Z'(k_f)FZ(k_f)] \right\} \\
&= \frac{1}{2} [C'FCX(k_f) + C'FCX(k_f) - C'FZ(k_f) - C'F'Z(k_f)]
\end{aligned}$$

As $F' = F$ being symmetric:

$$\lambda(k_f) = C'FCX(k_f) - C'FZ(k_f) \quad (21)$$

The state and co-state system at (equation 20) along with the initial condition $X(k_0) = 0$ on the state and the final condition at (equation 21) on the co-state becomes a two point boundary value problem (TPBVP). The state $X^*(k)$ is solved forward starting from initial condition $X(k_0)$ and co-state $\lambda^*(k)$ is solved backwards starting from its final condition $\lambda(k_f)$ given by (equation 21) [62].

Boundary condition (equation 21) and solution of the system (equation 20) indicate that state and co-state are linearly related:

$$\lambda^*(k) = P(k)X^*(k) - g(k) \quad (22)$$

Where, $P(k)$ is $n \times n$ matrix and $g(k)$ is $n \times 1$ vector, and are yet to be determined to satisfy the canonical system (equation 20)

$$\lambda^*(k+1) = P(k+1)X^*(k+1) - g(k+1) \quad (23)$$

Putting $\lambda^*(k+1)$ in the state equation (19):

$$X^*(k+1) = AX^*(k) - E[P(k+1)X^*(k+1) - g(k+1)]$$

$$X^*(k+1) = AX^*(k) - EP(k+1)X^*(k+1) + Eg(k+1)$$

Solving it for $X^*(k+1)$:

$$X^*(k+1) + EP(k+1)X^*(k+1) = AX^*(k) + Eg(k+1)$$

$$X^*(k+1)[I + EP(k+1)] = AX^*(k) + Eg(k+1)$$

$$X^*(k+1) = [I + EP(k+1)]^{-1}[AX^*(k) + Eg(k+1)] \quad (24)$$

Now using equation (22), (23) and (24) in the co-state equation:

$$\lambda^*(k) = VX^*(k) + A'\lambda^*(k+1) - WZ(k)$$

$$P(k)X^*(k) - g(k) = VX^*(k) + A'[P(k+1)X^*(k+1) - g(k+1)] - WZ(k)$$

$$P(k)X^*(k) - g(k) = VX^*(k) + A'P(k+1)[I + EP(k+1)]^{-1}[AX^*(k) + Eg(k+1)] - A'g(k+1) - WZ(k)$$

$$-P(k)X^*(k) + g(k) + VX^*(k) + A'P(k+1)[I + EP(k+1)]^{-1}AX^*(k) + A'P(k+1)[I + EP(k+1)]^{-1}Eg(k+1) - A'g(k+1) - WZ(k) = 0$$

$$\{-P(k) + A'P(k+1)[I + EP(k+1)]^{-1}A + V\}X(k) + \{g(k) + A'P(k+1)[I + EP(k+1)]^{-1}Eg(k+1) - A'g(k+1) - WZ(k)\} = 0$$

This equation must hold good for all values of $X^*(k)$ which means, co-efficient of $X(k)$ and other terms must be zero which gives:

$$-P(k) + A'P(k+1)[I + EP(k+1)]^{-1}A + V = 0$$

$$P(k) = A'P(k+1)[I + EP(k+1)]^{-1}A + V$$

$$P(k) = A'[P^{-1}(k+1) + E]^{-1}A + V \text{ (25) And,}$$

$$g(k) + A'P(k+1)[I + EP(k+1)]^{-1}Eg(k+1) - A'g(k+1) - WZ(k) = 0$$

$$g(k) = -A'[P^{-1}(k+1) + E]^{-1}Eg(k+1) + A'g(k+1) + WZ(k)$$

$$g(k) = A'\{I - [P^{-1}(k+1) + E]^{-1}E\}g(k+1) + WZ(k)$$

$$g(k) = \{A' - A'P(k+1)[I + EP(k+1)]^{-1}E\}g(k+1) + WZ(k) \quad (26)$$

To obtain the boundary conditions for equation (25) and (26), comparison of equation (21) and (22) yields:

$$P(k_f) = C'FC \quad (27)$$

$$g(k_f) = C'FZ(k_f) \quad (28)$$

Equation (25) is a non-linear matrix difference Riccati equation (DRE) which is solved backwards using the final condition given by equation (27) and linear vector difference equation (equation 26) is solved backwards using final condition given by equation (28) [62,64,65]. Once solutions are obtained offline, equation (22) relating co-state in terms of state at final time, is used in the control equation (18) to get close-loop optimal control as a function of state in the following form:

$$u^*(k) = -R^{-1}B'[P(k+1)X^*(k+1) - g(k+1)]$$

$$u^*(k) = -R^{-1}B'P(k+1)[AX^*(k) + Bu^*(k)] + R^{-1}B'g(k+1)$$

Multiplying by R :

$$R u^*(k) = -R^{-1}B'P(k+1)AX^*(k)R - RR^{-1}B'P(k+1)Bu^*(k) + RR^{-1}B'g(k+1)$$

$$R u^*(k) + B'P(k+1)Bu^*(k) = -B'P(k+1)AX^*(k) + B'g(k+1)$$

$$u^*(k)[R + B'P(k+1)B] = -B'P(k+1)AX^*(k) + B'g(k+1)$$

Optimal feed rate which will produce thrust force and torque as given in reference trajectory during drilling in composite laminate is given as [60]:

$$u^*(k) = -L_b(k)X^*(k) + L_f(k)g(k+1)$$

where, $L_b(k)$ is feedback gain and $L_f(k)$ is feed-forward gain given as:

$$L_b(k) = [R + B'P(k+1)B]^{-1}B'P(k+1)A$$

$$L_f(k) = [R + B'P(k+1)B]^{-1}B'$$

And optimal states of thrust force and torque trajectory as given by optimal controller at optimal feed-rate are given as:

$$X^*(k+1) = [A - BL_b(k)]X(k) + BL_f(k)g(k+1)$$

CONCLUSION

The following conclusions can be drawn from the presented optimal controller:

- a) Optimal controller can track both thrust force and torque at the same time by assigning relative weightage to corresponding element of the error weighted matrix 'Q'. This is advantage over the conventional PID controller where only one parameter can be tracked at a time.
- b) By defining a reference thrust force and/or torque trajectory 'Z', optimal controller can track the references by minimizing error 'e'.
- c) Delamination free holes can be drilled using the optimal controller by giving delamination free thrust force and/or torque trajectories as reference input.

REFERENCES

- [1] Tsao CC, Chiu YC. Evaluation of drilling parameters on thrust force in drilling carbon fiber reinforced plastic (CFRP) composite laminates using compound core-special drills. *International Journal of Machine Tools and Manufacture* 2011; 51: 740-744.
- [2] Singh AP, Sharma M, Singh I. Drilling of fiber reinforced plastic composites: A review. *Journal of Manufacturing Technology Today* 2008; 7(6): 24-30.
- [3] Abrao AM, Faria PE, Rubio JCC, Reis P, Davim JP. Drilling of fiber reinforced plastics: A review. *Journal of Materials Processing Technology* 2007; 186(1-3): 1-7.

-
- [4] Hocheng H, Tsao CC. The path towards delamination-free drilling of composite materials. *Journal of Materials Processing Technology* 2005; 167: 251-264.
 - [5] Shyha I, Soo SL, Aspinwall D, Bradley S. Effect of laminate configuration and feed rate on cutting performance when drilling holes in carbon fibre reinforced plastic composites. *Journal of Materials Processing Technology* 2010; 210: 1023-1034.
 - [6] Singh I, Bhatnagar N, Viswanath P. Drilling of uni-directional glass fiber reinforced plastics: Experimental and finite element study. *Materials and Design* 2008; 29(2): 546-553.
 - [7] Hocheng H, Dharan CKH. Delamination during drilling in composite laminates. *Transactions of the ASME Journal of Engineering for Industry* 1990; 112: 236-239.
 - [8] Hocheng H, Tsao CC. Comprehensive analysis of delamination in drilling of composite materials with various drill bits. *Journal of Materials Processing Technology* 2003; 140: 335-339.
 - [9] Davim JP (Ed.). Drilling of composite materials. NOVA Publishers, New York, 2009.
 - [10] Singh AP, Sharma M, Singh I. A review of modelling and control during drilling of fiber reinforced plastic composites. *Composites Part B: Engineering* 2013; 47: 118-125.
 - [11] Bhattacharyya D, Horrigan DPW. A study of drilling in Kevlar composites. *Composites Science and Technology* 1998; 58: 267-283.
 - [12] Davim JP (Ed.). Machining composite materials. ISTE-Wiley, London, 2009.
 - [13] Davim JP, Rubio JC, Abrao AM, A novel approach based on digital image analysis to evaluate the delamination factor after drilling composite laminates, *Composites Science Technology* 2007; 67: 1939-1945.
 - [14] Davim JP, Reis P. Drilling carbon fiber reinforced plastics manufactured by autoclave-experimental and statistical study. *Materials and Design* 2003; 24(5): 315-324.
 - [15] Hough CL, Lednicky TE, Griswold N. Establishing criteria for a computerized vision inspection of holes drilled in carbon fiber composites. *Journal of Testing and Evaluation* 1988; 16(2): 139-145.
 - [16] Davim JP, Reis P. Study of delamination in drilling carbon fiber reinforced plastics (CFRP) using design experiments. *Composite Structures* 2003; 59: 481-487.
 - [17] Durao LMP, De Moura MFSF, Marques AT. Numerical simulation of the drilling process on carbon/epoxy composite laminates. *Composites Part-A: Applied Science and Manufacturing* 2006; 37: 1325-1333.
 - [18] Khashaba UA. Delamination in drilling GFR-thermoset composites. *Composite Structures* 2004; 63: 313-327.
 - [19] Karnik SR, Gaitonde VN, Rubio JC, Correia AE, Abrao AM, Davim JP. Delamination analysis in high speed drilling of carbon fiber reinforced plastics (CFRP) using artificial neural network model. *Materials and Design* 2008; 29: 1768-1776.
 - [20] Konig W, Grab P. Quality definition and assessment in drilling of fiber reinforced thermosets. *CIRP Annals-Manufacturing Technology* 1989; 38(1): 119-124.
 - [21] Bhatnagar N, Naik NK, Ramakrishnan N. Experimental investigations of drilling of CFRP composites. *Materials and Manufacturing Processes* 1993; 8(6): 683-701.
 - [22] Gaitonde VN, Karnik SR, Rubio JC, Correia AE, Abrao AM, Davim JP. Analysis of parametric influence on delamination in high-speed drilling of carbon fiber reinforced plastic composites. *Journal of Materials Processing Technology* 2008; 203: 431-438.

-
- [23] Caprino G, Diterlizzi A, Tagliaferri V. Damage in drilling glass fiber reinforced plastics, advancing with Composites. In: International Conference on Composite Materials, Milan Italy, 1988, p. 493-503.
- [24] Tagliaferri V, Caprino G, Diterlizzi A. Effect of drilling parameters on the finish and mechanical properties of GFRP composites. *International Journal of Machine Tool and Manufacturing* 1990; 30 (1): 77-84.
- [25] Caprino G, Tagliaferri V. Damage development in drilling glass fiber reinforced plastics. *International Journal of Machine Tools and Manufacture* 1995; 35(6): 817-829.
- [26] Abrao AM, Rubio JC, Faria PE, Davim JP. The effect of cutting tool geometry on thrust force and delamination when drilling glass fibre reinforced plastic composite. *Materials and Design* 2008; 29: 508-513.
- [27] Davim JP, Reis P, António CC. Drilling fiber reinforced plastics (FRPs) manufactured by hand lay-up: Influence of matrix (Viapal VUP 9731 and ATLAC 382-05). *Journal of Materials Processing Technology* 2004; 155-156: 1828-1833.
- [28] Capello E, Tagliaferri V. Drilling damage of GFRP and residual mechanical behavior-Part I: Drilling damage generation. *Journal of Composites, Technology and Research* 2001; 23(2): 122-130.
- [29] Capello E, Tagliaferri V. Drilling damage of GFRP and residual mechanical behavior-Part II: Static and cyclic bearing loads. *Journal of Composites, Technology and Research* 2001; 23(2): 131-137.
- [30] Davim JP, Reis P, Antonio CC. Experimental study of drilling glass fiber reinforced plastics (GFRP) manufactured by hand lay-up. *Composites Science and Technology* 2004; 64: 289-297.
- [31] Tsao CC, Hocheng H. Taguchi analysis of delamination associated with various drill bits in drilling of composite material. *International Journal of Machine Tools and Manufacture* 2004; 44: 1085-1090.
- [32] Ramulu M, Branson T, Kim D. A study on the drilling of composite and titanium stacks. *Composite Structures* 2001; 54: 67-77.
- [33] Rubio JC, Abrao AM, Faria P, Correia AE, Davim JP. Effects of high speed in the drilling of glass fibre reinforced plastic: Evaluation of the delamination factor. *International Journal of Machine Tools and Manufacture* 2008; 48: 715-720.
- [34] Singh I, Bhatnagar N. Drilling induced damage in uni-directional glass fiber reinforced plastic (UD-GFRP) composite laminates. *International Journal of Advanced Manufacturing Technology* 2006; 27: 877-882.
- [35] Singh I, Bhatnagar N. Drilling of uni-directional glass fiber reinforced plastic (UD-GFRP) composite laminates. *International Journal of Advanced Manufacturing Technology* 2006; 27: 870-876.
- [36] Lachaud F, Piquet R, Collombet F, Surcin L. Drilling of composite structures. *Composite Structures* 2001; 52: 511-516.
- [37] Zhang L-B, Wang L-J, Liu X-Y. A mechanical model for predicting critical thrust forces in drilling composite laminates. *Proceedings of the Institution of Mechanical Engineers, Part B: Journal of Engineering Manufacture* 2001; 215(2): 135-146.
- [38] Stone R, Krishanmurthy K. A neural network thrust force controller to minimize delamination during drilling of graphite-epoxy laminates. *International Journal of Machine Tools and Manufacture* 1996; 36(9): 985-1003.

-
- [39] Kawaji S, Arao M, Chen Y. Thrust force control of drilling system using neural network. In: IEEE/ASME International conference on Advanced Intelligent Mechatronics Proceedings, Corno, Italy; 2001, p. 476-481.
- [40] Kim M, Matsunga N, Kawaji S. Estimation of cutting torque in drilling system based on flexible neural network. In: *IEEE Proceedings of the International Joint Conference on Neural Networks*, 20-24 July 2003; 1: 642-647.
- [41] Mishra R, Malik J, Singh I. Prediction of drilling-induced damage in unidirectional glass-fibre-reinforced plastic laminates using an artificial neural network. *Proceedings of the Institution of Mechanical Engineers Part B: Journal of Engineering Manufacture* 2010; 224(5): 733-738.
- [42] Chung B-M, Tomizuka M. Fuzzy logic modeling & control for drilling of composite laminates. In: IEEE International Fuzzy Systems Conference, Melbourne, Australia, 2001, p. 509-512.
- [43] Mishra R, Malik J, Singh I, Davim JP. Neural network approach for estimating the residual tensile strength after drilling in uni-directional glass fiber reinforced plastic laminates. *Materials and Design* 2010; 31(6): 2790-2795.
- [44] Bhatnagar N, Jalutharia MK, Singh I. Prediction of thrust force and torque when drilling composite materials. *International Journal of Materials and Product Technology* 2008; 32(2/3): 213-225.
- [45] Kim JB, Lee S-Jo, Park Y-Pil. Stable and efficient drilling process by active control of the thrust force. *Mechanical Systems and Signal Processing* 1994; 8(5): 585-595.
- [46] Haber-Haber R, Haber R, Schmittiel M, del Toro RM. A classic solution for the control of a high-performance drilling process. *International Journal of Machine Tools and Manufacture* 2007; 47: 2290-2297.
- [47] del Toro RM, Schmittiel M, Haber-Guerra RE, Haber-Haber R. System identification of the high performance drilling process for network-based control. In: Proceedings of the ASME 2007 International Design Engineering Technical Conferences and Computers and Information in Engineering Conference, Las Vegas, Nevada, USA, 2007, p. 827-834.
- [48] Sheng Y, Tomizuka M, Ozaki M. Dynamic modeling and adaptive predictive control (APC) of drilling of composite materials. In: Proceedings of the American Control Conference, Chicago, Illinois, 2000, p. 2568-2572.
- [49] Kawaji S, Suenaga Y. Control of cutting torque in the drilling process using disturbance observer. In: Proceedings of American Control Conference, Seattle, Washington, USA, 1995, p. 723-728.
- [50] Furness RJ, Tsao T-C, Rankin JS-II, Muth MJ, Manes KW. Torque control for a form tool drilling operation. *IEEE Transactions on Control System Technology* 1999; 7(1): 22-30.
- [51] Oh YT, Kim GD, Chu Chong N. Design of a drilling torque controller for a machining center. *International Journal of Advanced Manufacturing Technology* 2003; 22: 329-335.
- [52] Singh AP, Sharma M. Modelling of thrust force during drilling of fibre reinforced plastic composites. *Procedia Engineering* 2013; 51: 630-636.
- [53] Singh AP, Sharma M. Modeling and PID control of thrust force during drilling in composite laminates. In: Proceedings of Recent Advances in Engineering and Computational Sciences, Panjab University, Chandigarh, India, 2014, p. 1-5.

- [54] Singh AP, Sharma M, Singh I. PID control of torque during drilling in GFRP Laminates. *Multidiscipline Modeling in Materials and Structures* (Accepted).
- [55] Dutton K, Thompson S, Barraclough B. *The art of control engineering*. Addison-Wesley, Boston, 1997.
- [56] Astrom KJ, Wittenmark B. *Adaptive control*. Addison-Wesley, Boston, 1995.
- [57] Sanchez M, Rodellar J. *Adaptive predictive control: From the concepts to plant optimization*. Prentice Hall PTR, 1996.
- [58] Shaw MC, Oxford Jr. CJ. On the drilling of metals: Part 2-The torque and thrust in drilling. *Transactions of ASME* 1957; 79: 139-148.
- [59] Dharan CKH, Won MS. Machining parameters for an intelligent machining system for composite laminates. *International Journal of Machine Tools and Manufacture* 2000; 40: 415-426.
- [60] Singh AP, Sharma M, Singh I. Optimal control during drilling in GFRP composite laminates (Communicated).
- [61] Rockafellar RT. Conjugate convex functions in optimal control and the calculus of variations. *Journal of Mathematical Analysis and Applications* 1970; 32(1): 174-222.
- [62] Naidu DS. *Optimal control systems*. Boca Raton Florida, CRC Press, 2003.
- [63] Sideris A, Rodriguez LA. A Riccati approach for constrained linear quadratic optimal control. *International Journal of Control* 2011; 84(2): 370-380.
- [64] Kalman RE. The theory of optimal control and calculus of variations. In R Bellman (Ed.), *Mathematical optimization techniques*, University of California Press, Berkeley, CA, 1963, p. 309-331.
- [65] Vaughan DR. A nonrecursive algebraic solution for the discrete Riccati equation. *IEEE Transactions Automatic Control* 1970; AC-15: 597-599.

Chapter 5

**QUALITY IN THE MACHINING:
CHARACTERISTICS AND TECHNIQUES
TO OBTAIN GOOD RESULTS**

***C. H. Lauro^{1,*}, L. C. Brandão², S. M. Ribeiro Filho²
and J. P. Davim¹***

¹University of Aveiro, Portugal

²Federal University of São João del Rei, Brazil

ABSTRACT

To obtain great results in the machining of new materials, the manufacture industry required development of tools and techniques. Enhanced knowledge of these tools and techniques can offer a decreasing of cost, time, and risk to operator. This chapter debates the quality of the machined surface, the aspects and characteristics to analyse the desired quality. Furthermore, it presents some developments (tool and techniques) applied in the machining process to obtain the quality of surface.

Keywords: Machining; Machinability; Surface integrity; Burr, Damages, Tools

INTRODUCTION

The material industry has developed increasingly specific materials to satisfy other industries, i.e., material that can present low corrosion, or low weight, or high tenacity and others properties. An example is the automobile industry that aims the decrease the weight of components to offer car more efficient, mainly because fuel consum is reduced. Thus, new materials (alloys, composites, ceramics and others) arise each day. However, these materials require great commitments of material industry because characteristics, as machinability or conformability, can be affected by some their constituents.

* E-mail: carlos.lauro@ua.pt.

Although the machinability or conformability can be saved in many cases, there are cases that these properties are reduced that can complicate obtaining complex shapes, for example. This fact requires great development by manufacture industry that need develop techniques and/or tool to transform the crude material to finished product. The parameters definition is also studied to make the processes more efficiently and safe, such as, in the machining of composite or ceramic materials that can fracture. To instance this context, the processes as hand lay-up or filament winding are used to fabricate Carbon Fiber-Reinforced Plastic (CFRP) composites, but is applied the machining at final production stage to obtain the finished components (Gaitonde et al., 2011).

The machining process that is a process widely used, techniques are studied to obtain the smallest roughness surface or to avoid metallurgical changes. In the literature is possible find many High Speed Machining (HSM) studies that have the objectives previously cited. This chapter debates about the important aspects to obtain great results in the machining processes. There is a remarkable that the machinability is must important aspect; however, some technique can help to obtain the great results. Furthermore, the care that should observed in the machining, mainly in the composite material.

MACHINABILITY

The machinability is a quality or propriety of material that can often be measured in terms of the numbers of components produced per hour. The costs of machining the component or the quality of the finish are critical on a surface quality. However, a material may have good machinability by one criterion, but poor machinability by another, because a different type of operation is being carried out - turning versus milling - or when the tool material is changed. The machinability may be assessed by one or more of the criteria, such as, Tool life; Limiting rate of metal removal; Cutting forces; Surface finish and Chip shape (Trent and Wright, 2000).

Sanchez et al. (2014) affirmed that the difficult-to-machine materials can present a relation between mechanical resistance and temperature that causes a moderated decreasing of the resistance in low temperatures, but a remarkable reduction with the progressive raising of temperature. The understanding of the temperature in the metal cutting is important because tool flank wear is strongly influenced by the interactions between cutting tool and workpiece in the form of contact stress and cutting temperature (Isik, 2007). According to Trent and Wright (2000), the temperature of the body of the chip is not greatly influenced by the cutting speed, in most operations when cutting steel the chip body reaches a temperature in the range 200 to 350° C. An indicator of the temperature of steel chips is their colour:

- When steel is machined with high speed without the use of a coolant, the chip is seen to change colour, usually to a brown or blue, a few seconds after leaving the tool, that indicate a temperature on the order of 250 to 350°C;
- With very low speeds the chip does not change colour, indicating a lower temperature, usually associated with a built-up edge;
- When cutting fully hardened steel or certain nickel alloys at high speed, chips have been seen to leave the tool red hot at temperature over 650°C

In turning operation three force components exist: the Cutting Force (force occurs along the direction of cutting speed, tangential to turned surface), Feed Force (force occurs along the direction of the tool feed whereas radial force acts perpendicular to the turned surface) and Radial Force, among these forces, the Cutting force and feed force play a major role in determining the machinability of any material (Thakur et al. 2009).

Jaffery and Mativenga (2008) cited that titanium alloys have high strength, corrosion resistance, fatigue endurance, and biocompatibility. The authors comment that machining is highly expensive because they have poor machinability. Thus, the optimization of the parameters of influence is of greater significance for the industry. In their paper, they developed a wear map for turning the Ti-6Al-4V titanium alloy.

Chinchanikar and Choudhury (2013) studied the machinability of AISI 4340 steel at three levels of hardness (35, 45 and 55 HR_C) using cemented carbide inserts coated with single-layer TiAlN and CVD coated multi-layer and analysed the tool life, surface roughness and cutting forces. They observed that the cutting forces varied almost linearly with the feed rate and depth of cut. However, they showed a different trend with cutting speed, they decreased with the increase in cutting speed but almost unaltered in higher cutting speed range.

Arrazola et al. (2009a) compared the machinability of two kinds of titanium alloys. In the maximum cutting speed, the machinability of Ti-555.3 was approximately 56% of Ti-6Al-4V. In the specific cutting force (K_c) and the specific feed force (K_f) aspects, a cutting speed of 50 m/min provided 2300 N·mm⁻² and 1270 N·mm⁻² for Ti-6Al-4V to 2810 N·mm⁻² and 1950 N·mm⁻² for the Ti555.3 alloy, respectively.

To analyse the machinability of Ti-6Al-4V and Ti54M titanium alloy, Armendia et al. (2010) used as criteria the measurements of flank and crater wear, cutting forces, chip formation and SEM (Scanning Electronic Microscopy). According to the authors, the machinability of Ti54M could be approximately 10 to 15% greater than Ti-6Al-4V. They cited the speed cutting maximum for Ti-6Al-4V is approximately 80 m/min and around 90 m/min for Ti54M.

Arrazola et al. (2009b) investigated the machinability of AISI 4140 Standard and AISI 4140 MECAMAX[®] Plus using three types of tungsten carbide inserts (uncoated, TiN-Al₂O₃-TiCN coated and TiN-Al₂O₃-TiCN coated with chip breaker). They concluded that the temperatures for the AISI 4140 MECAMAX[®] Plus were less than those for the AISI 4140 Standard. In addition, the temperatures in both coated tools (the coated tool with a chip breaker are less than the coated) were less than those in the uncoated tool.

In the machinability study of austempered ductile iron (G2 and G3), Carvalho et al. (2013) analysed the chip, surface roughness, cutting forces and tool life. The authors observed that the higher the feed rate showed a tendency to form thicker chips is for the cutting speed and insert selected. The cutting parameters used in finishing and roughing operations generated segmented chips and the round end of chips observed for depths of cut greater than 1 mm can be explained by the existence of the nose radius of the inserts.

Sayuti et al. (2012) studied the decreasing of the friction in the tool-chip interface in milling of AL-2017-T4 (118 HV) aluminium alloy using cutting speed of 75.408 m/min, feed rates of 100 mm/min and depths of 1.0 mm. They applied different lubrication modes (0.0, 0.5, 1.0, and 1.5% wt of carbon onion mixed with Alumicut oil), followed by sonification using Sono Bright ultrasonic vibration to suspend the particles homogeneously in the mixture. They observed that the highest carbon onion concentration (1.5% wt) produces the lowest

cutting force, 21.99%, and best surface quality, 46.32%, when compared with ordinary lubrication oil.

SURFACE INTEGRITY

Surface Integrity (SI) is important to safety critical industries (as aerospace) or critical to the economics of the processes (as forging dies, plastic moulds, and press tools). The influence of each parameter needs to be known, together with interactions, in order to allow at least, a “pseudo-optimisation” of SI. The parameters, tools, and operation selection are very important on the machining (Axinte and Dewes, 2002). The authors cited the Field et al. proposed, whose a ‘minimum’ SI data set involve surface roughness, macrostructure, microstructure, microhardness, residual stress, minimal fatigue, stress corrosion tests and a host of mechanical tests (tensile, stress rupture, creep, fracture toughness, etc.).

The performance of a component is influenced by quality and reliability of the surface produced in terms of topography, metallurgical, and mechanical states of the surface and subsurface layers (Suresh et al., 2013). To obtain a high surface integrity is need a significance control in manufacturing processes, i.e., the effects on engineering properties of workpiece have to be carefully analyzed, (Saini et al., 2012).

In his study about the surface integrity in the turning of Inconel 718, Umbrello (2013) measured the surface roughness (R_a), the surface and subsurface hardness and metallurgy changes. The authors observed that better surface roughness was obtained applying the lower feed and higher speed cutting values, however, the variation in microhardness values was obtained with the lower feed and speed cutting values.

Surface Roughness

Between the many methods to quantify the surface integrity, the surface roughness is a method widely used and considered as the primary indicator of the quality of the surface finish (Ulutan and Özel, 2011). International standards define that surface roughness is deviation from the nominal surface relative to periodic grooves, cracks, and dilapidations (third- and fourth-order), and deviations refer to workpiece material structure (fifth- and sixth-order) (Benardos and Vosniakos, 2003).

Umbrello (2013) highlighted that roughness surface values between 0.10 to 0.20 μm is called “turning replaces grinding” because it produces comparable R_a values with grinding, and a smooth surface with better surface roughness would prevent the initiation of cracks under cyclic loads. Benardos and Vosniakos (2003) cited that the desired surface quality is of great importance for the functional behavior of a part because it is a widely used as quality index mainly in mechanical products. The surface roughness formation mechanism and the numerous uncontrollable factors, that influence it, make almost impossible a straightforward solution. However, the process parameters selection is the most common applied strategy, but it neither guarantees the desired surface finish nor attains high metal removal rates.

According to Piotrowska et al. (2009) the surface roughness is also influenced by several factors, as geometry of the tool, vibrations, the elastic deformations, depth of cut, the feed

rate, the workpiece material, and its hardness. Palani et al. (2013) cited that it is possible to find surface roughness studies that exhibit mathematical models based on direct measurements of certain machining parameters. However, their effectiveness requires large amounts of accurate data gathered under varying machining conditions and/or the use of expensive instrumentation, furthermore, the surface roughness tends to be stochastic and non-stationary.

Upadhyay et al. (2013), the surface roughness prediction model using cutting parameters as input were good enough only for selection of cutting parameters to achieve a desired surface finish, where vibrations/cutting forces were some inputs to serve this purpose. They developed this model using multiple regression method as a function of acceleration amplitudes of vibration in radial, axial and tangential directions. They tested the prediction ability using an Artificial Neural Network (ANN) model using the feed rate, depth of cut, acceleration amplitude of vibration in radial and tangential direction as input parameters and the Levenberg-Marquardt (LM) to train the learning rule. These developed models can be effectively used for in process prediction of surface roughness, which showed average percentage error for ANN model was 4.11% and maximum percentage error was 6.42%.

Hessainia et al. (2013) classified the surface roughness (R_a) modelling techniques into three groups: experimental models; analytical models; and artificial intelligence (AI) based models. They proposed an experimental model through the Response Surface Methodology (RSM) in hard turning of AISI 4140 (56 HR_C), which found a quadratic model of RMS with correlation coefficient of 99.9% and 96.4% for models R_a and R_t respectively.

White Layers

According to Umbrello and Filice (2009), in some machining processes occur changes to the microstructure, few tens micrometers into the subsurface, that affect mechanical properties and quality of the surface called as dark and white layers. The dark layer is a higher thickness (20 - 40 microns) and it is soft and ductile due to the presence of overtempered martensite that is detrimental because it has a significant impact on the magnitude of maximum residual stress and on the location of the compressive residual stress peak. The white layer is disadvantageous to the fatigue life of the part and is concerned with three main theories:

- rapid heating and quenching, which results in sudden microstructural transformation;
- severe plastic deformation, which produces a homogenous structure and/or a very fine grain size microstructure;
- surface reaction with the environment, such as in nitriding processes.

Chou and Evans (1999) identified by classical metallographic methods the white layer phenomenon in hard turned surfaces. They observed that in hard machining, the martensite is a metastable structure that will decompose to ferrite and cementite when heated and the XRD analysis, about 10 mm thick, showed a volume fraction of 33% austenite, an increase of 22% (or double) compared to the bulk material. According to authors, this increase of austenite is probably due to insufficient cooling rate or lack of tempering when the machined surfaces encounter heating (rehardening) and self-quenching during cutting.

Duan et al. (2013) affirmed that the cutting parameters influence the thickness of white layer, i.e., variations of cutting speed, depth of cut, flank wear, and chamfer geometry of tool vary significantly the thickness of white layer. Applying the cutting speeds between 50 and 420 m/min, they observed that the thickness of white layer increases at first with the increase of cutting speed, and after 250 m/min, there is a slight of diminution, due to there ar a influence of cutting speed on the workpiece temperature. For the depth of cut, white layer is getting thicker with the increase of deph of cutting, because it increases the contact area between tool and workpiece, so temperature and stress all increase with the increase of depth of cut. The white layer is more thickness with the increase flank wear, because the heat in the contact area between tool and machined surface accumulates with the increase of flank wear and the rubbing action between flank and machined surface results in large stress and deformation in subsurface. The thickness of white layer increases with the increase of chamfer length, because it is the effect of negative rake angle becomes more and more significant with the increase of chamfer length.

Is possible find in the literature researches developes using Finite Elements Method (FEM). Attanasio et al. (2012) used numeric (2D and 3D) and experimental tests to study the layers formation on the orthogonal hard turning of AISI 52100. They found that the thickness of white and dark layers increases with increasing of tool flank wear and higher cutting speed generates thicker white layers and thinner dark layers. A small feed rate increases the white layers thickness; on the other hand, the high feed rate decreases the dark layer thickness.

Ramesh and Melkote (2008) used the FEM to study the white layer formation in orthogonal machining of AISI 52100 (62 HRC) using the CBN tool. They used a model explicitly incorporates the effects of stress and strain on the transformation temperature, volume expansion and transformation plasticity that showed predicted values and trends of white layer thickness. These effects are in good agreement with the measured values and trends when compared to experimental validation.

Residual Stress

Rossini et al. (2012) define the residual stresses as the stresses that remain into material after manufacture and material processing in the absence of external forces, or thermal gradients, or service loading that leads to inhomogeneous plastic deformation, which can occur by differential plastic flow; or differential cooling rates; or phase transformations with volume changes etc. They can be classified into three types:

- Macro residual stress (a component on a scale larger than the grain size of the material);
- Micro residual stresses (vary on the scale of an individual grain); and
- Micro residual stresses (result of the presence of dislocations and other crystalline defects).

The effects on the residual stress can improve the fatigue life of hard turned that has been investigated by many researchers, as the improvement of fatigue life induced by residual stresses or the influence of cutting edge geometry. Diversity in the results is found in the

literature due to this phenomenon is hard to measure or model, which can be due to different workpiece materials and cutting conditions used as well as the differences in tool parameters (Saini et al., 2012).

Dahlman et al. (2004) studied influence of the cutting parameters in the residual stresses for AISI 52100 (62 HR_C). They observed that the cutting depth does not affect residual stresses; increased feed generates significantly higher compressive stresses; greater negative rake angle gives higher compressive stresses; and compressive stresses are always generated below the surface.

BURR

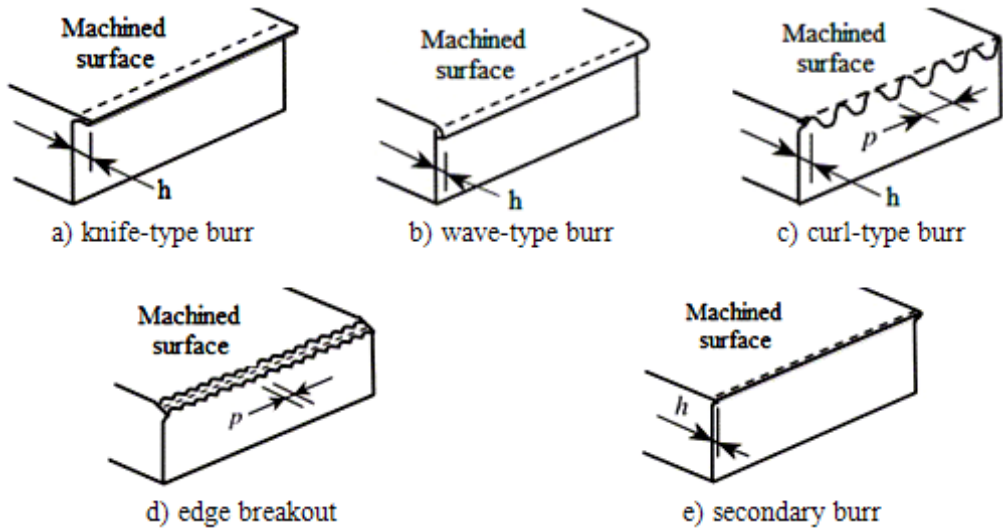
In machining processes is common observed a small portion in the surface machined that was not perfectly cutted that is called of burr. According to Aurich et al. (2009) this phenomena is knowed thousands of years ago, only in 1784, Erasmus Darwin, grandfather of Charles Darwin, called it by burr. They presented some burr definitions, as bellow, but they affirmed that CIRP dictionary do not have a definition of the burr.

- "rough ridge or edge left on metal or other substance after cutting, punching, etc";
- "undesirable or unwanted projections of the material formed as the result of the plastic flow from cutting and shearing operations";
- "the part of a workpiece which is produced through manufacturing processes on an edge or a surface and which lies outside the desired geometry".

According to Souza Júnior et al. (2005), burrs in the milling processes are extremely undesirable because they can happen accident to the operators in the assembly lines, can hinder contacts between surfaces, and the burr removal is an expensive time consuming operation. Thus, the knowledge of the phenomenon of burr formation is of great importance because the milling process can be controlled, particularly the cutting parameters

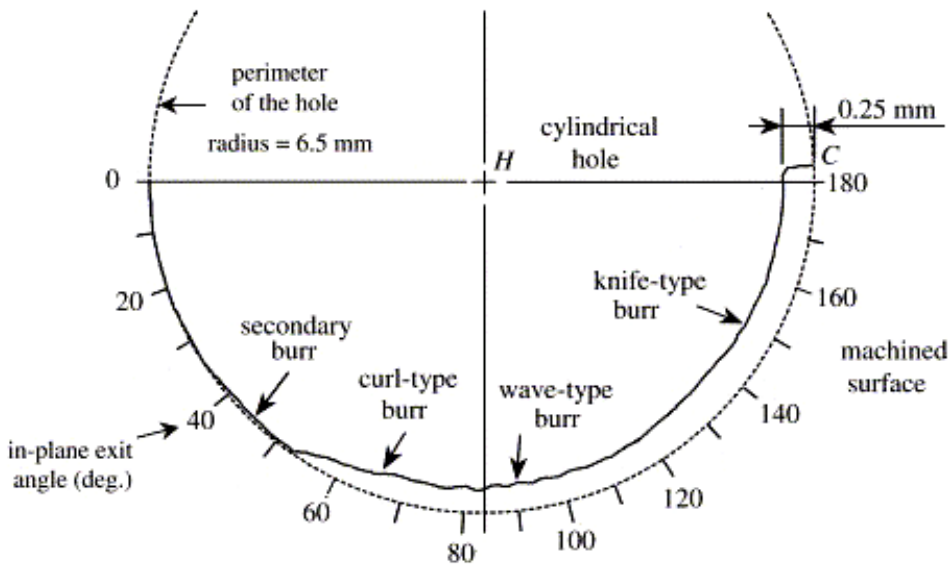
Chern (2006) analysed the of in-plane exit angle (Ψ) influence in the burr of milling of the different kind of aluminum alloys. The in-plane exit angle is defined as the angle in the machining plane between the cutting velocity vector and the edge of the workpiece to be machined. They observed that the variation of in-plane exit angle provided five types of burrs, Figure (1), that can vary the burr height also along the perimeter of the hole, Figure (2).

Wyen et al. (2012) analysed the burr formation in the milling of Ti-6Al-4V titanium alloy with a cutting edge radius (r_n) varying between $06\pm 2\mu\text{m}$ and $50\pm 1\mu\text{m}$. They observed that it increases with the cutting edge radius and is especially pronounced in up milling. Cedergren et al. (2012) studied the burr formation in the interrupted turning of Alloy 718, nickel iron-based superalloy, with two grain size. They observed that for the high grain size happened the burr formation in both feed rates and for the small grain size material happened the burr formation only to higher feed that are associated shear-localized chip edges.



(Adapted from Chern (2006), with permission from Elsevier).

Figure 1. Types of burrs in the milling of aluminium alloys.



(Adapted from Chern (2006), with permission from Elsevier).

Figure 2. Variation of burr size and burr type along edge of cylindrical hole Al 2024-T4, depth of cut=0.25 mm, feed=0.16 mm/tooth.

DAMAGES IN MACHINING OF COMPOSITE MATERIAL

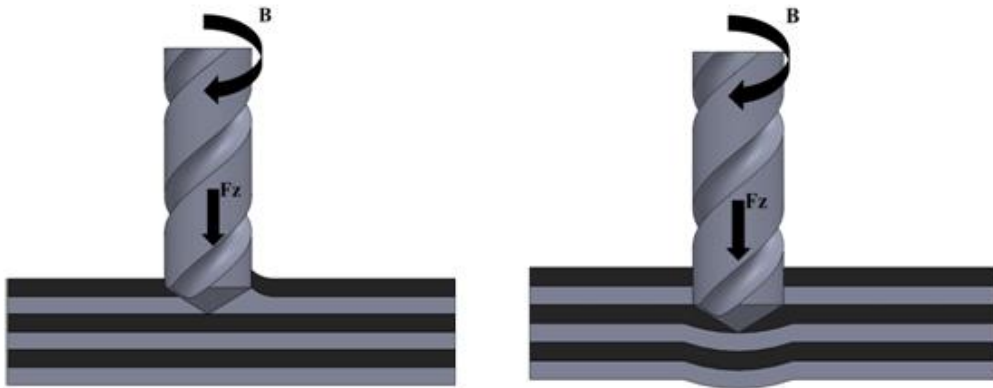
In the literature is easily to find drilling of composite material studies. It is because the carbon fibre composites are used widely in aerospace structures due to high strength-to-weight ratios. These structures contain holes for various purposes that is difficult to achieve

good hole quality. The most widely method to make these holes is the machining method, drilling, that can reduce the strength are delamination, chip-out of fibres/matrix, and degradation of matrix due to overheating (Persson et al. 1997).

According to König and Graß (1989), the the delamination is the separation of the surface layers at the entrance and exit of the tool has to be distinguished from the cracks formation in the inner parts of workpiece. The Figure (3) shows a delamination scheme; (a) a first phase was concerned with delamination at the entrance and (b) a second phase with delamination at the exit during the drilling (Davim and Reis, 2003).

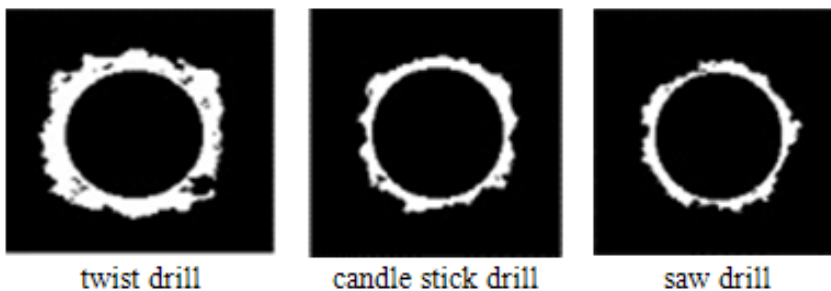
To analyse the delamination, Tsao and Hocheng (2004) used image data into a gray level array, whose the values, 0 (black) to 255(white), corresponding to differences in laminates density, Figure (4). They tested three different type drills (twist drill, candle stick drill and saw drill) and determined the drilling delamination factor (F_d), Eq. (1), by the ratio of the maximum diameter (D_{max}) of the delamination zone to the hole diameter (D), Figure (5). They observed that the candle stick drill and saw drill cause a smaller delamination factor than twist drill.

$$F_d = \frac{D_{max}}{D} \quad (1)$$



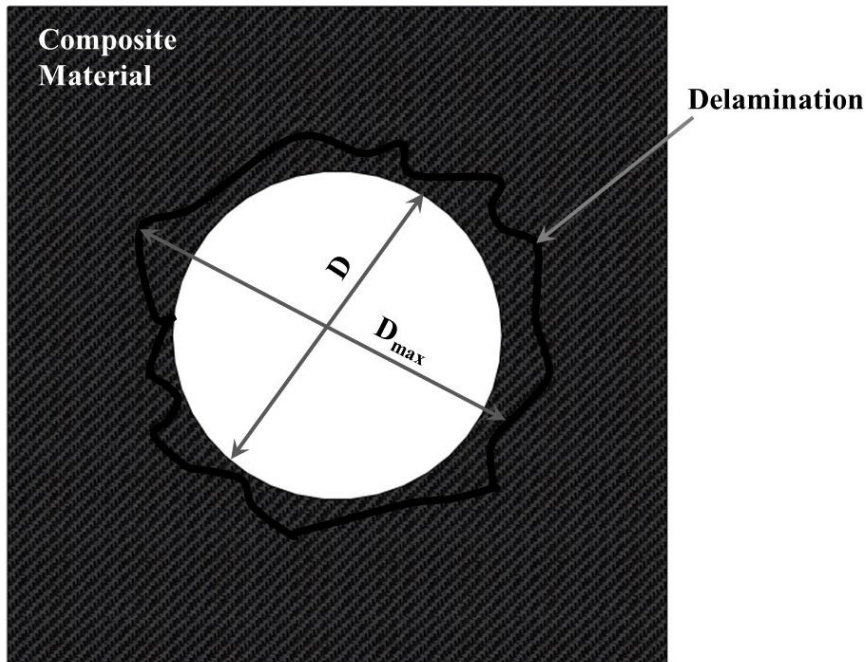
(Adapted from Davim and Reis (2003), with permission from Elsevier).

Figure 3. Delamination in the drilling CFRP composite laminate.



(Adapted from Tsao and Hocheng (2004), with permission from Elsevier).

Figure 4. Ultrasonic scanning of delaminated holes drilled.



(Adapted from Tsao and Hocheng (2004), with permission from Elsevier).

Figure 5. Scheme of the delamination factor.

Gaitonde et al. (2011) studied the minimization of delamination damage in the high-speed drilling of CFRP composites using cemented carbide tools. They analysed the process parameters (spindle speed, feed, and point angle) to obtain the optimal setting (levels) to minimize the delamination. Among the applied parameters values, the combination of higher spindle speed, lower values of feed, and lower point angle resulted in a smaller delamination. It occurred because the high speed generates a less damage due to thermal softening of tool materials; smaller values of point angle reduce the thrust force. The low feed generates a less fracture, as compared to high feed, due to it decreases chatter effects and produce less heat generation.

Hocheng and Tsao (2005) developed a delamination drilling of composite material review. According to authors, a special drill bits and larger feed rate combination can offer holes without delamination damage compared to the twist drill. It occurs due to special drills show different level of the drilling thrust force varying with the feed rate and the feed rate strategy can avoid delamination caused by the thrust in drilling. Furthermore, the step drill and pilot hole reduce of drilling thrust that significantly avoids the delamination and back-up plate prevents the deformations from leading to exit delaminations. They presented also the advantages and disadvantages of non-traditional drilling methods (Waterjet, Ultrasonic, Laser, EDM and vibration-assisted).

The matrix can clog the tool and make further machining impossible and their damage can occur due to drilling thrust or torque is too high, friction and the flux heat, which that can cause the matrix to soften (Persson et al., 1997) . Furthermore, the fibres did not cut, fuzzing, are considered a machining error that can be corrected by further machining (König and Graß, 1989). When the fibres were not cut, the tensile and compressive forces caused by rotation of

the tool cause the fibres and matrix to be torn out of the hole surface, resulting in a rough surface. It happens commonly in laminates with fibres predominantly in one direction (Persson et al., 1997).

Ferreira et al. (2001) studied the turning of CFRC composite (finishing and Rough operations) using diamond (PCD), cubic boron nitride (CBN), and different cemented carbides tools. They cited a difference between the cutting mechanism of CFRC and conventional materials due to anisotropic structure. The fibres orientation and fibre/matrix composition and fabrication methods influence the cutting. They observed that the choice of the best tool is important because the CFRC is abrasive and the kind of machining operation it's a necessary oxidation process control. The diamond tool is best option for the finishing operation and the coated cemented carbide for rough operation.

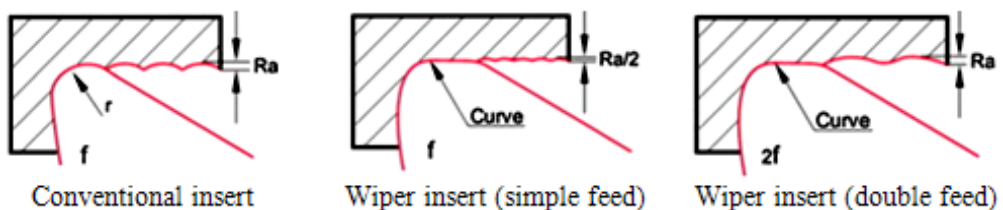
TOOLS AND TECHNIQUES

According to Fallböhmer et al. (2000), there is an increase development of new cutting tool materials, improved design of cutting tool inserts, new strategies, and improvement of cutting process conditions.

Wiper

The Wiper Tool is widely applied due to it shows best surface roughness than conventional tool. The use of this tool can provide same surface finish using double the conventional values of feed rates that can provide new levels of productivity in the hardness turning, such as, a reduce machining time about 90% for specific type of cutting (Grzesik and Wanat, 2006). The wiper geometry is a tool used in machining technology and designed for finish cutting that uses special geometry multi-radii to obtain it, Figure (6). The wiper inserts have a lot of area in contact with the workpiece, so they exert a lot of force on the workpiece (Correia and Davim, 2011). In the Table (1) is exhibited same values of surface roughness (R_a) found in the literature for conventional and wiper inserts.

Correia and Davim (2011) observed that wiper inserts used in the finish, a low feed rate provided a similar surface roughness and high feed rate provided low values of surface roughness when compared with conventional inserts. They affirmed also that applying a high feed rate, 0.25 mm/rev, can obtain surface quality in workpiece of mechanics precision without cylindrical grinding operations, values of R_a of less than 0.8 μm .



(Adapted from Elbah et al. (2013), with permission from Elsevier).

Figure 6. Comparison of the surface roughness in the cutting with conventional and wiper inserts.

Table 1. Comparison of surface roughness (R_a) values between conventional and wiper inserts

Researchers	Material	Cutting Speed (m/min)	Feed (mm/rev)	R_a (Conv.)	R_a (Wiper)
Elbah et al. (2013)	AISI 4140 (60 HRC)	80, 115, 150	0.08, 0.11, 0.14	0.64 – 1.38	0.22 – 0.45
Gaitonde et al. (2009)	AISI D2 (59/61HRC)	80	0.1	0.39 – 1.94	0.30 – 0.88
Grzesik and Wanat (2006)	AISI 5140 (60±1 HRC)	100	0.04 – 0.4	0.24 – 5.47	
			0.1 – 0.8		0.25 6.03

In the turning of AISI 4140 steel with an initial grain size of about 120 μm and hardness of 60 HR_C, Elbah et al. (2013) used wiper and conventional inserts. They observed that a flank wear (VB) of 0.3mm provided an roughness surface (R_a) for wiper insert (not exceed 0.88 μm) less than conventional insert (0.99 μm). Gaitonde et al. (2009) used three kinds of ceramic inserts in the turning of AISI D2 (59-61 HR_C), which were analysed the machining force (F_m), power (P), specific cutting force (K_s), surface roughness (R_a) and tool wear. They observed that wiper insert performs better surface roughness and tool wear, and conventional insert showed lower values of the machining force, power and specific cutting force.

Guddat et al. (2011) used wiper and conventional inserts, new and worn, in the turning of AISI 52100 (60HR_C). In the analysis of 3D-topography of surfaces, they observed that the worn wiper insert provided S_a (94nm) and S_z (771nm) values lower than new conventional insert, S_a (120nm) and S_z (818nm). The analysis of residual stress, the wiper insert induces higher compressive stresses than the conventional insert at all settings.

In the milling of GH 190 UNI gray cast iron (200 HV) with two different wiper insert (ceramics and PCBN), Souza Júnior et al. (2005) applied constant spindle speed of 1270 rpm ($v_c=1000$ m/min), feed per tooth (f_z) of 0.06 mm/tooth, and depth of cut (doc) of 0.3 mm. In the analysis of the burr height, they observed an increase of burr height as a function of the number components machined, values between 0 and 0.24mm. The ceramic cutting inserts tend to produce higher burrs, which the higher wear is responsible for these results.

Ball Nose and Complex Geometric

The complex machining is used in die and mold industry widely, where the surface finish is an important criterion. In the machining of free form surfaces, ball nose is a versatile process and it is used in both rough and finish machining (Kaymakci and Lazoglu, 2008). Ball nose is an important in three-dimensional machining due to its ability to machine three-dimensional curves easily (Chiang et al., 1995).

According to Axinte and Dewes (2002), the ball nose and radius end mills, 2 to 16 mm in diameter, and HSM are commonly used in the machining moulds/dies in their hardened state. The use of HSM, ball nose, and low depths of cut offers good surface integrity results due to high cutting forces and a high mechanical effect. Furthermore, a low thermal effect, temperatures less than 400°C, happens in the cutting with centre and with worn tools. They

used a ball nose with 6 mm diameter and obtained Ra values between 0.36 to 2.18 μm in the milling of AISI H13 (47-49).

Bouzakis et al. (2003) studied the milling with ball end tools aiming to understand the chip formation mechanisms, the cutting force, the tool deflections, and achieve low roughness values. They analysed the influence of the tool axis inclination on the surface roughness at various cutting kinematics, whose the roughness increase caused by the cutting tool deflection at different tool inclination angles is also considered.

Brandão et al. (2008) studied the temperature in the up-and-downward milling of AISI H13 (52 HRC) and AISI D2 (58 HRC) using different types of ball noses end mills and cooling systems. They embedded thermocouples on the internal part of the workpiece that were placed at 2 mm below the milling surface. The temperature ranges were for the AISI H13 of 29.7 to 48.9 (dry condition), 27.2 to 32.9 (compressed air), and 23.9 to 30.8 (cold air) and for the AISI D2 of 34.7 to 48.5 (dry condition), 28.3 to 33.7 (compressed air), and 24.0 to 29.8 (cold air). They affirmed that the compressed air can be the most appropriate cooling systems due to the temperature is kept closer to the ambient. Furthermore, the other cooling systems can affect workpiece dimension, dry condition (thermal expansion) and cooled air (thermal contraction).

To study the finishing of AISI P20, Arruda et al. (2014) used a ball nose with diameter of 6 mm and coating of TiAlN. They analysed the cutting forces and surface roughness applied in different strategies (radial depth of cut $>$ feed rate, radial depth of cut = feed rate, and radial depth of cut $<$ feed rate) and contact angle (axis' tool and workpiece surface) of 10°, 45° and 90°. They obtained a best result applying lower values of contact angle, feed rate, and depth of cut for the feed rate direction and middle value contact angle with lower values feed rate and depth of cut for the radial depth of cut direction.

Souza et al. (2014) studied the phenomena of milling of free-form geometry using ball nose tool and four values of cutting speed in the AISI P20 ($\pm 30 \text{ HR}_C$). They measured the surface roughness (R_a) perpendicularly to the feed direction in the beginning and end of workpiece for each of the four cutting speeds. They observed that the Ra was influenced by the engagement (or not) of the tool center into the cut and the Ra can be twice as bad in the areas where the tool uses its center. The Ra values were, approximately, 0.28 to 0.32 for beginning of path and 0.31 to 0.64 for the end of path, where the lower values were obtained applying the higher speed.

High Speed Machining

Many advantages obtained with the use of HSM were cited by researchers, such as (Schulz and Moriwaki, 1992). The authors affirm that the main advantages are increase of accuracy in machining, especially in machining of thin webs due to reduced chip load; better surface finish and reduction in the damaged layer; reduced bur formation; better chip disposal; possibility of higher stability in cutting due to stability lobes against chatter vibration; simplified tooling, etc. The speed applied in the HSM will depend on material and process combination. Kitagawa et al. (1997) comments in their paper, that the high-speed machining of Ti-6Al-6V-2Sn alloy using sintered carbide tool with 628 m/min of cutting speed is feasible to end milling and no more than 200 m/min is attainable for continuous turning.

Some of the first researches about HSM have sponsored in USA by Defense Advanced Research Project Agency (DARPA), working with a range from 0.0013 m/min to 24,500 m/min, and in Germany by the Ministry of Research and Technology (BMFT). Many of these researches were applied in machining of light alloy, mainly aluminium alloys because of the use in the aircraft industry (Schulz and Moriwaki, 1992). The start developed in several companies and laboratories in machining of hardened steel dies, showing that it is possible to obtain better material remove rate (MRR's) than with Electrical Discharge Machining (EDM) (Tlustý, 1993). The HSM has been applied to a range of applications in the aerospace industry, originally for the machining of aluminium alloys and more recently in titanium alloys and nickel-based super alloys (Coldwell et al., 2003).

Krajnik and Kopač (2004) cited market exigencies from manufacturing companies to produce high-quality products at acceptable prices with shortest interval of time possible. Thus, manufacturers of tooling and die modernize their equipment, processes, and organization, knowing all advantages and disadvantages of rather expensive investments in new technologies, or they can go to bankrupt. They show an evolution of machining time of mould and die manufacturing between 1985's and 2000's, where the manufacturing time improved 43% with HSM in comparison to conventional process. Coldwell et al. (2003) affirmed that benefits with HSM approach include significant cost/lead time, reduction through the elimination of multiple processes including hand finishing and a product manufactured using the traditional route can take over 20 weeks.

Bartarya and Choudhury (2012) affirmed that experiments showed that cemented carbides performed better with speeds up to 120m/min while CBN-(High) tools are superior with high cutting speeds (up to 200m/min). According to Axinte and Dewes (2002), due to high cutting forces, the HSM using ball nose end mills and low depths showed "good" surface integrity results. Table (2) shows roughness values of some researches results using HSM in the machining on hardness steel, because it is the low machinability materials and generally need low surface roughness.

In their research using the HSM on the turning of Inconel 718, Pawade et al. (2007) observed the surface roughness is lower when the cutting speed increases, and it represents a higher MRR. Lima et al. (2005) observed during the machining of AISI 4340 steel hardened using coated carbide (42 HRC) and PCBN (50 HRC) tools that the best surface finish occurred when the cutting speed was elevated and the feed rate was decreased. However, depth of cut showed little effect on the Ra values. Furthermore, the AISI D2 steel (58 HRC) with mixed alumina inserts allowed a surface finish as good as that produced by cylindrical grinding, ranging from 0.28 to 1.12 μm .

Suresh et al. (2012) studied the machinability in the turning of AISI 4340 (48 HRC) and observed that the combination of low feed rate, low depth of cut, and low machining time with high cutting speed is beneficial for minimizing the machining force. Gaitonde et al. (2010) studied the machinability of tungsten-copper (WCu25) machining with cemented carbide and observed the formation of continuous coiled chips during the machining of tungsten-copper composite and with usage of HSM, the formation of longer and smoother tubular structured chips. Silva et al. (2013) investigated the wear mechanisms of PCD tools when turning Ti-6Al-4V alloy at high speed (175, 200, 230 and 250 m/s) conditions using high pressure coolant supplies. They observed the substantial improvement in tool life and it presented dominant the flank and nose wear and the adhesion and attrition are dominant wear mechanisms.

Table 2. Some roughness values of investigations about HSM

	Researchers	Material (AISI)	Speed Machining (m/min)	Roughness ($R_a - \mu\text{m}$)
Milling	Urbanski et al. (2000)	H13(52 HR _C)	250, 350	approximately 1 μm
	Rodrigues and Coelho (2007)	H13 (50 HR _C)	400	0.22 - 0.64 μm
	Elbestawi et al. (1997)	H13 (45 -55 HR _C)	10, 60 krpm	0.2 - 0.66
	Axinte and Dewe (2002)	H13 (47-49 HR _C)	200, 300	0.36 - 2.18
	Koshy et al. (2002)	D2 (58 HR _C)	50 - 200	1 - 6 (carbide) 0.1 - 0.2 (PCBN)
Turning	Suresh et al. (2012)	4340 (48 HR _C)	80, 140, 200, 260	0.50 - 2.45
	Paiva et al. (2012)	52100 (49-52 HR _C)	186.4, 200, 220, 240, 253.6	0.211 - 0.471
	Asiltürk and Akkuş (2011)	4140 (51 HR _C)	90, 120, 150	1.17 - 4.22
	Sahin and Motorcu (2008)	1050 (48 HR _C)	103, 138, 173, 208, 243	0.553 - 1.192
	Lima et al. (2005)	4340 (42 HR _C)	60, 120, 180	approximately 0.6 μm
		4340 (50 HR _C)	60, 120, 180	1.3 - 1.9
		D2	80, 150, 220	0.31 - 1.09

Rodrigues and Coelho (2007) affirmed that the main factor that limits the HSM evolution depends basically on tool developments, such as coatings, substrates and cutting edge geometries. In their paper, they investigated the influence of different tool edge geometric in comparison between conventional speed machining and high speed machining. They, using the specific cutting energy, observed that the influence is due to the combination between tool chip breaker geometry and depth of cut.

Small cut depths with intermediate and high cutting speeds may imply a fully tensile surface influence zone and an increase in cutting speed implies a reduction in longitudinal residual stress until tool breakdown starts to occur (Madyira et al., 2013). Yap et al. (2013) researched the turning Ti-5Al-4V-0.6Mo-0.4Fe (Ti54) titanium ally using the HSM (100 m/s). They found surface roughness values 0.236 μm (R_a), 0.305 μm (R_q) and 1.85 μm (R_{max}) in dry condition. When they applied cryogenic liquid nitrogen, the values decreased to 0.208 μm (R_a), 0.272 μm (R_q) and 1.69 μm (R_{max}).

A problem in the HSM is the tool premature wear or high tool-wear rate. Özel et al. (2007) observed in the finish turning of AISI D2 steels (60 HRC) using ceramic wiper inserts, a value of $V_{BC} = 0.15$ mm around 15 min of cutting time at high cutting speeds due to elevated temperatures. According to Davim and Figueira (Davim and Figueira, 2007), in the turning of AISI D2 using ceramic tools, the tool wear is highly influenced by the cutting

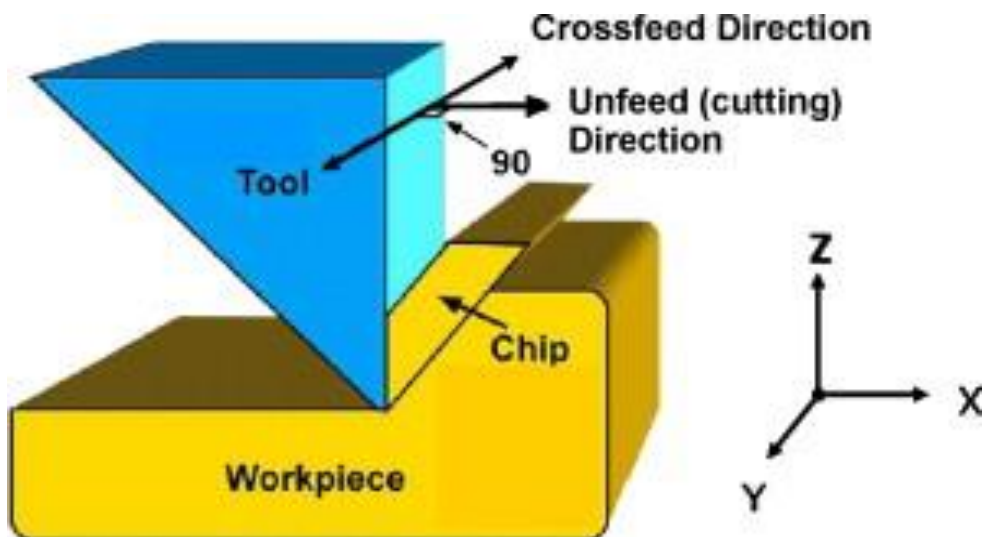
velocity (57.4%) and the cutting time (13.4%), in a smaller degree. Arrazola et al. (2009b) cited the importance of tool geometry on temperature and tool wear in their research about HSM of hardness steel using tools with uncoated/coated and with or without chip breaker.

Assisted Machining

The use of vibration-assisted machining (VAM) can offer an improvement in the surface finishes, better form accuracy, extended tool life (diamond tools cutting ferrous materials), near-zero burr, reduction of machining forces and chips through the small-amplitude, high-frequency tool displacement to the cutting motion of the tool. The tool tip can be driven in a small reciprocating (1D VAM) or elliptical motion (2D VAM) whose centroid moves in the direction of the cutting velocity. The Figure (7) describes the coordinate system of this technique, which the X-axis is in the primary cutting direction and is designated the “upfeed” direction, the Y-axis lies along the “crossfeed” direction, and the Z-axis is normal to the nominal uncut surface of the workpiece and is the direction of the depth of cut (Brehl and Dow, 2008).

According to Patil et al. (2014), the ultrasonic assisted turning (UAT) is an advanced machining technique developed in 1960s in which high frequency ultrasonic vibrations, up to 30,000 low energy vibro-impacts, are superimposed on the conventional movement of cutting tool.

It can provide benefits as an improvement in the dynamic cutting stability; a reduction in the cutting forces and improvement in tool life; a reduction in surface roughness of machined surface; a reduction in residual stresses in the machined workpiece; a reduction in cutting temperature.



(Adapted from Brehl and Dow (2008), with permission from Elsevier).

Figure 7. Coordinate system.

They used experimental tests, analysing surface roughness, microstructure and chip, and FEM tests, which realized that cutting tool in ultrasonically assisted turning is subjected to considerably lower stresses than in conventional turning, except in the penetration stage that is equal and UTA showed a considerable (45 to 50%) reduction in the cutting forces than in conventional turning.

In the drilling of aluminum matrix composites with SiC particles (5, 15 and 20 wt%), Kadivar et al. (2014) applied a ultrasonic vibration technique or ultrasonic-assisted machining (UAM), which is a discontinuous process, while, the conventional machining is a continuous cutting process. In ultrasonic vibration drilling process, also called ultrasonic assisted drilling (UAD), a high frequency and low amplitude vibration are added to conventional drilling in the feed direction. Although the ultrasonic vibration drilling provided a higher thrust force than the conventional drilling, it resulted in smaller burr size and better surface roughness.

According to Muhammad et al. (2012) the ultrasonically assisted turning (UAT) is a non-conventional machining technique that employs the superposition of high-frequency (~ 20 kHz) and low-amplitude ($\sim 15 \mu\text{m}$) vibro-impacts on the cutting tool. They used this technique in Ti15V3Cr3Al3Sn titanium alloy using a frequency of 20 kHz and a vibration amplitude of $8\mu\text{m}$. They observed a significant reducing cutting forces using the ultrasonic vibration compared to conventional turning, maximum reduction of 77%, which offers substantial benefits, as the elimination of the chatter noise during operations and better surface finish. Dong et al. (2012) applied the ultrasonic vibration in the turning of Al 2024 aluminium alloy reinforced with SiC particles with volume fraction of 45% and average size is $3 \mu\text{m}$, which the vibration frequency was 20 kHz and vibration amplitude was $10\mu\text{m}$. They used a cutting speed of 30 m/min, feed of 0.02 mm/rev, and depth of cut of 0.1 mm and obtain a surface roughness between 0.2 and $0.4\mu\text{m}$, approximately.

According to Wang et al. (2014), the Ultrasonic Vibration Assisted Grinding (UAG) have a small grinding force, high material removal rate (6-10 times of common grinding, and 4 times of ultrasonic machining), high machining quality, reduces the cutting force, and lengthen the grinding tool life. This technique can provide a smaller surface roughness and the improved surface integrity. They applied a high frequency (14 and 28 KHz) and vibration amplitude (5 and $10\mu\text{m}$) in the grinding of Si₃N₄. They analysed the 3D topography of the ground surface (S_q and S_a), which was observed more surface quality in the UAG than conventional grinding. The best result, low roughness and waviness value, was obtained using frequency of 14 kHz and vibration amplitude of $5\mu\text{m}$ (S_a of 5592 nm and S_q of 7028 nm), and the conventional grinding provided a S_a of 6701 nm and S_q of 8191 nm.

Abdullah et al. (2008) studied the surface integrity in the WC-Co composite with 10% wt Co content (ISO K15-30) machined by EDM and ultrasonic vibration EDM with frequency of 25kHz (approximately) and maximum amplitude of $5\mu\text{m}$. They observed that the ultrasonic vibration in finishing machining showed a decreasing of the thickness of the heat-affected zone (HAZ) and recast layer that reduces the numbers, size and depth of normal and transverse cracks. Although the ultrasonic vibration showed higher hardness and surface roughness than the conventional EDM, the authors affirmed that the ultrasonic vibration could significantly improve the surface integrity this material.

Sanchez et al. (2014) studied turning of SAE XEV-F, which is a difficult-to-machine steel because it has low thermal conductivity that concentrates heat at the tool tip and can deteriorate the cutting tool wear due to precipitate chromium carbides. They applied the hot machining using three quartz resistances of 500 W each one that found temperatures around

230°C in preliminary test. In comparison with conventional machining, their results showed a meaningful tool life increase (80% to 340%), as a surface roughnesses smaller (difference of 0.15 to 1.14 μm). Furthermore, they compared also the conventional, dry and wetter, with hot machining, where, the cutting force and tool wear in the hot machining was smaller than wetter.

Ranganathan et al. (2010) analysed the the surface roughness in the hot turning of 316 stainless steel temperature at temperatures of 200°C, 400°C, and 600°C. They observed poor surface roughness values at 200C, hpwever, temperatures of 400°C and 600°C showed a satisfactory surface finish due to the material shows recrystallization property. Futhermore, they found that the main contribution factor was the feed rate (1.3% at 200°C, 29% at 400°C, and 20.1% at 600°C), the second factor was combination of cutting speed and feed rate (11.92% at 200°C, 15.14% at 400°C, and 20.1% at 600°C), and the depth of cut is the least significant factor.

To improve the machinability, some researchers use the assisted machining methods, such as vibration, laser and others. Dandekaret al. (2010) studied the improvement of machinability of Ti-6Al-4V titanium alloy using Laser-Assisted Machining (LAM) and hybrid machining method (HYB). They used FEM and experimental method and observed the reduced specific cutting energy. The surface roughness and tool life was improved 1.7 times (LAM) or 2 (HYB) compared with conventional machining at speed of 107 m/min.

Masood et al. (2011) studied the hard turning of AS2027 Grade Cr27, high chromium white cast iron with approximately 60 HRC, applying laser-assisted machining. The inputs were varying depth of cut, laser power, temperature and axial laser position and the outputs were the cutting forces, surface temperature and chips. Their results of cutting force showed that the laser spot closer to the cutting tool reduces turning forces, a reduction of 8.3% to 24% for all depths of cut, a reduction of 12% to 22% for feed force. They affirmed that a increase in the laser power resulted in an increase in surface temperature and depth of heat penetration and the chip formation showed more frequent shearing of material, and surface profile results point to less uniform surface formation.

Muhammad et al. (2014) studied the turning of Ti-15333 applying the conventional turning (CT), hot conventional turning (HCT) and hot ultrasonically assisted turning (HUAT) that is form a new hybrid turning process. A band-resistance heater was used as a heat source to increase the temperature of the workpiece to $300^{\circ}\text{C} \pm 10^{\circ}\text{C}$. They observed a substantial reduction in component forces, 47.2 N to 150.9 N for CT, 33.9 N to N 140.1 for HCT, and 2.7 N to 27.5 N for HUAT in the tangential direction, and 25.6 N to 60.5 N for CT, 21.8 N to 44.6 N for HCT, and 2.1 N to 11.9 N for HUAT in the radial direction. In the surface roughness analysis, they observed that HUAT improved the surface topography parameters in excess of 50%

REMARKS

The quality in the machined surface is a goal that industries and researchers attempt daily. To obtain the desired quality is need know the events that affect the machined surface, as also to know as these events occur. Thus, these knowledge, “what” and “how” occur in machining processes, possible to define the ideal condition to avoid or reduce undesired

events. Furthermore, development of new techniques/tools or to improvement of existing techniques/tools become also a need to obtain the desired quality, mainly when the machined material has poor machinability.

ACKNOWLEDGMENT

The authors would like to thank to the Ministry of Education's Coordination for the Improvement of Higher Education Personnel (CAPES). The author Carlos Lauro would like to thank Elsevier for granting permission for reuse of the published materials.

REFERENCES

- Abdullah, A. et al. - Effect of ultrasonic-assisted EDM on the surface integrity of cemented tungsten carbide (WC-Co). *The International Journal of Advanced Manufacturing Technology*. ISSN 0268-3768. 41:3-4 (2008) 268–280. doi: 10.1007/s00170-008-1476-7.
- Armendia, M. et al. - Comparison of the machinabilities of Ti6Al4V and TIMETAL® 54M using uncoated WC-Co tools. *Journal of Materials Processing Technology*. ISSN 09240136. 210:2 (2010) 197–203. doi: 10.1016/j.jmatprotec.2009.08.026.
- Arrazola, P. J.; Garay, A.; et al. - Machinability of titanium alloys (Ti6Al4V and Ti555.3). *Journal of Materials Processing Technology*. ISSN 09240136. 209:5 (2009) 2223–2230. doi: 10.1016/j.jmatprotec.2008.06.020.
- Arrazola, P. J.; Arriola, I.; Davies, M. A. - Analysis of the influence of tool type, coatings, and machinability on the thermal fields in orthogonal machining of AISI 4140 steels. *CIRP Annals - Manufacturing Technology*. ISSN 00078506. 58:1 (2009) 85–88. doi: 10.1016/j.cirp.2009.03.085.
- Arruda, E. M. et al. - Integrated optimization using mixture design to confirm the finishing of AISI P20 using different cutting strategies and ball nose end mills. *Measurement*. ISSN 02632241. 47:2014) 54–63. doi: 10.1016 /j.measurement. 2013.08.052.
- Asiltürk, İ.; Akkuş, H. - Determining the effect of cutting parameters on surface roughness in hard turning using the Taguchi method. *Measurement*. ISSN 02632241. 44:2011) 1697–1704. doi: 10.1016/j.measurement.2011.07.003.
- Attanasio, A. et al. - Tool wear effects on white and dark layer formation in hard turning of AISI 52100 steel. *Wear*. ISSN 00431648. 286-287:2012) 98–107. doi: 10.1016/j.wear.2011.07.001.
- Aurich, J. C. et al. - Burrs—Analysis, control and removal. *CIRP Annals - Manufacturing Technology*. ISSN 00078506. 58:2 (2009) 519–542. doi: 10.1016/j.cirp.2009.09.004.
- Axinte, D. A.; Dewes, R. C. - Surface integrity of hot work tool steel after high speed milling—experimental data and empirical models. *Journal of Materials Processing Technology*. ISSN 09240136. 127:3 (2002) 325–335. doi: 10.1016/S0924-0136(02)00282-0.
- Bartarya, G.; Choudhury, S. K. - State of the art in hard turning. *International Journal of Machine Tools & Manufacture*. ISSN 08906955. 53:1 (2012) 1–14. doi: 10.1016/j.ijmachtools.2011.08.019.

- Benardos, P. G.; Vosniakos, G.-C. - Predicting surface roughness in machining: a review. *International Journal of Machine Tools & Manufacture*. ISSN 08906955. 43:8 (2003) 833–844. doi: 10.1016/S0890-6955(03)00059-2.
- Bouzakis, K.-D.; Aichouh, P.; Efstathiou, K. - Determination of the chip geometry, cutting force and roughness in free form surfaces finishing milling, with ball end tools. *International Journal of Machine Tools & Manufacture*. ISSN 08906955. 43:5 (2003) 499–514. doi: 10.1016/S0890-6955(02)00265-1.
- Brandão, L. C.; Coelho, R. T.; Rodrigues, A. R. - Experimental and theoretical study of workpiece temperature when end milling hardened steels using (TiAl)N-coated and PcBN-tipped tools. *Journal of Materials Processing Technology*. ISSN 09240136. 199:1-3 (2008) 234–244. doi: 10.1016/j.jmatprotec.2007.07.049.
- Brehl, D. E.; Dow, T. A. - Review of vibration-assisted machining. *Precision Engineering*. ISSN 01416359. 32:3 (2008) 153–172. doi: 10.1016/j.precisioneng.2007.08.003.
- Carvalho, M. V. De; Montenegro, D. M.; Gomes, J. O. - An analysis of the machinability of ASTM grades 2 and 3 austempered ductile iron. *Journal of Materials Processing Technology*. ISSN 09240136. 213:4 (2013) 560–573. doi: 10.1016/j.jmatprotec.2012.11.004.
- Cedergren, S. et al. - The effects of grain size and feed rate on notch wear and burr formation in wrought Alloy 718. *The International Journal of Advanced Manufacturing Technology*. ISSN 0268-3768. 67:5-8 (2012) 1501–1507. doi: 10.1007/s00170-012-4584-3.
- Chern, G.-L. - Experimental observation and analysis of burr formation mechanisms in face milling of aluminum alloys. *International Journal of Machine Tools & Manufacture*. ISSN 08906955. 46:12-13 (2006) 1517–1525. doi: 10.1016/j.ijmactools.2005.09.006.
- Chiang, S.-T.; Tsai, C.-M.; Lee, A.-C. - Analysis of cutting forces in ball-end milling. *Journal of Materials Processing Technology*. ISSN 09240136. 47:3-4 (1995) 231–249. doi: 10.1016/0924-0136(95)85001-5.
- Chinchanikar, S.; Choudhury, S. K. - Investigations on machinability aspects of hardened AISI 4340 steel at different levels of hardness using coated carbide tools. *International Journal of Refractory Metals and Hard Materials*. ISSN 02634368. 38:2013) 124–133. doi: 10.1016/j.ijrmhm.2013.01.013.
- Chou, Y. K.; Evans, C. J. - White layers and thermal modeling of hard turned surfaces. *International Journal of Machine Tools & Manufacture*. ISSN 08906955. 39:12 (1999) 1863–1881. doi: 10.1016/S0890-6955(99)00036-X.
- Coldwell, H. et al. - Rapid machining of hardened AISI H13 and D2 moulds, dies and press tools. *Journal of Materials Processing Technology*. ISSN 09240136. 135:2-3 (2003) 301–311. doi: 10.1016/S0924-0136(02)00861-0.
- Correia, A. E.; Davim, J. P. - Surface roughness measurement in turning carbon steel AISI 1045 using wiper inserts. *Measurement*. ISSN 02632241. 44:5 (2011) 1000–1005. doi: 10.1016/j.measurement.2011.01.018.
- Dahlman, P.; Gunnberg, F.; Jacobson, M. - The influence of rake angle, cutting feed and cutting depth on residual stresses in hard turning. *Journal of Materials Processing Technology*. ISSN 09240136. 147:2 (2004) 181–184. doi: 10.1016/j.jmatprotec.2003.12.014.
- Dandekar, C. R.; Shin, Y. C.; Barnes, J. - Machinability improvement of titanium alloy (Ti-6Al-4V) via LAM and hybrid machining. *International Journal of Machine Tools &*

-
- Manufacture*. ISSN 08906955. 50:2 (2010) 174–182. doi: 10.1016/j.ijmachtools.2009.10.013.
- Davim, J. P.; Figueira, L. - Machinability evaluation in hard turning of cold work tool steel (D2) with ceramic tools using statistical techniques. *Materials & Design*. ISSN 02613069. 28:4 (2007) 1186–1191. doi: 10.1016/j.matdes.2006.01.011.
- Davim, J. P.; Reis, P. - Drilling carbon fiber reinforced plastics manufactured by autoclave—experimental and statistical study. *Materials & Design*. ISSN 02613069. 24:5 (2003) 315–324. doi: 10.1016/S0261-3069(03)00062-1.
- Dong, G. et al. - Experimental Investigation on Ultrasonic Vibration Assisted Turning of Sicc/Al Composites. *Materials and Manufacturing Processes*. ISSN 1042-6914. v 28, n 9:2012) 120813105547003. doi: 10.1080/10426914.2012.709338.
- Duan, C. et al. - Modeling of white layer thickness in high speed machining of hardened steel based on phase transformation mechanism. *The International Journal of Advanced Manufacturing Technology*. ISSN 0268-3768. 69:1-4 (2013) 59–70. doi: 10.1007/s00170-013-5005-y.
- Elbah, M. et al. - Comparative assessment of wiper and conventional ceramic tools on surface roughness in hard turning AISI 4140 steel. *Measurement*. ISSN 02632241. 46:9 (2013) 3041–3056. doi: 10.1016/j.measurement.2013.06.018.
- Elbestawi, M. A. et al. - High-speed Milling of Dies and Molds in Their Hardened State. *CIRP Annals - Manufacturing Technology*. 46:1 (1997) 57–62.
- Fallböhrmer, P. et al. - High-speed machining of cast iron and alloy steels for die and mold manufacturing. *Journal of Materials Processing Technology*. 98:1 (2000) 104–115.
- Ferreira, J. R.; Coppini, N. L.; Levy Neto, F. - Characteristics of carbon–carbon composite turning. *Journal of Materials Processing Technology*. ISSN 09240136. 109:1-2 (2001) 65–71. doi: 10.1016/S0924-0136(00)00776-7.
- Gaitonde, V. N. et al. - Machinability investigations in hard turning of AISI D2 cold work tool steel with conventional and wiper ceramic inserts. *International Journal of Refractory Metals and Hard Materials*. ISSN 02634368. 27:4 (2009) 754–763. doi: 10.1016/j.ijrmhm.2008.12.007.
- Gaitonde, V. N. et al. - Machinability analysis in turning tungsten–copper composite for application in EDM electrodes. *International Journal of Refractory Metals and Hard Materials*. ISSN 02634368. 28:2 (2010) 221–227. doi: 10.1016/j.ijrmhm.2009.10.002.
- Gaitonde, V. N. et al. - A study aimed at minimizing delamination during drilling of CFRP composites. *Journal of Composite Materials*. ISSN 0021-9983. 45:22 (2011) 2359–2368. doi: 10.1177/0021998311401087.
- Grzesik, W.; Wanat, T. - Surface finish generated in hard turning of quenched alloy steel parts using conventional and wiper ceramic inserts. *International Journal of Machine Tools & Manufacture*. ISSN 08906955. 46:15 (2006) 1988–1995. doi: 10.1016/j.ijmachtools.2006.01.009.
- Guddat, J. et al. - Hard turning of AISI 52100 using PCBN wiper geometry inserts and the resulting surface integrity. *Procedia Engineering*. ISSN 18777058. 19:2011) 118–124. doi: 10.1016/j.proeng.2011.11.089.
- Hessainia, Z. et al. - On the prediction of surface roughness in the hard turning based on cutting parameters and tool vibrations. *Measurement*. ISSN 02632241. 46:5 (2013) 1671–1681. doi: 10.1016/j.measurement.2012.12.016.

- Hocheng, H.; Tsao, C. C. - The path towards delamination-free drilling of composite materials. *Journal of Materials Processing Technology*. ISSN 09240136. 167:2-3 (2005) 251–264. doi: 10.1016/j.jmatprotec.2005.06.039.
- Isik, Y. - Investigating the machinability of tool steels in turning operations. *Materials & Design*. ISSN 02613069. 28:5 (2007) 1417–1424. doi: 10.1016/j.matdes.2006.03.025.
- Jaffery, S. I.; Mativenga, P. T. - Assessment of the machinability of Ti-6Al-4V alloy using the wear map approach. *The International Journal of Advanced Manufacturing Technology*. ISSN 0268-3768. 40:7-8 (2008) 687–696. doi: 10.1007/s00170-008-1393-9.
- Kadivar, M. A. et al. - Investigating the effects of vibration method on ultrasonic-assisted drilling of Al/SiCp metal matrix composites. *Robotics and Computer-Integrated Manufacturing*. ISSN 07365845. 30:3 (2014) 344–350. doi: 10.1016/j.rcim.2013.10.001.
- Kaymakci, M.; Lazoglu, I. - Tool Path Selection Strategies for Complex Sculptured Surface Machining. *Machining Science and Technology*. ISSN 1091-0344. 12:1 (2008) 119–132. doi: 10.1080/10910340801913979.
- Kitagawa, T.; Kubo, A.; Maekawa, K. - Temperature and wear of cutting tools in high-speed machining of Inconel 718 and Ti-6Al-6V-2Sn. *Wear*. 202:2 (1997) 142–148.
- König, W.; Gras, P. - Quality Definition and Assessment in Drilling of Fibre Reinforced Thermosets. *CIRP Annals - Manufacturing Technology*. ISSN 00078506. 38:1 (1989) 119–124. doi: 10.1016/S0007-8506(07)62665-1.
- Koshy, P.; Dewes, R. C.; Aspinwall, D. K. - High speed end milling of hardened AISI D2 tool steel (~58 HRC). *Direct*. 127:2 (2002) 266–273.
- Krajnik, P.; Kopač, J. - Modern machining of die and mold tools. *Journal of Materials Processing Technology*. ISSN 09240136. 157-158:2004) 543–552. doi: 10.1016/j.jmatprotec.2004.07.146.
- Lima, J. G. et al. - Hard turning: AISI 4340 high strength low alloy steel and AISI D2 cold work tool steel. *Journal of Materials Processing Technology*. 169:2005) 388–395.
- Madyira, D. M. et al. - High speed machining induced residual stresses in grade 5 titanium alloy. *Journal of Materials : Design and Applications*. 227:2013) 208–215.
- Masood, S. H.; Armitage, K.; Brandt, M. - An experimental study of laser-assisted machining of hard-to-wear white cast iron. *International Journal of Machine Tools and Manufacture*. ISSN 08906955. 51:6 (2011) 450–456. doi: 10.1016/j.ijmactools.2011.02.001.
- Muhammad, R. et al. - Numerical Modelling of Vibration-Assisted Turning of Ti-15333. *Procedia CIRP*. ISSN 22128271. 1:2012) 347–352. doi: 10.1016/j.procir.2012.04.062.
- Muhammad, R. et al. - Thermally enhanced ultrasonically assisted machining of Ti alloy. *CIRP Journal of Manufacturing Science and Technology*. ISSN 17555817. 7:2 (2014) 159–167. doi: 10.1016/j.cirpj.2014.01.002.
- Özel, T. et al. - Modelling of surface finish and tool flank wear in turning of AISI D2 steel with ceramic wiper inserts. *Journal of Materials Processing Technology*. ISSN 09240136. 189:1-3 (2007) 192–198. doi: 10.1016/j.jmatprotec.2007.01.021.
- Paiva, A. P. et al. - A multivariate robust parameter design approach for optimization of AISI 52100 hardened steel turning with wiper mixed ceramic tool. *International Journal of Refractory Metals and Hard Materials*. ISSN 02634368. 30:1 (2012) 152–163. doi: 10.1016/j.ijrmhm.2011.08.001.
- Palani, S.; Natarajan, U.; Chellamalai, M. - On-line prediction of micro-turning multi-response variables by machine vision system using adaptive neuro-fuzzy inference

- system (ANFIS). *Machine Vision and Applications*. ISSN 0932-8092. 24:1 (2013) 19–32. doi: 10.1007/s00138-011-0378-0.
- Patil, S. et al. - Modelling and simulation of effect of ultrasonic vibrations on machining of Ti6Al4V. *Ultrasonics*. ISSN 1874-9968. 54:2 (2014) 694–705. doi: 10.1016/j.ultras.2013.09.010.
- Pawade, R. S. et al. - An investigation of cutting forces and surface damage in high-speed turning of Inconel 718. *Journal of Materials Processing Technology*. ISSN 09240136. 192-193:2007) 139–146. doi: 10.1016/j.jmatprotec.2007.04.049.
- Persson, E.; Eriksson, I.; Zackrisson, L. - Effects of hole machining defects on strength and fatigue life of composite laminates. *Composites Part A: Applied Science and Manufacturing*. ISSN 1359835X. 28:2 (1997) 141–151. doi: 10.1016/S1359-835X(96)00106-6.
- Piotrowska, I. et al. - Mathematical model of micro turning process. *The International Journal of Advanced Manufacturing Technology*. ISSN 0268-3768. 45:1-2 (2009) 33–40. doi: 10.1007/s00170-009-1932-z.
- Ramesh, A.; Melkote, S. N. - Modeling of white layer formation under thermally dominant conditions in orthogonal machining of hardened AISI 52100 steel. *International Journal of Machine Tools & Manufacture*. ISSN 08906955. 48:3-4 (2008) 402–414. doi: 10.1016/j.ijmachtools.2007.09.007.
- Ranganathan, S.; Senthilvelan, T.; Sriram, G. - Evaluation of Machining Parameters of Hot Turning of Stainless Steel (Type 316) by Applying ANN and RSM. *Materials and Manufacturing Processes*. ISSN 1042-6914. 25:10 (2010) 1131–1141. doi: 10.1080/10426914.2010.489790.
- Rodrigues, A. R.; Coelho, R. T. - Influence of the Tool Edge Geometry on Specific Cutting Energy at High - Speed Cutting. *Journal of the Brazilian Society of Mechanical Sciences and Engineering*. XXIX:3 (2007) 279–283.
- Rossini, N. S. et al. - Methods of measuring residual stresses in components. *Materials & Design*. ISSN 02613069. 35:2012) 572–588. doi: 10.1016/j.matdes.2011.08.022.
- Sahin, Y.; Motorcu, A. R. - Surface roughness model in machining hardened steel with cubic boron nitride cutting tool. *International Journal of Refractory Metals and Hard Materials*. ISSN 02634368. 26:2 (2008) 84–90. doi: 10.1016/j.ijrmhm.2007.02.005.
- Saini, S.; Ahuja, I. S.; Sharma, V. S. - Residual Stresses, Surface Roughness, and Tool Wear in Hard Turning: A Comprehensive Review. *Materials and Manufacturing Processes*. ISSN 1042-6914. 27:6 (2012) 583–598. doi: 10.1080/10426914.2011.585505.
- Sanchez, L. E. A. et al. - Hot turning of a difficult-to-machine steel (sae xev-f) aided by infrared radiation. *The International Journal of Advanced Manufacturing Technology*. ISSN 0268-3768. 2014). doi: 10.1007/s00170-014-5879-3.
- Sayuti, M. et al. - Cutting force reduction and surface quality improvement in machining of aerospace duralumin AL-2017-T4 using carbon onion nanolubrication system. *The International Journal of Advanced Manufacturing Technology*. ISSN 0268-3768. 65:9-12 (2012) 1493–1500. doi: 10.1007/s00170-012-4273-2.
- Schulz, H.; Moriwaki, T. - High-speed Machining. *Annals of the CIRP*. 41:1992) 637–643.
- Silva, R. B. Da et al. - Tool life and wear mechanisms in high speed machining of Ti–6Al–4V alloy with PCD tools under various coolant pressures. *Journal of Materials Processing Technology*. ISSN 09240136. 213:8 (2013) 1459–1464. doi: 10.1016/j.jmatprotec.2013.03.008.

- Souza, A. F. et al. - Investigating the cutting phenomena in free-form milling using a ball-end cutting tool for die and mold manufacturing. *The International Journal of Advanced Manufacturing Technology*. ISSN 0268-3768. 71:9-12 (2014) 1565–1577. doi: 10.1007/s00170-013-5579-4.
- Souza JR., A. M. DE et al. - Performance of single Si₃N₄ and mixed Si₃N₄+PCBN wiper cutting tools applied to high speed face milling of cast iron. *International Journal of Machine Tools and Manufacture*. ISSN 08906955. 45:3 (2005) 335–344. doi: 10.1016/j.ijmachtools.2004.08.006.
- Suresh, R. et al. - Machinability investigations on hardened AISI 4340 steel using coated carbide insert. *International Journal of Refractory Metals and Hard Materials*. ISSN 02634368. 33:2012) 75–86. doi: 10.1016/j.ijrmhm.2012.02.019.
- Suresh, R. et al. - State-of-the-art research in machinability of hardened steels. *Proceedings of the Institution of Mechanical Engineers, Part B: Journal of Engineering Manufacture*. ISSN 0954-4054. 227:2 (2013) 191–209. doi: 10.1177/0954405412464589.
- Thakur, D. G.; Ramamoorthy, B.; Vijayaraghavan, L. - Study on the machinability characteristics of superalloy Inconel 718 during high speed turning. *Materials & Design*. ISSN 02613069. 30:5 (2009) 1718–1725. doi: 10.1016/j.matdes.2008.07.011.
- Thusty, J. - High-Speed Machining. *CIRP Annals - Manufacturing Technology*. ISSN 00078506. 42:2 (1993) 733–738. doi: 10.1016/S0007-8506(07)62536-0.
- Trent, E.; Wright, P. - *Metal Cutting*. 4. ed. Woburn : Butterworth–Heinemann, 2000. 446 p. ISBN 075067069X.
- Tsao, C.; Hocheng, H. - Taguchi analysis of delamination associated with various drill bits in drilling of composite material. *International Journal of Machine Tools and Manufacture*. ISSN 08906955. 44:10 (2004) 1085–1090. doi: 10.1016/j.ijmachtools.2004.02.019.
- Ulutun, D.; Özel, T. - Machining induced surface integrity in titanium and nickel alloys: A review. *International Journal of Machine Tools & Manufacture*. ISSN 08906955. 51:3 (2011) 250–280. doi: 10.1016/j.ijmachtools.2010.11.003.
- Umbrello, D. - Investigation of surface integrity in dry machining of Inconel 718. *The International Journal of Advanced Manufacturing Technology*. ISSN 0268-3768. 69:9-12 (2013) 2183–2190. doi: 10.1007/s00170-013-5198-0.
- Umbrello, D.; Filice, L. - Improving surface integrity in orthogonal machining of hardened AISI 52100 steel by modeling white and dark layers formation. *CIRP Annals - Manufacturing Technology*. ISSN 00078506. 58:1 (2009) 73–76. doi: 10.1016/j.cirp.2009.03.106.
- Upadhyay, V.; Jain, P. K.; Mehta, N. K. - In-process prediction of surface roughness in turning of Ti–6Al–4V alloy using cutting parameters and vibration signals. *Measurement*. ISSN 02632241. 46:1 (2013) 154–160. doi: 10.1016/j.measurement.2012.06.002.
- Urbanski, J. P. et al. - High speed machining of moulds and dies for net shape manufacture. *Materials & Design*. ISSN 02613069. 21:4 (2000) 395–402. doi: 10.1016/S0261-3069(99)00092-8.
- Wang, Y. et al. - Study on the system matching of ultrasonic vibration assisted grinding for hard and brittle materials processing. *International Journal of Machine Tools and Manufacture*. ISSN 08906955. 77:2014) 66–73. doi: 10.1016/j.ijmachtools.2013.11.003.

-
- Wyen, C.-F.; Jaeger, D.; Wegener, K. - Influence of cutting edge radius on surface integrity and burr formation in milling titanium. *The International Journal of Advanced Manufacturing Technology*. ISSN 0268-3768. 67:1-4 (2012) 589–599. doi: 10.1007/s00170-012-4507-3.
- Yap, T. C.; El-Tayeb, N. S. M.; Brevern, P. - Cutting forces, friction coefficient and surface roughness in machining Ti-5Al-4V-0.6Mo-0.4Fe using carbide tool K313 under low pressure liquid nitrogen. *Journal of the Brazilian Society of Mechanical Sciences and Engineering*. ISSN 1678-5878. 35:1 (2013) 11–15. doi: 10.1007/s40430-013-0001-6.

Chapter 6

A COMPARISON OF MILLING CUTTING PATH STRATEGIES FOR ALUMINIUM 6262-T6 ALLOYS FABRICATION

*W. O. Leite¹, J. C. Campos Rubio², J. Tejero,³
F. Mata^{3,*} and I. Hanafi⁴*

¹Universidade Federal de Minas Gerais, Programa de Pós-Graduação
em Engenharia de Produção, Pampulha, Belo Horizonte, Minas Gerais - Brasil

²Universidade Federal de Minas Gerais – Departamento de Engenharia Mecânica –
Laboratório de Usinagem e Automação, Pampulha, Belo Horizonte,
Minas Gerais – Brasil

³Escuela de Ingeniería Minera e Industrial de Almadén,
Almadén, Ciudad Real, España

⁴Ecole Nationale des Sciences Appliquées d'Al Hoceima (ENSAH),
Al Hoceima, Morocco

ABSTRACT

This chapter presents a comparison of milling cutting path strategies for Aluminium 6262-T6. To search for more efficient cutting path strategies for machined parts, an interactive process planning and analyzing method is introduced. Several rigid combinations of machining parameters are examined based on the evaluation of surface finish, thickness accuracy and machining time in the visual charts. In order to obtain the best cutting path strategy, CAM software have been used to utilize the cutting path for machining Aluminium alloy parts into CNC end milling machine. The resulting of cutting path strategies is solved by experimental method. From the experiment, it was found that the circular path strategy provided 17% less time, fewer errors, and worse accuracy. The Z level from bottom to top strategy had lowers circularity and better accuracy compared to Z level from top to bottom.

* Correspondence: 3 Escuela de Ingeniería Minera e Industrial de Almadén, Plaza de Manuel Meca- 1, Almadén, Ciudad Real, España Tel.: +34 926295300, Ext.: 6044. jose.tejero@uclm.es francisco.mcabrera@uclm.es.

Keywords: CNC milling machine, CAM software, process planning, machining efficiency

INTRODUCTION

The Computer-aided design and Computer-aided manufacturing (CAD/CAM) came to change the manufacturing concepts. Since the 1960, to the present, they have contributed to the reduction of manufacturing costs, becoming more accessible to the manufacturers. Phasing into the life of companies has provided new technological challenges, including the need to ensure the end product quality. As the machining become faster, deviations that were previously considered insignificant proportions make the production viable, if they are not corrected. The study of the sources of error in machining with CAD /CAM systems and correction becomes, thus, a precondition for ensuring the end result.

The high quality and high productivity in machining of complex parts has been of primary interest in manufacturing industries. To improve the efficiency of CNC machining, high speed milling is now widely used in manufacturing industries [1]. The complex shapes of these machined parts are rather defined as complex features which are mainly represented by their geometric parameters [2]. The geometric representation of features has been widely explored in several works [3-4]. In conventional machining, the geometric features are associated to machining features through a recognition process [5-6].

The quality of the surface produced depends on various technological parameters, such as the cutting conditions as well as the cutting tool and the workpiece specification. Additionally, it is very important to select the appropriate cutting strategy. However, the application of this cutting strategy results in new limitations for the manufacturing process, both in relationship to machining time and in terms of geometric quality [7]. Faced with these limitations, new manufacturing processes for machined surfaces must be developed to increase the efficiency of the machining process and also to reduce its costs.

The machining strategies applied, such as Z level or parallel planes [8-9], lead to the manufacturing of the whole part in a single sequence [10]. At this stage, the geometric parameters are not sufficient for the development of an efficient machining process. The strategy chosen to generate the tool path can influence in important parameters (machining time, cutting forces, length of the tool path, surface roughness). It can be considered in two main stages; the global and local strategy. The former is related to selection of the approach for material removal whereas the latter considers process parameters used in the tool path. For example, in case of machining of turbine engine compressors, there are several global strategies such as flank milling, point milling and plunge milling, whereas some of the local strategies are zig, zig-zag, helical, raster and trochoidal. The required configuration and specifications of the machine tool, the required cutting tools to be utilized in the process and overall productivity depend on the selected global strategy. However, this is not a straight forward task as several aspects such as geometry, mechanics and dynamics of the process, and the nonlinear relation between them, should be taken into account.

Several authors investigated the effects of tool path pattern on the process, [11,12]. Most of the studies on machining strategy selection are concentrated on the tool trajectory where cutting forces, tool deflections and maximum feed rate maps are utilized to decide tool feed direction and select the best tool path pattern. CNC milling experiments were performed to

identify various 3D tool paths, and then their scallop heights distribution and tool path distance were theoretically analyzed. The effect of various 3D tool path strategies was investigated on their surface texture height, surface roughness, and form errors [13]. The experimental results indicates that the surface texture height, the surface roughness, and the form errors were nearly identical on the machined flat location and surface for various tool path strategies, whereas their surface quality and form accuracy are easily destroyed on the abrupt ones except for the parallel tool paths.

Design of Experiment

A number of cutting experiments was carried out on a ROMI model DISCOVERY 760 milling machine, controlled by the Siemens control 810D. In the production of formed surfaces (Roughing/ Finishing), cylindrical / end ball milling cuts are mainly used. These cutting tools are marked as monolithic milling cutter or as tools with indexable insert (Figure 1).

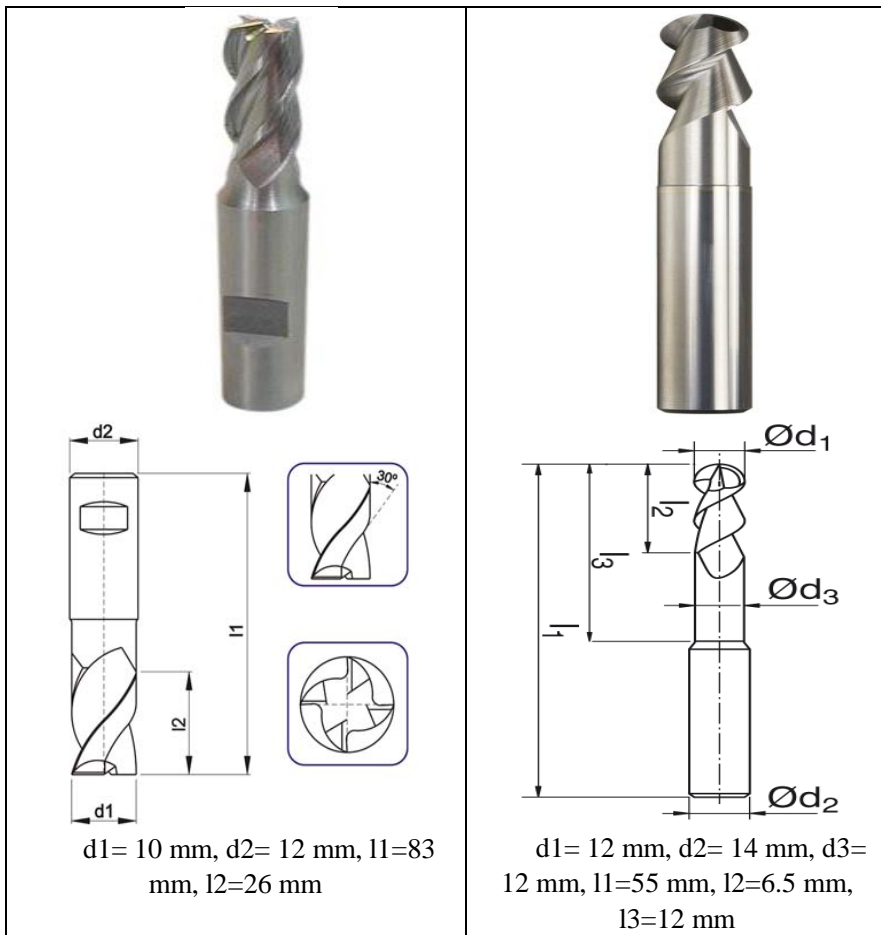


Figure 1. Monolithic Roughing/ Finishing milling cutters.

Al6262-T6 was selected as a workpiece material has the following dimensions: width = 50.8 mm; length = 220 mm; height = 50.8 mm (see Figure 3), because it has been widely used for structural components and especially for aircraft and aerospace structures. Al6262-T6 offers a combination of high strength, with moderate toughness and corrosion resistance, and for this reason is widely preferred in the structural components manufacturing industry. Figure presents the workflow for the execution of the complete experimental work. The resulted surfaces were measured with the use of a Taylor Hobson Surtronic 25 Compact surface roughness tester.

Based from the problem statement and the objective, a flow chart was used to demonstrate the project being implemented from the beginning until the end of the project as explained in Figure 2.

The project planning involves with the selection of end mills tool, CNC milling machine, machine parameters, machining process and strategies, safety features and report which need to be used in this work.

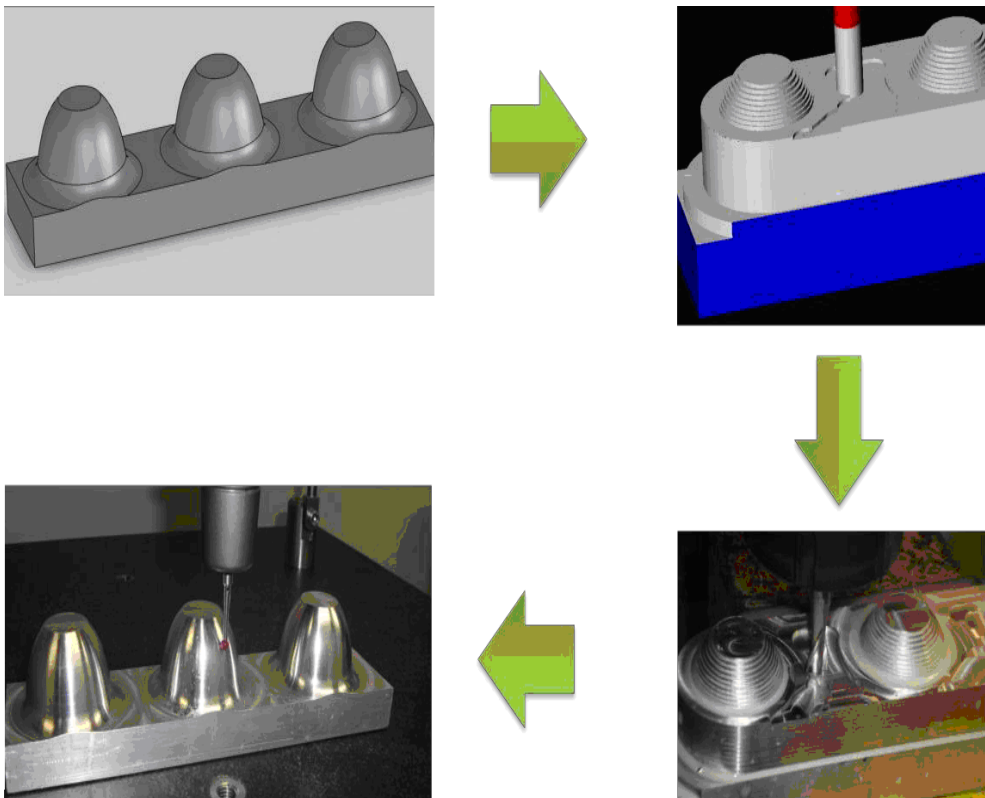


Figure 2. The workflow of the experimental work.

Machining Setting and Programming based on Cutting Strategies Before running the CNC end milling machine, there are several setting need to be done in order to get the right process method for machining the product. CAM software was used to select the milling cutting path strategies of each cutting process. The parameters also must be allocated to accomplish the condition of machining such as cutting speed, feed rate and depth of cut which is important in order to observe the correct parameters for the correct process. All the

parameters are in a constant value of setting. Then, the experiments can be done accordingly to the machining cutting path strategies. There are three cutting path strategies are being used for this work: Circular, Z level from bottom to top and Z level from top to bottom.

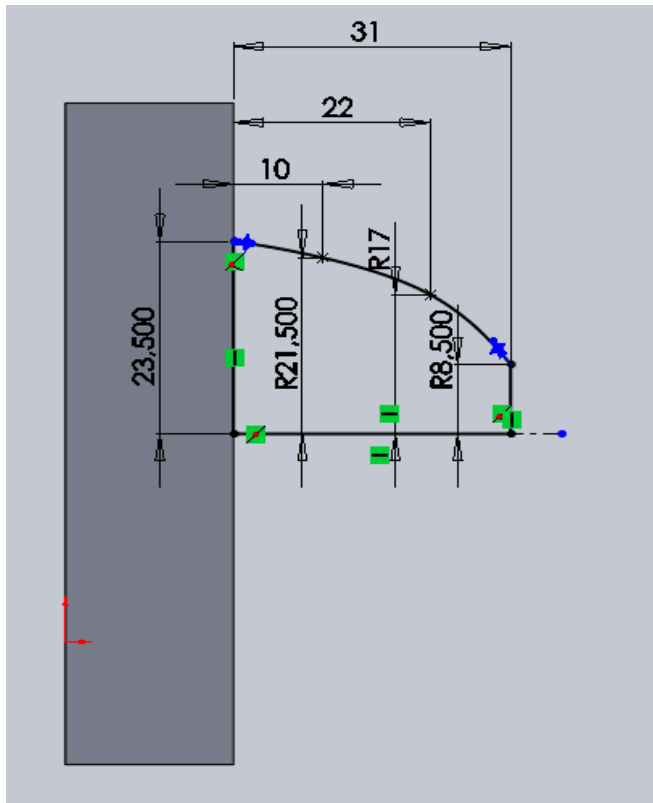


Figure 3. Workpiece dimensions.

The milling parameters level used are given in Table 1. The same technological parameters were programmed into the CAM system for all studied strategies.

Table 1. Experimental tests

	Roughing milling cutter	Finishing milling cutter
Cutting Tool	HSS Ø10 mm	Ball Nose Ø12 mm
Vc (m/min)	160	245
Vf (m/min)	480	665
Depth per cut ap (mm)	1.5	0.5
Stepover (mm)	4.35	0.127
Time	02:55:32	03:32:21

As illustrated in Figure, the strategy was adopted to collect the point coordinates along the virtual planes parallel to the plane of the top of the workpiece using the TESA Micro-Hite[®] 3D coordinate measuring machine to evaluate the surface deviations of machined part. The measurements were made at various levels of depth (Figure 4).

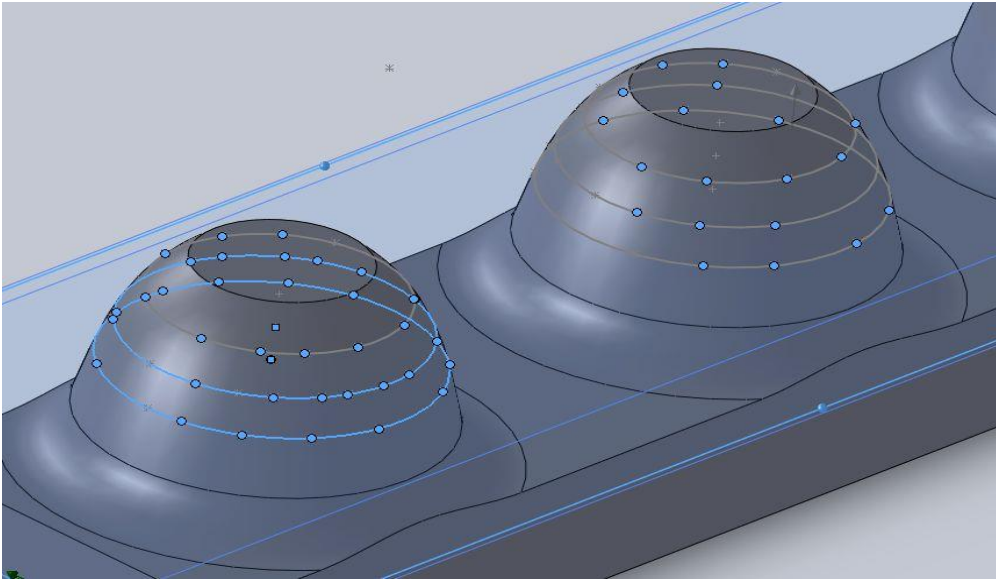


Figure 4. The depth of the different layers.

Collecting the point coordinates allowed us to measure the following parameters, shown in Figure 5:

- Standard Error: The distance between the real and theoretical surface for a given depth measured from the top of the piece.
- Radial deviation: The error on the XY plane, measured on the orthogonal plane to the axis of revolution of the tool.
- Angle α : The angle between the axis of rotation of the tool and the orthogonal plan to the machined surface.

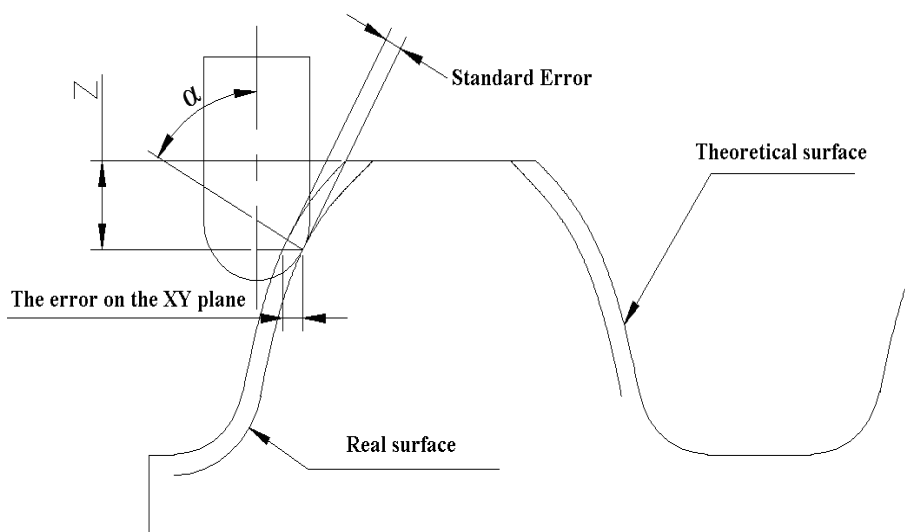


Figure 5. Description of the standard error, the error on XY plan and the α angle.

Those parameters allow us to find the deviations of a real surface from its ideal form, the circularity tolerance and the error surface of the circles formed by the intersections of the different measurement planes and the surfaces of the workpiece.

The circularity tolerance "t" provides a circular zone in which all points of the cross section e slice of the surface must lie. The tolerance zone is the two concentric circles that are the stated tolerance apart [14]. Figure 6 illustrates the concept of circularity tolerance.

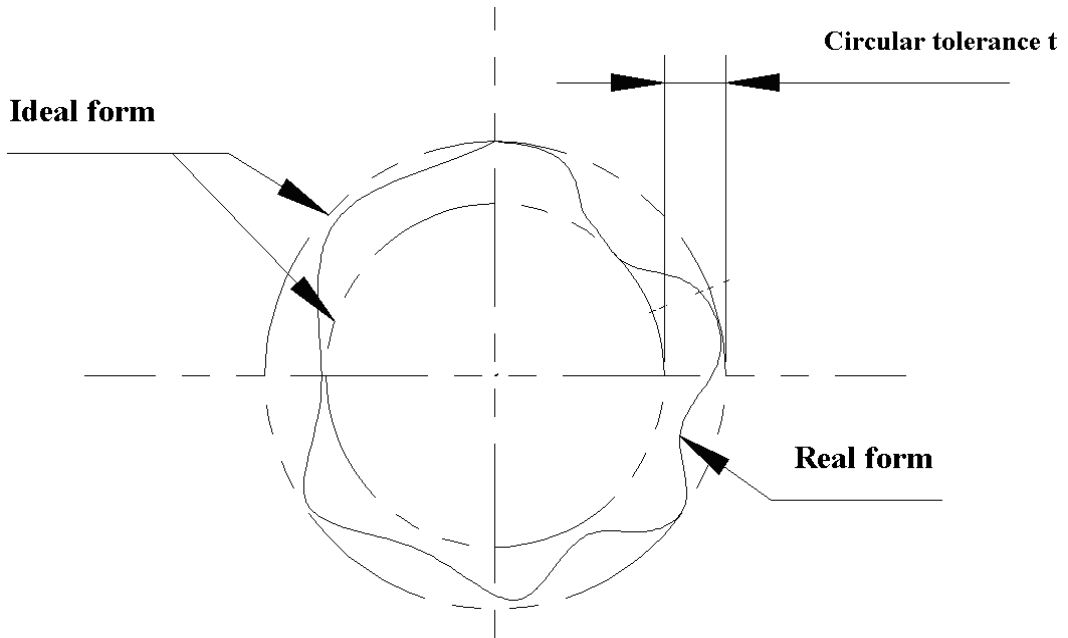


Figure 6. Circularity tolerance.

Results and Discussion

The milling cutter starts out above the machined part and is moved in a circular path as it shown in Figure (7-a). The vibration of the cutting tool increases as the depth of cut increases. The micro-abrasions caused probably by the accumulated of chip, has been detected using The Z level machining from the top to the bottom (Figure (7-b)). In terms of vibration and surface roughness, the best results are achieved using The Z level machining from the bottom to the top (Figure (7-c))

The figure 8 presents the deviation variation as function of the depth and the angle. As observed in a the figure there was a reduction in the radial deviation as the depth increases and the angle α tends to 90° when using the both Z level machining strategies. The greatest error of these two strategies compared to the circular path, can be attributed to the steps cutting tool in points with Z zero, since there is a convergence of the lines representing the trajectories of the same phenomenon does not occur with the third strategy. For small values of α , the pattern of variations in the two curves can be correlated, and it can lead to heavy tool instability. The milling cutter moved in circular path has better stability, especially for lower angles $\alpha (< 51^\circ)$, as the deviation tends to increase with α for circular path, it tends to

decrease for the two Z level machining. Also, there is a clear convergence of values of the deviation when the angle tends to 90° .

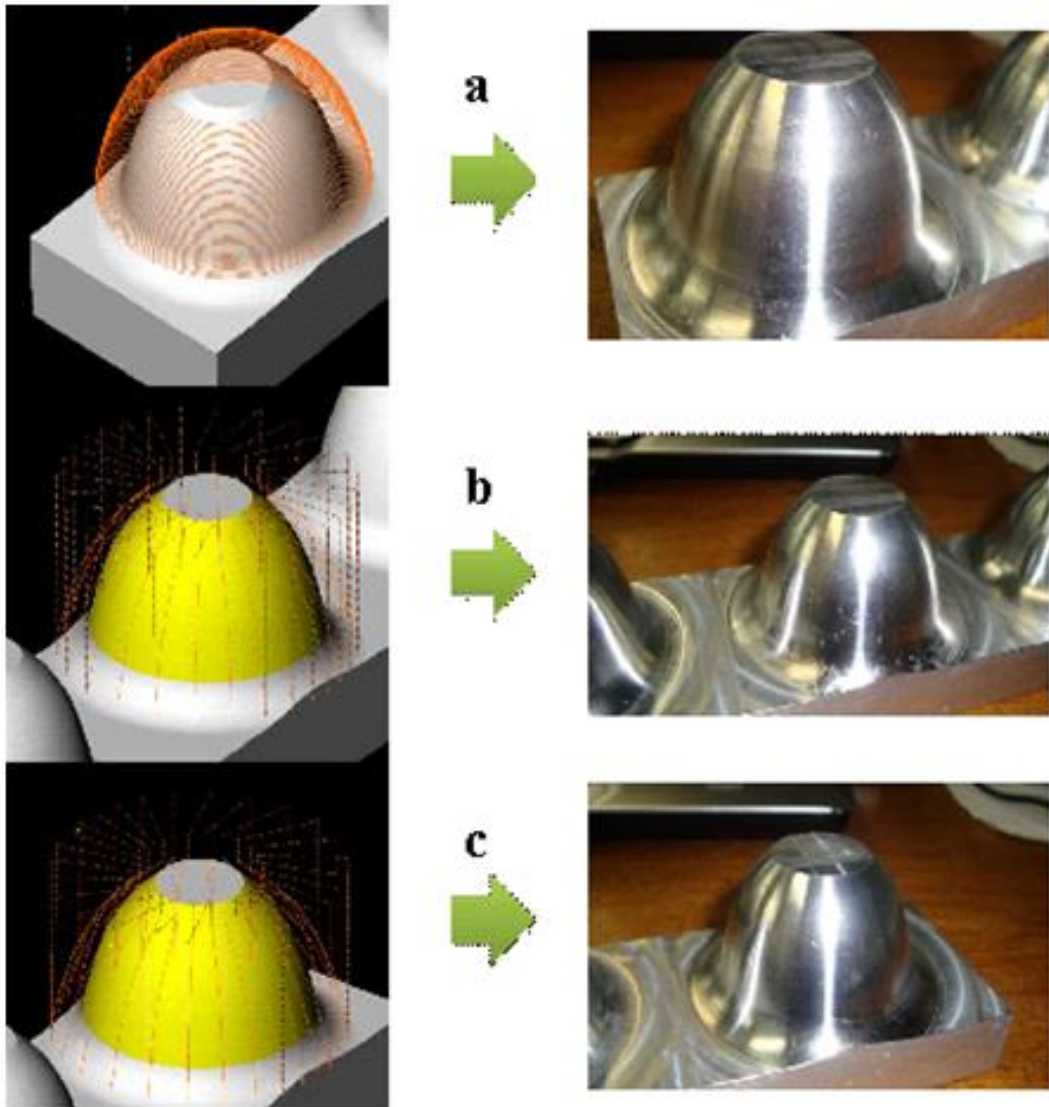


Figure 7. Milling cutter strategy and visual results.

The figure 9 presents the error as function of the depth. A clear disadvantage of Z level from top to bottom compared to the other strategies is observed. It presents higher errors values and greater variation in its amplitude. This result was expected because, theoretically, such a strategy would provide us sudden changes in the configuration of the cutting forces as quickly the cutting tool move down. There is a clear relation of variation of circularity vis-à-vis the depth or angle α . The machining using the Z level from bottom to top gives the best results. The circular path strategy presented average circularity error values that were not expected because, theoretically, this strategy produces a slowly forces configuration changes when the tool slowly descends the z axis, with very gradual changes in α .

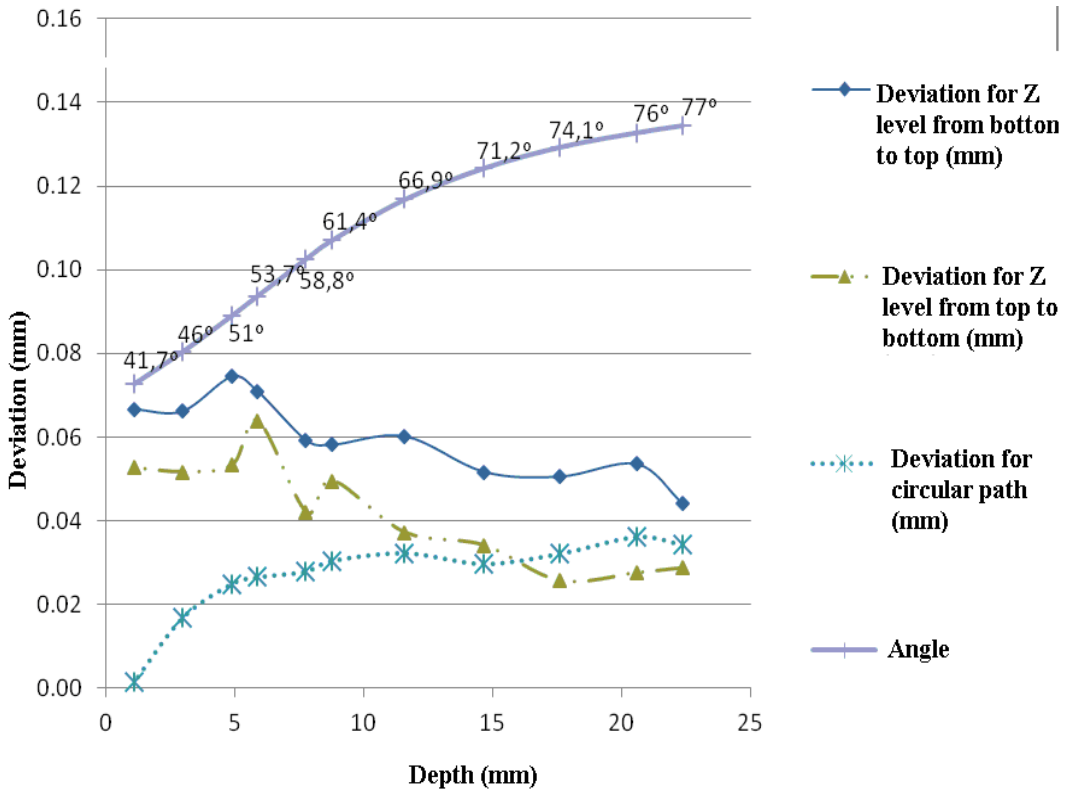


Figure 8. Deviation variation as a function of depth and angle.

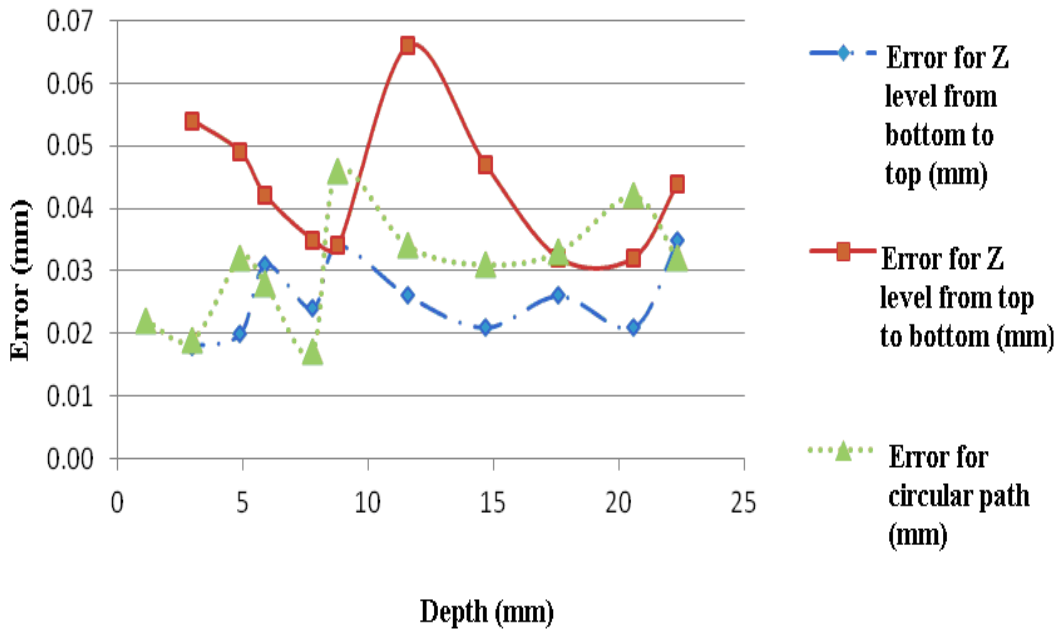
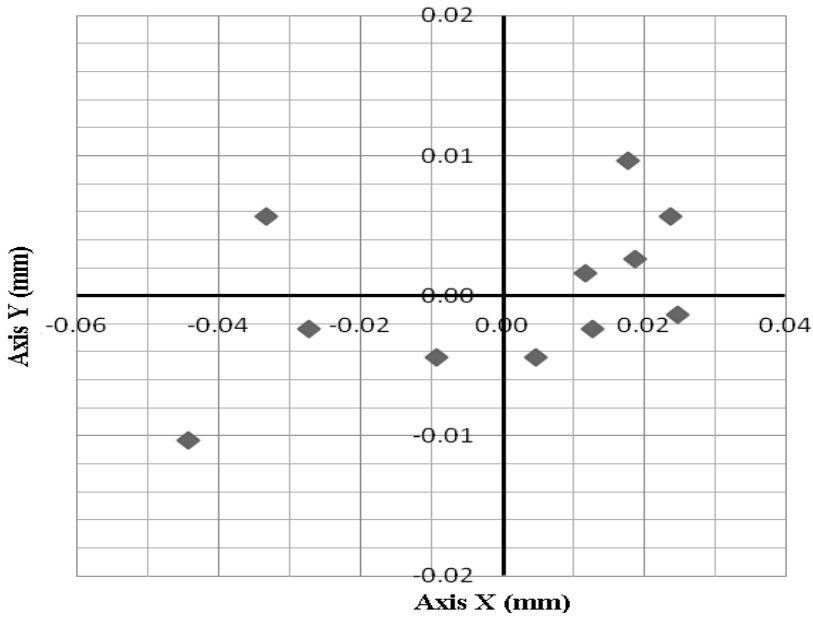
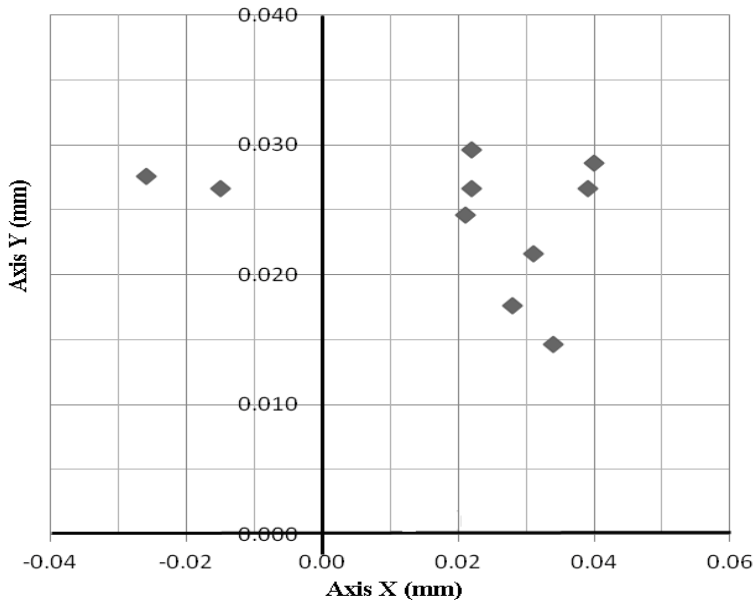


Figure 9. Error variation as a function of depth.

The machining using the Z level from bottom to top generates a better centres of the circles dispersions compared to the other strategies, suggesting a fixed recirculating ball screw fitted on the machines X axis, as shown in figures 10 (a-c).



(a) Z level from bottom to top



(b) Z level from top to bottom

Figure 10. (Continued).

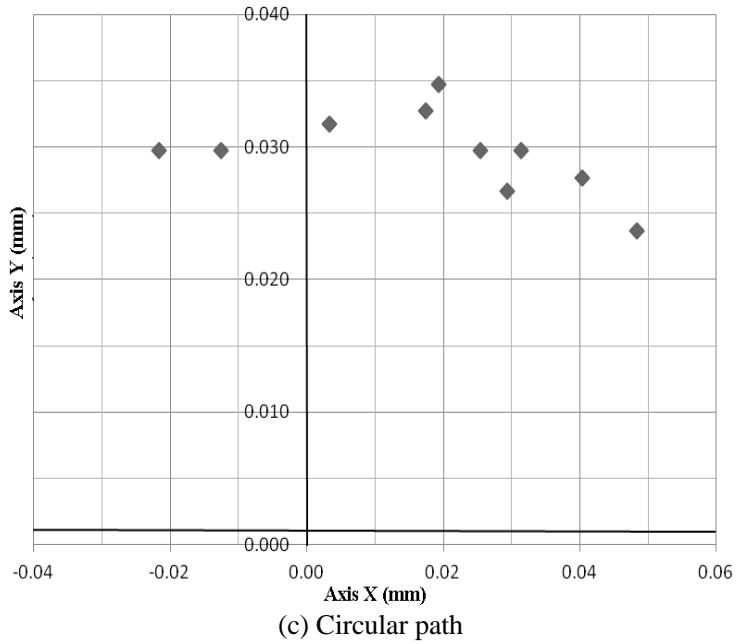
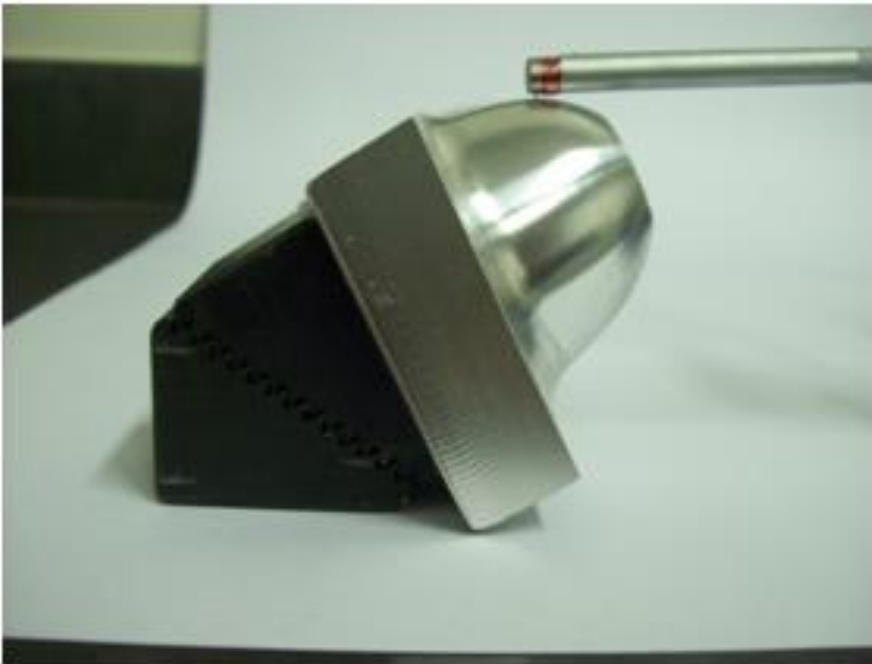


Figure 10. Dispersion of the centers of the circles.

Various surface roughness measurements were performed in two ways: parallel and orthogonal to the axe of symmetry, as shown in the Figure 11. The results are presented in Table 2.



(a)

Figure 11. (Continued).



(b)

Figure 11. Surface roughness measurement Paralleled (a) and orthogonal (b) to the axe of symmetry.

For roughness measurement in parallel axes, the machining performed on normal trajectories to the direction of measurement showed higher roughness values and no significant change in the result of Z level from bottom to top roughness, suggesting that the direction of the path would be an important factor for the finish quality. For roughness measurement in orthogonal axes, the machining using the Z level from top to bottom strategy showed lower roughness values. Suggesting that the surface finish will depend on the radial force.

Table 2. Experimental results

Surface roughness	Ra (μm)		
	Circular path	Z level from top to bottom	Z level from bottom to top
Parallel	0.69	1.07	1.01
Orthogonal	1.01	0.72	1.10

From the Table 3, shows the experimental results of machining time. The highest machining time is Z level cutting strategies with the machining time of 58 minutes. Whereby, the Circular path cutting strategy has less machining time compared to the others machining strategies with the time taken of 48 minutes. The reason is the machining pattern of Circular path cutting strategy used down cut or down milling process in cutting condition. In down milling process, the workpiece is fed in the same direction as that of the cutter's tangential

velocity. The cutter enters the top of the workpiece and removes the chip that gets progressively thinner as the cutter tooth rotates.

Table 3. experimental results of machining time

Machining Strategies	Time
Circular path	00:48:38
Z level from top to bottom	00:58:28
Z level from bottom to top	00:58:28

CONCLUSION

Machining strategies adopted in this work present advantages and disadvantages depending on the chosen evaluation parameter. During this work three strategies and parameters related to machining time were studied and tested in order to find a standard procedure for its determination. The circular path strategy provided 17% less time, fewer errors, and worse accuracy. The Z level from bottom to top strategy had lowers circularity and better accuracy compared to Z level from top to bottom. It's known that machining time is one objective factor to improve the manufacturing of machined surfaces but it has to be combined to other factors. Thus, another suggestion to other works related to this paper is to study in more details the influence of feed rate variation on surface quality. In the case of industrial applications, with similar resources, it is suggested that the choice of the strategy must be made based on the most important customer satisfaction parameter.

REFERENCES

- [1] P. Fallböhmer, C.A. Rodriguez, T. Özel, T. Altan, "High-speed machining of cast iron and alloy steels for die and mold manufacturing", *Journal of Materials Processing Technology*, vol. 98, pp. 104- 115, 2000.
- [2] K. Mawussi, A. Bernard, "Complex dies representation and definition with complex feature-based model", Proc. of the 15th International Computers in Engineering Conference (ASME), September 17- 21, Boston (USA).
- [3] Eelco van den Berg, Willem F. Bronsvort, Joris S.M. Vergeest, "Freeform feature modelling: concepts and prospects", *Computers in Industry*, vol.49, pp.217-233, 2002.
- [4] V. Sundararajan, P.K. Wright, "Volumetric feature recognition for machining components with freeform surfaces", *Computer-Aided Design*, vol. 36, pp. 11-25, 2004.
- [5] X. Yan, K. Yamazaki, J. Liu, "Recognition of machining features and feature topologies from NC programs", *Computer-Aided Design*, vol. 32, pp. 605-616, 2000.
- [6] Xingquan Zhang, Jie Wang, Kazuo Yamazaki, Masahiko Mori, "A surface based approach to recognition of geometric freeform surface machining", *Computer-Aided Design*, vol. 36, pp. 735-744, 2004.
- [7] Ramos, A. M., C. Relvas, e J. A. Simões. "The influence of finishing milling strategies on texture, roughness and dimensional deviations on the machining of complex

- surfaces.” *Journal of Materials Processing Technology*, 10 de January de 2003: 209-216.
- [8] C.-M. Chuang, H.-T. Yau, “A new approach to Z-level contour machining of triangulated surface models using file endmills”, *Computer-Aided Design*, vol. 37, pp. 1039-1051, 2005.
- [9] Davim, J. Paulo, e A. Esteves Correia. *Maquinagem a Alta Velocidade*. Porto: Publindústria Edições Técnicas, 2006.
- [10] A. Flutter, J. Todd, “A machining strategy for toolmaking”, *Computer-Aided Design*, vol. 33, pp. 1009-1022, 2001.
- [11] Lim, E. M., Menq, C.H., 1997, Integrated planning for precision machining of complex surfaces. Part 1: Cutting path and federate optimization, *Int. J. Mach. Tools & Manufacture* Vol. 37, No.1, pp. 61-75.
- [12] Lazoglu, I., Manav C., Murtezaoglu, Y., 2009, Tool path optimization for free form surface machining, *CIRP Annals-Manufacturing Technology*, Vol. 58:1,pp. 101-104.
- [13] Zhang, X. F.; Xie, J.;Xie, H.F.; Li, L. H. Experimental investigation on various tool path strategies influencing surface quality and form accuracy of CNC milled complex freeform surface. *The International Journal of Advanced Manufacturing Technology*, 59, 647-654, 2012.
- [14] Agostinho, Oswaldo Luiz, Antonio Carlos dos Santos Rodrigues, e João Lirani. *Tolerâncias, ajustes, desvios e análise de dimensões*. São Paulo: Edgard Blücher Ltda, 1977.

Chapter 7

APPLICATION OF FUZZY LOGIC IN MODELING AND OPTIMIZATION OF SURFACE ROUGHNESS IN TURNING

*Arup Kumar Nandi**

Mechanical and Aerospace Engineering Department
Missouri University of Science and Technology,
Rolla, Missouri, US

ABSTRACT

This chapter presents the application of fuzzy logic in modeling and optimization of surface roughness of hard materials through a machining process, turning. Modeling of surface roughness in turning process presented in this chapter uses TSK-type fuzzy logic rule followed by a genetic algorithm (GA) is used to optimise the critical machining parameters based on the developed model. In order to construct the optimal knowledge base of the fuzzy model, the genetic linear regression approach is adopted which introduces the multiple regression in the framework of a GA.

This chapter is organized by presenting first, an overview on the fundamentals of fuzzy logic and fuzzy inference systems towards formulating a rule based model (called fuzzy rule based model, FRBM).

After that, a brief introduction on the working principle of a GA is discussed. In the next section, various fuzzy rule based models are discussed.

Then, the genetic linear regression approach is presented to construct the knowledge base of TSK-type FRBM. Results on the effectiveness of FRBM and optimization of machining parameter for surface roughness of AISI D2 Steel in turning are presented.

Keywords: Surface roughness, Turning, Fuzzy logic, Genetic algorithm, Modeling, Optimization

* Corresponding Author Email: nandiarup@yahoo.com / nandia@mst.edu.

INTRODUCTION

Surface roughness is one of the benchmarks, based on which the quality of a machined component is determined. Prediction of surface roughness on the machined surface is an important issue in automated manufacturing system. Several methods were utilized in the past, to develop surface roughness model for turning operation. Response surface methodology was used by Taraman and Lambert (Taraman & Lambert, 1974) to establish a mathematical model of the surface roughness for a turning operation. A common mathematical model based on the regression analysis discussed by Draper and Smith (Draper & Smith, 1981), was utilized by Choudhury and El-Baradie (Choudhury & El-Baradie, 1997) to predict surface roughness in turning of high-strength steel based on factorial design of experiment. In addition, attempts were also made to develop mathematical models for fine turning (Sundaram & Lambert, 1981) as well as for finish turning (Wang & Feng, 2002). Furthermore, computer vision techniques were utilized by various researchers to predict surface roughness in turning. Lee and Tarn (Lee & Tarn, 2001) adopted a polynomial network using a self-organizing adaptive learning tool called polynomial network to construct the relationships between the feature of the surface image and the actual surface roughness under a variation of turning operations to predict the surface roughness of a turned part. Abouelatta and Madl (Abouelatta & Madl, 2001) derived mathematical models to predict roughness parameter based on cutting parameters and machine tool vibration in turning operations. An abductive network which is composed of a number of functional nodes being self-configured based on a predicted square error (PSE) criterion was adopted by Lin et al. (Lin et al., 2001) to construct a prediction model for surface roughness in turning operation. Cheung and Lee (Cheung & Lee, 2000a) developed a model-based simulation system to predict surface roughness generated in ultra-precision diamond turning. This system is based on a surface roughness model, which takes into account the effect of tool geometry, process parameters and relative tool-work vibration. They had also used multi-spectrum analysis method to investigate the formation of surface roughness in ultra-precision diamond turning (Cheung & Lee, 2000b). Taguchi method, a powerful tool for design optimization was used by Yang and Tarn (Yang & Tarn, 1998), Davim (Davim, 2001) to find optimal cutting parameters for turning operations. The fractal geometry and image-processing techniques were used by Zhang and Gopalakrishnam to implement a practical area-based surface finish monitoring system (Zhang & Gopalakrishnam, 1996).

However, due to non-linearity of the cutting parameters, tool-work combination and rigidity of machine tool, soft computing (i.e., neural network, fuzzy logic, genetic algorithm and their hybridizations) is used for prediction of important parameters in manufacturing. Fuzzy logic concept was used in (Nandi, 2003) in order to predict surface roughness in ultraprecision turning operation, in (Fang & Jawahir, 1994) to predict total machining performance in finish turning of the machinability parameters. Neural network-based approach was used by Grzesik and Brol (Grzesik & Brol, 2003), Risbood et al. (Risbood et al., 2003), Mainsah and Ndumu (Mainsah & Ndumu, 1998), Abburi and Dixit (Abburi & Dixit, 2006), Kohli and Dixit (Kohli & Dixit, 2005) to assess surface roughness in turning. Ho et al. (Ho et al., 2002) described a method using an adaptive neuro-fuzzy inference system (ANFIS) to establish a relationship between the features of surface image and the actual surface roughness, and tried to predict surface roughness based on the three cutting

parameters (cutting speed, feed rate and depth of cut). There are various surface roughness amplitude parameters used in industry, such as roughness average (R_a), maximum peak-to-valley roughness (R_t), root-mean-square roughness (R_q), etc. In this chapter, R_a and R_t parameters are mainly concentrated for optimization of machining parameters in hard turning of AISI D2 steel using ceramic inserts, because these are the two important parameters in manufacturing (Davim, 2001). The primary objective of this optimization task is to minimize the R_a as well as the ratio of R_a and R_t , ($\frac{R_a}{R_t}$).

FUZZY LOGIC AND INFERENCE SYSTEMS

Crisp Set and Fuzzy Set

A set (A) is a collection of any objects ($a_1, a_2, a_3, \dots, a_n$), which according to some law can be considered as a whole and it is usually written as

$$A = \{a_1, a_2, \dots, a_n\} \text{ or}$$

$A = \{x | P(x)\}$, means A is the set of all elements (x) of universal set X for which the proposition P(x) is true (e.g., $P(x) > 3$). In crisp set, the function $X_A(x)$ (so-called characteristic function) assigns a value of either 1 or 0 to each individual object, x in the universal set, thereby discriminating between members and non-members of the crisp set, A under consideration. That means there is no uncertainty or vagueness in the fact that the object belongs to the set or does not belong to the set. Set A is defined by its characteristic function, $X_A(x)$ as follows

$$X_A(x) = \begin{cases} 1 & \text{for } x \in A \\ 0 & \text{for } x \notin A \end{cases}$$

In the year, 1965, Lotfi A. Zadeh (Zadeh, 1965) proposed a completely new and elegant approach to vagueness and uncertainty in a seminal paper, called *fuzzy set theory*. In his approach an element, x can belong to a set to a degree, k ($0 \leq k \leq 1$) in contrast to classical set theory where an element must definitely belong or not to a set. A fuzzy set, \tilde{A} is usually written as $\tilde{A} = \{x, \mu_{\tilde{A}}(x) | x \in X\}$. The function $\mu_{\tilde{A}}(x)$ is called membership function (MF) of the (fuzzy) set \tilde{A} and defined as $\mu_{\tilde{A}}(x) \rightarrow (0,1)$. The value of $\mu_{\tilde{A}}(x)$ is called the degree of membership of x in the fuzzy set \tilde{A} .

Fuzzy Membership Function

Graphically, a membership function is represented as a curve (as shown in Figure 1) that defines how each element in the set is mapped to a membership value (or degree of membership) between 0 and 1. There are many ways to assign membership values or

functions to fuzzy variables compared to that to assign probability density function to random variables. The membership function assignment process can be intuitive or based on some algorithmic or logical operations.

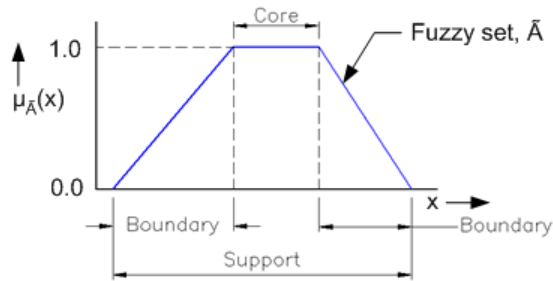


Figure 1. A graphical representation of fuzzy set.

Some Key Properties of Fuzzy Set

- Having two fuzzy sets \tilde{A} and \tilde{B} based on X , then both are *equal* if their membership functions are equal, i.e., $\tilde{A} = \tilde{B} \Leftrightarrow \mu_{\tilde{A}}(x) = \mu_{\tilde{B}}(x)$ for all $x \in X$
- Given a fuzzy set \tilde{A} defined on X and any number $\alpha \in (0,1)$, the α -cut, ${}^{\alpha}\tilde{A}$, and the *strong* α -cut, ${}^{\alpha+}\tilde{A}$, are the crisp sets: ${}^{\alpha}\tilde{A} = \{x \mid \tilde{A}(x) \geq \alpha\}$ and ${}^{\alpha+}\tilde{A} = \{x \mid \tilde{A}(x) > \alpha\}$
- The *height* of a fuzzy set is the largest membership grade obtained by any element in that set i.e., $\text{height}(\tilde{A}) = \max_{x \in X} \mu_{\tilde{A}}(x)$
- The *crossover points* of a membership function are defined as the elements in the universe for which a particular fuzzy set A has values equal to 0.5, i.e., for which $\mu_{\tilde{A}}(x) = 0.5$
- A fuzzy set \tilde{A} is called *normal* when $\text{height}(\tilde{A}) = 1$ and *subnormal* when $\text{height}(\tilde{A}) < 1$.
- The *support* of a fuzzy set \tilde{A} is the crisp set that contains all the elements of X that have nonzero membership grades, i.e., $\text{support}(\tilde{A}) = \{x \in X \mid \mu_{\tilde{A}}(x) > 0\}$, refer to Figure 1.
- The *core* of a normal fuzzy set \tilde{A} is the crisp set that contains all the elements of X that have the membership grades of one in \tilde{A} , i.e., $\text{core}(\tilde{A}) = \{x \in X \mid \mu_{\tilde{A}}(x) = 1\}$, refer to Figure 1.
- The *boundary* is the crisp set that contains all the elements of X that have the membership grades of $0 < \mu_{\tilde{A}}(x) < 1$ in \tilde{A} , i.e., $\text{boundary}(\tilde{A}) = \{x \in X \mid 0 < \mu_{\tilde{A}}(x) < 1\}$, refer to Figure 1.
- Having two fuzzy sets \tilde{A} and \tilde{B} based on X , then both are *similar* if $\text{core}(\tilde{A}) = \text{core}(\tilde{B})$ and $\text{support}(\tilde{A}) = \text{support}(\tilde{B})$.
- If the support of a normal fuzzy set consists of a single element x_0 of X , which has the property $\text{support}(\tilde{A}) = \text{core}(\tilde{A}) = \{x_0\}$, this set is called a *singleton*.

- A fuzzy set \tilde{A} is said to be a *convex* fuzzy set if for any elements x, y and z in fuzzy set \tilde{A} , the relation $x < y < z$ implies that $\mu_{\tilde{A}}(y) \geq \min[\mu_{\tilde{A}}(x), \mu_{\tilde{A}}(z)]$. The intersection of two convex fuzzy sets is also a convex fuzzy set, i.e., if \tilde{A} and \tilde{B} are *convex* fuzzy sets, then $\tilde{A} \cap \tilde{B}$ is also convex fuzzy set.
- If \tilde{A} is convex single-point normal fuzzy set defined on the real line, then \tilde{A} is often termed as a *fuzzy number*.
- Any fuzzy set \tilde{A} defined on a universe X is a *subset* of that universe.

Various Types of Fuzzy Membership Function and its Mathematical Representation

The The common types of membership function (MF) used in FRBM are triangular, (higher order) polynomial, trapezoidal, Gaussian, etc.

Triangular MF: Mathematically a triangular MF can be represented by Equation (1) as follows (Figure 2(a)):

$$\mu_{\tilde{A}}(x, a, b, c, d) = \begin{cases} 0 & x \leq a \\ \frac{x-a}{b-a} & a \leq x \leq b \\ \frac{c-x}{c-b} & b < x < c \\ 0 & c \leq x \end{cases} \quad \text{for} \quad \begin{cases} x \leq a \\ a \leq x \leq b \\ b < x < c \\ c \leq x \end{cases} \quad (1)$$

Trapezoidal MF: Mathematically a trapezoidal MF can be represented by Equation (2) as follows (Figure 2(b)):

$$\mu_{\tilde{A}}(x, a, b, c, d) = \begin{cases} 0 & x < a, x > d \\ \frac{x-a}{b-a} & a \leq x \leq b \\ 1 & b < x < c \\ \frac{d-x}{d-c} & c \leq x \leq d \end{cases} \quad \text{for} \quad \begin{cases} x < a, x > d \\ a \leq x \leq b \\ b < x < c \\ c \leq x \leq d \end{cases} \quad (2)$$

The controlling parameters towards the configuration of trapezoidal MF (as shown in Figure 2(b)) are $b_1=b-a$, $b_2=c-b$ and $b_3=d-c$.

Polynomial MF: A polynomial MF can be expressed mathematically by Equation (3) as follows (Figure 2(c)):

$$\mu_{\tilde{A}}(x, a, b, c, d) = \begin{cases} 0 & x < a, x > c \\ f_1(x, b_1) & a \leq x < b \\ 1 & x = b \\ f_2(x, b_2) & b < x \leq c \end{cases} \quad \text{for} \quad \begin{cases} x < a, x > c \\ a \leq x < b \\ x = b \\ b < x \leq c \end{cases} \quad (3)$$

where the functions f_1 and f_2 are the polynomial type. Polynomial MF is treated as triangular type MF when the functions, f_1 and f_2 of the above empirical expression are linear. f_1 and f_2 may be also exponential or any other kind of functions.

The controlling parameters towards the configuration of polynomial MF (as shown in Figure 2(b)) are $b_1=b-a$ and $b_2=c-b$. Mathematically, the second order polynomial function can be represented as $\mu_{\tilde{A}}(x) = c_0x + c_1x^2$, where x is the distance measured along the base-width of membership function distributions, $\mu_{\tilde{A}}(x)$ is the fuzzy membership function value and, c_0 and c_1 are the coefficients which can be determined based on some specified conditions, such as

$$\mu_{\tilde{A}} = \begin{cases} 1 \text{ at } x = b_1 \\ 0 \text{ at } x = 0 \end{cases} \text{ and } \frac{\partial \mu_{\tilde{A}}}{\partial x} = 0, \text{ at } x = b_1,$$

Finally the coefficients of the 2nd order polynomial function become $c_0 = \frac{2}{b_1}$ and $c_1 = -\frac{1}{b_1^2}$

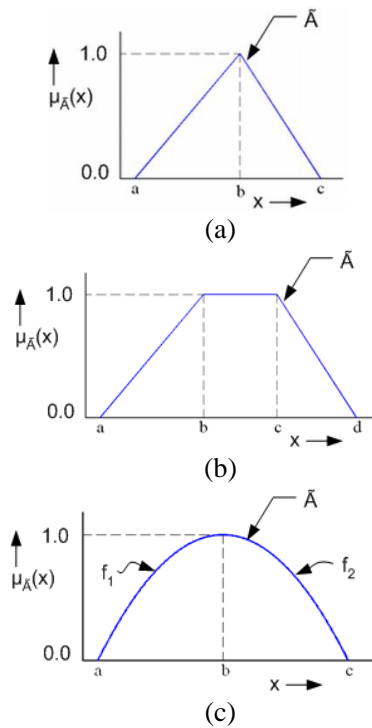


Figure 2. Membership function configuration (a) Triangular (b) Trapezoidal (c) Polynomial.

From the Figure 2, it has been seen that for a given value of support of the membership function of a fuzzy set, only one parameter, b_1 is required to describe triangular and polynomial type MFDs (membership function distributions) with 3 fuzzy sub-sets, whereas two parameters, b_1 and b_2 are required to explain the (semi) trapezoidal MFDs with two fuzzy

sub-sets. The number of controlling parameter increases with increasing the number of fuzzy sub-sets involved in the MFDs.

Fuzzy Set Operator

Defining the fuzzy sets \tilde{A} and \tilde{B} on the universe X , for a given element x of the universe, the fuzzy set operations, intersection (t-norm), union (t-conorm) and complement are expressed as follows and the corresponding Venn diagrams are shown in Figure 3.

- Intersection: $\mu_{\tilde{A} \cap \tilde{B}}(x) = \mu_{\tilde{A}}(x) \wedge \mu_{\tilde{B}}(x)$
- Union: $\mu_{\tilde{A} \cup \tilde{B}}(x) = \mu_{\tilde{A}}(x) \vee \mu_{\tilde{B}}(x)$
- Complement: $\mu_{\tilde{A}^c}(x) = 1 - \mu_{\tilde{A}}(x)$

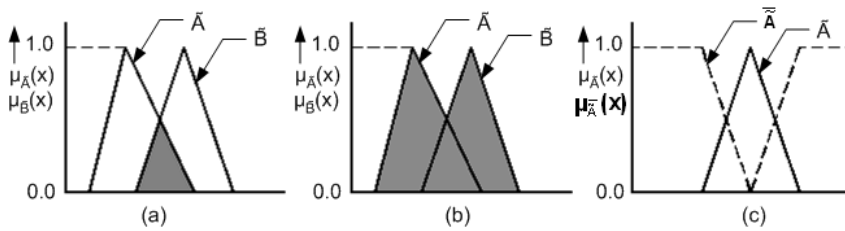


Figure 3. (a) Intersection of fuzzy sets \tilde{A} and \tilde{B} (b) Union of fuzzy sets \tilde{A} and \tilde{B} (c) Complement of fuzzy set \tilde{A} .

Classical Logical Operations and Fuzzy Logical Operations

Classical logic deals with classical proposition (P) which is a collection of elements, that is, a set, where all the truth values, $T(P)$ for all elements in the set are either all true (1) or all false (0), and follows the two-valued logical operations and Boolean algebra.

Let the sets A and B are defined from universe X and the proposition, P measures the truth of the statement that an element, x from the universe X is contained in set, A and Q measures the truth of the statement that this element, x is contained in set, B , i.e., if $x \in A, T(P) = 1$; otherwise $T(P) = 0$ and if $x \in B, T(Q) = 1$; otherwise $T(Q) = 0$. There are five logical connectives (defined as follows) used to combine multiple simple propositions and to form new propositions:

- Disjunction (OR): $P \vee Q: x \in A \text{ or } x \in B, \text{ Hence, } T(P \vee Q) = \max(T(P), T(Q))$
- Conjunction (AND): $P \wedge Q: x \in A \text{ or } x \in B, \text{ Hence, } T(P \wedge Q) = \min(T(P), T(Q))$
- Negation: If $T(P) = 1$, then $T(\bar{P}) = 0$; if $T(P) = 0$, then $T(\bar{P}) = 1$
- Implication: $P \rightarrow Q: x \notin A \text{ or } x \in B, \text{ Hence, } T(P \rightarrow Q) = T(\bar{P} \cup Q)$
- Equivalence: $(P \leftrightarrow Q): T(P \leftrightarrow Q) = \begin{cases} 1 \text{ for } T(P) = T(Q) \\ 0, \text{ for } T(P) \neq T(Q) \end{cases}$

For two different universes of discourse where P is a proposition described by set A, which is defined on universe X, and Q is a proposition described by set B, which is defined on universe Y. Then the implication $P \rightarrow Q$ (which is also equivalent to the linguistic rule form, IF A THEN B) can be represented in set-theoretic terms by the relation, R which is defined by

$$R = (A \times B) \cup (\bar{A} \times Y) \equiv \text{IF } A, \text{ THEN } B$$

IF $x \in A$, where $x \in X$ and $A \subset X$
 THEN $y \in B$, where $y \in Y$ and $B \subset Y$

The other connectives are applicable to two different universes of discourse as usual. Classical logical compound propositions that are always true irrespective of the truth values of the individual simple propositions are called tautologies.

Fuzzy propositional logic generalizes the classical propositional operations by using the truth set (0, 1) instead of either 1 or 0. The above logical connectives are also defined for a fuzzy logic. Like classical logic, the implication connective in fuzzy logic can be modeled in rule-based form: $\tilde{P} \rightarrow \tilde{Q}$ is, IF x is \tilde{A} THEN y is \tilde{B} (where IF part is called *antecedent* and THEN part is called *consequent*) and it is equivalent to the fuzzy relation $\tilde{R} = (\tilde{A} \times \tilde{B}) \cup (\bar{\tilde{A}} \times Y)$ where the fuzzy proposition \tilde{P} is assigned to fuzzy set \tilde{A} which is defined on universe X, and the fuzzy proposition \tilde{Q} is described by fuzzy set \tilde{B} , which is defined on universe Y. The membership function of \tilde{R} is expressed by $\mu_{\tilde{R}}(x,y) = \max[\mu_{\tilde{A}}(x) \wedge \mu_{\tilde{B}}(y), (1 - \mu_{\tilde{A}}(x))]$. The implication connective can be defined in several distinct forms. While these forms of implication are equivalent in classical logic, their extensions to fuzzy logic are not equivalent and result in distinct classes of fuzzy implications.

Fuzzy Implication Methods

The fuzzy implication operation is used to find the fuzzy relation \tilde{R} between two fuzzy sets \tilde{A} and \tilde{B} which are defined on the universes of discourse X and Y, respectively based on the rule IF x is \tilde{A} , THEN y is \tilde{B} , where $x \in X$ and $y \in Y$. Mathematically, the fuzzy relation, \tilde{R} is defined as $\tilde{R}(x,y) = \wp[A(x), B(y)]$, where \wp is called the implication operator. Besides the implication method as presented in Section 2.6, there are other forms of implication operator, among them *min* and *product* implication operators are mostly used in fuzzy inference system for practical applications.

The membership function values of fuzzy relation \tilde{R} defined on the Cartesian product space $X \times Y$ using min and product implication operators are obtained by the Equation (4) and Equation (5), respectively and graphically represented in Figure 4.

$$\text{min: } \mu_{\tilde{R}}(x,y) = \min[\mu_{\tilde{A}}(x), \mu_{\tilde{B}}(y)] \quad (4)$$

$$\text{product: } \mu_{\tilde{R}}(x,y) = \mu_{\tilde{A}}(x) \bullet \mu_{\tilde{B}}(y) \quad (5)$$

In Figure 4, the MF value, 0.7 of $\mu_{\tilde{B}}(x)$ corresponds to rule weight obtained after decomposition of the IF part of rule.

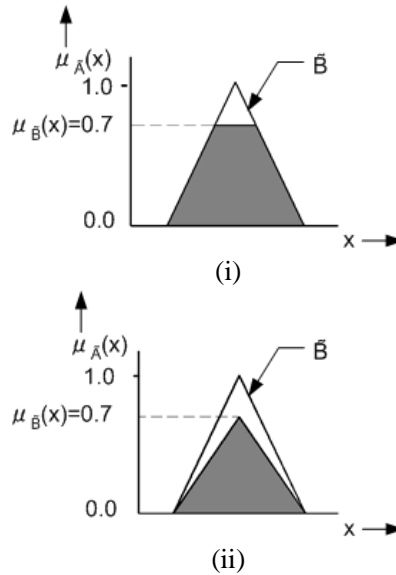


Figure 4. Graphical representation of fuzzy implication (i) min (ii) product.

Decomposition of Compound Rules

The most common techniques for decomposition of compound linguistic rules into simple canonical forms are described as follows:

Multiple conjunctive antecedents: IF x is \tilde{A}_1 AND x is \tilde{A}_2 ... AND x is \tilde{A}_L THEN y is \tilde{B}_S
 This fuzzy rule can be written in canonical form as: IF \tilde{A}_S THEN \tilde{B}_S .

Where the fuzzy subset \tilde{A}_S is defined as $\tilde{A}_S = \tilde{A}_1 \cap \tilde{A}_2 \cap \dots \cap \tilde{A}_L$ with the membership function $\mu_{\tilde{A}_S}(x) = \min[\mu_{\tilde{A}_1}(x), \mu_{\tilde{A}_2}(x), \dots, \mu_{\tilde{A}_L}(x)]$ obtained by the definition of the fuzzy intersection operation.

Multiple disjunctive antecedents: IF x is \tilde{A}_1 OR x is \tilde{A}_2 ... OR x is \tilde{A}_L THEN y is \tilde{B}_S .

Assuming a new fuzzy subset \tilde{A}_S (as $\tilde{A}_S = \tilde{A}_1 \cup \tilde{A}_2 \cup \dots \cup \tilde{A}_L$) expressed by means of membership function $\mu_{\tilde{A}_S}(x) = \max[\mu_{\tilde{A}_1}(x), \mu_{\tilde{A}_2}(x), \dots, \mu_{\tilde{A}_L}(x)]$ based on the definition of the fuzzy union operation, the compound rule may be written in canonical form as: IF \tilde{A}_S THEN \tilde{B}_S .

Aggregation of Rule

The technique of obtaining the overall rule consequent by combining the individual consequents contributed by each rule in the rule base (which comprises multiple rules) is known as aggregation of rules. The most popular aggregation techniques of fuzzy rules are as follows:

Conjunctive system of rules (MIN): In the case of a system of rules that must be jointly satisfied, the rules are connected by AND connectives. In this case, the aggregated consequent, y is obtained by fuzzy intersection of all individual rule consequents (y_1, y_2, \dots, y_r), as $y = y_1 \cap y_2 \cap \dots \cap y_r$ which is defined by the membership function:

$$\mu_y(y) = \min[\mu_{y_1}(y), \mu_{y_2}(y), \dots, \mu_{y_r}(y)] \text{ for } y \in Y.$$

Disjunctive system of rules (MAX): For the case of a disjunctive system of rules where the satisfaction of at least one rule is required, the rules are connected by the OR connectives. In this case, the aggregated consequent, y is obtained by fuzzy union of the individual rule consequents as $y = y_1 \cup y_2 \cup \dots \cup y_r$ which is defined by the membership function:

$$\mu_y(y) = \max[\mu_{y_1}(y), \mu_{y_2}(y), \dots, \mu_{y_r}(y)] \text{ for } y \in Y.$$

Composition Technique of Fuzzy Relation

Let R and S are the relations that relate elements from universe X to universe Y , and elements from universe Y to universe Z , respectively. Now, composition is an operation to find another relation, T that relates the same elements in universe X that R contains to the same elements in universe Z that S contains.

The composition operation of fuzzy relation reflects the inference of a fuzzy rule based system and is expressed by $\tilde{B} = \tilde{A} \circ \tilde{R}$, where \tilde{A} is the input, or antecedent defined on the universe X , \tilde{B} is the output or consequent defined on universe Y and \tilde{R} is a fuzzy relation characterizing the relationship between specific input(s), x and specific output(s), y . Among various methods of composition of fuzzy relation, max-min and max-product are the most commonly used techniques and defined by membership function-theoretic expressions as follows.

$$\text{max-min: } \mu_{\tilde{B}}(y) = \max_{x \in X} \{ \min[\mu_{\tilde{A}}(x), \mu_{\tilde{R}}(x, y)] \} \quad (6)$$

$$\text{max-product: } \mu_{\tilde{B}}(y) = \max_{x \in X} [\mu_{\tilde{A}}(x) \bullet \mu_{\tilde{R}}(x, y)] \quad (7)$$

The method of composition of fuzzy relation basically includes the implication method and technique of aggregation of fuzzy rule.

In the above methods of composition of fuzzy relation, max is the aggregation technique of rule, whereas min and product are the implication methods used in Equation (6) and Equation (7), respectively.

Fuzzy Inference System

Inference is a process of combining the measurement of input(s)/antecedent(s) with one or more relevant fuzzy rules in a proper manner to infer the output(s)/consequent(s). Figure 5 describes the layout of a fuzzy inference system.

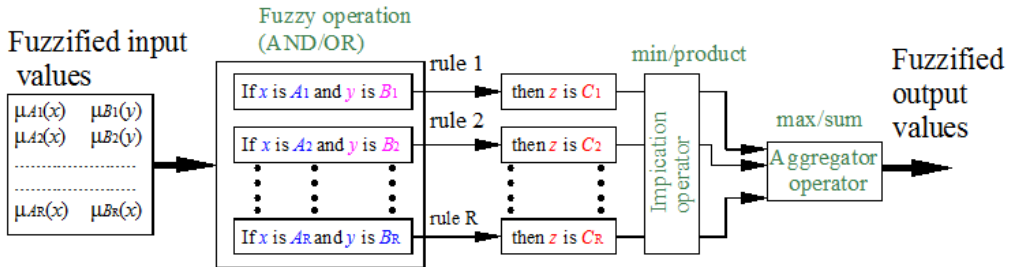


Figure 5. Layout of a fuzzy inference system.

In order to demonstrate the inference method, let consider a system of one input (antecedent) and a single output (antecedent) described by two IF-THEN rules as follows:

Rule 1: if input1 is \tilde{A}_1 , then output1 is \tilde{B}_1

Rule 2: if input1 is \tilde{A}_2 , then output1 is \tilde{B}_2

Now given the IF-THEN rules (Rule 1 and Rule 2) and a fact/measurement “Input1 is \tilde{A} ” it is inferred that “output1 is \tilde{B} ”, where $\tilde{A}, \tilde{A}_1 \in F(\chi)$ and $\tilde{B}, \tilde{B}_1 \in F(Y)$, where $F(\chi)$ and $F(Y)$ denote the sets of all ordinary fuzzy sets that can be defined within the X and Y , respectively. χ and Y are the sets of values (x and y) of variables, input1 (condition variable) and output1 (action variable), respectively. In order to determine B , method of interpolation is used which consists of two steps explained as follows:

Step 1: Calculate the *degree of consistence*, $r_j(x)$ between the given fact/measurement and the antecedent of each rule, j in terms of the *height* of intersection of the associated sets \tilde{A}_1 and \tilde{A} . $r_j(x)$ is expressed using the standard fuzzy intersection and the definition of height of a fuzzy set (described in Section 2.3) as follows:

$$r_j(x) = \max_{x \in X} \min [\mu_{\tilde{A}}(x), \mu_{\tilde{A}_j}(x)], \quad j=1, 2 \quad (8)$$

Step 2: Calculate the conclusion \tilde{B} by truncating each set \tilde{B}_j by the value of $r_j(x)$ (i.e., *min* implication method) which expresses the degree to which the antecedent \tilde{A}_j is compatible with the given fact \tilde{A}_1 , and taking the union of the truncated sets as the rules are satisfied independently (i.e., *max* aggregation method).

$$\mu_{\tilde{B}}(y) = \max_{j=1,2} \min [r_j(x), \mu_{\tilde{B}_j}(y)] \quad \text{for all } y \in Y \quad (9)$$

The above steps are graphically presented in Figure 6.

$$\begin{aligned}
 \text{Now, } \mu_{\tilde{B}}(y) &= \max_{j=1,2} \min[r_j(x), \mu_{\tilde{B}_j}(y)] \\
 &= \max_{j=1,2} \min \left[\max_{x \in X} \min(\mu_{\tilde{A}_j}(x), \mu_{\tilde{A}_j}(x)), \mu_{\tilde{B}_j}(y) \right] \\
 &= \max_{j=1,2} \max_{x \in X} [\min(\mu_{\tilde{A}_j}(x), \mu_{\tilde{A}_j}(x)), \mu_{\tilde{B}_j}(y)] \\
 &= \max_{x \in X} \max_{j=1,2} \min \left[\mu_{\tilde{A}}(x), \min(\mu_{\tilde{A}_j}(x), \mu_{\tilde{B}_j}(y)) \right] \\
 &= \max_{x \in X} \min \left[\mu_{\tilde{A}}(x), \max_{j=1,2} \min(\mu_{\tilde{A}_j}(x), \mu_{\tilde{B}_j}(y)) \right] \\
 &= \max_{x \in X} \min[\mu_{\tilde{A}}(x), \mu_{\tilde{R}}(x,y)], \tag{10}
 \end{aligned}$$

which is equivalent to the expression of max-min composition presented in Equation (6) and accordingly, this inference method is also called max-min inference method. In the above step 2, if *product* implication technique and *max* aggregation method are used, we can obtain the expression (defined in Equation 10) similar to max-product composition (Equation (7)). Moreover, the above inference method may also be applicable to the system with any number of fuzzy rule (j) and inputs (Input1, input2). In case of multiple inputs/antecedents of fuzzy rule, the (effective) *degree of consistence*, $r_j(x)$ between the given facts/measurements and the antecedents of each rule is obtained by first finding the *degree of consistence* between each fact/measurement and the related antecedent of the rule (using Equation (8)), then adopting the technique of decomposition of compound rules according to the type of logical connectives (AND or OR) as explained graphically in Figure 7 for the following two IF-THEN rules as follows:

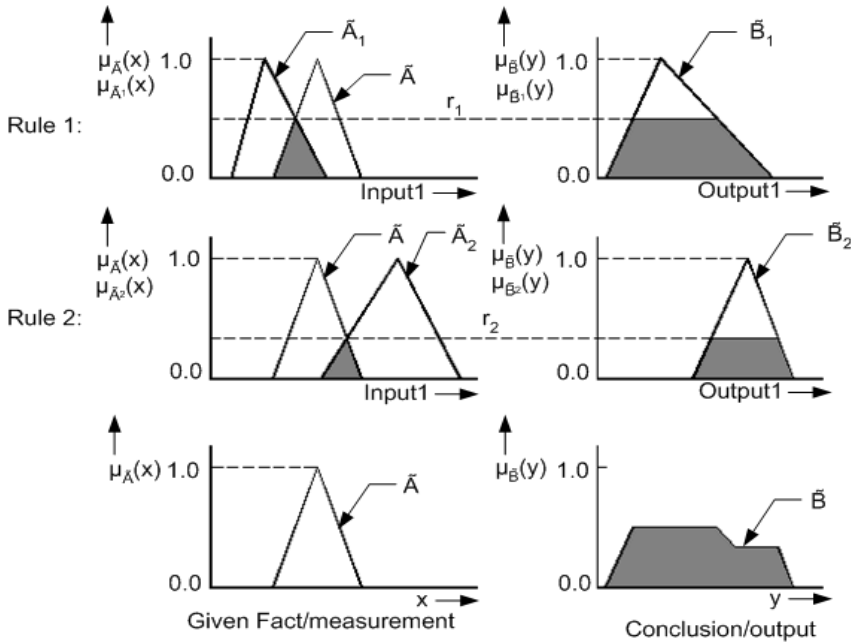


Figure 6. Illustration of the method of interpolation in fuzzy inferences.

Rule 1: if input1 is \tilde{A}_{11} AND input2 is \tilde{A}_{12} then output1 is B_1
 Rule 2: if input1 is \tilde{A}_{21} AND input2 is \tilde{A}_{22} then output1 is B_2
 Fact: input1 is \tilde{A}_1 AND input2 is \tilde{A}_2
 Conclusion: output1 is B

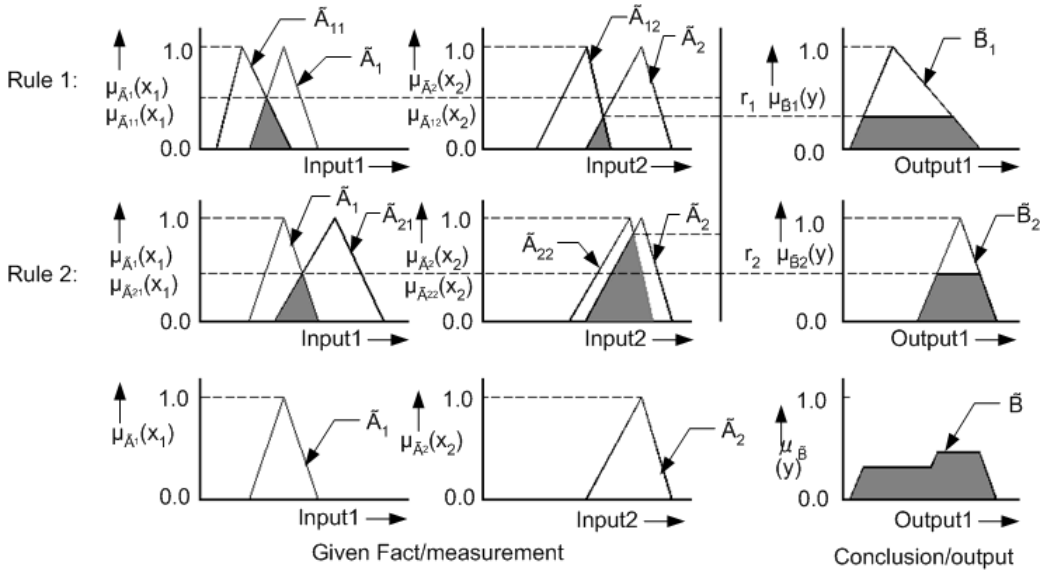


Figure 7. Illustration of the method of interpolation in fuzzy inferences with multiple inputs.

In the above illustration of fuzzy inference, we have considered fuzzy value (\tilde{A}) for the variable input1.

Figure 8 demonstrates the above (max-min) inference method for a two input and a single output system where the values of input variables are considered as crisp type (for instance, Fact: input1 is x_1 AND input2 is x_2) and the (max-product) inference method for the same system is demonstrated in Figure 9.

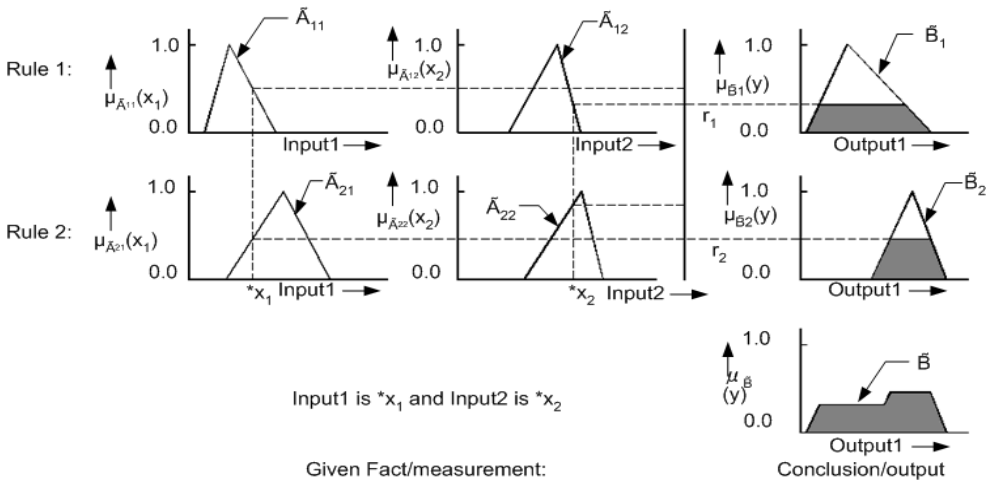


Figure 8. Graphical representation of max-min inference method with crisp type of input values.

Fuzzification and De-Fuzzification

L fuzzification is a process of transforming the crisp value into a grade of membership using a membership function of the associated fuzzy set as shown in Figure 10. Figure 10 demonstrates that the given (crisp) value x_0 of variable x belongs to a grade of $\mu_{\tilde{A}_1}(x_0)=0.8$ to the fuzzy set \tilde{A}_1 and with a grade of $\mu_{\tilde{A}_2}(x_0)=0.2$ to the fuzzy set \tilde{A}_2 . Fuzzification is required in the fuzzy inference system when the values of input variables to system are considered as crisp type (as described in Figure 8 and Figure 9).

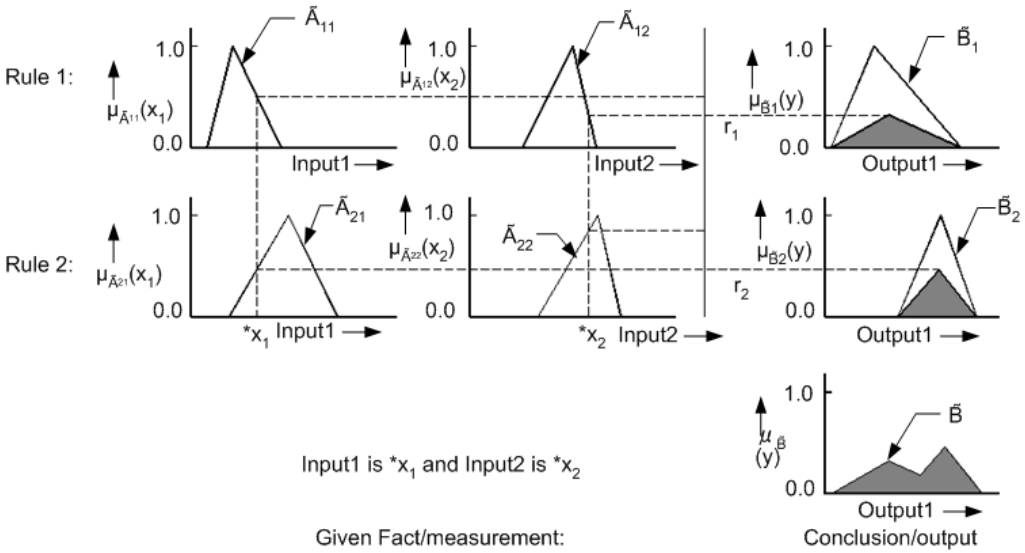


Figure 9. Graphical representation of max-product inference method with crisp type of input values.

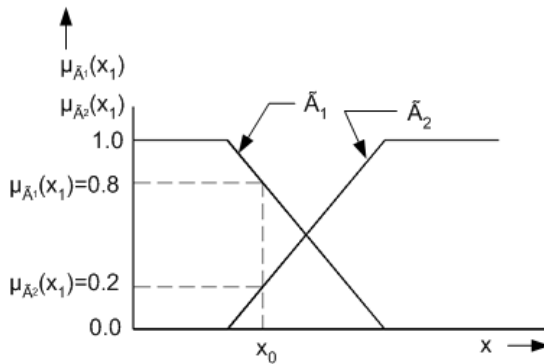


Figure 10. Fuzzification method.

Defuzzification is the conversion of a fuzzy quantity to a crisp quantity analogous to fuzzification. Defuzzification is used in fuzzy inference system to convert the fuzzy value of the output (i.e., \tilde{B} of output1 in Section 2.11) to a crisp value ($*y$). Among various defuzzification methods available in the literature, centroid method (also called centre of area (COA) or centre of gravity) is most popular, which is mathematically expressed by Equation (11) and graphically expressed in Figure 11.

$$y_{COA} = \frac{\int \mu_{\tilde{B}}(y) \cdot y dy}{\int \mu_{\tilde{B}}(y) dy} \quad (11)$$

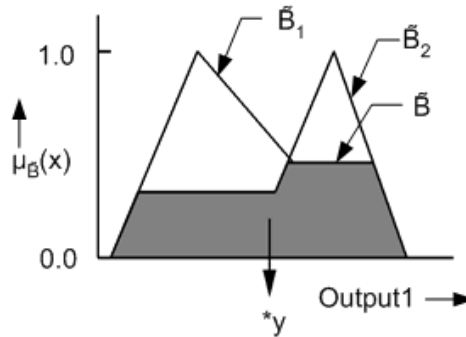


Figure 11. Centroid defuzzification methoded.

GENETIC ALGORITHM

Genetic algorithm is a search and optimization technique which mimics the principle of natural selection and natural genetics (Goldberg, 1989) to find the best solution for a specific problem.

Genetic algorithms operate on a population of feasible solutions by applying the principle of survival of the fittest to produce better approximations to a solution. At each generation, a new set of approximations is created by the process of selecting individuals according to their level of fitness in the problem domain and breeding them together using operators borrowed from natural genetics. This process leads to the evolution of populations of individuals that are better suited to their environment than the individuals that they were created from, just as in natural adaptation.

Coding and Initialization of GA

Binary Coding

The most commonly used representation of chromosomes in the GA is that of the single-level binary string. Here, each decision variable (say, d and h) in the parameter set is encoded as a binary string (s_d and s_h , respectively) and these are concatenated to form a chromosome as shown in Figure 12. Binary-coded GAs are not restricted to use only integer and for the given lower bound (d_{\min}) and upper bound (d_{\max}) of a variable (say, d), the value of the variable (d) is calculated from the GA-string using the decoding scheme represented by Equation (12).

$$d = d^{\min} + \frac{d^{\max} - d^{\min}}{2^{l_d} - 1} DV(s_d) \quad (12)$$

where l_d is the string length used to code the d variable and $DV(s_d)$ is the decoded value of the string s_d . This mapping function allows:

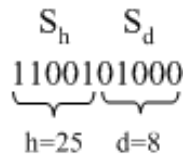


Figure 12. A schematic representation of a chromosome with 5 bits for S_d and 5 bits for S_h .

Real Coding

For a continuous search space, binary-coded GA faces many problems such as

- Hamming cliffs associated with certain strings (e.g., 01111 and 10000) from which a transition to a neighboring solution requires the alteration of many bits.
- Inability to achieve any arbitrary precision in the optimal solution. The more the required precision, the larger is the string length, results more computational complexity

In real coding, the variables are directly represented in real type as $\frac{25}{h} \frac{8}{d}$.

Initialization of GA

Initial population of a GA is normally determined at random. With a binary population of N_{ind} individuals whose chromosomes are L_{ind} bits long, $N_{ind} \times L_{ind}$ random numbers uniformly distributed from the set $\{0, 1\}$ would be produced.

Objective Function and Fitness Function

The objective function is used to provide an analytical measure of how individuals have performed in the problem domain. The objective function, f is a function of decision variable(s). The fitness value of an individual/solution in the population is determined based on the fitness function which consists of the objective function value and the penalty value for constraint violation which is determined by a penalty function, $f_{constraint}$. Thus, the fitness value is calculated as follows:

$$\text{Fitness value} = f + f_{constraint}$$

Since GAs mimic the survival-of-the-fittest of the nature to make a search process, GAs are suitable for maximization problem where objective function is directly use as fitness function $F(x)$.

In the case of a minimization problem, the fit individuals will have the lowest numerical value of the associated objective function. This situation is handled using a conversion of the objective function into an equivalent maximization problem and used as fitness function so that the optimum point remain unchanged.

Selection

Selection guides the tool to find the optimized solution by preferring individuals/members of the population with higher fitness over one with lower fitness. It is the operator which generates the mating pool. This operator determines that the number of times a particular individual will be used for reproduction and the number of offspring that an individual will produce. Some of the popularly used selection methods are as follows:

Roulette Wheel Selection Methods: Roulette wheel selection scheme chooses a certain individual with a probability proportional to its fitness as shown in Equation (13).

$$p[I_{j,t}] = \frac{f(I_{j,t})}{\sum_{k=1}^n f(I_{k,t})} \quad (13)$$

where $p[I_{j,t}]$ is the probability of getting selected of any j^{th} individual at a generation t , $f(I_{j,t})$ and $\sum_{k=1}^n f(I_{k,t})$ are corresponding individual fitness and the sum of the fitness of the population with size n , respectively.

The property as represented by Equation (13) is satisfied by applying a random experiment that has some similarity with a generalized roulette game. In the roulette game, the slots are not equally wide, that is why different outcomes occur with different probabilities. Figure 13 gives a graphical representation of how this roulette wheel game works.

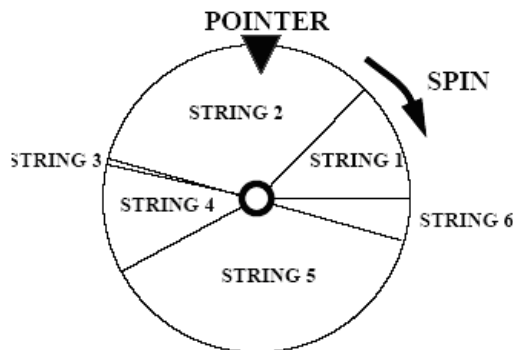


Figure 13. Graphical representation of the Roulette wheel selection mechanism.

Linear rank selection: In this plan, a small group of individuals is taken from the population and the individual with best fitness is chosen for reproduction. The size of the group chosen is called the tournament size. A tournament size of two is called binary tournament.

In addition another scheme for selection is applied along with all three selection schemes discussed above which is called ‘elitism’. The idea of elitism is to avoid the observed best-fitted individual dies out just by selecting it for the next generation without any random experiment. Elitism significantly influences the speed of the convergence of a GA. But it can lead to premature convergence also.

Crossover

The basic operator for producing new chromosomes in the GA is that of crossover or called recombination. Like natural reproduction, crossover produces new individuals so that some genes of a new child come from one individual while others comes from the other individual. In essence, crossover is the exchange of genes between the chromosomes of the two parents. The process may be described as cutting two strings at a randomly chosen position and swapping the two tails. It is known as the single-point crossover, and the mechanism is visualized in Figure 13. An integer position, i is selected at random with a uniform probability between one and the string length, l , minus one (i.e., $i \in (1, l-1)$). When the genetic information is exchanged among the parent individuals (represented by the strings, P_1 and P_2) about this point, two new offspring (represented by the strings, O_1 and O_2) are produced. The two offspring in Figure 14 are produced when the crossover point, $i=4$ is selected.

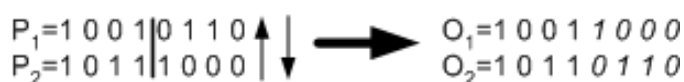


Figure 14. A typical example of single point crossover.

For multi-point crossover, multiple crossover positions (m) are chosen at random with no duplicates and sorted into ascending order. Then the bits between two successive crossover points are exchanged between the two parents to produce two new offspring. The process of multi-point crossover is illustrated in Figure 15 with shaded color.



Figure 15. Typical example of multi-point crossover (with $m=5$).

The idea behind multi-point crossover is that the parts of the chromosome representation that contribute to the most to the performance of a particular individual may not necessarily be contained in adjacent substrings. Further, multi-point crossover appears to encourage the exploration of the search space, thus making the search more robust.

Mutation

Mutation is nothing but deformation of the genetic information of an individual (solution) by means of some external influences. The bit-wise mutation operator changes a bit, 1 to 0, and vice versa, with a prescribed probability (called, mutation probability) as shown in Figure 16. In real reproduction, the probability that a certain gene is mutated is almost equal for all genes. So, it is near at hand to use the mutation technique for a given binary string, where there is a given probability that a single gene is modified. The probability should be rather low in order to avoid chaotic behavior of the GA.

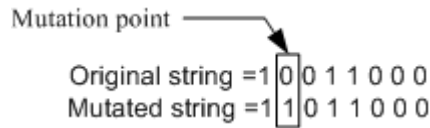


Figure 16. Mutation effect on offspring's strings.

Termination of GA

Because the GA is a stochastic search method, it is difficult to formally specify convergence criteria. As the fitness of a population may remain static for a number of generations before a superior individual is found, the application of conventional termination criteria becomes problematic. A common practice is to terminate the GA after a pre-specified number of generations and then test the quality of the best members of the population against the problem definition. If no acceptable solutions are found, the GA may be restarted or a fresh search can be initiated. Attaining a pre-specified fitness function value or when best fitness of the population does not change appreciably over successive iterations may be also considered as a termination criteria.

Description of Working Principle of GA

The working principle of a (binary-coded) GA is described here with an engineering optimization problem, namely designing a can (Deb, 2001), as shown in Figure 17. The objective of the problem is to determine the optimum values of the diameter (d , in cm) and height (h , in cm) of the can in order to minimize its cost, $f(d, h)$ subject to some constraints and the problem is defined as follows:

$$\text{Minimize } f(d, h) = c \left(\frac{\pi d^2}{2} + \pi dh \right), \quad (14)$$

Subject to

$$g(d, h) = \frac{\pi dh^2}{4} \geq 300,$$

$$\begin{aligned} d_{\min} &\leq d \leq d_{\max} \\ h_{\min} &\leq h \leq h_{\max} \end{aligned},$$

where c is the cost of the can material per square cm, which is taken as 0.005 and the minimum and maximum values of d and h are taken as, $d_{\min}=h_{\min}=0$ and $d_{\max}=h_{\max}=31$.

Therefore, in this problem the number of decision variables is two (d and h). The population size of GA is considered as six and it is kept constant throughout the GA-operation. GA operates in a number of iterations until a specified termination criterion is satisfied and in the Figure 17, the maximum number of iteration/generation (i.e., max_gen) is treated as the termination criteria.

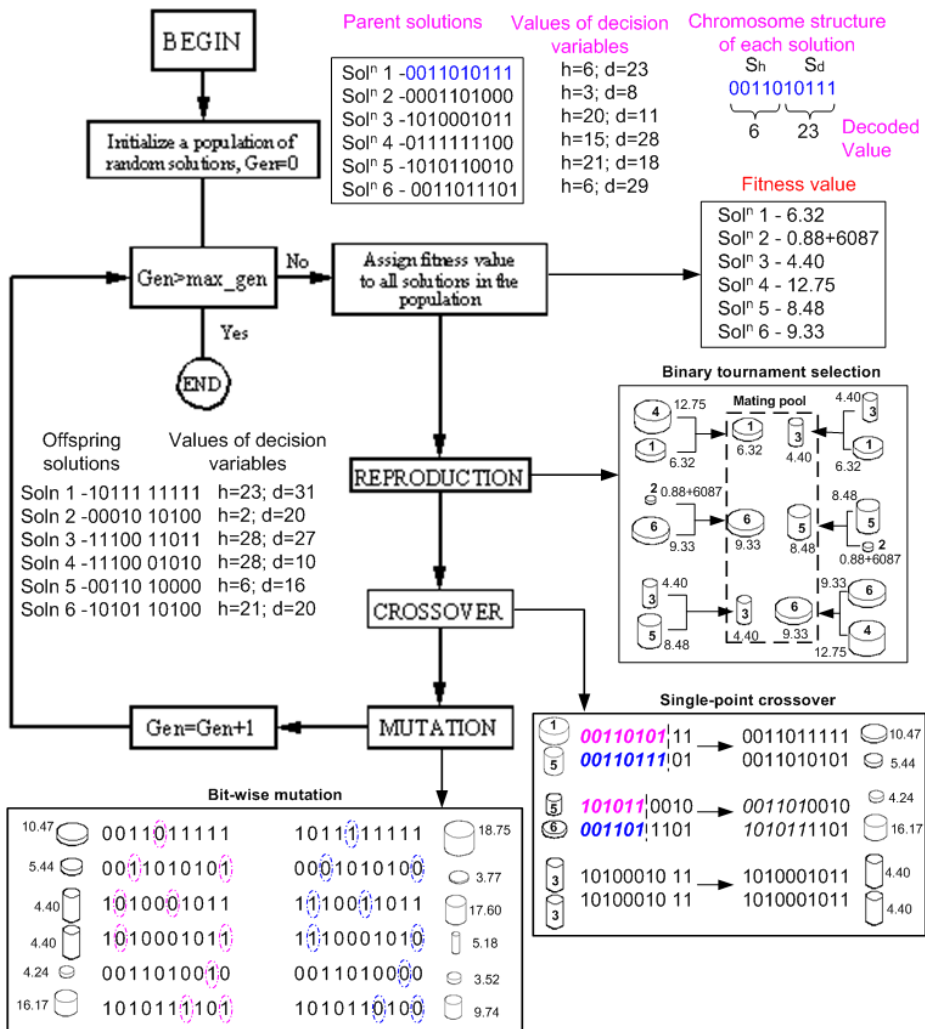


Figure 17. Working principle of a genetic algorithm..

GA iteration starts with the creation of six random solutions which are treated as the parent solutions. The chromosome structure of each solution is the same as presented in Figure 12. The real values of decision variables are calculated from the binary coded GA-string using Equation (12). Then, the fitness values of all the parent solutions in the population are calculated using following fitness function (discussed in Section 3.3).

$$\text{Fitness value} = \begin{cases} f(d,h) + P_p \times [300 - g(d,h)] & \text{if } g(d,h) \leq 300 \\ f(d,h) & \text{if } g(d,h) > 300 \end{cases} \quad (15)$$

where P_p is the penalty parameter and the value of P_p is taken as 25.

After that selection/reproduction (discussed in Section 1.3.2.3) operation is performed on the parent solutions based on the fitness values of solutions (as depicted in the binary tournament selection table in Figure 17) to form the mating pool. The number of solutions contained in the mating pool is to be equal to the number of parent solution in order to maintain a constant population size throughout the GA-iteration. After that, crossover operator (discussed in Section 3.5) is applied among the two randomly chosen solutions from the mating pool based on a given probability (crossover-probability, say 0.9). Then, bit-wise mutation (discussed in Section 3.6) is carried out on each of the six solutions obtained after employing the crossover operator using a given mutation probability (say 0.02) and produces six new (offspring) solutions.

The objective function values corresponding to each solution are depicted in the single-point crossover and bit-wise mutation tables in Figure 17. It completes one iteration/generation of GA. Now, the checking of GA-termination criterion is performed and if it satisfies the termination criteria, stop the GA-iteration process, otherwise starts another generation/iteration with treating the six offspring solutions obtained in the previous iteration as the parent solutions and then assigning fitness value to all the solutions in the population and continue the same iteration procedure as described above.

FUZZY RULE BASED MODEL

Working Principle of a Fuzzy Rule Based Model

A fuzzy rule base, a fuzzy inference engine, fuzzification, and de-fuzzification: these are the four modules involved in a FRBM (Fuzzy rule based model). Figure 18 shows a schematic diagram explaining the working cycle of a FRBM. The following steps are involved in the working cycle of a FRBM:

- The output(s) (action) and input(s) (condition) variables needed to control a particular process are chosen and measurements are taken of all the condition variables.
- The measurements taken in the previous steps are converted into appropriate fuzzy sets to express measurement uncertainties (called fuzzification as described in Section 2.12).
- The fuzzified measurements are then used by the interference engine to evaluate the control rules stored in the rule base and a fuzzified output is determined (as discussed in Section 2.11).
- The fuzzified output is then converted into a single (crisp) value (called a defuzzification as illustrated in Section 2.12). The de-fuzzified value(s) represent action(s)/prediction(s) to be made by the FRBM in controlling a process.

The kernel of a FRBM that is the knowledge base (KB) is constituted by rule base, RB (a set of fuzzy logic rules) and membership functions/membership function distributions, MFDs (fuzzy subsets). Two types of fuzzy logic rules (FLRs) that are commonly used for constructing the RB of a FRBM are Mamdani-type and TSK-type. In both types of FLRs, the input variables are expressed by linguistic terms (fuzzy subsets) in the rule antecedent part. But the main difference between these two types of fuzzy rules lies in the rule consequent part. The output variable in Mamdani-type FLR is defined by linguistic term also, whereas in TSK-type FLR, it is not defined by linguistic term rather it is defined by a linear combination of the input variables. The shape of fuzzy subsets (MFDs of input-output variables) is also an important factor that is to be decided appropriately to achieve the best performance of a FRBM for a typical process.

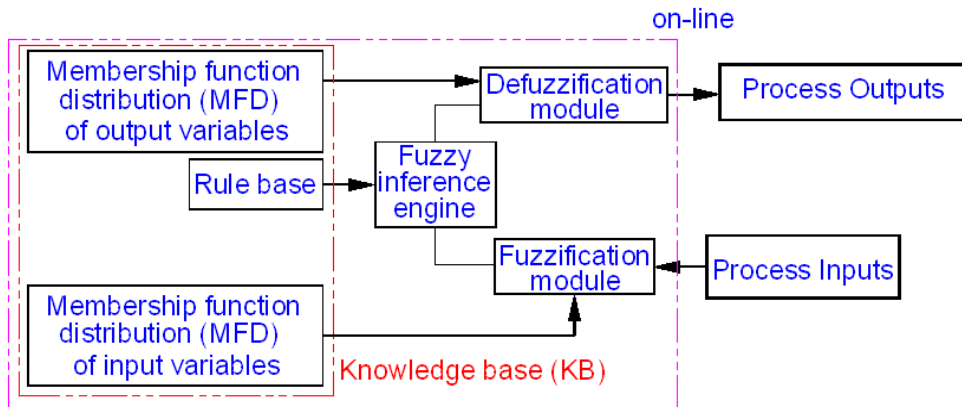


Figure 18. A schematic diagram of the working cycle of a FRBM.

Various Types of Fuzzy Rule Based Model

Mamdani-type (Mamdani & Assilian, 1975):

The structure of Mamdani-type fuzzy logic rule is expressed as follows:

IF x_1 is A_1 AND x_2 is A_2 AND.....AND x_n is A_n THEN y is B

where x_i ($i=1, 2, \dots, n$) are input variables and y is the output variable. A_1, A_2, \dots, A_n and B are the linguistic terms (say, Low, Medium, High, etc.) used for the fuzzy subsets (membership function distributions) of the corresponding input and output variables, respectively.

Sugeno-type (Sugeno & Kang, 1988):

The Sugeno-type fuzzy rule is defined as follows:

IF x_1 is A_1 AND x_2 is A_2 AND.....AND x_n is A_n THEN $y = f(x_1, x_2, \dots, x_n)$

Unlike Mamdani-type, the rule consequent/output is expressed by a function of the input variables.

Tsukamoto (Tsukamoto, 2004):

The Tsukamoto -type fuzzy rule is defined as follows:

IF x_1 is A_1 AND x_2 is A_2 AND.....AND x_n is A_n THEN $y = z$, where z is a monotonical membership function.

Mamdani-Type Fuzzy Rule Based Model

The output of a Mamdani-type FRBM whose rule base (RB) is constructed using Mamdani-type fuzzy logic rule is obtained as follows (when centroid method is considered for defuzzification):

$$Y = \frac{\sum_{r=1}^{R_f^1} A^{\alpha r} C_{A^{\alpha r}}}{\sum_{r=1}^{R_f^1} A^{\alpha r}} \quad (16)$$

where $A^{\alpha r}$ is the area of fuzzy subset of output variable, covered by α membership value (equivalent to *degree of consistence* as obtained in Step 1 in Section 2.11) that is obtained by r^{th} rule after fuzzy inference method. $C_{A^{\alpha r}}$ is the centre distance of the area, $A^{\alpha r} \cdot R_f^1$ ($R_f^1 \subseteq R_f$) is the number of rules fired out of a total of R_f rules present in the rule base for a set of input values.

In order to determine the output in Equation 16, all the four modules (fuzzy rule base, a fuzzy inference engine, fuzzification, and de-fuzzification) as mentioned in Section 4.1 are involved in a Mamdani-type FRBM. The performance of a Mamdani-type fuzzy model is relied on the appropriate fuzzy subsets of rule consequents and antecedent, and the type of fuzzy subsets (membership function distributions) considered for input-output variables. Therefore, the tasks of designing FRBMs with Mamdani-type FLRs are:

- construct of an optimal set of rules (R_f) with its appropriate outputs (B),
- selection of shape of fuzzy subsets/MFDs for both the input and output variables
- tuning of MFDs

TSK-Type Fuzzy Rule Based Model

The TSK-type fuzzy logic rule is defined as follows (Sugeno & Kang, 1988, Takagi & Sugeno, 1985):

If x_1 is A_1 and x_2 is A_2 and.....and x_n is A_n , then $y = \sum_{j=1}^K c_j f_j(x_1, \dots, x_n)$

where A_1, \dots, A_n are the fuzzy subsets of the respective input variables, x_1, \dots, x_n . The output function of fuzzy rule is a linear function (say, polynomial) in the form of

$$y = \sum_{j=1}^K c_j f_j(x_1, \dots, x_n) = c_1 f_1(x_1, \dots, x_n) + c_2 f_2(x_1, \dots, x_n) + \dots + c_k f_k(x_1, \dots, x_n) \quad (17)$$

The overall output of the TSK-type fuzzy model can be obtained for a set of inputs (x_1, x_2, \dots, x_n) using the following empirical expression.

$$Y = \frac{\sum_{r=1}^{R_f} \left(\prod_{v=1}^n \mu_v(x_v) \right) \sum_{j=1}^K c_j^r f_j^r(x_1, \dots, x_n)}{\sum_{r=1}^{R_f} \left(\prod_{v=1}^n \mu_v^r(x_1, \dots, x_n) \right)} \quad (18)$$

Π is the product representing a conjunction decomposition method. $\sum_{j=1}^K c_j^r f_j^r(x_1, \dots, x_n)$ is the output function of r^{th} rule and c_j^r are the function coefficients of the corresponding rule consequent, where K is the number of coefficients present in the consequent function of each rule.

Unlike Mamdani-type FRBM, TSK-type FRBM includes only the fuzzy rule base, a fuzzy inference engine, and fuzzification module to determine the output in Equation (18). The performance of a TSK-type fuzzy model is mainly depended on the optimal values of the rule output (consequent) functions which are depended on the coefficients (c_j), the exponential parameters of the input variables (not shown in the Equation (17)) and choice of the fuzzy subsets (membership function distributions). Thus, the steps of developing FRBM with TSK-type FLRs are:

- construction of an optimal set of rules (R_f) with the appropriate structures of rule output/consequent functions
- selection of shapes of fuzzy subsets/MFDs of input variables
- determination of optimal values of coefficients and power terms of rule consequent functions
- tuning of MFDs of the input variables.

GENETIC LINEAR REGRESSION APPROACH TO CONSTRUCT FRBM

Genetic Linear Regression (GLR) approach (Nandi, 2006) is one of the most popular GA-fuzzy approaches in designing the KB of TSK-type FRBM. In genetic linear regression (GLR) approach, the GA is introduced partly in the multiple regression method. The GLR method will take the advantages of both the regression technique and GA, and have a capability to find global optimum and good convergence properties.

In this approach, the KB of the FRBM is optimized using the combined method of linear regression (LR) approach and genetic algorithm. In this method the coefficients of output function of each rule are determined using a linear regression approach whereas the input variables' exponential parameters are simultaneously optimized using a GA. In addition to that, the MFDs are also tune using a GA. In order to accomplish this, besides the exponential

parameters of input variables, the controlling parameter(s) describing the MFDs (as discussed in Section 2.4) are considered as GA-variables. The working principle of GLR approach (as illustrated in Figure 19) consists of following four major steps:

- Step-I: Set an initial set (population) of values of power terms of a given regression function at random
- Step-II: Evaluate the function coefficients based on least square method
- Step-III: Checking of fitness value (if satisfied terminate the iteration procedure)
- Step-IV: Update the values of power terms of regression function using GA-operators and repeat Step-II

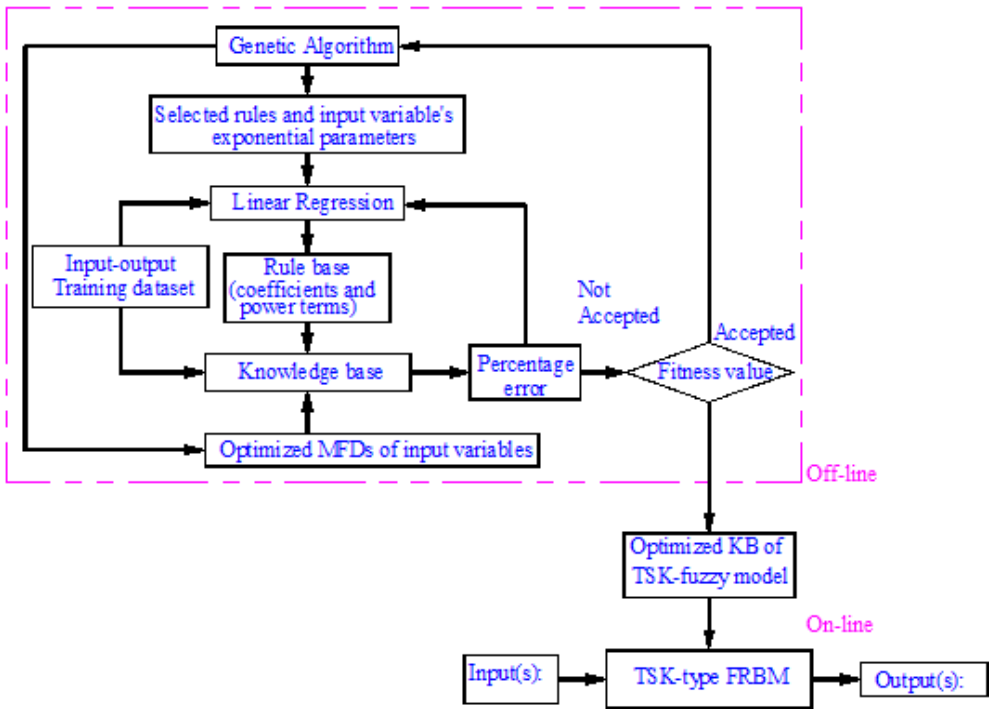


Figure 19. Flow chart of genetic linear regression approach to construct KB of a FRBM.

The GA-string of GLR approach will look as described in Figure 20.

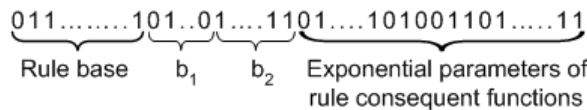


Figure 20. A GA-string representing the rule base, parameters related to membership functions of input variables and exponential parameters of rule consequent functions of a TSK-type FRBM

The proposed GLR has an added facility to carryout the task of tuning MFDs of input variables simultaneously in the same framework of GA.

In order to determine the coefficients of the output functions of TSK-type fuzzy rules, a general expression of multiple linear regression system with TSK-fuzzy model is derived as follows. The Equation (18) may be rewritten by denoting $\prod_{v=1}^n \mu_v(x_1, \dots, x_n) = \eta_r$ for simplicity, in the following form:

$$\begin{aligned}
 Y &= F(x_1, \dots, x_n) \\
 &= \frac{\sum_{r=1}^{R_f} \eta_r (a_1^r f_1^r(x_{1..n}) + a_2^r f_2^r(x_{1..n}) + \dots + a_k^r f_k^r(x_{1..n}))}{\sum_{r=1}^{R_f} \eta_r} \\
 &= \frac{\eta_1 (a_1^1 f_1^1(x_{1..n}) + \dots + a_k^1 f_k^1(x_{1..n})) + \dots + \eta_{R_f} (a_1^{R_f} f_1^{R_f}(x_{1..n}) + \dots + a_k^{R_f} f_k^{R_f}(x_{1..n}))}{\eta_1 + \eta_2 + \dots + \eta_{R_f}} \tag{19}
 \end{aligned}$$

Let us assume we have a set of input-output tuple (D) of S number of sample data where the output $y^{(i)}$ is assigned to the input $(x_1^{(i)}, x_2^{(i)}, \dots, x_n^{(i)})$

$$D = \{(x_1^{(1)}, \dots, x_n^{(1)}, y^{(1)}), (x_1^{(2)}, \dots, x_n^{(2)}, y^{(2)}), \dots, (x_1^{(s)}, \dots, x_n^{(s)}, y^{(s)})\}$$

Now, the total quadratic error that is caused by the TSK-type FLC with respect to the given data set:

$$E = \sum_{i=1}^s (f(x_1^{(i)}, x_2^{(i)}, \dots, x_n^{(i)}) - y^{(i)})^2 \tag{20}$$

In order to minimise E, we have to choose the parameters, $\{(a_1^1, \dots, a_k^1), (a_1^2, \dots, a_k^2), \dots, (a_1^{R_f}, \dots, a_k^{R_f})\}$ appropriately.

where the parameter a_j^r indicates the j th coefficient of the output function of r th rule.

To determine the above parameters, we take the partial derivatives of E with respect to the each parameter and require them to be zero, i.e., $\frac{\partial E}{\partial a_j^r} = 0$, where $j = \{1, 2, \dots, k\}$ and

$$r = \{1, 2, \dots, R_f\}$$

Now, we obtain the partial derivation of E with respect to the parameter $a_{t_j}^{tr}$,

$$\frac{\partial E}{\partial a_{t_j}^{tr}} = \sum_{i=1}^s 2 \cdot (f(x_1^{(i)}, \dots, x_n^{(i)}) - y^{(i)}) \cdot \frac{\partial f(x_1^{(i)}, \dots, x_n^{(i)})}{\partial a_{t_j}^{tr}}$$

$$\begin{aligned}
 &= 2 \cdot \sum_{l=1}^S \left(\frac{\sum_{r=1}^{R_f^l} \eta_r (a_1^r f_1^r(x_{1,\dots,n}^1) + \dots + a_k^r f_k^r(x_{1,\dots,n}^1))}{\sum_{r=1}^{R_f^l} \eta_r} - y^l \right) \cdot \frac{\eta_{t_r} \cdot f_{t_j}^{tr}(x_{1,\dots,n}^1)}{\sum_{r=1}^{R_f^l} \eta_r} \\
 &= 2 \left(\left(\frac{\sum_{l=1}^S \sum_{r=1}^{R_f^l} \eta_r (a_i^r) f_i^r(x_{1,\dots,n}^1) \eta_{t_r} f_{t_j}^{tr}(x_{1,\dots,n}^1)}{\left(\sum_{r=1}^{R_f^l} \eta_r \right)^2} \right) + \dots + \left(\frac{\sum_{l=1}^S \sum_{r=1}^{R_f^l} \eta_r (a_k^r) f_k^r(x_{1,\dots,n}^1) \eta_{t_r} f_{t_j}^{tr}(x_{1,\dots,n}^1)}{\left(\sum_{r=1}^{R_f^l} \eta_r \right)^2} \right) \right) \\
 &\quad - 2 \left(\frac{\sum_{l=1}^S y^l \cdot \eta_{t_r} f_{t_j}^{tr}(x_{1,\dots,n}^1)}{\sum_{r=1}^{R_f^l} \eta_r} \right) = 0, \tag{21}
 \end{aligned}$$

Thus, the Equation (20) provides the following system of linear equations from which we can compute the coefficients $\{(a_1^1, \dots, a_k^1), (a_1^2, \dots, a_k^2), \dots, (a_1^{R_f}, \dots, a_k^{R_f})\}$:

$$\begin{aligned}
 &\sum_{r=1}^{R_f} \sum_{j=1}^K a_j^r \sum_{l=1}^S \frac{\prod_{v=1}^n \mu_v^r(x_{1,\dots,n}^1)}{\left(\sum_{r=1}^{R_f} \prod_{v=1}^n \mu_v^r(x_{1,\dots,n}^1) \right)^2} f_j^r(x_{1,\dots,n}^1) \cdot f_{t_j}^{tr}(x_{1,\dots,n}^1) \cdot \prod_{v=1}^n \mu_v^{tr}(x_{1,\dots,n}^1) \\
 &= \sum_{l=1}^S \frac{y^l \prod_{v=1}^n \mu_v^{tr}(x_{1,\dots,n}^1)}{\sum_{r=1}^{R_f} \prod_{v=1}^n \mu_v^r(x_{1,\dots,n}^1)} f_{t_j}^{tr}(x_{1,\dots,n}^1) \tag{22}
 \end{aligned}$$

In matrix form, Equation (22) will be written as:

$$\begin{bmatrix} \alpha_{11}^r & \alpha_{12}^r & \cdot & \alpha_{1K}^r \\ \alpha_{21}^r & \alpha_{22}^r & \cdot & \alpha_{2K}^r \\ \cdot & \cdot & \cdot & \cdot \\ \alpha_{k1}^r & \alpha_{k2}^r & \cdot & \alpha_{kK}^r \end{bmatrix} \begin{bmatrix} a_1^r \\ a_2^r \\ \cdot \\ a_k^r \end{bmatrix} = \begin{bmatrix} \beta_1^r \\ \beta_2^r \\ \cdot \\ \beta_K^r \end{bmatrix} \tag{23}$$

where $\alpha_{ij}^r = \sum_{l=1}^S f_j^r(x_1^l, x_2^l, \dots, x_n^l) f_i^r(x_1^l, x_2^l, \dots, x_n^l)$; $\beta_i^r = \sum_{l=1}^S y^l f_i^r$, where s is the number of training (input-output) sample data. Thus, Equation (22) provides a solution of the function coefficients (a_j^r) of the TSK-type fuzzy rule consequents for a given of values of the input

variable's exponential terms. To solve the Equation (22) in order to find the values of function coefficients, the Gauss Algorithm with Column Pivot Search Method is used here. More generally, any conventional numerical method, which provides a representative solution of Equation (22), may be adopted.

SURFACE ROUGHNESS MODELS IN TURNING

In this chapter, two surface roughness models (R_a , average roughness and R_t , maximum peak-to-valley roughness) are presented in order to determine the optimized values of cutting speed, feed rate and cutting time to achieve a desired surface roughness on a machined surface in turning (Nandi & Davim, 2009). These models are constructed based on TSK-type fuzzy rule using a genetic fuzzy approach as discussed in Section 4. For this application, the rule consequent function of each TSK-fuzzy rule (Equation 3) is considered as a linear function of machining parameters (such as cutting speed, feed rate and cutting time) in turning and it is expressed as follows:

$$y = a_1 V_c^{p_1} + a_2 f^{p_2} + a_3 T_c^{p_3} \quad (24)$$

The machining parameters (i.e., cutting speed V_c , feed rate, f and cutting time, T_c) that are primarily affecting to the surface roughness are treated as (input) variables to the surface roughness model. Each of the input variables (V_c , f and T_c) are considered to have two fuzzy sub-sets (linguistically called, say, LOW and HIGH) of the type of semi-trapezoidal in their corresponding range of (80, 220), (0.05, 0.15) and (5, 15), respectively. These two semi-trapezoidal fuzzy sub-sets of a variable may be defined by two parameters (b_1 and b_2) as shown in Figure 21. In order to optimize the fuzzy sub-sets, the appropriate values of these parameters (b_1 and b_2) are to be determined using GA. As each input variable has two fuzzy sub-sets in their range in the input space, there are a maximum of $2 \times 2 \times 2 = 8$ rules to be present in the rule-based system. Now the task is to find the appropriate values of the parameters: output function coefficients (a_1 , a_2 and a_3) of each rule rules (total of $8 \times 3 = 24$), variable's exponential parameters (p_1 , p_2 , p_3) (total of $8 \times 3 = 24$) and the parameters b_1 and b_2 associated to semi-trapezoidal fuzzy sub-sets for three input variables (total of $3 \times 2 = 6$). During optimization, the values of the exponential terms of each input variables are kept in the range of 0 to 1. The parameters (b_1 and b_2) for cutting speed, feed rate, and cutting time are allowed to vary in the range of (10, 150 and 0, 60), (0.01, 0.1 and 0, 0.06) and (1, 10 and 0, 8), respectively. During optimization, the fitness value of GA is considered as the mean percentage error of training data and the objective is to run the GA for minimizing the fitness value until a satisfactory result is obtained.

Model of R_a

Through a rigorous parametric study, the optimum values of GA-parameters for R_a model are set as follows for the best performance of GA:

Population size: 200
 Chromosome length: 600
 No of bits used for each input variable: 20
 No of bits used for each variable for power factor: 20
 Selection (reproduction) method: Tournament selection
 Crossover probability: 0.97
 Mutation probability: 0.01

The optimum value of the parameters (b_1, b_2) for cutting speed, feed rate, and cutting time are obtained as (56.83, 33.76), (0.028, 0.027) and (9.91, 0.0375), respectively. All rules of the rule based system for R_a model are described in Table 1.

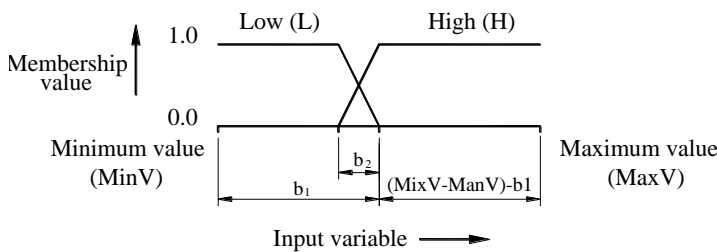


Figure 21. Two semi-trapezoidal fuzzy subsets.

Table 1. Rule base of FRBM of R_a

Rule No.	Rule antecedent			Rule consequent function
	Vc	f	Tc	
1	L	L	L	$y_1 = -2.67212V_c^{0.144105} + 28.7472f^{0.558778} + 0.0246824T_c^{0.631831}$
2	L	L	H	$y_2 = 0.103425V_c^{0.275274} + 84557.1f^{0.582791} - 1130.79T_c^{0.948508}$
3	L	H	L	$y_3 = 0.028222V_c^{0.796081} - 2.62769f^{0.345424} + 0.806025T_c^{0.154388}$
4	L	H	H	$y_4 = 0.11638V_c^{0.582911} - 1.07163f^{0.468166} - 0.0294324T_c^{0.629089}$
5	H	L	L	$y_5 = -0.161968V_c^{0.2984521} - 17.1405f^{0.807206} + 2.30398T_c^{0.0789466}$
6	H	L	H	$y_6 = 0.981749V_c^{0.347674} - 18194.1f^{0.436945} + 1481.04T_c^{0.442519}$
7	H	H	L	$y_7 = -4.81052V_c^{0.00000001} + 4.12005f^{0.358391} + 3.1042T_c^{0.0956505}$
8	H	H	H	$y_8 = 140.947V_c^{0.0045235} + 2.8470f^{0.362736} - 48.9195T_c^{0.399538}$

Model of R_t

The optimum values of GA parameters for R_t model are set as follows:

Population size: 200
 Chromosome length: 600
 No of bits used for each input variable: 20
 No of bits used for each variable for power factor: 20
 Selection (reproduction) method: Tournament selection
 Crossover probability: 0.985
 Mutation probability: 0.011

The optimum value of the parameters (b1, b2) for cutting speed, feed rate, and cutting time are obtained as (82.22, 43.59), (0.098, 0.030) and (9.913, 0.015), respectively. All rules of the rule based system for R_t model are illustrated in Table 2.

Discussion on Model Validation

Before, carrying out the optimization of machining parameters to obtain a desired surface roughness, it is very much important to validate surface roughness models. In order to validate the surface roughness models (R_a and R_t), a rigorous testing of the models has been made. First of all, the characteristics behaviours of these models (R_a and R_t) are studied here. In order to accomplish this, the variations of surface roughness with the cutting time for a given cutting speed and feed rate obtained from the models are compared with that found in the experimental study of surface roughness in turning AISI D2 Steel (those are used for learning the models) as described in Figure 22 and Figure 23 for the models R_a and R_t , respectively. In Figures 22 and 23, it has observed the nature of the characteristics curves are monotonic like the experimental data for a given values of cutting speed and feed rate.

Table 2. Rule base of FRBM of R_t

Rule No.	V_c	f	T_c	Rule consequent function
1	L	L	L	$y_1 = 0.0154091V_c^{0.999953} + 23.2713f^{0.999987} + 0.0235612T_c^{0.999579}$
2	L	L	H	$y_2 = 0.0527879V_c^{0.87782} + 11.700f^{0.522283} - 1.2434T_c^{0.124275}$
3	L	H	L	$y_3 = 44.6805V_c^{0.186297} - 138.049f^{0.176562} + 0.293344T_c^{0.368142}$
4	L	H	H	$y_4 = 18.2314V_c^{0.300686} + 2613.24f^{0.274002} - 196.085T_c^{0.779424}$
5	H	L	L	$y_5 = -2.76997V_c^{0.0000141} + 20.347f^{0.591166} + 0.530914T_c^{0.50938}$
6	H	L	H	$y_6 = 15.4595V_c^{0.0730525} + 28.0004f^{0.186995} - 9.0932T_c^{0.506985}$
7	H	H	L	$y_7 = 1.80671V_c^{0.507232} - 63879.4f^{0.94982} + 10513.2T_c^{0.000138}$
8	H	H	H	$y_8 = 145.073V_c^{0.0712262} - 580.29f^{0.911143} - 54.9844T_c^{0.235217}$

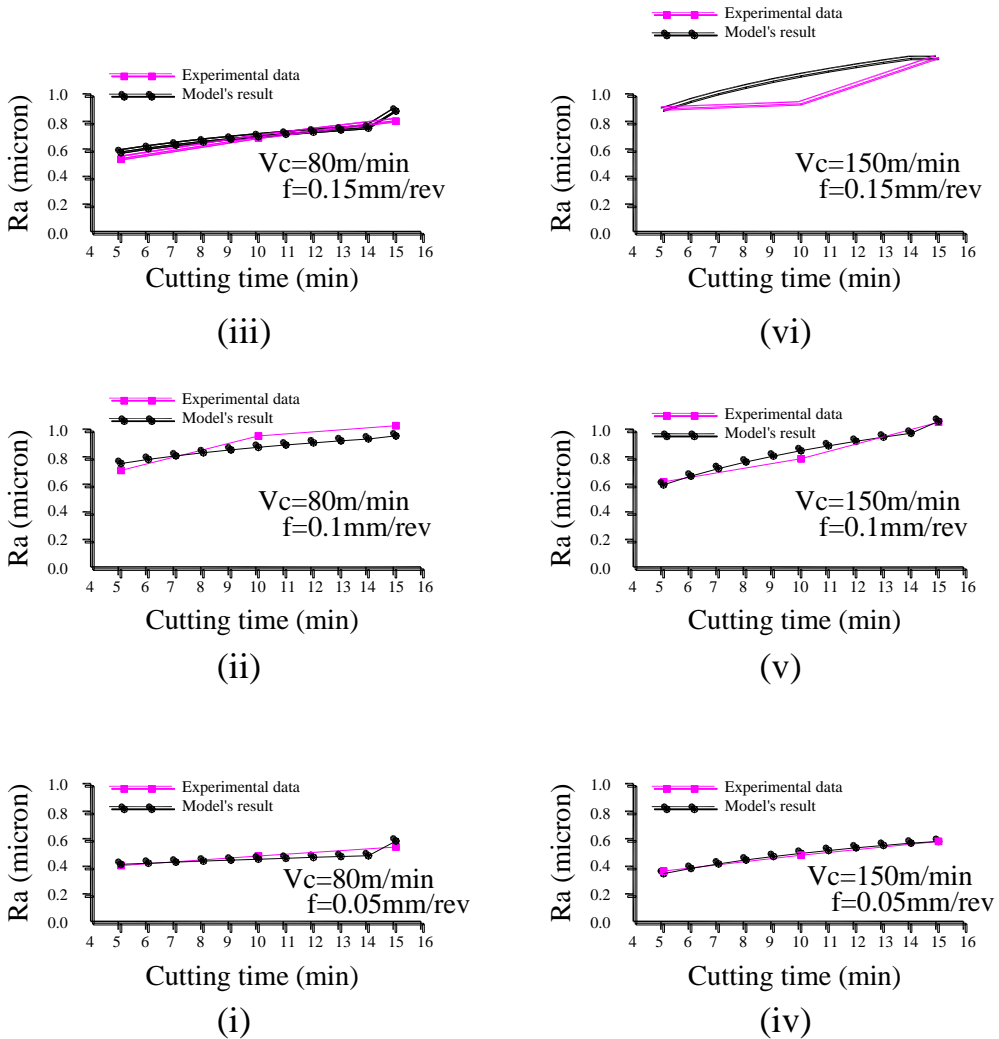
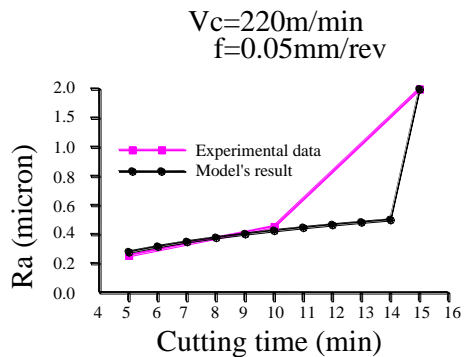


Figure 22(a). Comparisons of experimental data and R_a model's results.

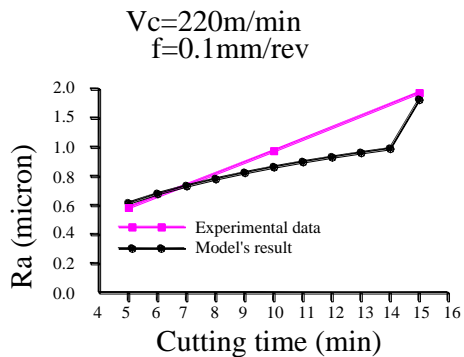
For further investigation to awards validation of the models, we have considered another 9 test cases (experimental data), and the results of the models are compared with these test data as described in Table 3.

In Table 3, Error I and Error II are the percentage values of the deviations of results of the models from those obtained using real experiments for surface roughness components R_a and R_t , respectively. It has been observed that for most of the cases, the errors are below 10 percent which may be acceptable in shop floor, and the mean percentage values of Error I and Error II are 6.78 and 4.08, respectively. From the above discussions regarding validation of the models it may be argued that these models may be accepted to carry out the optimization of surface roughness.

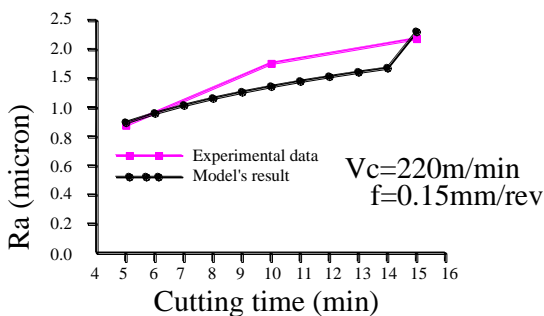
Generally, the accuracy of a rule-based model may be increased with increasing the number of rules. The number of TSK-type fuzzy rules depends on the number of fuzzy subsets considered for each input variable. However, increasing the number of rules means the enhancement of complexity in the model.



(vii)



(viii)



(ix)

Figure 22(b). Comparisons of experimental data and Ra model's results.

Table 3. Comparison of results obtained from surface roughness model and Experimental values

Cutting velocity, V_c (m/min)	Feed rate, f (mm/rev)	Cutting time, T_c (min)	R_a (micron) (Experimental value)	R_a (micron) (Result of model)	% Error I	R_t (micron) (Experimental value)	R_t (micron) (Result of model)	% Error II
115	0.05	5	0.29	0.26	12.01	3.31	3.22	2.81
115	0.05	10	0.32	0.33	3.57	3.32	3.30	0.62
115	0.05	15	0.43	0.45	4.83	4.31	4.11	4.74
115	0.10	5	0.87	0.92	5.30	4.73	4.51	4.71
115	0.10	10	1.07	1.08	0.87	4.95	4.59	7.28
115	0.10	15	1.06	1.17	10.85	4.97	5.17	4.11
115	0.15	5	1.00	0.90	9.94	9.99	9.92	0.66
115	0.15	10	1.12	1.06	5.02	9.01	10.08	11.84
115	0.15	15	1.31	1.19	8.79	11.33	11.32	0.02

Sometimes, it is required to increase the number of rules to obtain a desired performance of the model when the complexity of the process is high. In the present study of developing models of surface roughness for Hard Turning operation of AISI D2 Steel using Ceramic Inserts, it has been investigated that 8 rules (means two fuzzy sub-sets for each of the variables cutting speed, feed rate and Cutting time) are enough to achieve a desired model performances.

OPTIMIZATION OF MACHINING PARAMETERS USING GA

Once, the surface roughness models are obtained, a GA is used to determine the optimized value of machining parameters to obtain a desire surface roughness. To carry out the optimization process, we have considered a binary coded-GA with the following values of GA parameters:

Population size: 50
 Chromosome length: 45
 No of bits used for each input variable: 15
 Selection (reproduction) method: Tournament selection
 Crossover probability: 0.98
 Mutation probability: 0.1

However, the values of above parameters may be different for different cases for obtaining a best result. For this optimization, the optimum value of the machining parameters will lie in the range of total input space. Therefore, the maximum and minimum value of input variables, cutting speed, feed rate, and cutting time are kept as (220, 80), (1.5, 0.05) and (15, 5), respectively. A typical GA-string of these variables is presented in Figure 24.

The objective of this study of optimization is to determine the optimum values of machining parameters (cutting speed, feed rate and time of cut) by minimizing the error of desired surface roughness from that obtained using the models.

In this optimization process two surface roughness parameters R_a and R_t are considered. The objective function of this optimization process includes the R_a and the ratio of R_a and R_t ($\frac{R_a}{R_t}$). Therefore, the fitness criteria (F_c) of this GA-based optimization process is defined as:

$$F_c = (R_{ad} - R_{am}) + \frac{R_{ad} - R_{am}}{R_{td} - R_{tm}} \quad (25)$$

where, R_{ad} and R_{am} are the desired surface roughness value of R_a and that obtained from the model, respectively. R_{td} and R_{tm} values are the desired surface roughness of R_t and the model output, respectively. Now, the aim of this optimization task is to minimize the value of F_c . The Table 4 shows the result of some of the case (including few known cases, first twelve entries of the Table) considered at random for optimization of surface roughness. The rests of the entries of Table 4 are the some unknown cases. For each case, the values of GA-parameters are kept as fixed.

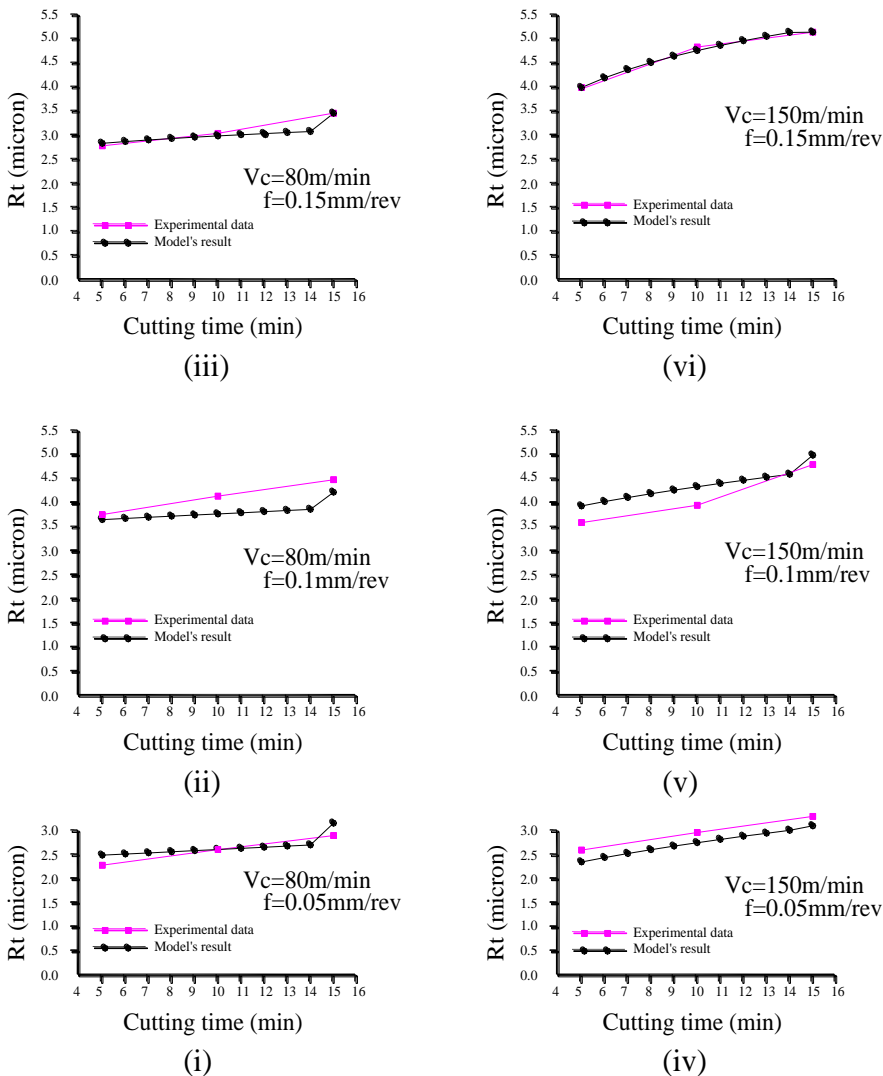


Figure 23(a). Comparisons of experimental data and R_t model's results.

Table 4. Results of optimization of surface roughness in turning

Sl. No.	R_a (micron)	R_t (micron)	$\frac{R_a}{R_t}$	Cutting velocity, V_c (m/min)	Feed rate, f (mm/rev)	Cutting time, T_c (min)
1	0.43	4.31	0.0997	118.26	0.065	14.596
2	0.87	4.73	0.1839	115.78	0.131	5.724
3	1.12	9.01	0.1243	120.03	0.143	10.175
4	0.425	2.305	0.1843	78.78	0.057	5.726
5	0.72	3.78	0.1904	85.60	0.101	6.114
6	0.82	3.48	0.2356	87.29	0.160	18.024

Sl. No.	R_a (micron)	R_t (micron)	$\frac{R_a}{R_t}$	Cutting velocity, V_c (m/min)	Feed rate, f (mm/rev)	Cutting time, T_c (min)
7	0.5	2.985	0.1675	150.81	0.072	8.329
8	0.785	3.615	0.2171	145.02	0.115	5.881
9	1.32	5.165	0.2555	152.32	0.165	13.227
10	1.4	2.885	0.4852	220.035	0.042	16.239
11	0.585	3.985	0.1468	220.01	0.128	5.292
12	1.475	6.035	0.2444	219.67	0.156	10.103
13	0.2	2.0	0.1	199.01	0.055	5.609
14	0.4	4.0	0.1	152.16	0.067	7.420
15	0.6	6.0	0.1	135.749	0.065	6.580
16	0.8	8.0	0.1	210.99	0.071	12.023
17	1.0	10.0	0.1	214.73	0.078	13.251
18	1.2	12.0	0.1	216.02	0.107	14.005
19	1.5	15.0	0.1	219.89	0.0834	14.002
20	0.2	1	0.2	215.34	0.061	7.921
21	0.4	2.0	0.2	219.25	0.08	9.227
22	0.6	3.0	0.2	219.73	0.012	5.001
23	0.8	4.0	0.2	220.00	0.0612	5.283
24	1.0	5.0	0.2	143.459	0.062	5.303
25	1.2	6.0	0.2	133.616	0.050	6.592
26	1.5	7.5	0.2	167.921	0.0867	8.159

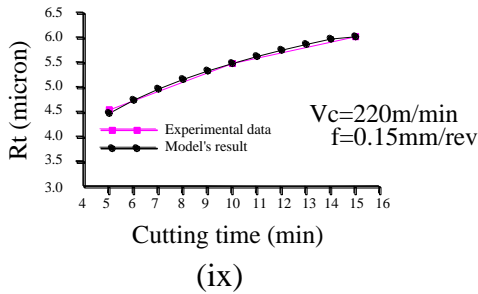
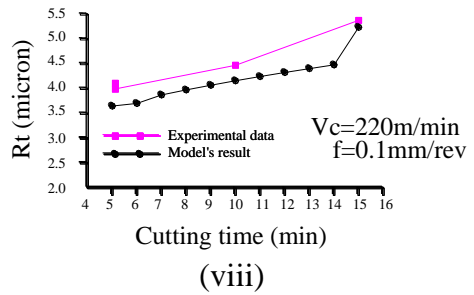
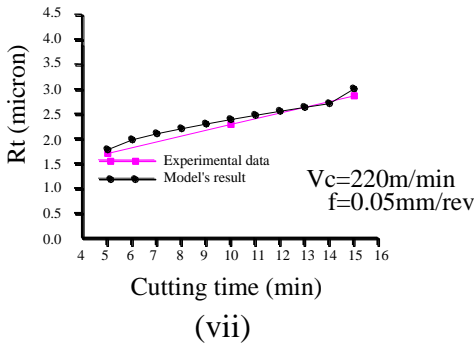


Figure 23(b). Comparisons of experimental data and R_t model's results.

From the results as depicted in Table 4, it may be stated that the GA-based optimization procedure gives almost accurate results for most of the cases as found in the known cases. For other cases, it has been observed that the deviations of results are occurred. This is happen due to the fact that the optimization of machining parameters to obtain a desired surface roughness is a kind of multi-modal optimization problem, where a number of solutions may exist for a given value of surface roughness.

$$\underbrace{100111\dots\dots10011\dots\dots010\dots\dots01}_{\text{Cutting speed}} \quad \underbrace{\hspace{1.5cm}}_{\text{Feed rate}} \quad \underbrace{\hspace{1.5cm}}_{\text{Cutting time}}$$

Figure 24. A typical GA-string of cutting variables.

CONCLUSION

In this chapter, the surface roughness obtained in turning process is modeled and optimized using soft computing tools. The average surface roughness and maximum peak-to-valley roughness are modeled using fuzzy logic rule, namely TSK-type fuzzy logic rule and considering a linear function of machining parameters as a rule-consequent function. The knowledge base of the fuzzy model is constructed and optimized using a proposed GA-fuzzy approach, namely genetic linear regression approach. Based on the developed models of surface roughness, the values of machining parameters such as cutting speed, feed rate, and cutting time are optimized using genetic algorithm for obtaining a better surface roughness on machined surface in turning operation. The results of the developed fuzzy models and optimized values machining parameters are compared with the real experimental values found in turning of AISI D2 Steel and this comparative study suggests that the developed models may be implemented in industrial applications specifically in automated manufacturing system.

REFERENCES

- A. Taraman, K., Lambert, B., 1974. A surface roughness model for a turning operation. *International Journal of Production Research*, Vol. 12, No. 6, pp. 691-703.
- Abhuri, N.R., Dixit, U.S., (2006). A knowledge-based system for prediction of surface roughness in turning process. *Robotics and Computer-Integrated Manufacturing*, Vol. 22, No. 4, pp. 363-372.
- Abouelatta, O.B., Madl, J., (2001). Surface roughness prediction based on cutting parameters and tool vibrations in turning operations. *Journal of Materials Processing Technology*, Vol. 118, pp. 269-277.
- Cheung, C.F., Lee, W.B., (2000). A multi-spectrum analysis of surface roughness formation in ultra-precision machining. *Precision Engineering*, Vol. 24, pp. 77-87.
- Cheung, C.F., Lee, W.B., (2000). A theoretical and experimental investigation of surface roughness formation in ultra-precision diamond turning. *International Journal of Machine Tools and Manufacture*, Vol. 40, No. 7, pp. 979-1002.

- Choudhury, I.A., El-Baradie, M.A., (1997). Surface roughness prediction in the turning of high-strength steel by factorial design of experiments. *Journal of Materials Processing Technology*, Vol.67, No.1-3, pp. 55-61.
- Davim, J.P., (2001). A note on the determination of optimal cutting conditions for surface finish obtained in turning using design of experiments. *Journal of Materials Processing Technology*, Vol. 116, pp. 305-308.
- Deb, K., (2001). *Multi-Objective Optimization using Evolutionary Algorithms*. John Wiley & Sons Ltd, England.
- Draper, N.R., Smith, H., (1981). *Applied Regression Analysis*, 2nd Edition, John Wiley & Sons, Inc, New York.
- Fang, X.D., Jawahir, I.S., (1994). Predicting total machining performance in finish turning using integrated fuzzy-set models of the machinability parameters. *International Journal of Production Research*, Vol. 32, No. 4, pp. 833-849.
- Goldberg, D.E., (1989). *Genetic Algorithms in Search, Optimization and Machine Learning*. Addison-Wesley, Reading, Mass., USA.
- Grzesik, W., Brol, S., (2003). Hybrid approach to surface roughness evaluation in multistage machining processes. *Journal of Materials Processing Technology*, Vol. 134, No. 2, pp. 265-272.
- Ho, S., Lee, K., Chen, S., Ho, S., (2002). Accurate modeling and prediction of surface roughness by computer vision in turning operations using an adaptive neuro-fuzzy inference system, *Int. J. Mach. Tools Manufact.* 42 (13) (2002) 1441-1446.
- Kohli, A., Dixit, U.S., (2005). A neural-network-based methodology for the prediction of surface roughness in a turning process. *International Journal of Advanced Manufacturing Technology*, Vol. 25, No. 1-2, pp. 118-129.
- Lee, B.Y., Tarn, Y.S., (2001). Surface roughness inspection by computer vision in turning operations. *International Journal of Machine Tools and Manufacture*, Vol. 41, No. 9, pp. 1251-1263.
- Lin, W.S., Lee, B.Y., Wu, C.L., (2001). Modeling the surface roughness and cutting force for turning. *Journal of Materials Processing Technology*, Vol. 108, No. 3, pp. 286-293.
- Mainsah, E., Ndumu, D.T., (1998). Neural network application in surface topography. *International Journal of Machine Tools and Manufacture*, Vol. 38, No. 5-6, pp. 591-598.
- Mamdani, E.H., Assilian, S., (1975). An experiment in linguistic synthesis with a fuzzy logic controller. *International Journal of Man-Machine Studies*, Vol. 7, No. 1, pp. 1-13.
- Nandi, A.K. (2006). TSK-Type FLC using a combined LR and GA: surface roughness prediction in ultraprecision turning. *Journal of Material Processing Technology*, Vol. 178, No. 1-3, pp. 200-210.
- Nandi, A.K., (2003). Prediction of Surface roughness in Ultraprecision Turning Using Fuzzy Logic. Proceedings of the 3rd International Conference in Fuzzy Logic and Technology (EUSFLAT2003), pp. 408-413, Zittau, Germany, September 10-12, 2003.
- Nandi, A.K., Davim, J.P., (2009). Optimisation of surface roughness in hard turning AISI D2 steel using TSK-type fuzzy logic rules. *International Journal of Materials and Product Technology*, Vol. 35, No. 1/2, pp. 167-183.
- Risbood, K.A., Dixit, U.S., Sahasrabudhe, A.D., (2003). Prediction of surface roughness and dimensional deviation by measuring cutting forces and vibrations in turning process. *Journal of Materials Processing Technology*, Vol. 132, No. 1-3, pp. 203-214.

- Sugeno, M., Kang, G.T., (1988). Structure identification of fuzzy model. *Fuzzy Sets and Systems*, Vol. 28, No. 1, pp. 15-33.
- Sundaram, R.M., Lambert, B.K., (1981). Mathematical model to predict surface finish in fine turning of steel. Part I. *International Journal of Production Research*, Vol. 19, No. 5, pp. 547-564.
- Takagi, T., Sugeno, M., (1985). Fuzzy identification of systems and its application to modeling and control. *IEEE Transactions on Systems, Man, and Cybernetics*, Vol. 15, No. 1, pp. 116-132.
- Tsukamoto, Y., (2004). Fuzzy information theory. Daigaku Kyoiku Pub.
- Wang, X.F., Feng, C.X., (2002). Development of empirical models for surface roughness prediction in finish turning. *International Journal of Advanced Manufacturing Technology*, Vol. 20, No. 5, pp. 348-356.
- Yang, W.H., Tarn, Y.S., (1998). Design optimization of cutting parameters for turning operations based on the Taguchi method. *Journal of Materials Processing Technology*, Vol. 84, No. 1-3, pp. 122-129.
- Zadeh, L.A., (1965). Fuzzy sets. *Information and control*, Vol. 8, No. 3, pp. 338-353.
- Zhang, G., Gopalakrishnam, S., (1996). Fractal geometry applied to on-line monitoring of surface finish. *International Journal of Machine Tools and Manufacture*, Vol. 36, No. 10, pp. 1137-1150.

Chapter 8

PERSPECTIVE OF WIRE ELECTRICAL DISCHARGE MACHINING: A REVIEW

S. K. Garg^{1}, A. Manna² and Ajai Jain³*

¹NIT, Kurukshetra, India &

JMIT, Radaur Yamunanagar, Haryana, India

²Mechanical Engineering Department, PEC University
of Technology, Chandigarh, India

³Mechanical Engineering Department, NIT, Kurukshetra, India

ABSTRACT

Wire electrical discharge machining (WEDM) is a specialized thermal machining process capable of accurately machining parts of hard materials with complex shapes. Parts having sharp edges that pose difficulties to be machined by the main stream machining processes can be easily machined by the WEDM process. WEDM is used not only for making tools and dies but also evolved as the best alternative of producing micro-scale parts with the highest degree of dimensional accuracy and surface finish quality.

This chapter presents the detail of various process parameters of WEDM and their effect on machining performance characteristics. It presents the review of the various modeling method used to optimize the WEDM process parameters and performance of WEDM for conventional tool and die materials, Metal matrix composites (MMC) and ceramics. The final part of the chapter presented the future scope of WEDM.

1. INTRODUCTION

Wire cut electrical discharge machining (WEDM) or Electrical discharge wire cutting is a spark erosion process used to produce two and three dimensional complex shapes through electrically conductive work-pieces. In WEDM process, a small diameter wire ranging from

* Research Scholar and Associate Professor; Corresponding author, e-mail: sanjeevkgarg@rediffmail.com.

0.05 to 0.25 mm is applied as the tool electrode. It is essential to hold the wire in a designed position against the object because the wire repeats complex oscillations due to electro-discharge between the wire and the workpiece. The wire is continuously supplied from the supply spool through the work piece by the wire traction rollers. A DC power supply delivers high-frequency pulses of electricity to the wire and the workpiece. The gap between the wire and workpiece is flooded with deionised water, which acts as the dielectric. The work-piece is mounted on the table of the machine and the dielectric medium is ejected to the sparking area (Bannerjee et al., 1993).

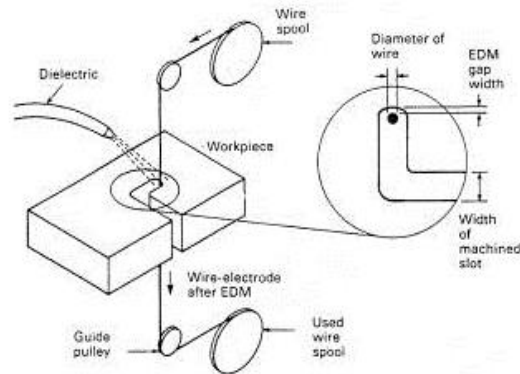


Figure 1. WEDM Process (Manna, 2006).

Material is eroded ahead of the travelling wire by spark discharges, which are identical with those in conventional EDM. There is no mechanical contact between the wire and the workpiece in WEDM. In WEDM, material is eroded from the workpiece by a series of discrete sparks occurring between the workpiece and the wire separated by a stream of dielectric fluid, which is continuously fed to the machining zone. The wire workpiece gap usually ranges from 0.025 to 0.05 mm and is constantly maintained by a computer controlled positioning system (Bannerjee et al., 1993). The WEDM process make use of electrical energy generated in a channel of plasma between the cathode and anode (Bannerjee et al., 2010) and turns it into thermal energy at a temperature in the range of 8000-12000 °C or as high as 20000 °C initializing a substantial amount of heating and melting on each pole. When the DC power supply in pulsating form 20000 and 30000 Hz (Cabanés et al., 2008) is turned off, the plasma channel breaks down. This causes a sudden decrease in the temperature allowing the circulating dielectric fluid to implore the plasma channel and flush the molten particles from the pole surfaces in the form of microscopic debris.

With WEDM technology, complicated cutouts can be made through difficult to cut machine metals without the need to use either high cost grinding or expensive formed EDM electrodes. The high degree of accuracy obtainable and the fine surface finishes make WEDM particularly value-able for applications involving the manufacture of press stamping dies, extrusion dies, prototype parts and even for the fabrication of conventional EDM electrodes.

WEDM was first introduced to the manufacturing industry in the late 1960s. Then various technological and NC aspects (Daniel and Philips, 1976) of the WEDM process were analyzed. The Short circuit gap (Kinoshita et al., 1976), properties of servo gap sensor

(Tanimura et al., 1977) and prevention of wire electrode from breaking (Kinoshita et al., 2010).

2. WEDM PROCESS PARAMETERS

Proper knowledge about the WEDM process parameters and their effect on the machining performance is essential to control the process and enhance the efficiency and productivity with minimum cost. There are numerous parameters which affect the WEDM process performance (Figure 1) and the most important of them will now be further discussed.

2.1. Pulse Width

The pulse width means the duration of a fully positive or fully negative half cycle of the alternating discharge current. Pulse width differs from the pulse duration. A positive or negative half cycle of the current is made up of a series of positive or negatives pulses, each with a duration defined as the ‘pulse duration’. The surface roughness does not change within the period of the pulse width. The main purpose of alternating the voltage is to prevent various damaging effects including oxide erosion, micro-cracks and rust spot when machining is performed in de-ionized water. Varying the length of the pulsing period does not change the discharge energy, so it has a minimal influence on surface roughness (Ramakrishnan and Karunamoorthy, 2006).

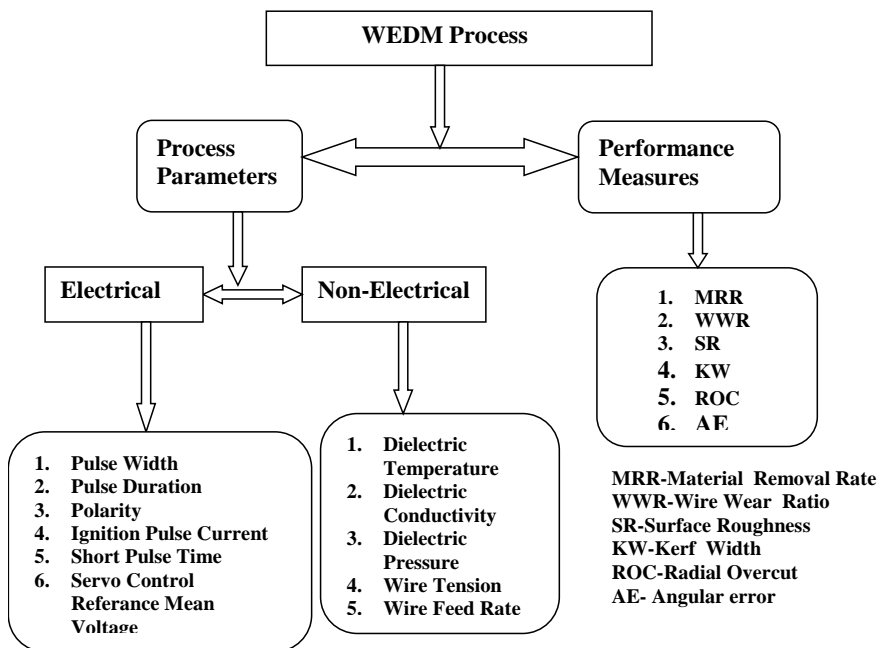


Figure 2. WEDM Process Parameters and Machining Performance Characteristics.

2.2. Pulse Duration

Pulse duration expressed in micro-seconds, is the time during which the pulse remains 'ON'. It is also known as pulse ON time. The surface quality of WEDM generated surface is related to the material removal per discharge determined by the pulse energy per discharge. The pulse energy per discharge can be expressed as follows:-

$$E = \int_0^{t_{on}} u(t) i(t) dt$$

where t_{on} is the pulse on time or pulse duration, $u(t)$ is the discharge voltage, $I(t)$ is the discharge current and E is the pulse energy per discharge.

Since the discharge voltage $u(t)$ remains constant during the discharge, the pulse energy per discharge is determined by the pulse on time (t_{on}) and discharge current $i(t)$.

2.3. Polarity

In WEDM, there are mainly two power supply modes: normal polarity machining and reversed polarity machining, in which the workpiece is connected with positive terminal, or negative terminal respectively. While the discharge is taking place between the workpiece and the electrode, electrons from the cathode in the dielectric arouse the ionization which produces an ionized channel. The particles with a positive charge bombard the cathode while electrons bombard the anode in ionized channel. In this process, electron, which are smaller and lighter, thus accelerate faster and reach higher speeds, whereas particles with a positive charge accelerate more slowly and do not reach high speeds. As a result, electrons transfer more energy to the anode than positively charged particles transfer to the cathode. This difference leads to material removal in the anode that is greater than the material removal in the cathode.

2.4. Ignition Pulse Current

The value of surface roughness increases as the ignition pulse current increases when the pulse duration is kept constant. When the pulse duration is kept constant, an increase in the discharge current will increase the discharge energy. Higher discharge energy will worsen surface roughness because of the increase in diameter and depth of the discharging craters. It was found that improving the surface roughness means the pulse energy per discharge must be controlled in the WEDM finish cut (Mahapatra and Patnaik, 2006).

2.5. Short Pulse Time

The crater volume and the width of the heat effected increases with increasing short pulse time. The diameter and depth of the craters increase with increasing short pulse time owing to

the large energy content of spark discharges. The most effective parameters for determining the crater diameter and crater depth are open circuit voltage and short pulse time (Tosun et al., 2003).

2.6. Servo Control Reference Mean Voltage

It is the mean voltage supplied to the servo control. If servo control reference mean voltage is increased, material removal rate will increase and the workpiece tends to become concave. If servo control reference mean voltage is decreased, material removal rate will decrease and the workpiece tend to become convex. This effect increases with the increase of the height of the part. It is also accentuated by an excessively low wire tension (Han et al., 2006).

2.7. Wire Tension

Wire mechanical tension expressed in daN(kg) is the tension force applied to the wire which keeps it in the straight position. It can be checked with a tension meter. Wire tension affects the shape geometry. If wire tension increases precision will increase. (Manna and Bhattacharyya, 2006).

2.8 Wire Feed Rate

Wire feed rate is expressed in meters per minute. Increasing the wire speed increases the depth and diameter of the wire crater. For longer pulse durations and higher wire speeds, the wire travel will be longer in front of the spark plasma channel which will result in larger crater diameters (Tosun et al., 2003). Wire feed rate affects the cutting rate and part parallelism. Since the wire feed rate is higher in roughing (due to setting), the cutting rate will be faster in roughing than finishing.

2.9. Dielectric Flushing Pressure

Injection pressure ensures the evacuation of metal particles during machining. As a general rule, it is recommended to decrease the injection pressure for evolutive surface parts so as to prevent creation of turbulence. Wire speed and dielectric flushing pressure were less effective factors for determining the crater diameter and crater depth (Tosun et al., 2003).

2.10. Dielectric Conductivity

As a medium of impulse discharge, the dielectric working fluid should be sufficiently capable of insulating the electrodes, because when the dielectric is broken down, its low

conductivity can narrow the ionized channel and limit the electrical arc column to a small area. This arc can melt or vaporize the material and the dielectric can also resume insulator after the spark. The conductivity of the dielectric should be appropriate. Excessively high conductivity will prevent sparking from taking place, whereas a dielectric with an excessively low conductivity will not break down easily enough, which will shorten the discharge gap and result in a short circuit. The value of surface roughness increases gradually accompanying an increase of conductivity of the dielectric. This is because increasing the conductivity increases the gap capacity. A higher gap capacity leads to a higher pulse energy per discharge, which worsen the surface roughness. However, it was also found that the influence of conductivity on surface roughness is not very significant (Han et al., 2006).

3. MAJOR AREAS OF WEDM RESEARCH

The WEDM research can be divided into the following major areas, however authors reviews the research work related with WEDM process parameters and performance of WEDM for conventional tool and die materials, Metal matrix composites (MMC) and ceramics;

1. Transition of WEDM Technology
2. WEDM process optimization
3. Thermal loads on the wire
4. Ultrasonic Vibration to the wire electrode
5. Development of wire electrode
6. Prevention of wire electrode breaking
7. Accuracy improvement of WEDM
8. WEDM for conventional materials
9. WEDM for Metal Matrix Composites
10. WEDM for Ceramics
11. Advanced application of WEDM

3.1. Transition of WEDM Technology

Zewang et al. (1991) introduced new concept distance parameter for the intricate ruled surface machining by WEDM. The formula to calculate the maximum inclination angle of ruling and the formula to calculate coordinates of points on ruled surface were obtained. A new method of 4-axis simultaneous control programming introduced in this paper can be applied to different top and bottom profile ruled surface machining.

Yan et al. (1995) developed an algorithm for surface design and tool path generation for WEDM. This paper proposed a CAD/CAM mathematical model to design ruled surface. The algorithm, being different from conventional methods, can present a surface or tool path concisely and uniquely.

Qu et al. (2002) analyzed a cylindrical wire EDM process. They investigated through a mathematical model concept, design, material removal rate, surface integrity and roundness

of cylindrical WEDM parts using brass as a wire material and carbide as a work material. They found through the model a good estimate of the surface finish and roundness of cylindrical WEDM parts.

Wang et al. (2003) investigated into computer aided contouring operation for travelling WEDM. It includes development of a computational method for numerical control (NC) of travelling WEDM operation from geometric representation of a desired cut profile in terms of its contours. Normalized arc length parameterization of the contour curves was used to represent the cut profile. Subdivision algorithm was developed together with kinematic analyses to generate the required motions of the machine tool axis.

Many wire EDM machines have adopted the pulse-generating circuit using low power for ignition and high power for machining. However, it is not possible for finishing process since the energy generated by the high voltage sub-circuit is too high to obtain a desired fine surface, no matter how short the pulse on-time is assigned. Liao et al. (2004) modified the pulse generating circuit for finishing process.

Liao et al. (2004) investigated the effect of specific discharge energy in WEDM and its applications. The specific discharge energy (SDE) defining as the real energy required to remove a unit volume of material. The SDE is constant for a specific material. Experimental results revealed that the relative relationship of SDE between different materials is invariant as long as all materials are machined under the same machining conditions, it was also found that the materials having close value of SDE demonstrate very similar machining characteristics such as machining speed, discharge frequency, groove width & surface finish of the machined surface under the same machining conditions. These results could be applied for the determination of the settings of machining parameters for different materials.

Lautre and Manna (2006) presented a binary relational analysis and expert system based module for maintenance and fault diagnosis of CNC WEDM. To explain the fault diagnosis and to realize the importance of maintenance through suggestions, the detection of faults was investigated through forward and backward propagation of matrix transformation. The developed system could help the trainers, operators and manufacturing engineers in achieving trouble free machining through quick detection of faults and proper maintenance of machines in actual practice.

Yan et al. (2007) studied a combined two-degrees-of freedom controller and Disturbance Observer (DOB) to improve the contouring accuracy of a linear synchronous motor drive WEDM machine. It was concluded that a conventional Proportional Integral Derivative (PID) control commonly used in commercial CNC machine tool could only improve the contouring accuracy to a very limited range. The proposed controller achieved a high contouring accuracy of $\pm 0.3\mu\text{m}$ as well as provided adequate disturbance rejection and robustness. The maximum contour error of circular trajectory at a feed rate of 40mm/min was reduced from 8.5 to 3.2 μm in comparison with the PID controller.

Lin and Liao (2009) developed the methodology for generating the wire-radius-compensated NC data equations required to carry out the machining. The results proved that the components manufactured using the proposed effective wire radius compensation are more geometrically precise than those produced using the conventional WEDM compensation method.

Haddad et al. (2010) experimentally investigated the cylindrical wire electrical discharge turning process to generate precise cylindrical forms on hard, difficult to machine materials. The level of importance of machining parameters on the roundness was determined by using

Analysis of Variance (ANOVA). Based on the ANOVA method, the highly effective parameters for the roundness were found as spindle rotational speed, voltage, power, and interaction effects between voltage and spindle rotational speed, whereas pulse off-time was a less effective parameter. The regression model between the machining parameters and machining performance was established.

Das et al. (2010) studied Modeling of spark erosion rate in micro wire-EDM. A comprehensive mathematical model has been developed to incorporate plasma features, moving heat source characteristics, multi spark phenomenon, and wire vibration effect to predict the cathode erosion rate for a single- and multi-spark in micro-WEDM. It was concluded that the plasma current and plasma radius increase with time. The temperature of the plasma increases gradually overtime and is independent of the wire velocity. The temperature around wire periphery is affected directly by the diameter of the wire. The erosion rate of the work piece is directly proportional to the temperature of the plasma and thus is independent of the velocity of the wire but decreases with increasing wire diameter. The erosion rate increases gradually with pulse on-time but a lot of fluctuations were seen because of its direct dependence on the plasma current.

Sarkar et al. (2011) studied a novel method for determination of wire lag for enhanced profile accuracy in WEDM. A novel method to measure gap force intensity and wire lag under any given machining condition has been proposed by developing an analytical model. Experiments were carried out to verify the proposed model. Beside this, the impact of wire deflection on profile accuracy during cutting cylindrical job has been investigated. It was observed that the level of inaccuracy due to wire lag is higher for smaller radius job, where the accuracy requirement is generally higher. It is analytically developed and also experimentally proved that the required wire lag compensations inversely proportional to programmed radius.

3.2. WEDM Process Optimization

WEDM is a complex machining process controlled by a large number of process parameters. The setting of the various process parameters required in the WEDM process play a crucial role in producing an optimal machining performance such as Cutting Rate (CR), Material Removal Rate (MRR), Surface Roughness (SR), Wire Wear Ratio (WRR) and Kerf Width (KW). The selection of appropriate machining conditions for the WEDM process is based on the relationship between the various process parameters to the machining performances. Traditionally, this was carried out by relying heavily on the operator's experience, thumbs rules or the conservative technological data provided by the WEDM manufacturer, which produced inconsistent machining performance. Moreover, the parameter setting given by the manufacturers are only valid for the common steel grades so for advanced materials, parameters setting have to be optimized experimentally.

Scott et al. (1991) have presented a study for the optimization of cutting parameters, which were effective for material removal rate and surface finish. They found that the surface finish increases with increasing discharge current, pulse duration and wire speed.

Liao et al. (1997) proposed an optimization technique for the selection of machining parameters. In the study, Taguchi quality design method is used to determine the significance of the machining parameters on the workpiece removal rate. Spedding and Wang (1997)

attempted the optimization of the process parameter settings by using artificial neural network to character the surfaces produced by WEDM. Response surface methodology and artificial neural networks models were developed and experiment showed that both the models are able to predict the process performance such as cutting speed, surface roughness and surface waviness within a reasonable large range of input factor levels. However, relative importance of the machining parameters on the performance measures (i.e., workpiece removal rate and surface topography) has not been considered in the above mentioned last two studies (Liao et al., 1997; Spedding and Wang, 1997). Huang and Liao (1999) made an attempt to understand the effect of machining parameters on the cutting rates and cutting width for machining a precision workpiece.

Tosun et al. (2003) found that increasing the wire speed increases the depth and diameter of the wire crater. For longer pulse durations and higher wire speeds, the wire travel will be longer in front of the spark plasma channel which will result in larger crater diameters. However the most effective parameters for determining the crater depth and crater diameter are open circuit voltage and pulse duration. It was found that increasing the pulse duration, open circuit voltage, and wire speed increases the crater size whereas increasing the dielectric flushing pressure decreases the crater size. Huang and Liao (2003) optimized the machining parameters of WEDM based on Grey relational and statistical analysis. It was found that the table feed rate had a significant influence on the metal removal rate, while the gap width and surface roughness were mainly influenced by pulse on time.

Tosun et al. (2004) investigated a study on kerf & material removal rate in WEDM based on Taguchi method. The experimental studies were conducted under varying pulse duration, open circuit voltage, wire speed & dielectric flushing pressure. Based on ANOVA method, the highly effective parameters for both the kerf and MRR were found as open circuit voltage & pulse duration, whereas wire speed & dielectric flushing pressure were less effective parameters. Liao et al. (2004) analyzed the different process parameters using Taguchi quality design, ANOVA and F-test to achieve a fine surface finish in wire-EDM and found that the machining voltage, current-limiting resistance, type of pulse-generating circuit and capacitance were identified as the significant parameters affecting the surface roughness in finishing process. Kuriakose Shunmugam (2005) optimized the WEDM process by non-dominated sorting genetic algorithm and found that there was no single optimal combination of cutting parameters, as their influences on the cutting velocity and the surface finish are quite opposite. It was found that cutting velocity and surface finish were most significant parameters which decide the cutting performance. Optimization of WEDM helps to increase the production rate considerably by reducing the machining time.

Ramakrishnan and Karunamoorthy (2006) used multi response optimization method using Taguchi's robust design approach for WEDM. Each experiment had been performed under different cutting conditions of pulse on time, wire tension, delay time, wire feed speed and ignition current intensity. Three responses namely material removal rate, surface roughness and wire wear ratio had been considered for each approach. It was observed that the Taguchi's parameter design is a simple, systematic, reliable and more efficient tool for optimization of the machining parameters. It was indentified that the pulse on time and ignition current had influenced more than the other parameters. The research showed that multiple performance characteristics such as material removal rate, surface roughness and wire wear ratio can be improved concurrently. Further research in this field might attempt to consider surface waviness, surface flatness and form accuracy as output parameters.

Table 1. Summary of literature review related to WEDM based on optimization method

S.N.	Reference	Year	Modeling/Analysis / Optimization method	Remarks
1.	Speeding and Wang	1997	Response Surface Methodology, Artificial Neural Network	A response surface model based on a central composite rotatable experiment design and a 4-16-3 size back-propagation neural network (ANN) was developed. Both models provided the accurate results for the process. 4-32-3 ANN model fit the process better than the 4-16-3 but was time consuming.
2.	Lok and Lee	1997	Weibull Modulus	The variability of test results were analyzed by the Weibull statistical method.
3.	Konda et al.	1999	Design of experiment	Experimental design technique was used to solve the multi-objective optimization problem.
4	Huang and Liao	2003	Grey relational and statistical analysis, Taguchi Design	Grey relational analysis was applied to determine the optimal selection of machining parameters for the WEDM. Taguchi Design L ₁₈ mixed orthogonal array was chosen for the experiment.
5	Kuriakose and Shunmugam	2005	Regression model, Genetic Algorithm	A multiple regression model was used to represent relationship between input and output variables and a multi-objective optimization method based on a Non-Dominated Sorting Genetic Algorithm was used to optimize WEDM process.
6	Puri and Bhattacharyya	2005	Response Surface Methodology	An experimental plan for rotatable central composite design of second order involving four variables with five levels was employed to carry out the experimental investigation and subsequently to establish the mathematical model correlating the input process parameters with the response.
7	Hewidy et al.	2005	Response Surface Methodology (RSM)	The RSM was used to correlate the inter-relationship of various WEDM machining parameters with the process performances.
8	Mahapatra and Patnaik	2006	Taguchi Method, Genetic Algorithm	Taguchi experimental design method is used to obtain the optimum parameter combination for maximization of Material Removal Rate(MRR), Surface Finish(SF) as well as minimization of kerf. In order to optimize for all the three objectives, mathematical models were developed using the non-linear regression method.
9	Tosun et al.	2006	Analysis of Variance (ANOVA)	ANOVA was used to obtain the relationship between the response with input parameters.
10	Ramakrishnan and Karunamoorthy	2006	Multi-Response Signal to Noise ratio(MRSN), ANOVA	MRSN ratio was applied to measure the performance characteristics deviating from the actual value. Analysis of Variance (ANOVA) was employed to identify the level of importance of the machining parameters on the multiple performance characteristics.
11	Chiang and Chang	2006	Grey Relational Analysis	Grey Relational Analysis was used to formulate the response table and response graph for each level of the machining parameters.
12	Kanlayasiri and Boonmung	2007	Design of experiments and regression model	ANOVA was used to determine the effect of parameters on the process performances. Assumptions of ANOVA were tested using residual analysis. Quantitative testing methods were employed in place of the typical qualitative testing techniques. Finally a mathematical model was developed using multiple regression method.
13	Guiqin et al.	2007	Neural-fuzzy modeling and Genetic Algorithm	The model combined modeling function of fuzzy interference with the learning ability of artificial neural network. Integrated with the genetic optimization procedure, the fuzzy inference systems were used to optimize the model of WEDM.

S.N.	Reference	Year	Modeling/Analysis / Optimization method	Remarks
14	Yuan et al.	2008	Gaussian Process Regression(GPR), Multi Objective Genetic Algorithms, Back-Propagation Neural Network	GPR models have the advantage over other models in terms of model accuracy, feature scaling and probabilistic variance
15	Sarkar et al.	2008	Response surface methodology (RSM), Desirability Function approach, Pareto Optimization algorithm.	A second order mathematical model was developed using RSM. Finally, the operation was optimized by Desirability Function approach and Pareto Optimization algorithm. It was observed that performance of the developed Pareto Optimization algorithm was superior compared to Desirability Function approach
16	Saha et al.	2008	Back-Propagation Neural Network, Multi-variable regression model	Back-Propagation Neural Network and Multi-variable regression model was developed to correlate the input process parameters with the process performances.
17	Shah et al.	2009	Taguchi method, Analysis of Variance (ANOVA)	The design of experiment was based on Taguchi design with 8 control factors with three levels each. ANOVA was carried out after obtaining the responses to determine the significant factors.
18	Manna and Kumar	2009	Taguchi Method (L ₁₈), ANOVA	Taguchi method L ₁₈ mixed orthogonal array was used to determine to determine S/N ratio, analysis of variance and F-test value for indicating the most significant parameters affecting the process performance.
19	Gauri and Chakraborty	2009	Grey Relational analysis (GRA), Multiple Response Signal to Noise ratio (MRSN), Weighted Signal to Noise ratio (WSN) and Vlse Kriterijumska Optimizacija I Kompromisno Resenje in serbian (VIKOR)	GRA, MRSN, WSN and VIKOR was used to model and optimize the process but result showed that WSN ratio method was the best
20	Gauri and Chakraborty	2009	Weighted Principal Component (WPC)	WPC method was used to optimize the multiple responses of WEDM processes. The result showed that the WPC method offers significantly better overall quality than the other approaches.
21	Lin and Liao	2009	Modified Denavit- Hartenberg (D-H) notation	The modified D-H notation was employed to derive the machine's ability matrix and to generate the desired were location matrix.
22	Patil and Brahmkar	2010	Dimension Analysis, Semi-empirical model, Response Surface Methodology	The model was developed by using dimension analysis and non-linear estimation technique such as quasi-Newton and simplex. In addition, an empirical model, based on Response Surface was also developed.
23	Guyen et al.	2010	Back Propagation(BPNN), General Regression Neural Networks (GRNN)	Both the BPNN and GRNN were used to determine and compare the WEDM parameters with the feature of surface roughness. It was found BPNN has the better learning capabilities and generalization ability for WEDM than the GRNN.

Yuan et al. (2008) developed the reliable multi-objective optimization based on Gaussian process regression (GPR) to optimize the high speed wire-cut electrical discharge machining process, considering mean current, on-time and off-time as input features and material removal rate and surface roughness as output responses. The experiment results showed that GPR models have the advantage over other regressive models in terms of model accuracy, feature scaling and probabilistic variance.

Singh et al. (2009) studied the effects of process parameters on material removal rate in WEDM. The effects of various parameters of WEDM like pulse on time, pulse off time, gap voltage, peak current, wire feed & wire tension have been investigated to reveal their impact on material removal rate of hot die steel. It was concluded that MRR directly increases with increase in pulse on time & peak current while decreases with increase in pulse off time & servo voltage.

3.4. Ultrasonic Vibration to the Wire Electrode

The machining performance was greatly influenced by the wire tool vibration occurring during machining. Guo et al. (1997) showed that wire vibration induced by ultrasonic action has a significant effect on the overall performance of the WEDM process. It was found that there exists an optimum relationship between the vibration amplitude of the wire and the discharge energy, by which the highest cutting rate and the best machined surface quality can be obtained.

Guo et al. (1997) also investigated the machining mechanism of WEDM with ultrasonic vibration of the wire. By means of experiments employing single pulse discharge it has been established that the high frequency vibration of wire electrode is able to bring about multiple channel discharges so that better surface quality and a high cutting rate can be obtained simultaneously.

Puri and Bhattacharyya (2003) depicted the influence of the pulse discharge frequencies under various wire tensions on the maximum amplitude of the wire vibration. A high tension without wire rupture is always beneficial to reduce the amplitude of wire tool vibration. Thickness of the workpiece also affects the amplitude of vibration and higher the thickness of the workpiece, larger will be the maximum amplitude of vibration for a given span of the wire between the guides. It is clarified from the solution that wire vibration during machining is mainly manipulated by the first order mode. The density of spark discharges also depends upon the shape of mode of a vibration. This minimization of imprecision and inaccuracy due to wire tool vibration will find the potential industrial application for manufacturing job with ultra precision contours.

3.5. Development of Wire Electrode

Kuroda et al. (2003) developed the high performance coated wire electrodes for high-speed cutting and accurate machining. They have developed two types of wire electrodes: both consist of a thin copper zinc alloy layer and core material, one being a copper zinc alloy coated with a brass layer while the other is a Cu-Sn-In alloy with high heat resistance and high electrical conductivity.

3.6. Prevention of Wire Electrode Breaking

Tanimura and Heuvelman (1977) developed a short circuit detecting system to avoid short sparks which causes the wire to rupture, which was performed by adjusting the choke inductance of the pulse generator. They reported that the unusual high rate of short circuit pulses during a period of 30 μ s or more causes the wire rupture.

Kinoshita et al. (1982) analyzed the various types of wire breaking. To prevent the wire breaking they developed a control system by means of monitoring the pulse frequency. Once a sudden rise of pulse frequency was detected, the pulse generator and servo system were turned off instantaneously to prevent the wire rupture. However the machining efficiency was much reduced by such control strategy but the efficiency was good up to 20 mm work-piece thickness.

The probable causes leading to wire rupture are failure under excessive thermal load, failure through short circuiting and wire vibration, the most important among these being the thermal load (Rajurkar and Wang, 1993).

Banerjee et al. (1993) determined the temperature distribution in the material of the wire and there by predicted failure due to thermal load. A simple computational model was developed which will give the temperature values for varying magnitudes of parameters, viz. input power, pulse on time, wire velocity and wire diameter.

Luo (1995) analyzed the energy distribution strategy in fast cutting wire EDM. It was experimentally confirmed that a stable high cutting speed can be achieved without detriment to the electrode wire only by applying discharge pulses with high power density and then raising the pulse density to the greatest possible extent. An extreme long discharge duration causes low energy efficiency, while excessively high pulse density results in incurable instability with low discharge efficiency.

Luo (1999) investigated the effect of the mechanical strength of the wire to find the wire rupture mechanism in WEDM. He emphasized the importance of the wire tension and spark energy in wire rupture.

Abnormal spark is one of the reasons for wire breaking. Lee and Liao (2003) developed the self-tuning fuzzy control for wire rupture prevention. By the concurrent adjustment of the arc off-time and the servo reference voltage, the abnormal sparks can be regulated at the proper level. As a result, the problems of wire rupture in most WEDM processes can be successively solved.

The thermal model accounts for the input energy density caused by different wire velocity. A temperature distribution along the wire electrode indicates that the highest temperature occurs near to the exit of the workpiece region.

Saha et al. (2004) used the finite element modeling and optimization to prevent wire breakage in electro-discharge machining. The model successfully predicted the thermal distribution profile accurately for various wire materials, for increased wire velocity and for reduction in heat transfer co-efficient. The developed model may lead to the development of a smart electro-discharge machining system with a sensor and feedback control to increase the cutting speed and minimize breakage. The results of the modeling and optimization showed that non uniform heating is the most important variable affecting the temperature and thermal strain. The future scope includes complex 3-d finite element analysis models for accurate prediction of wire breakage and erosion during machining.

Cabanes et al. (2008) proposed an on-line supervision system that monitors and diagnoses in advanced degraded cutting regimes in WEDM. The distribution of the anticipation time before wire breakage was also studied. The results showed that the detection strategy provides an anticipation time longer than 50 ms in approximately 80% of the total wire breakage cases. The results of the analysis revealed new symptoms that allow to predict wire breakage. These symptoms were related to the occurrence of an increase in discharge energy, peak current, as well as increase and / or decrease in ignition delay time.

Bannerjee et al. (2010) investigated into Numerical evaluation of transient thermal loads on a WEDM wire electrode under spatially random multiple discharge conditions with and without clustering of sparks. In the present investigation, a one-dimensional explicit finite difference thermal model was proposed for estimating the transient temperature distribution along the length of the wire under the conditions of randomly located spatial sparks with and without the formation of clusters. An optimum combination of power and duty factor as well as a critical value of frequency seemed to exist for better machining without wire rupture risks. For long elapsed time under multiple spark conditions, increase in wire velocity reduces the maximum temperature. The one-dimensional thermal models can be used for setting rules of selection for an expert system for the safe operating conditions of WEDM.

3.7. Accuracy Improvement of WEDM

Dauw and Albert (1992) developed a mathematical model to analyze the wire deflection during machining. The deviation of the wire position relative to the programmed wire path position was continuously measured and corrections were made during machining of complex shapes, arc and contours. In this study, substantial gain of machining time and improvement in corners accuracy was obtained.

Beltrami et al. (1996) experimentally measured the deviation of the wire position relative to the programmed wire path position

Puri and Bhattacharyya (2003) also analyzed the geometrical inaccuracy due to wire lag phenomenon in WEDM. The Taguchi methodology is employed to find out the main parameters that affect the different machining criteria, such as average cutting speed, surface roughness and the geometrical inaccuracies. It was clarified from the solution that wire vibration during machining was mainly manipulated by the first order mode. The density of spark discharges also depends upon the shape of mode of a vibration. This minimization of imprecision and inaccuracy due to wire tool vibration will find the potential industrial application for manufacturing job with ultra precision contours.

Yan et al. (2004) studied the accuracy improvement of WEDM by real time wire tension control. A closed loop wire tension control system for a WEDM machine is presented to improve the machining accuracy. Dynamic models of the wire feed control apparatus & wire tension control apparatus were derived to analyze & design the control system. Experimental results not only demonstrate that the developed control system with dynamic absorbers could obtain fast transient response & small steady state error than an open loop control system, they also indicate that the geometrical contour error of corner cutting was reduced with approximately 50% & the vertical straightness of a workpiece could be improved significantly.

Mohammadi et al. (2007) studied the effects & the optimization of machining parameters on the surface roughness & roundness in the TWEDM. A new machining parameter such as rotational speed is introduced, which changes the normal machining conditions in conventional WEDM. It was concluded that only power has a significant effect on the surface roughness. The effects of wire speed, power & servo on roundness were more significant than time off, voltage, wire tension & rotational speed.

3.8. Application of WEDM

3.8.1. WEDM for Conventional and Advanced Materials

Guo et al. (2002) experimentally investigated the shaping of Al_2O_3 particle- reinforced material (6061 alloy) by WEDM. It was found that the selection of the electric parameters had an important effect on the cutting rate. When low energy was used to cut particle-reinforced material, it was likely to bring about wire breakage especially for small pulse duration and low machining voltage. In operation, how the electric parameters were selected has little influence on the surface roughness. Whether high energy or low energy was used, a coarse surface was always obtained. In operation, large pulse duration, a high voltage, a large machining current and a proper pulse interval should be selected for high machining efficiency.

Hewidy et al. (2005) modeled the machining parameters of Inconel 601 using response surface methodology. Inconel 601 is a nickel base super alloy with a high content of iron, chromium and niobium, strengthened mainly with Ni_3Nb . The volumetric metal removal rate increased with the increase of the peak current value and water pressure. The wear ratio increased with the increase of peak current. The surface roughness increased with the increase of peak current and decreased with the increase of duty factor and wire tension.

Ramakrishnan and Karunamoorthy (2006) optimized the machining parameters for heat-treated tool steel using robust design of experiments. The effect of various machining parameters such as pulse on time, wire tension, delay time, wire feed speed and ignition current intensity on material removal rate, surface roughness and wire wear ratio have been considered. The research showed that multiple performance characteristics such as material removal rate, surface roughness and wire wear ratio can be improved concurrently. Further research in this field might attempt to consider surface waviness, surface flatness and form accuracy as output parameters.

Ozdemir and Ozek (2006) investigated the machinability of nodular cast iron by WEDM using different parameters machining voltage, current, wire speed and pulse duration. Three zones were identified in rough regimes of machining for all samples: de-carburized layer, heat effected layer and bulk metal. High machining efficiency can be obtained when the proper electrical parameters are selected, but whether high energy or the low energy is used, a coarse surface is always obtained. The variation of surface roughness and cutting rate with machining parameters was mathematically modeled by using the regression analysis method.

Sarkar et al. (2006) optimized WEDM of γ titanium aluminide alloy through an artificial neural network model. The three most important parameters- cutting speed, surface roughness and wire offset had been considered as measure of the process performance. Pulse on time, Pulse off time, Peak current, Wire tension, Dielectric flow rate and Servo reference voltage were used as a control parameters. Mahapatra and Patnaik (2006) used a 0.25 mm diameter

zinc coated copper wire for a block of D2 tool steel workpiece in their experimental work and took Discharge current, Pulse duration, Pulse frequency, Wire speed, Wire tension, Dielectric flow rate as a process parameters. Minimum wire tension gives maximum MRR but maximum wire tension gives maximum surface finish and minimum kerf. Factors like discharge current, pulse duration and dielectric flow rate and their interactions was found to play a significant role in rough cutting operations for maximization of material removal rate, minimization of surface roughness and cutting width. The future scope includes using different work material and hybrid optimization techniques.

Parashar et al. (2009) investigated the optimization of surface roughness for WEDM of SS 304L using Taguchi dynamic experiments. Each experiment was performed under different cutting conditions of gap voltage, pulse on time, pulse off time, wire feed & dielectric flushing pressure. It was found that pulse on time was the most influencing machining parameter for surface roughness. The gap voltage, pulse off time, flushing pressure and wire feed has little effect on surface roughness.

3.8.2. WEDM for Ceramics

Lok and Lee (1997) analyzed the processing of advanced ceramics (Sialon and Al₂O₃-TiC) using the wire-cut EDM process. The volumetric material removal rate for processing these ceramic materials were found to be very low as compared with alloy steels and the surface roughness achieved was generally inferior to that with the die sinking EDM process. The simulation of the dynamic characteristics of the wire electrode under the action of continuous discharge forces showed that ultrasonic vibration facilitates the shift of the discharge points and improves their distribution. The results showed that the WEDM process is a viable material processing method for the machining of advanced ceramics, but work have to be carried out to further study the ways and means of improving the surface finish and surface integrity of the machined ceramics such as to give a more reliable service life of components made of advanced ceramics.

Obara et al. (2004) studied the corrosion of cemented carbide during wire WEDM and found that a wire close to the cemented carbide surface causes corrosion of the cemented carbide in water, even if an AC voltage is applied to them. Jühr et al. (2004) improved cemented carbide properties after WEDM by pulse shaping and showed that it is important to use the correct parameter selection for main cut and post cut. Deterioration in the material properties by processing with high pulse energies can be corrected only up to a limited extent in the post cut. It is possible to reduce the rim damages in significant dimensions. The improved material properties can be proved by increased bending fraction stress. The considerable reduction of the post cuts leads to an increase in the total productivity of the machining and significantly lowering the cost. Tani et al. (2004) used a new assisting electrode material to avoid the breaking of the same for machining of the insulating ceramics (Si₃N₄). Using a carbonized layer as the assisting electrode, a ceramic plate of 100 mm thickness could be cut under high discharge current conditions.

Saha et al. (2007) developed the second order multi-variable regression model and a feed forward back-propagation neural network (BPNN) model to correlate the input process parameters (Pulse on-time, pulse off-time, peak current and capacitance) with the performance measures (Cutting speed and surface roughness) for the WEDM of tungsten carbide-cobalt composite material. It was observed that the increase in both peak current and capacitance lead to the increment of cutting speed and surface roughness.

Table 2. Summary of literature review related to WEDM based on workpiece material

S. No.	Workpiece Material	Wire Used	Process Parameters	Process performances/ Responses	Exp. Design	Optimization methods	Remarks	References
1	Titanium alloy (Ti6Al4V)	Brass, Zinc or Al coated	Time Between two pulses, Pulse duration, Servo control reference voltage, Maximum servo-speed variation, wire speed, wire tension, injection pressure	Cutting velocity, surface finish	Taguchi L-18	Non-dominated Sorted Genetic Algorithm	Non-dominated solution set was reported	Kuriakose and Shunmugam, 2005
2	Tungsten Carbide	Brass	Material thickness, Open voltage, Pulse ON time, pulse OFF time, Servo Voltage, Wire feed velocity, Wire Tension, dielectric pressure	Material Removal Rate, Kerf, Surface Roughness	Taguchi L-27	ANOVA	Material thickness had little effect on MRR and Kerf but was a significant factor in terms of surface roughness.	Shah et al., 2009
3	Al/SiC-MMC	Brass	Pulse ON time, pulse OFF time, Peak current, pulse peak voltage, wire feed rate, wire tension, spark gap voltage	Material Removal Rate, Surface Roughness, gap current, spark gap	Taguchi L-18, Gauss Elimination method	ANOVA, F-test	Optimal combination of WEDM was determined	Manna and Bhattacharyya, 2005
4	Al-4Cu-6Si alloy/ SiC-MMC	Brass	Pulse current, gap voltage, pulse duration	Material Removal Rate, Surface Roughness, tool wear rate, Radial over cut	Taguchi L-27	ANOVA	A second order non-linear mathematical model was developed	Dhar et al., 2007
5	Heat treated Tool steel	Zinc coated Brass wire	Pulse on time, Wire tension, Delay time, Wire feed speed, Ignition current intensity	MRR, SR, WWR	Taguchi L-16	ANOVA	Level of importance of machining parameters on the multiple performance characteristics was considered	Ramarishnan and Karunamoorthy 2006
6	D2 tool Steel	Stratified (Zinc coated copper wire)	Discharge current, pulse duration, pulse frequency, wire speed, wire tension, dielectric flow	MRR, SF, Kerf	Taguchi L-27, Non-linear regression analysis	Genetic Algorithm	Importance of machining parameters on the multiple performance characteristics was determined	Mahapatra and Patnaik, 2006

Table 2. (Continued)

S. No.	Workpiece Material	Wire Used	Process Parameters	Process performances/ Responses	Exp. Design	Optimization methods	Remarks	References
7	1.7131 Cemented Steel	-	Power, time-OFF, Voltage, Servo Voltage, wire Tension, Wire speed, rotational speed	SR, Roundness	Taguchi L-18	ANOVA	Optimized the machining parameters in Travelling-WEDM operations	Mohammadi <i>et.al.</i> , 2007
8	SS 304 L	Brass wire	Gap voltage, Pulse ON time, pulse OFF time, Wire feed, dielectric pressure	SR	Taguchi L-32	-	Effect of various parameters on surface roughness was studied	Parashar <i>et al.</i> , 2009
9	M2- Hardened and annealed die steel	Brass wire	Pulse on time	White layer depth		Response surface methodology	Rough cutting and trim cutting was performed. Effect of process parameters on response was studied	Puri and Bhattacharyya, 2005
10	Alloy Steel (Cr 12)	-	Discharge current	SR		FEA model in ANSYS	Thermo analysis was carried out to study the effect of discharge current on SR	Han <i>et. al.</i> , 2006
11	Nodular Cast Iron (GGG 40)	Brass Wire	Machining Voltage, Current, Wire speed, Pulse Duration.	Cutting Rate, SR	--	Regression Analysis	Variation of surface roughness and cutting rate with machining parameters was mathematically modeled	Ozdemir and Ozek (2006)
12	Tungsten Carbide Cobalt composite	Uncoated Brass	Pulse ON time, Pulse OFF time, Peak Current setting, Capacitance	Cutting speed and SR	Back propagation Neural Network (4-11-2)	Multivariable regression model	Studied the effect of input parameters on performances	Saha <i>et. al.</i> , 2008
13	Quenched and Tempered Martensitic Stainless Steel	Brass	----	Thickness of recast layer	--	---	Thickness of recast layer varied with the heat treatment condition of the workpiece.	Huang <i>et. al.</i> 2004

S. No.	Workpiece Material	Wire Used	Process Parameters	Process performances/ Responses	Exp. Design	Optimization methods	Remarks	References
14	AlSi ₇ Mg/SiC and AlSi ₇ Mg/Al ₂ O ₃	Brass	Pulse-ON-time, Discharge Current	Cutting feed rate, surface roughness	---	---	The machining feed rate of WEDM cutting composites significantly depends on the kind of reinforcement.	Roznek <i>et. al.</i> 2001
15	AISI 4140 Steel	Brass	Pulse Duration, Open Circuit Voltage, Wire Speed, Dielectric Flushing Pressure	Wire crater size	ANOVA	----	Effect on cutting parameters on wire crater size was determined	Tosun et al. 2003
16	Sialon, Al ₂ O ₃ -TiC	Brass	Peak current	Material Removal Rate, Surface Finish	Weibull Modulus	--	Viability of WEDM process was determined to machine the advanced Ceramics	Lok and Lee 1997
17	SKD 11 Alloy Steel	Brass	Feed Rate, Pulse-ON-time, Pulse-OFF-Time, Wire Velocity, wire Tension, Fluid Pressure	Metal Removal Rate, Gap Width, Surface Roughness	Taguchi Method	Grey Relational and Statistical Analysis	Optical machining parameters setting for maximum metal removal rate, minimum surface roughness, minimum gap width was determined	Huang and Liao 2003
18	Alloy Steel (Cr 12)	Brass	Pulse Duration, Discharge Current, Sustained Pulse Time, Pulse Interval Time, Polarity effect.	Surface Roughness	----	-----	Experimentally investigated the influence of machining parameters on surface roughness.	Han et. al. 2006
19	ZrO ₂ -WC composite	CuZn 37 Brass	Gap Voltage, Pulse Duration, Pulse Interval, Reference Servo Voltage, Flushing pressure, Ignition current, Wire tension, Wire speed	Material Removal Rate, Surface Roughness	---	---	Experiment revealed a significant influence of the microstructure of the secondary WC-phase on WEDM behavior and frictional characteristics.	Bonny et. al., 2008
20	AISI 4340 Low Carbon Steel	---	On-Time Pulses. Open circuit Voltage, Machine Cutting Speed, Dielectric Fluid Pressure	Thermal damage	Finite Element Method	----	A Finite Element Method program was developed to model temperature distribution in the workpiece under the conditions of different cutting parameters.	Hargrove and Ding 2007

Table 2. (Continued)

S. No.	Workpiece Material	Wire Used	Process Parameters	Process performances/ Responses	Exp. Design	Optimization methods	Remarks	References
21	γ Titanium Aluminide alloy	Brass	Pulse-ON time, Pulse-OFF-time, Peak current, Wire Tension, Dielectric Flow Rate, Servo Reference voltage	Cutting Speed, Surface Roughness , Wire Offset	---	Artificial Neural Network	Experiment results demonstrated that the machining model was suitable and the optimization strategy satisfied the practical requirements.	Sarkar et al.,2006
22	E0300 Alloy Steel	Brass	Open Circuit Voltage, Pulse ON time, Pulse OFF time, Pulse Peak Current, Wire Feed Rate, Wire Tension, Spark gap Voltage	Wire Crater Depth, Electrode Wear Rate, Surface Finish	Taguchi Method	ANOVA	Mathematical models were developed for wire crater depth, electrode wear rate and surface finish during machining of E0300 alloy Steel.	Manna and Kumar
23	AISI 4340 Steel	Brass	Pulse Duration, Open Circuit voltage, Wire Speed and Dielectric flushing pressure	Surface Roughness	Back Propagation(BPNN), General Regression Neural Networks (GRNN)	----	It was found BPNN had the better learning capabilities and generalization ability for WEDM than the GRNN.	Guyen <i>et. al.</i> 2010
24	DC 53 Die Steel	Cu-35wt % Zn	Pulse ON time, Pulse OFF time, Pulse Peak Current, Wire Tension	Surface Roughness	Design of experiment	Regression Model	Result from the analysis showed that pulse on time and pulse peak current were significant variables to the surface roughness of WEDM of DC 53 Die Steel.	Kanlayasiri and Boonmung 2007
25	Al ₂ O ₃ particle reinforced material (6061alloy)	Pure Copper	ON time of discharging, OFF time of discharging, arc ON time of discharging, arc OFF time of discharging, Servo Voltage, Wire Feed, Water Flow	Surface removal rate, Surface Roughness	Grey Relational Analysis	--	Presented an effective approach for the optimization of the WEDM process of Al ₂ O ₃ particle reinforced material (6061alloy) with multiple performance characteristics.	Chiang and Chang

S. No.	Workpiece Material	Wire Used	Process Parameters	Process performances/ Responses	Exp. Design	Optimization methods	Remarks	References
26	Al/ SiC Metal Matrix Composite	--	Pulse ON time, Pulse OFF time, Average Voltage	Material Removal rate	Dimensional Analysis	--	Present work proposed a semi-empirical model for Material Removal rate in WEDM based on thermo-physical properties of the workpiece and machining parameters.	Patil and Brahmkar
27	Inconel 601	Brass	Peak current, Pulse-ON time, Pulse-OFF-time, Wire Tension, Dielectric fluid, Wire Diameter, Water pressure	Metal Removal rate, Wear Ratio, Surface Roughness	Response Surface Methodology	----	Developed the model for correlating the inter-relationship of various WEDM machining parameters of Inconel 601 material with the process performances.	Hewidy et. al.
28	Beryllium Copper alloys	Brass	Pulse duration, Charge current, Charge frequency, Capacitance	Material removal rate, Surface Roughness	Design of experiment	---	Multi-objective optimization technique was applied to find the parameters setting for optimum cutting speed as well as optimum surface roughness.	Konda et. al. 1999

The SEM analysis confirmed that the machined surface was characterized by loosely bounded tungsten carbide grains and a lot of micro cracks, which were radially spread over the machined surface. It was also observed that at high energy level, the size of the micro-cracks increases.

Bonny et al. (2009) performed the dry reciprocating sliding experiments on wire-electrical discharge machined ZrO_2 -WC composites samples against WC-Co cemented carbide, performed using a pin-on-plate testing rig, and revealed a significant influence of the microstructure of the secondary WC-phase on wire-EDM behavior and frictional characteristics.

Shah et al. (2010) investigated the effect of all critical WEDM parameters for the machining of tungsten carbide cobalt composites such as open voltage, servo voltage, pulse on-time, pulse off-time, wire feed speed, wire tension, dielectric pressure and also thickness of tungsten carbide material on machining characteristics such as material removal rate, surface roughness and kerf. The workpiece thickness was expected to have a major effect on the material removal rate but showed to be significant in the case of surface roughness only. It was concluded that the material thickness had little effect on the material removal rate and kerf but was significant factor in terms of surface roughness. For thinner work-pieces, in order to obtain a fine surface finish, the spark energy will have to be reduced, which also reduces the material removal rate.

3.8.3 WEDM for Metal Matrix Composites

Rozenek et al. (2001) experimentally investigated the effect of machining parameters (discharge current, pulse-on-time, pulse-off-time, voltage) on the machining feed rate and surface roughness during wire electrical discharge machining of metal matrix composites AlSi7Mg/SiC and AlSi7Mg/Al₂O₃. The maximum cutting speed of AlSi7Mg/SiC and AlSi7Mg/Al₂O₃ metal matrix composites were approximately 3 times and 6.5 times lower than the cutting speed of aluminium alloy respectively.

Yan et al. (2005) examined the wire electrical discharge machining of Al₂O₃_p/ 6061 Al composite. The experiment results indicated that the material removal rate, surface roughness and width of slit of cutting test material significantly depend on volume fraction of reinforcement (Al₂O₃ particles). Test results revealed that in machining Al₂O₃_p/ 6061 Al composites a very low wire tension, a high flushing rate and a high wire speed were required to prevent wire breakage; an appropriate servo voltage, a short pulse-on-time, and a short pulse-off-time which were normally associated with a high cutting speed had little effect on the surface roughness.

Manna and Bhattacharyya (2006) used Taguchi and Gauss elimination method for the parametric optimization of aluminium reinforced silicon carbide metal matrix composite. Effect of machining parameters such as pulse on-time, pulse off-time, peak current, pulse peak voltage, wire feed rate, wire tension and spark gap voltage on machining performance criteria such as metal removal rate, surface roughness, gap current, and spark gap were studied. Open gap voltage and pulse on time were most significant and significant influencing machining parameters respectively for controlling the material removal rate. Wire tension and wire feed rate were most significant and significant influencing machining parameters respectively for controlling the surface roughness. Wire tension and spark gap voltage setting were most significant and significant influencing machining parameters respectively for controlling the spark gap.

Patil and Brahmankar (2010) experimentally investigated the effect of electrical as well as non-electrical machining parameters on performance in WEDM of metal matrix composite (Al/ Al₂O_{3p}). Taguchi orthogonal array was used to study the effect of combination of reinforcement, current, pulse on-time, off-time, servo reference voltage, maximum feed speed, wire speed, flushing pressure and wire tension on cutting speed, surface finish and kerf width. Reinforcement percentage, current and on-time was found to have significant effect on cutting rate, surface finish and kerf width separately.

Garg et al. (2010) conducted a review of research work in sinking EDM and WEDM on metal matrix composite materials. Most of the published work belongs to SiC reinforced metal matrix composites. Not so much work is reported Al₂O₃ reinforced and other MMCs types. Most of the research work had been carried out on optimization of process parameters for improvement of performance measures. In most of research work, mainly electrical process parameters and flushing pressure as non-electric parameter have been taken into account. Very little work has been reported on effect of non-electrical parameters like work piece rotation and electrode rotation. Many MMCs are yet to be explored for suitable electrode material and electrode design since very little research work has been reported in these areas.

Patil et al. (2010) determined the material removal rate in wire electro-discharge machining of metal matrix composites using dimensional analysis. This work proposed a semi-empirical model for material removal rate in WEDM based on thermo-physical properties of the work piece and machining parameters such as pulse on time and average gap voltage. The model was developed by using dimensional analysis and non-linear estimation technique such as quasi-Newton and simplex. Predictability of the proposed model is more than 99% for all work materials studied. The work materials were silicon carbide particulate reinforced aluminium matrix composites. Pulse on-time and thermo-physical properties such as coefficient of thermal expansion, thermal diffusivity and melting point temperature are significant parameters on material removal rate. The experimental results show that increased percentage of ceramic particulates in the MMC causes decreased material removal rate.

Kumar et al. (2011) investigated into wire electrical discharge Machining of Al6063/SiCp composites. The effect of WEDM parameters such as pulse-on time , pulse-off time , gap voltage and wire feed on material removal rate and surface roughness in metal matrix composites (MMCs) consisting of aluminium alloy (Al6063) and silicon carbide (SiCp) is discussed. It was found that the increase in volume percentage of SiC resulted in decreased material removal rate and increased surface roughness. The microstructure of stir cast composite shows discrete localized pool/agglomeration of SiC particles indicating constrain of the process for attaining uniform microstructure. It was found that the influence of gap voltage (V) is more significant than that of other parameters for material removal rate.

Jangra et al. (2011) studied a Digraph and matrix method to evaluate the machinability of tungsten carbide composite with WEDM. A methodology based on digraph and matrix method was proposed to evaluate the machinability of tungsten carbide in terms of material removal rate. This methodology builds a flexible and comprehensive model, which has the capability to consider the interdependencies between various factors and sub-factors affecting the machinability. Factors affecting the machinability of tungsten carbide were grouped into five main factors namely work material, machine tool, tool electrode, cutting conditions, and geometry to be machined. Graph theoretic approach revealed that the machine tool had

highest index value. Therefore, it was the most influencing factor affecting the machinability of tungsten carbide.

Shandilya et al. (2012) obtained the parametric optimization during WEDM of Al 6061/10% wt. SiC_p MMC using RSM and also analyzed the machined surface. Authors found that fine surface finish was obtained when machining was done at a combination of lower levels of input process parameters. Jangra et al. (2012) optimized the multi-machining characteristics i.e., MRR,SR, angular error and radial overcut in WEDM of WC-5.3% CO composite using integrated approach of Taguchi, GRA and entropy method.

3.8.4. Modern Tooling applications

Metal bonded diamond wheels are generally used for grinding difficult-to-cut materials but the poor dressability of it limits its applications. Weingartner et al. (2009) developed a wire electrical discharge dressing unit to dress metal-bonded grinding wheels. Cylindrical plunge grinding tests on silicon nitride work-pieces than in comparison to conventionally dressed wheels, smaller cutting forces and wheel wear are achieved by using EDM dressed grinding wheels.

Taper cutting is a common application of the wire electrical discharge machining process used for the production of parts with complex geometry such as extrusion dies in wear-resistant materials, cutting dies etc. Plaza et al. (2009) developed the original model for the prediction of angular error in wire-EDM taper cutting. Results showed that part thickness and taper angle were the most influencing variables.

3.9. Surface Characteristics Machined by WEDM

To prevent corrosion, recent WEDM machines use an AC power generator which provides a positive and a negative voltage to the gap between the wire and the workpiece alternatively and makes the mean working voltage between the gap 0 V. cemented carbide having cobalt as a binder is corroded during wire EDM, when it is submerged for a long time in water, even if an AC power generator is used to machine the workpiece. A cemented carbide material using nickel as a binder and binder less cemented carbide do not suffer from corrosion, when they are submerged in water for a long duration (Obara et al. (2004))

Schacht et al. (2004) showed by the examination of the wire's impedance, that the skin-effect becomes a predominant phenomenon in WEDM, while machining with ferromagnetic wires. The skin effect raises the electrical resistance of the wire. Using thick conductive coating solve this problem.

Puri and Bhattacharyya (2005) model the white layer depth through response surface methodology comprising a rough cut followed by a trim cut. The white layer depth increases with increasing pulse on time during the first cut. The white layer depth decreases with increasing pulse on time during trim cutting. The white layer depth reduces with decreasing wire tool offset during trim cutting. With increasing cutting speed in trim cutting, the white layer depth first reduces and then starts increasing. This break even trim cutting speed was found to be 3mm/min.

The material removal process in WEDM may result in workpiece surface damage due to the material thermal properties and the cutting parameters. Hargrove and ding (2006) modeled the temperature distribution in the workpiece under the conditions of different

cutting parameters. This model is helpful for developing advance control strategies to enhance the complex contouring capabilities and machining rate while avoiding harmful surface damage. In finish machining of wire electrical discharge machining (WEDM). The discharge current has distinct influences on the machined surface. Han et al. (2007) studied the surface morphology under various pulse durations; thermo-analysis was carried out to investigate the mechanism of erosion of the workpiece material using the finite element method. Under the same discharge energy, a discharge current with a short-duration pulse and a high peak value removes the workpiece material mainly by gasifying, while a discharge current with a long duration pulse and a low peak value removes the workpiece material mainly by melting.

3.10. Future Scope of WEDM

Spedding and Wang (1995) studied the modeling of WEDM process through response surface methodology and artificial neural networks. The pulse width, time between two pulses, wire tension and injection set point were selected as factors while the cutting speed, surface roughness and surface waviness were selected as the responses. From the results presented in this paper it can be concluded that these techniques can be extended to processes exhibiting similar stochastic character and complexity.

Wang and Ravani (2002) studied computer aided contouring operations for traveling WEDM. Here a computational method for NC of traveling WEDM from geometric representation of a desired cut profile in terms of its contour was developed. Normalized arc length parameterization of the contour curves was used to represent the cut profile and a sub division algorithm was developed together with kinematic analysis to generate the required motion of the machine tool axis. It is hoped that this study would enhance further applications of computational geometry in manufacturing and would contribute to CAD /CAM integration for WEDM.

Puri and Bhattacharyya (2003) depicted the influence of the pulse discharge frequencies under various wire tensions on the maximum amplitude of the wire vibration. A high tension without wire rupture was always beneficial to reduce the amplitude of wire tool vibration. Thickness of the workpiece also affects the amplitude of the vibration and higher the thickness of the workpiece, larger will be the maximum amplitude of vibration for a given span of the wire between the guides. It was clarified from the solution that wire vibration during machining was mainly manipulated by the first order mode. The density of spark discharges also depends upon the shape of mode of a vibration. This minimization of imprecision and inaccuracy due to wire tool vibration will find the potential industrial application for manufacturing jobs with ultra precision contours.

Saha et al. (2003) used the finite element modeling and optimization to prevent wire breakage in electro-discharge machining. The model successfully predicted the thermal distribution profile accurately for various wire materials, for increased wire velocity and for reduction in heat transfer co-efficient. The developed model may lead to the development of a smart electro-discharge machining system with a sensor and feedback control to increase the cutting speed and minimize breakage. The results of the modeling and optimization showed that non uniform heating was the most important variable affecting the temperature and

thermal strain. The future scope includes complex 3-D finite element analysis models for accurate prediction of wire breakage and erosion during machining.

Ramakrishnan and Karunamoorthy (2005) investigated into a multi response optimization of WEDM operations using Taguchi's robust design. The effect of various parameters such as pulse on time, wire tension, delay time, wire feed speed and ignition current intensity has been studied through machining of heat-treated tool steel. The pulse on time and ignition current intensity has more influence than other parameters. Further research might attempt to consider other performance criteria such surface waviness, form accuracy and surface flatness as output parameters.

Manna and Bhattacharyya (2005) investigated into parametric optimization of CNC wire cut EDM of PRAISiMMC. The results showed that open gap voltage and pulse on period were the most significant and significant influencing machining parameters for MRR. Wire tension and wire feed rate were the most significant and significant influencing machining parameters for SR. Wire tension and spark gap voltage were the most significant and significant influencing machining parameters for gap width. The effective machining of PRAISiMMC is challenge to manufacturing industries. The Taguchi method based approach for searching out significant WEDM parameters during machining of PRAISiMMC will provide efficient guide lines for manufacturing engineers.

Miller et al. (2005) investigated the WEDM of thin cross section and compliant mechanisms. Effects of EDM process parameters such as spark cycle time and spark on time on thin cross section cutting of Nd-Fe-B magnetic material, carbon bipolar plate and titanium were investigated. Although results presented were machine dependent, this research provides the guide lines and procedures for the development of WEDM process to manufacture miniature features on advanced engineering materials.

Mahapatra and Patnaik (2006) studied the optimization of WEDM process parameters using Taguchi method. Factors like discharge current, pulse duration, and dielectric flow rate and their interactions have been found to play a significant role in rough cutting operations for maximization of MRR, minimization of surface roughness and minimization of cutting width. In future, the study can be extended using different work materials and hybrid optimization techniques.

Cabanes et al. (2007) studied the industrial application for online detection of instability and wire breakage in wire EDM. Here a methodology was proposed that guarantees an earlier detection of instability that can be used to avoid the detrimental effects associated to both unstable machining and wire breakage. Future work will involve the development of real time control strategy so as different parameters of the machine are automatically readjusted. In this respect the no. and thresholds of alarms can be extended in order to assure recovering of stable operations. Therefore the final aim is to increase cutting process performance while avoiding wire breakage.

Cheng et al. (2007) studied the experimental determination of convective heat transfer coefficient in WEDM. A special device was developed to measure the average temperature increment of the wire after a period of short circuit discharges and the thermal load imposed on the wire is also tracked and recorded in advance. The values of convective coefficient change with the kerf conditions and flushing pressure of the coolant. With this method introduced in this paper, a complete estimation of the convective coefficient for WEDM may be possible in the future.

Plaza et al. (2008) investigated the prediction of angular error in Wire EDM taper cutting. Through this method, the maximum angular deviation reached in machined parts has been 4'52". In 75% of results obtained from the two models proposed, the angular deviation is below 3'45". When compared with industrial practice based on trial and error experiments, the models proposed here are more general and permit deeper insight into the scientific knowledge of problem. In case of numerical model, the results set the base for research of new guide geometries and new generations of wire.

Parashar et al. (2009) investigated the optimization of surface roughness for wire cut EDM of SS 304L using Taguchi dynamic experiments. Each experiment was performed under different cutting conditions of gap voltage, pulse ON time, pulse OFF time, wire feed & dielectric flushing pressure. It was found that pulse ON time is the most influencing machining parameter for surface roughness. The gap voltage, pulse OFF time & flushing pressure had little effect on surface roughness. The wire feed had the lowest effect on the surface roughness. This methodology can also be applied for the various other unconventional machining operations to improve the performance characteristics simultaneously.

Now a days, there are various advance optimization techniques used for the optimization of process such as genetic algorithm, neural networks, fuzzy logic and swam particle optimization. In future these techniques can be used for optimization of WEDM process parameters. (Speeding and Wang, 1995)

In future, the automation of WEDM can be achieved by application of computational geometry in manufacturing and CAD/CAM integration of WEDM (Wang and Ravani, 2002). Hybridization of processes such as wire tool vibration and WEDM hybridization will find potential industrial application for manufacturing jobs with ultra precision contours (Puri and Bhattacharyya, 2003). WEDM has a huge potential for machining miniature and complex geometries.

Further WEDM can also be used to machine intricate geometries and ultra precision contours. (Miller et al., 2005)

Further study might also include hybridization of the above mentioned advance optimization techniques and compare the effect of process parameters on process responses. Better results can be obtained by this approach. (Mahapatra and Patnaik, 2006). Since WEDM is best suited for the machining of metal matrix composites, the characteristic of WEDM of advanced metal matrix composites (Matrix: Al, Cu, Fe, Mg, Ti, Pb and particle reinforcement: Al_2O_3 , Al_4O_3 , TiB_2 , ZrO_2) should be investigated. Even hybridization of more than one particle reinforcement should be tried.

The WEDM frame work could be extended by further research to consider other performance characteristics such as surface waviness, form accuracy and surface flatness as output parameters. (Ramakrishnan and Karunamoorthy, 2006). In the area of development of wire electrodes, future research can include the use of tubular electrodes, coating of super conductors on the wire to increase the current carrying capacity, wire treatment and in process treatment of wire. Future work in WEDM can involve the development of a real time control strategy so as different parameters of the machine are automatically adjusted. (Cabanes et al. 2007)

REFERENCES

- Bannerjee, S., Prasad, B.V. S. S. S., (2010), "Numerical evaluation of transient thermal loads on a WEDM wire electrode under spatially random multiple discharge conditions with and without clustering of sparks". *International Journal of Advance Manufacturing Technology*, Vol.48 pp.571-580.
- Bannerjee, S., Prasad, B.V. S. S. S., Mishra, P. K. (1993), "A simple model to estimate the thermal loads on an EDM wire electrode". *Journal of Materials Processing Technology*, Vol. 39, pp.305-317.
- Bonny,K., Baets, P.D., Vleugels, J., Salehi, A., Biest, O.V., Lauwers,B., Liu,W.,(2009), "EDM machinability and frictional behavior of ZrO₂-WC composites", *International Journal of Advance Manufacturing Technology*, Vol. 41, pp. 1085-1093.
- Cabanes, I., Portillo, E., Marcos, M., Sanchez, J.A., (2008), "An industrial application for on-line detection of instability and wire breakage in WEDM", *Journal of Materials Processing Technology*, Vol.195, pp. 101-109.
- Cabanes, I., Portillo, E., Marcos, M., Sanchez, J.A.,(2008), "On-line prevention of wire breakage in wire electro-discharge machining", *Journal of Robotics and Computer Integrated Manufacturing*, Vol.24, pp. 287-298.
- Cheng, Gang., Han, Fuzhu., Feng, Zhijing., "Experimental determination of convective heat transfer coefficient in WEDM", *International Journal of Machine Tools And Manufacture*, Vol. 47, pp. 1744-1751.
- Chiang, Ko-Ta., Chang, F.P.(2006), "Optimization of the WEDM process of particle-reinforced material with multiple performance characteristics using grey relational analysis", *Journal of Materials Processing Technology*, Vol.180, pp. 96-101.
- Daniel ACM, Philips, Eindhoven (1976) NC wire spark erosion-a survey, *Ann CIRP* 25 (2):521-525.
- Das saradindu, Joshi, suhas.s (2010),"Modeling of spark erosion rate in microwire-EDM", *International Journal of Advance Manufacturing Technology*, Vol. 48, pp.581-596.
- Dauw, D. F. and Albert, L. (1992), "About the evolution of tool wear performance in wire EDM", *Annals CIRP*, Vol. 41(1), pp.221-225.
- G. Boothroyd, A. K. Winston, *Non-conventional Machining Processes, Fundamentals of Machining*, Marcel Dekker, Inc. 1989, pp 491.
- G. F.Benedict, *Electric Discharge Machining (EDM), Non-traditional Manufacturing Processes*, Marcel Dekker, Inc, New York & Basel, 1987, pp 231-232.
- Garg, R. K. , Singh, K. K., Sachdeva, Anish, Sharma, Vishal S., Ojha Kuldeep, Singh Sharanjit(2010) "Review of research work in sinking EDM and WEDM on metal matrix composite materials", *International Journal of Advance Manufacturing Technology*, Vol. 50, pp. 611-624.
- Gauri, S. K., Chakraborty, S. (2009), "A study on the performance of some multi-response optimisation methods for WEDM process", *International Journal of Advance Manufacturing Technology*, Vol. 49, pp. 155-166.
- Gauri, S.K., Chakraborty, S. (2009), "Optimisation of multiple responses for WEDM processes using weighted principal components", *International Journal of Advance Manufacturing Technology*, Vol. 40, pp. 1102-1110.

- Guiqin, L., Fanhui, K., Wenle, L., Qingfeng, Y., Minglum, F. (2007), "The Neural-fuzzy Modelling and Genetic Optimization in WEDM", ICCA 2007, *IEEE International Conference on Control and Automation*, pp. 1440-1443.
- Guo, Z. N., Lee, T. C., Yue, T. M., Lau, W. S. (1997), "A study of Ultrasonic-aided Wire Electrical Discharge Machining", *Journal of Materials Processing Technology*, Vol.63, pp.823-828.
- Guo, Z. N., Lee, T. C., Yue, T. M., Lau, W. S. (1997), "Study on the machining mechanism of WEDM with Ultrasonic vibration of the wire", *Journal of Materials Processing Technology*, Vol. 69, pp.212-221.
- Guo, Z. N., Wang, X., Huang, Z. G., Yue, T. M. (2002), "Experimental investigation into shaping particle-reinforced material by WEDM", *Journal of Materials Processing Technology*, Vol. 129, pp.56-59.
- Güven, O., Esme, U., Kaya, I. E., Kazancoglu, Y., Kulekci, M. K., Boga, C. (2010), "Comparative modeling of Wire Electrical Discharge Machining (WEDM) process using back propagation (BPN) and general regression neural networks (GRNN)", *Journal of Materials and Technology*, Vol. 44,3, pp.147-152.
- Haddad, M.J., Alihoseini, F., Hadi, M., Hadad, M., Tehrani, A.F., Mohammadi, A. (2010), "An experimental investigation of cylindrical wire electrical discharge turning process", *International Journal of Advance Manufacturing Technology*, Vol. 46, pp. 1119-1132.
- Han, F., Jiang, J., Dingwen, Y., (2007), "Influence of discharge current on machined surfaces by thermo-analysis in finish cut of WEDM", *International Journal of Machine Tools and Manufacture*, Vol.47, pp.1187-1196.
- Han, Fujhu., Jiang, Jun., Dingwen, Yu. (2006), "Influence of machining parameters on surface roughness in finish cut of WEDM", *International Journal of Advance Manufacturing Technology*, Vol. 34, pp. 538-546.
- Hargrove, S. Keith. and Ding, Duowen. (2006), "Determining cutting parameters in wire EDM based on workpiece surface temperature distribution" *International Journal of Advance Manufacturing Technology*, Vol. 34, pp. 295-299.
- Hewidy, M. S., Taweel, T.A., EI-Safty, M. F. (2005), "Modelling the machining parameters of wire electrical discharge machining of Inconel 601 using RSM". *Journal of Materials Processing Technology*, Vol. 169. pp. 328-336.
- Huang, C.A., Tu, G. C., Yao, H. T., Kuo, H. H, (2004), "Characteristics of the rough cut surface of quenched and tempered Martensitic stainless Steel using WEDM", *Metallurgical and Materials transactions*, Vol.35 A, pp. 1351-1357.
- Huang, J. T. and Liao, Y. S. (2003), "Optimization of machining parameters of wire EDM based on Grey relational and statistical analysis", *International Journal of Production Resources*, Vol.41, No.8, pp.1707-1720.
- Huang, J. T., Liao, Y. S., Hsue, W.J. (1999), "Determination of finish cutting operation number and machining parameters setting in wire electrical discharge machining", *Journal of Materials Processing Technology*, Vol.87, pp.69-81.
- Jain, V. K. (2004), "Advanced Machining Processes", *Allied Publishers Pvt. Limited*, Mumbai.
- Jameson, E. C. Description and development of electric discharge machining (EDM), Electrical Discharge Machining, Society of Manufacturing engineers, Dearborn, Michigan, 2001, pp 16.

- Jangra, Kamal., Grover, Sandeep. , Chan ,Felix T. S., Aggarwal ,Aman. (2011),“ Digraph and matrix method to evaluate the machinability of tungsten carbide composite with wire EDM”, *International Journal of Advance Manufacturing Technology*.
- Juhr, H., Schulze, H. P., Wollenberg, G., Kunanz, K. (2004), “Improved cemented carbide properties after wire-EDM by pulse shaping”, *Journal of Materials Processing Technology*, Vol.149, pp.178-183.
- Kinoshita N, Fukui M, Gamo G (1976) “Study on EDM with wire electrode; Gap phenomena”, *Ann CIRP* 25 (1): 141-145.
- Kinoshita, N., Fukui, M., Gamo,G. (1982), “Control of wire EDM preventing from breaking”, *Annals CIRP*, Vol.31, pp.111-114.
- Konda. R., Rajurkar. K. P., Bishu, R. R., Guha, A., Parson, M. (1999), “Design of experiments to study and optimize process performance”, *International Journal of Quality & Reliability Management*, vol.16, No.1, pp. 56-71.
- Krar, S. F., Check, A.F., Electrical discharge machining, Technology of Machine Tools, Glencoe/ McGraw- Hill, New York 1997, pp. 800.
- Kuriakose, Shajan. and Shunmugam, M. S. (2005), “Multi-objective optimization of wire-electro-discharge machining process by non-dominated sorting Genetic Algorithm”, *Journal of Materials Processing Technology*, Vol.170, pp.133-141.
- Kuroda, H., Aoyama, S., Kimura, T., Sawahata, K., Sato, T. (2003), “Development of high performance coated wire electrodes for high speed cutting and accurate machining” *Hitachi Cable Review*, no.22, pp. 51-56.
- Lautre, Nitin. K. and Manna, Alakesh. (2006), “ A study on fault diagnosis and maintenance of CNC-WEDM based on binary relational analysis and expert system” *International Journal of Advance Manufacturing Technology*, Vol. 29, pp.490-498.
- Lee, W. M. and Liao, Y. S. (2003), “Self-tuning fuzzy control with a grey prediction for wire rupture prevention in WEDM”, *International Journal of Advance Manufacturing Technology*, Vol. 22, pp.481-490.
- Liao, Y. S., Chiu, Y. Y., Yan, M. T. (1997), “Study of wire breaking process and monitoring of WEDM”, *International Journal of Machine Tools and Manufacture* , Vol.37(4), pp.555-567.
- Liao, Y. S., Huang, J. T., Chen, Y. H. (2004), “ A study to achieve a fine surface finish in wire-EDM”, *Journal of Materials Processing Technology*, Vol.149, pp.165-171.
- Liao, Y. S., Yu, Y. P. (2004), “Study of specific discharge energy in WEDM and its application”, *International Journal of Machine Tools & Manufacture*, vol.44, pp.1373-1380.
- Lin, D. P., Liao, T. T, (2009), “An effective-wire-radius compensation scheme for enhancing the precision of wire-cut electrical discharge machines”, *International Journal of Advance Manufacturing Technology*, Vol. 40, pp.324-331.
- Lok, Y. K. and Lee, T. C. (1997), “Processing of advanced ceramics using the wire-cut EDM process”, *Journal of Materials Processing Technology* ,Vol.63, pp.839-843.
- Luo, Y. F. (1999), “Rupture failure and mechanical strength of the electrode wire used in wire EDM”, *Journal of Materials Processing Technology*, Vol.94, pp.208-215.
- Luo. Y. F.(1995), “An energy distribution strategy in fast cutting wire EDM”, *Journal of Materials Processing Technology*,Vol.55,pp.380-390.

- Mahapatra, S. S. and Patnaik Amar. (2006), "Optimization of wire electrical discharge machining (WEDM) process parameters using Taguchi method", *International Journal of Advance manufacturing Technology*. Vol. 34(9-10), pp. 911-925.
- Mahapatra, S. S. and Patnaik, Amar. (2006), "Parametric Optimization of wire electrical discharge machining (WEDM) process using Taguchi method", *Journal of the Brazil Society of Mechanical Science & Engineering*, Vol 28, pp. 422-429.
- Manna, A. and Bhattacharya, B. (2006), "Taguchi and Gauss elimination method: a dual response approach for parametric optimization of CNC wire cut EDM of PRAISiCMMC", *International Journal of Advance Manufacturing Technology*, Vol. 28, pp. 67-75.
- Manna, A., Kumar, N. (2009), "A Study on Electrode Wear of WEDM during Cutting of E0300 Alloy steel", *IE (I) Journal- PR*, pp. 30-35.
- Masui, K., Sone, T. (1989), "Transfer coupling circuit for wire spark erosion with non-electrolytic affection" *Ann. ISEM* 9, 72.
- McGeough, J.A., *Electro-discharge Machining, Advanced methods of Machining*, Chapman & Hall, London, pp. 130.
- Miller, Scott. F, Kao, Chen-C., Shih, Albert J., Qu, Jun. "Investigation of wire electrical discharge machining of thin cross-sections and compliant mechanisms" *International Journal of Machine Tools and Manufacture*, 45, 1717-1725.
- Mishra, P. K. (1997), "Non conventional Machining", Narosa Publishing House, New Delhi.
- Mohammadi A. Tehrani Alireza Fadaei, Emanian Ehsan, Karimi Davoud (2007), "A new approach to surface roughness and roundness improvement in wire electrical discharge turning based on statistical analyses", *International Journal of Advance Manufacturing Technology*.
- Obara, Haruki., Satou, Harutoshi., Hatano, Masatoshi. (2004), "Fundamental study on corrosion of cemented carbide during wire EDM", *Journal of Materials Processing Technology*, Vol.149, pp.370-375.
- Ozdemir, N. and Ozek, Cebeli. (2006), "An investigation on machinability of nodular cast iron by WEDM", *International Journal of Advance Manufacturing Technology*, Vol. 28, pp.869-872.
- Pandey, P. C. and Shan, H. S. (2006), "Modern Machining Processes", Tata McGraw-Hill Publishing Company Limited, New Delhi.
- Parashar Vishal, Rehman. A, Bhagoria. J. L and Puri. Y. M, (2009), "Investigation and optimisation of surface roughness for wire cut electro discharge machining of SS304L using taguchi dynamic experiments", *International Journal of Engineering Studies*, vol.1, number 4 , pp.257-267.
- Patil, N. G. and Brahmkar, P. K. (2010), "Determination of material removal rate in wire electro-discharge machining of metal matrix composites using dimensional analysis", *International Journal of Advance Manufacturing Technology*, Vol. 51, pp.599-610.
- Patil, N. G. and Brahmkar, P. K. (2010), "Some studies into wire electro-discharge machining of alumina particulate-reinforced aluminum matrix composites", *International Journal of Advance Manufacturing Technology*, Vol. 48, pp.537-555.
- Plaza. S., Ortega, N., Sanchez, J.A., Pombo, I., Mendikute, A., (2009), "Original models for the prediction of angular error in wire-EDM taper cutting", *International Journal of Advance Manufacturing Technology*, Vol. 44, pp.529-538.

- Puri, B. A. and Bhattacharyya, B. (2003), "An analysis and optimisation of the geometrical inaccuracy due to wire lag phenomenon in WEDM", *International Journal of Machine Tools and Manufacture*, Vol.43, pp.151-159.
- Puri, B. A. and Bhattacharyya, B. (2003), "Modelling and analysis of the wire-tool vibration in wire-cut EDM", *Journal of Materials Processing Technology*, Vol.141, pp.295-301.
- Puri, B. A. and Bhattacharyya, B. (2005), "Modelling and analysis of white layer depth in a wire-cut EDM process through response surface methodology", *International Journal of Advance Manufacturing Technology*, Vol. 25, pp.301-307.
- Qu, Jun., Shih, Albert, J., Scattergood, Ronald. O. (2002), "Development of the Cylindrical Wire Electrical discharge Machining Process, Part 1 : Concept, Design, and Material Removal Rate", *Journal of Manufacturing Science and Engineering*, Vol.124, pp. 702-707.
- Qu, Jun., Shih, Albert. J., Scattergood, Ronald. O. (2002), "Development of the Cylindrical Wire Electrical discharge Machining Process, Part 2: Surface Integrity and Roundness" *Journal of Manufacturing Science and Engineering*, Vol.124, pp. 708-714.
- Rajurkar, K. P. and Wang, W. M. (1991), "On line monitor and control for wire breakage in WEDM", *Annals CIRP*, Vol. 40(1), pp. 219-222.
- Rajurkar, K. P. and Wang, W. M.(1993), "Thermal Modeling and on line Monitoring of Wire-EDM", *Journal of Materials Processing Technology*, Vol.38,pp.417-430.
- Ramakrishnan, R. and Karunamoorthy, L. (2004), "Surface roughness model for CNC wire electro-discharge machining", *Journal of Manufacturing Technology Today*, Vol. 3 (5), pp.8-11.
- Ramakrishnan, R. and Karunamoorthy, L. (2006), "Multi response optimization of wire EDM operations using robust design of experiments", *International Journal of Advance Manufacturing Technology*, Vol. 29, pp.105-112.
- Rozenek, M., Kozak, J., Dabrowski, L., Lubowski, K., (2001), "Electric discharge machining characteristics of metal matrix composites", *Journal of Materials Processing Technology*, Vol.109, pp.367-370.
- Saha, P., Singh, A., Pal, S.K., Saha, P., (2007), "Soft computing model based prediction of cutting speed and surface roughness in wire electro-discharge machining of tungsten carbide cobalt composite", *International Journal of Advance Manufacturing Technology*, Vol. 39, pp. 74-84.
- Saha, S., Pachon, M., Ghoshal, A., Schulz, M. J.,(2003), " Finite element modelling and optimisation to prevent wire breakage in electro-discharge machining" *Mechanics Research Communication* 31, 451-463.
- Sarkar, S., Mitra, S., Bhattacharyya, B. (2006), "Modelling and optimisation of wire electrical discharge machining of γ -TiAl in trim cutting operation", *Journal of Materials Processing Technology*, Vol.109, pp.367-370.
- Sarkar, S., Mitra, S., Bhattacharyya, B. (2008), "Parametric optimisation of wire electrical discharge machining of γ titanium aluminide alloy through an artificial neural network model", *International Journal of Advanced Manufacturing Technology*, Vol. 27, pp. 501-508.
- Sarkar, S., Sekh, M., Mitra, S., Bhattacharyya, B. (2011), "A novel method of determination of wire lag for enhanced profile accuracy in WEDM", *Precision Engineering*, Vol.35, pp.339-347.

- Satishkumar, D., Kanthababu, M., Vajjiravelu, V., Anburaj, R., Thirumalai Sundarrajan, N., Arul, H. (2011), "Investigation of wire electrical discharge machining characteristics of Al6063/SiCp composites", *International Journal of Advance Manufacturing Technology*.
- Schacht, B., Kruth, J. P., Lauwers, B., Vanherck, P. (2004), "The skin-effect in ferromagnetic electrodes for wire-EDM", *International Journal of Advance Manufacturing Technology*, Vol. 23, pp.794-799.
- Schumacher, B. M.(1983), "EDM technology for precise workpieces with excellent surface quality" *Ann. ISEM* 7, 126.
- Scott, D., Boyina, S., Rajurkar, K. P. (1991), "Analysis and optimization of parameter combinations in wire electrical discharge machining", *International Journal of Production Research*, Vol.29, No.8, pp.2189-2207.
- Shah, A., Mufti, N. A., Rakwal, D., Bamberg, E., (2010), "Material Removal rate, Kerf and Surface Roughness of Tungsten Carbide machined with wire electrical discharge machining" *Journal of Materials Engineering and Performance*, Vol. 20(1), pp 71-76.
- Shandilya, P., Jain, P. K., Jain, N. K. (2012), "Parametric optimization during wire electrical discharge machining using response surface methodology", *Procedia Engineering*, Vol. 38, pp. 2371-2377.
- Shobert, E. I., What happens in EDM, in: E. C. Jameson (Ed.), *Electrical Discharge Machining: Tooling, Methods and Application*, Society of Manufacturing Engineers, Dearborn, Michigan, 1983, pp 3-4.
- Singh, H, Garg, R. (2009), "Effects of process parameters on material removal rate in WEDM", *Journal of Achievements in Materials and Manufacturing Engineering*, vol.32, issue 1, pp. 70-74.
- Spedding, T. A. and Wang, Z. Q. (1997) "Study on modeling of wire EDM process", *Journal of Materials Processing Technology*, Vol. 69, pp.18-28.
- Spedding, T. A. and Wang, Z. Q. (1997), "Parameter optimization and surface characteristics of wire electrical discharge machining process", *International Journal of Precision Engineering*, Vol.20, pp.5-15.
- Tani, Takayuki., Fukuzawa, Yasushi., Mohri, Naotake., Saito, Nagao., Okada, Masaaki. (2004), "Machining phenomenon in WEDM of insulating ceramics" *Journal of Materials Processing Technology*, Vol. 149, pp.124-128.
- Tanimura, T. and Heuvelman, C. J. (1977), "The properties of servo gap sensor with sparking-erosion machining", *Annals CIRP*, Vol.26(1), pp. 59-63.
- Tosun, N., Cogun, C., Inan, A. (2003), "The effect of cutting parameters on workpiece surface roughness in wire EDM", *Journal of Machining Science and Technology*, Vol.7, No.2, pp.209-219.
- Tosun, N., Cogun, C., Pihtili, H. (2003), "The Effect of Cutting Parameter on Wire Crater Sizes in Wire EDM", *International Journal of Advance Manufacturing Technology*, Vol.21, pp.857-865.
- Tosun, N., Cogun, C., Tosun, Gul (2004), "A study on kerf and material removal rate in wire electrical discharge machining based on taguchi method", *Journal of Materials Processing Technology*, Vol.152, pp. 316-322.
- Wang, J., Ravani, B. (2003), "Computer aided contouring operation for travelling wire electric discharge machining (EDM)", *Computer Aided Design*, Vol.35, pp. 925-934.

- Weingartner, E. Jaumann, S., Kuster, F., Wegener, K., (2009), "On-machine wire electrical discharge dressing of metal-bonded grinding wheels", *International Journal of Advance Manufacturing Technology*, in press.
- Yan, B.W., Tsai, H. C., Huang, F.Y., Lee, L.C., (2005), "Examination of wire electrical discharge machining of Al₂O₃/ 6061 Al composites", *International Journal of Machine Tools and Manufacture*, Vol.45, , pp.251-259.
- Yan, H. S., Lee, R. S., Yang, Y. C. (1995), "An algorithm for surface design and tool path generation in wire- cut electrical discharge machining", *International Journal of Machine Tools and Manufacture* , Vol.35, No. 12, pp.1703-1714.
- Yan, Mu-Tian, Huang, Pin-Hsum, (2004), "Accuracy improvement of wire-EDM by real time wire tension control", *International Journal of Machine Tools and Manufacture*, Vol.44, pp.807-814.
- Yan, Mu-Tian, Shiu, Yau-jung (2007), "Theory and application of a combined feedback-feed forward control and disturbance observer in linear motor drive wire-EDM machines", *International Journal of Machine tools and Manufacture*.
- Yuan, Jin., Wang, Keshang., Yu, Tao., Fang, Minglun., (2008), "Reliable multi-objective optimization of high-speed WEDM process based on Gaussian process regression", *International Journal of Machine Tools & Manufacture*, Vol. 48, pp. 47-60.
- Zewang, Ni., Zhenxun, Liu. , Chengye, Yu. (1991), "Intricate ruled surface machining by wire-EDM", *Journal of Materials Processing Technology*, Vol. 28, pp.169-175.

Chapter 9

EXPERIMENTAL ANALYSIS OF DIE SINKING EDM PROCESS ON AISI P 20 TOOL STEEL USING RESPONSE SURFACE METHODOLOGY

G. K. Bose^{1,} and K. K. Mahapatra²*

¹Department of Mechanical Engineering , Haldia Institute of Technology, Haldia, India

²Technical Service, Central Institute of Plastic Engineering Technology,
Bhubaneswar, India

ABSTRACT

Electric Discharge Machining (EDM) is one of the most widely used non-traditional machining processes for machining intricate shapes in high strength electro-conductive materials by spark erosion. EDM has penetrated the commercial manufacturing field and has seen through technological development in various directions. The present study is focusing on the electric discharge machining (EDM) of AISI P – 20 tool steel for finding out the effect of machining parameters such as discharge gap current (GI), pulse on time (POT), pulse off time (POF) and spark gap (SG) on performance responses like Material removal rate (MRR), Surface Roughness (Ra) & Overcut (OC) using Square-shaped Cu tool with Lateral flushing. A well-designed experimental scheme is used to reduce the total number of experiments. The experiment is conducted with the L27 orthogonal array based on the Taguchi method and significant process parameters are identified using Analysis of Variance (ANOVA). It is found that MRR and Ra are significantly affected by gap current and pulse on time respectively. Whereas overcut is affected only by gap current. These experimental data are investigated using Response Surface Methodology (RSM) for effect of four EDM parameters on the responses. Response surfaces are considered to explore the importance of the variables and their levels so as to optimize the responses. Finally multi-response optimization is conceded out by means of overlaid contour plots and desirability functions.

Keywords: Electrical Discharge Machining; AISI P -20 tool steel; Material removal rate; Surface roughness; Overcut; Analysis of Variance; Response surface methodology

* Corresponding author, E-mail: gkbose@yahoo.com.

1. INTRODUCTION

Electric Discharge Machining (EDM) is one of the most thriving, convenient and commercial nontraditional machining process for machining newly developed, high strength alloys with high degree of accuracy and cost-effective production (Ghosh & Mallick, 1991). The process is well-matched for extensive application in manufacturing sector for machining of varieties of dies, moulds and precision components which are used widely in press tools and dies, aerospace, automotive, surgical components manufacturing industries etc. EDM is now a well-established technique for machining hard materials. The process has resolutely established itself as a standard process for machining of internal cavities in dies and press tools which have been previously hardened. The EDM process has become the workhorse of the tool making industry for the precise machining of conductive work pieces even with complicated contours. EDM uses high energy electro-thermal erosion to remove material. Material erodes from the work piece by a series of discrete sparks between the work and tool electrode immersed in a liquid dielectric medium. These electrical discharges melt and vaporize minute amounts of the work material, which are then ejected and flushed away by the dielectric (El Hofy, 2005).

Since EDM is an essential process in machining super alloys which requires precision and accuracy, hence it is in the limelight of several researchers for quite some time to augment its performance in terms of dimensional accuracy, surface integrity, high productivity, low electrode wear etc. Several researchers has contributed considerable amount of work in the field of EDM. Ojha et al. (2012), studied the material removal rate (MRR) and tool wear rate (TWR) on the powder mixed electrical discharge machining (PMEDM) of EN-19 (AISI-4140) steel where most important parameters affecting selected performance measures are identified and effects of their variations are observed. Bayramoglu (2005) describes the use of simple “profiled plate electrodes” for the generation of any linear and circular swept surfaces on CNC EDM machines and introduces the machining characteristic of these types of tools using statistical techniques. Bonny et al. (2009) executed EDM in demonized water through several consecutive gradually finer steps and correlated the Material Removal Rate (MRR), surface finish and EDM parameters. Suzuki et al. (2006) investigated the effect of various control parameters on the EDM of die-steel using electrically conductive CVD diamond with respect to electrode wear, efficiency and EDMed surface property. Singh and Singh (2012) studied the effect of different electrode materials on surface roughness produced and help in choosing right type of electrode material for specific purpose. Lauwers et al. (2005) studied the wire EDM machining of Si_3N_4 , ZrO_2 and Al_2O_3 based ceramics and validated the results of cutting and surface finish. Selvakumar et al. (2013) studied the experimental performance based on L-18 orthogonal array with pulse on time, pulse off time, peak current, wire tension, servo feed setting and corner angle as control factors. ANOVA has been performed to find the significance of the factors considered. Taguchi's additive model is used for prediction. Later, the responses are concurrently optimized based on Pareto optimality approach and a technology table has been tailored for handy use. Kapoor et al. (2012) investigated the effect of cryogenic treated brass wire electrode on surface roughness and material removal rate for WEDM. They described the influence of various machining parameters including pulse width, time between two pulses, wire tension and wire feed on surface roughness and material removal rate by using one

variable at a time approach. Ayesta et al. (2013) studied parameters related to the discharge process (current, pulse time and servo voltage) on machining time and electrode wear in EDM process for machining of narrow slots in low machinability materials, such as Ni based alloys used for aeronautical applications.

Salem et al. (2011) predicted the surface roughness by using experimental design methodology in EDM. Singh and Kalra (2013) optimized the machining parameters of EDM on OHNS steel using the Taguchi and ANOVA methodology respectively. Syed and Palaniyandi (2012) has studied the performance of electrical discharge machining using aluminium powder suspended distilled water and the Taguchi Design of Experiments is used to conduct experiments by varying the parameters peak current pulse, on time, concentration of the powder, and polarity. Kumar et al. (2012) presents an investigation on WEDM of pure titanium (grade-2). An attempt has been made to model the response variable i.e., surface roughness in WEDM process using multi response optimization. The ANOVA has been applied to identify the significance of the developed model. Mohanty et al. (2013) presented a thermal-structural model to analyze the process parameters and their effect on three important responses such as material removal rate, tool wear rate and residual stresses on work piece in EDM process. The numerical model is validated conducting experiments on a die-sinking EDM machine. Arikatla et al. (2013) studied the optimization of electric discharge machining response variables using design of experiment. Jana et al. (2011) established the significance of the machining parameter like speed feed and depth of cut over the performance responses like MRR and Ra in a single fast turning and analyzing by using response surface method.

The experimental work focuses on the characteristic features of the EDM process with various process parametric combinations like Gap Current (GI), Pulse on Time (POT), Pulse off Time (POF) & Spark Gap (SG) on Material removal Rate (MRR), Surface Roughness (Ra) & Overcut (OC). The significant process parameters are identified using Analysis of Variance (ANOVA). These experimental data are further investigated using Response Surface Methodology (RSM). The present paper is aimed at fulfillment of three basic but conflicting objectives concurrently during machining higher material removal rate (MRR), lower surface roughness (Ra) and overcut (OC) by employing a single set of optimal or near optimal process variables following response surface methodology (RSM). Response surfaces and studied to investigate the prominence of the variables and their levels so as to optimize the responses. Finally multi-response optimization is carried out using overlaid contour plots and desirability functions.

2. PLANNING FOR EXPERIMENTATION

In the present research work Electric Discharge Machine (ACTSPARK SP1, China) die-sinking type with servo-head (constant gap) and positive polarity for electrode is used for experimentation.

Commercial grade EDM-30 oil (specific gravity= 0.80 at 25°C, Viscosity of 3.11 CSt. @ 100°F (38°C)) is used as dielectric fluid. With external lateral flushing using a square-shaped Cu tool (12x12 mm) having a pressure 0.2 kgf/cm² is used. Experiments are conducted with positive polarity of electrode.

AISI P -20 tool steel work piece material is selected for the experiment. P20 tool steels are either nitrided or carburized and are pre-hardened to (29 – 33) HRC. These steels are capable of being machined into complex and large dies and molds. The presence of chromium and nickel enhances the toughness and hardness of P20 steels. The pulsed discharge current is applied in various steps in positive mode.

The EDM setup consists of dielectric reservoir, pump and circulation system, power generator and control unit, working tank with work holding device, X-Y table accommodating the working table, tool holder, the servo system to feed the tool part as shown in Figure 1.



Figure 1. (a) Working Tank with work holding (b) Tool holding devices (c) Tool holder (d) Work piece.

The servo control unit is provided to maintain the pre-determined gap. It senses the gap voltage and compares it with the current value and the difference in voltage is then used to control the movement of servo motor to adjust the gap.

The MRR is expressed as the ratio of the volume of the work piece material removed during machining the cavity to the machining time. Surface roughness of the cavity surface is expressed as R_a expressed in μm , is measured using stylus type profilometer named Perthometer-M1, of Mahr Gmbh make.

Overcut (OC) is expressed as half the difference of area of the cavity produced to the tool frontal area. Area of Cavity & frontal area of electrode can be calculated by measuring the respective length & width using Toolmaker's microscope.

While executing an experiment, varying the levels of the factors concurrently rather than one at a time is proficient in terms of time and cost and also permits for the study of interactions between the factors. Based on past research works and preliminary investigation, four parameters are chosen as input. Four input parameters are varied with three levels in twenty seven experimental run. The combination for factors and the three responses are shown in Table 1 below. There are other factors which may affect the measured performance like Duty cycle, Flushing pressure, Lift time etc., however, are kept constant during experimentation.

3. RESULTS ANALYSIS USING ANOVA

ANOVA is a functional method for estimating error variance and determining the relative importance of various process variables (Park, 1996). The experimental outcomes are explored to study the role of different process variables on various responses by using linear graphs and ANOVA. The result analysis is carried out by statistical software MINITAB, version 13.

3.1. Analysis of Test Results

The linear graphs exhibit the contribution of different control variables on various responses.

Table 1. Combination of factors and responses

EXPT NO.	POT (μSec)	POF (μSec)	GI (Amp)	SG (mm)	MRR (mm ³ /min)	Ra (μmm)	Overcut (mm ²)
1	20	12	11	0.18	0.007124	2.772	5.7312
2	24	20	9	0.18	0.089267	7.502	4.4166
3	24	16	11	0.18	0.141447	5.846	2.8788
4	20	20	7	0.18	0.172147	10.738	5.1352
5	16	16	11	0.18	0.078728	7.148	3.6724
6	20	16	7	0.16	0.009649	4.52	3.824
7	16	20	9	0.18	0.118636	7.34	6.6948
8	20	20	11	0.18	0.009851	5.262	3.4664
9	20	16	11	0.2	0.022883	2.626	3.6001
10	24	16	9	0.16	0.13117	6.243	7.6843
11	20	16	9	0.18	0.215712	10.462	8.8853
12	16	16	7	0.18	0.029763	2.217	6.084
13	20	12	9	0.2	0.288042	10.345	5.8502
14	16	16	9	0.16	0.022525	2.742	5.2415
15	20	16	9	0.18	0.090713	7.512	5.484
16	20	16	11	0.16	0.021019	2.356	7.6843
17	20	20	9	0.16	0.225082	6.817	6.847
18	20	16	9	0.18	0.004783	4.977	7.1376
19	20	20	9	0.2	0.093288	7.279	4.7739
20	20	12	9	0.16	0.036573	4.453	1.9083
21	20	16	7	0.2	0.114049	5.9776	3.6768
22	16	16	9	0.2	0.121345	7.944	3.4358
23	16	12	9	0.18	0.055672	6.343	7.441
24	24	12	9	0.18	0.088568	8.08	7.0674
25	24	16	9	0.2	0.01229	2.353	3.4818
26	24	16	7	0.18	0.23422	9.307	5.624
27	20	12	7	0.18	0.073723	6.611	6.198

The goal is to find out an optimal combination of control factor settings that achieve robustness against (insensitivity to) noise factors. S/N ratio analysis for MRR (mm³/sec) is carried out on the basis of larger is the better and the corresponding S/N ratio is expressed as follows:

$$n_{1=-10\log_{10}\left[\frac{1}{n}\sum_{i=1}^n\frac{1}{MRR^2}\right]} \quad (1)$$

S/N ratio analysis for Ra is modeled on the basis of smaller is the better and corresponding equation is

$$n_2 = -10 \log_{10} [1/n \sum_{i=1}^n Ra^2] \tag{2}$$

S/N ratio analysis for OC is modeled on the basis of smaller is the better and corresponding equation is

$$n_3 = -10 \log_{10} [1/n \sum_{i=1}^n OC^2] \tag{3}$$

3.1.1. Analysis of Test Results for MRR

The variations of MRR (mm³/Sec) with POT, POF, GI and SG are exhibited in figure 2 which shows that maximum MRR is obtained at the following parametric combination: POT – 20 μSec, POF – 12 μSec, GI – 11 amps and SG – 0.2 mm.

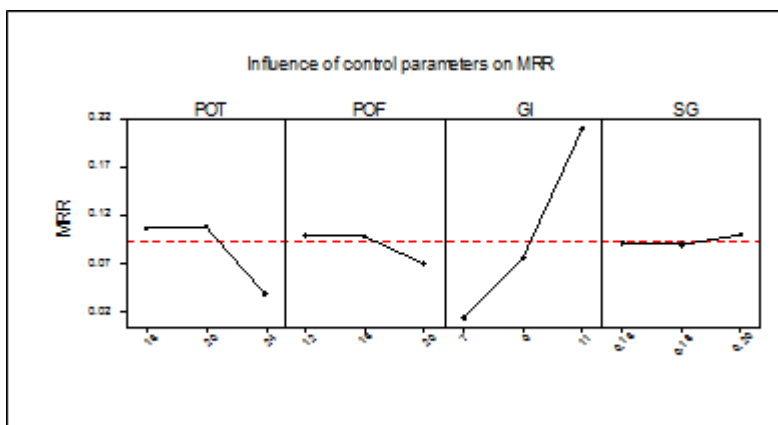


Figure 2. Linear graphs showing the effect of POT, POF, GI & SG on MRR.

Table 2 exhibits the ANOVA results for MRR. ANOVA results as exhibited from F-values and P-values of the process variables states that the F value of GI assumes a value of 84.58 followed by POT having a value of 14.33 in case of MRR. This implies that these variables have significant effects on MRR in contrast to the other two parameters and GI is the most significant amongst all.

Table 2. ANOVA for MRR

Source	DF	Seq SS	Adj SS	Adj MS	F – value	P - value
POT	2	0.022673	0.020409	0.010204	14.33	0.000
POF	2	0.005595	0.003867	0.001934	2.71	0.093
GI	2	0.120952	0.120474	0.060237	84.58	0.000
SG	2	0.000207	0.000207	0.000104	0.15	0.866
Error	18	0.012820	0.012820	0.000712		
Total	26	0.162247				

3.1.2. Analysis of Test Results for Ra

The change of Ra (μm) with POT, POF, GI and SG are exhibited in figure 3 which shows that minimum Ra is obtained at the following parametric combination: POT – 24 μSec , POF – 20 μSec , GI – 07 amps and SG – 0.18 mm.

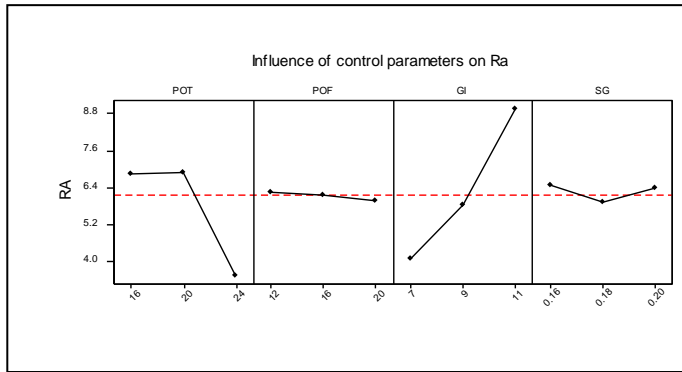


Figure 3. Linear graphs showing the effect of POT, POF, GI & SG on Ra.

Table 3 portrays the ANOVA results for Ra. ANOVA results as exhibited from F-values and P-values of the process variables states that the F value of GI assumes a value of 15.64 followed by POT having a value of 10.14 in case of Ra. This implies that these variables have significant effects on Ra in contrast to the other two parameters and GI is the most significant amongst all.

Table 3. ANOVA for Ra

Source	DF	Seq SS	Adj SS	Adj MS	F - value	P - value
POT	2	52.694	47.669	23.835	10.14	0.001
POF	2	1.194	0.582	0.291	0.12	0.884
GI	2	73.343	73.506	36.753	15.64	0.000
SG	2	0.228	0.228	0.114	0.05	0.953
Error	18	42.309	42.309	2.351		
Total	26	169.769				

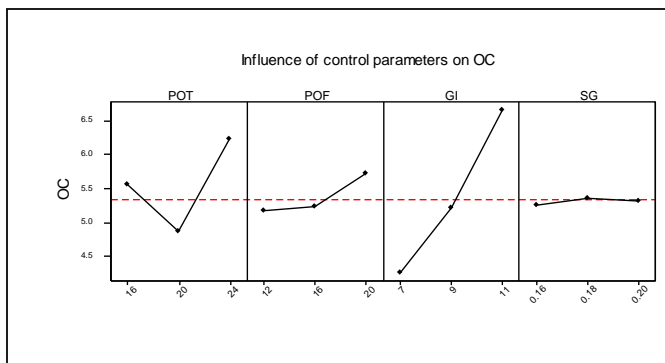


Figure 4. Linear graphs showing the effect of POT, POF, GI & SG on OC.

3.1.2. Analysis of Test Results for OC

The variations of OC (mm^2) with POT, POF, GI and SG are exhibited in figure 4 which shows that minimum OC is obtained at the following parametric combination: POT – 20 μSec , POF – 12 μSec , GI – 07 amps and SG – 0.20 mm.

Table 4 reveals ANOVA results for OC of the process variables. It is understood that the F value of GI assumes a value of approximately 4. This implies that this variable have significant effects on MRR in contrast to the others. Rest of the parameters remains insignificant in this regard.

Table 4. ANOVA for OC

Source	DF	Seq SS	Adj SS	Adj MS	F – value	P – value
POT	2	8.416	12.429	6.215	2.29	0.130
POF	2	2.141	4.010	2.005	0.74	0.492
GI	2	19.720	20.746	10.373	3.82	0.042
SG	2	1.416	1.416	0.708	0.26	0.774
Error	18	48.926	48.926	2.718		
Total	26	80.619				

3.2. Discussion

It can be inferred from the analysis through ANOVA that GI is the most significant parameter which affects all the responses simultaneously followed by POT while machining AISI P – 20 tool steel. The other two parameters remain quite insignificant in this regard. It is revealed that in order to have high MRR, GI should be set at 11 amps and POT at 24 μSec while for having low Ra and low OC, GI should be set at 07 amps and POT between 24 μSec to 20 μSec .

4. RESULTS ANALYSIS USING RESPONSE SURFACE METHODOLOGY (RSM)

The response surface (output) can be related with the number of controllable variables

$$x_1, x_2, \dots, x_k \text{ as } y = f(x_1, x_2, \dots, x_k) + \varepsilon.$$

A second order model is used to establish input-output relationship efficiently that takes the generic form:

The response surface (output) can be related with the number of controllable variables

$$x_1, x_2, \dots, x_k \text{ as } y = f(x_1, x_2, \dots, x_k) + \varepsilon \quad (4)$$

A second order model is used to establish input-output relationship efficiently that takes the generic form

$$y = \beta_0 + \sum_{i=1}^k \beta_i x_i + \sum_{i=1}^k \beta_{ii} x_i^2 + \sum_{i=1}^k \beta_{ij} x_i x_j + \varepsilon \tag{5}$$

The predicted response for the model is

$$\hat{y} = \hat{\beta}_0 + \sum_{i=1}^k \hat{\beta}_i x_i + \sum_{i=1}^k \hat{\beta}_{ii} x_i^2 + \sum_{i=1}^k \hat{\beta}_{ij} x_i x_j \tag{6}$$

In the present work, Box-Behenken Design is followed which is based on 2^k ($k = 4$) factorials with incomplete designs and found to be very efficient (Montgomery, 2000). The process variables combinations and the corresponding responses are presented in Table 1.

4.1. Analysis of Test Results for MRR

The empirical model for MRR is shown in equation (7) below:

The estimated regression surface equation for MRR is:

$$\text{MRR} = - 0.159 - 0.00862 \text{ POT} - 0.00361 \text{ POF} + 0.0494 \text{ GI} + 0.206 \text{ SG} \tag{7}$$

The empirical model has R^2 value of 82.7% and it provides good explanation of the relationship between parameters and responses. The details of the regression analysis result and subsequent ANOVA are presented in Table 5 and Table 6 respectively.

Table 5. Estimated Regression Coefficients for MRR

Term	Coef	SE Coef	T	P
Constant	0.10449	0.015112	6.914	0.000
POT	-0.03448	0.007556	-4.563	0.001
POF	-0.01443	0.007556	-1.909	0.080
GI	0.09884	0.007556	13.082	0.000
SG	0.00413	0.007556	0.546	0.595
POT*POT	-0.03394	0.011334	-2.995	0.011
POF*POF	-0.01603	0.011334	-1.414	0.183
GI*GI	0.02464	0.011334	2.174	0.050
SG*SG	-0.00074	0.011334	-0.066	0.949
POT*POF	0.01355	0.013087	1.036	0.321
POT*GI	-0.01553	0.013087	-1.187	0.258
POT*SG	0.00810	0.013087	0.619	0.547
POF*GI	-0.01613	0.013087	-1.232	0.241
POF*SG	-0.00972	0.013087	-0.743	0.472
GI*SG	0.01745	0.013087	1.333	0.207

Notes: S = 0.02617 R-Sq = 94.9% R-Sq(adj) = 89.0%.

Table 6. ANOVA for MRR

Source	DF	Seq SS	Adj SS	Adj MS	F - value	P - value
Regression	14	0.154026	0.154026	0.011002	16.06	0.000
Linear	4	0.134203	0.134203	0.033551	48.97	0.000
Square	4	0.015224	0.015224	0.003806	5.56	0.009
Interaction	6	0.004599	0.004599	0.000767	1.12	0.407
ResidualError	12	0.008221	0.008221	0.000685		
Lack-of-Fit	10	0.006066	0.006066	0.000607	0.56	0.781
Pure Error	2	0.002155	0.002155	0.001077		
Total	26	0.162247				

R-square as well as R-square (adjusted) assumes a value of 94.9% and 89.0% respectively, that implies the model is poised to explain 94.9% variability with process variable POT, POF, GI & SG. From the T values of the process variables, it can be concluded that GI is the most significant process variables followed by SG, POF and POT.

The normal plot of residuals for MRR is shown in Figure 5. It can be observed that the residuals are located on a straight line, which indicates that the errors are normally distributed and the non-linear models are fairly well fitted with the experimental values.

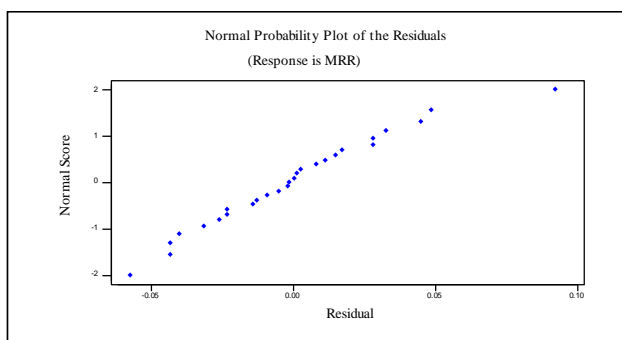


Figure 5. Normal Plot of Residuals for MRR.

4.2. Analysis of Response Surface Wireframe Plots for MRR

The mathematical model of equation (7) can be used to analyze the MRR according to processes parameters, known as Response Surface Analysis. The response surface plots of MRR with respect to GI, SG, POT and POF are shown in the following figures.

Figure 6 shows the trend of the surface plot for MRR which increases slowly with respect to POT in initial stage up to 18 then gradually decreases. Maximum MRR observed at POT value 18 as 0.30 mm³/min and minimum MRR is observed at POT value 24 sec as 0.20 mm³/min. Whereas MRR increases initially up to POF value 15 then decreases. Figure 7 shows the effects of POT and GI on MRR. From the trend of the above surface plot POT seems to have insignificant effect on MRR whereas GI is having significant parameter for MRR. Here MRR increases exponentially with respect to GI. Max MRR is predicted at POT value 18 and GI value of 11.

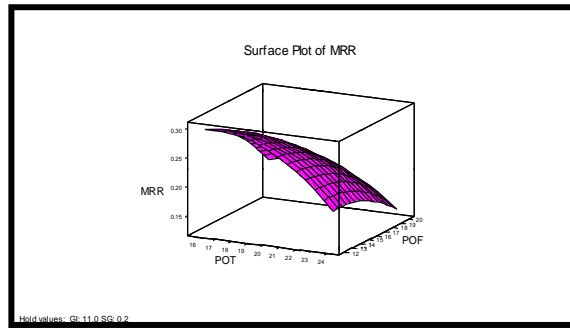


Figure 6. Effects of POT and POF on MRR.

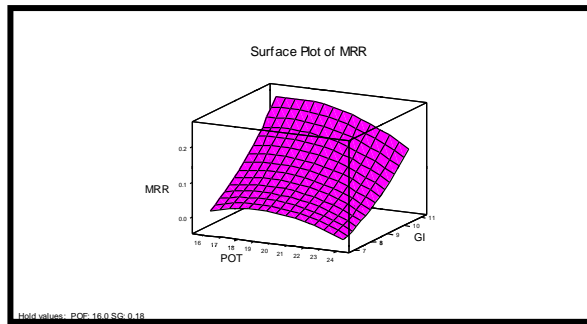


Figure 7. Effects of POT and GI on MRR.

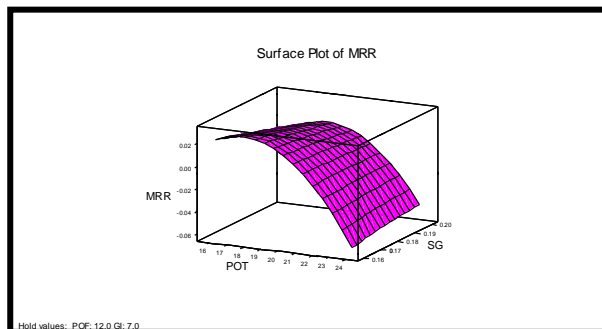


Figure 8. Effects of POT and SG on MRR.

Figure 8 exhibits the trend of surface plot for MRR while varying POT and SG. MRR initially increases gradually with respect to POT up to 18 and then gradually decreases. Maximum MRR is observed at POT value 18 and minimum MRR is observed at POT value of 24. MRR increases negligibly with change in SG. Figure 9 displays the surface plot of MRR with respect to POF and GI. It is revealed that MRR increases marginally with increase in POF up to 16 then slowly decreases. But GI shows an increasing trend and is having the most significant effect on MRR. MRR increases exponentially with respect to GI. Maximum MRR is observed at POF value of 16 and GI value of 11.

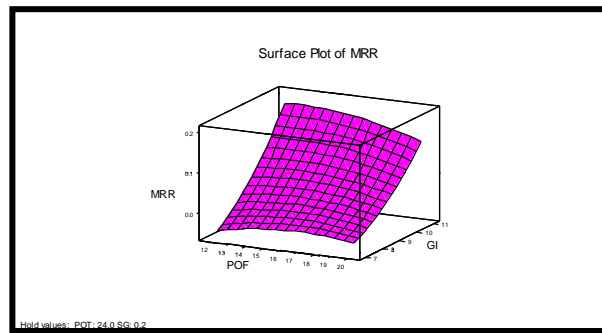


Figure 9. Effects of POF and GI on MRR.

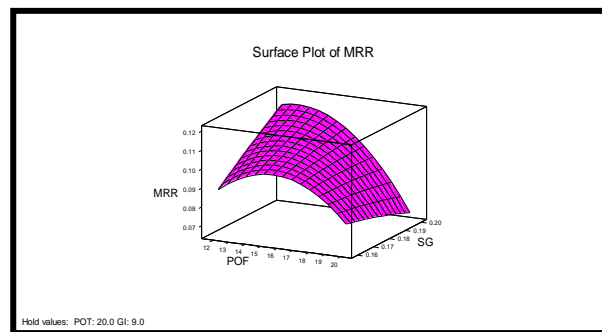


Figure 10. Effects of POF and SG on MRR

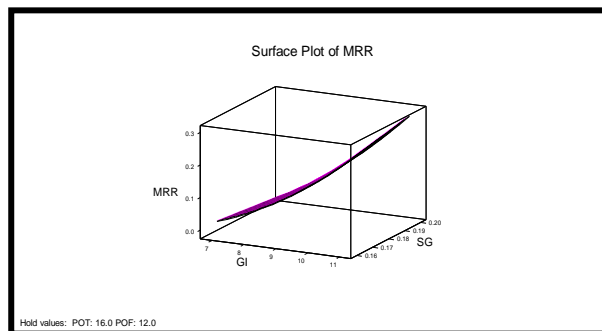


Figure 11. Effects of GI and SG on MRR.

Figure 10 shows the trend of the surface plot for MRR with varying POF and SG. It is revealed that MRR increases initially with respect to 16 and then gradually decreases. Maximum MRR is observed at POF value of 16 and minimum MRR is observed at POF of 20. But MRR decreases gradually with respect to SG. Figure 11 exhibits the effects of GI and SG on MRR. As per the trend of the surface plot, MRR increases exponentially with respect to GI and simultaneously increases with respect to SG. Max MRR predicted at GI value of 11 and SG value of 0.20.

4.2.1. Discussions

It is observed that high levels of the two variables out of four yield maximum responses. The GI & POT have the significant effect on MRR. Since the response is proportional to the

variables, there can not have any stationary point as evident from the surface plots. Further, the effect of GI is more pronounced than other three parameters.

4.3. Analysis of test results for Surface Roughness (Ra)

The empirical model for Ra is shown in equation (8) below:

The estimated regression surface equation for Ra is:

$$Ra = 4.28 - 0.413 POT - 0.036 POF + 1.23 GI - 2.3 SG \tag{8}$$

Table 7. Estimated Regression Coefficients for Ra

Term	Coef	SE Coef	T	P
Constant	6.758	1.0000	6.757	0.000
POT	-1.651	0.5000	-3.303	0.006
POF	-0.143	0.5000	-0.285	0.780
GI	2.465	0.5000	4.929	0.000
SG	-0.045	0.5000	-0.090	0.929
POT*POT	-1.674	0.7500	-2.232	0.045
POF*POF	-0.251	0.7500	-0.335	0.743
GI*GI	0.340	0.7500	0.453	0.659
SG*SG	0.195	0.7500	0.260	0.799
POT*POF	0.284	0.8661	0.328	0.749
POT*GI	-0.274	0.8661	-0.317	0.258
POT*SG	-0.005	0.8661	-0.006	0.995
POF*GI	1.085	0.8661	1.253	0.234
POF*SG	0.161	0.8661	0.186	0.856
GI*SG	-0.466	0.8661	-0.538	0.600

Notes: S = 1.732 R-Sq = 78.8% R-Sq(adj) = 54.1%.

Table 8. ANOVA for Ra

Source	DF	Seq SS	Adj SS	Adj MS	F – value	P – value
Regression	14	133.766	133.766	9.5547	3.18	0.026
Linear	4	105.882	105.882	26.4705	8.82	0.001
Square	4	21.578	21.578	5.3944	1.80	0.194
Interaction	6	6.306	6.306	1.0510	0.35	0.896
ResidualError	12	36.003	36.003	3.0003		
Lack-of-Fit	10	34.748	34.748	3.4748	5.54	0.163
Pure Error	2	1.255	1.255	0.6276		
Total	26	169.769				

The empirical model has R^2 value of 62.4% and it present satisfactory details of the relationship between parameters and responses. The particulars of the regression analysis outcome and subsequent ANOVA are presented in Table 7 and Table 8 respectively. R-square as well as R-square (adjusted) furnishes a value of 78.8% and 54.1% respectively that implies the model is balanced to explain 78.8% variability with process variable POT, POF, GI & SG. From the T values of the process variables, it can be concluded that GI is the most significant process variables followed by SG, POF and POT.

The normal plot of residuals for Ra is shown in Figure 12. It is pragmatic that the residuals are positioned on a straight line, which signifies that the errors are normally distributed and the non-linear models are moderately healthy fitted with the experimental values.

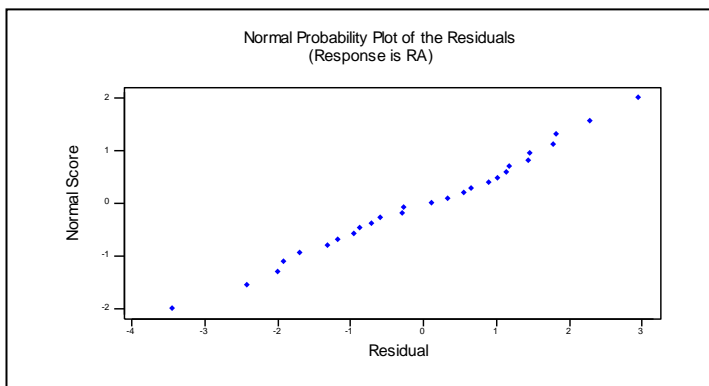


Figure 12. Normal Plot of Residuals for Ra.

4.4. Analysis of Response Surface Wireframe Plots for Ra

The mathematical model of equation (8) can be used to analyze the Ra according to processes parameters, recognized as Response Surface Analysis.

The response surface plots of Ra with respect to GI, SG, POT and POF are exhibited in the following figures.

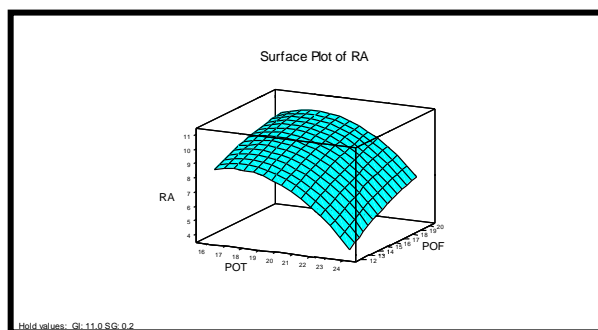


Figure 13. Effects of POT and POF on Ra.

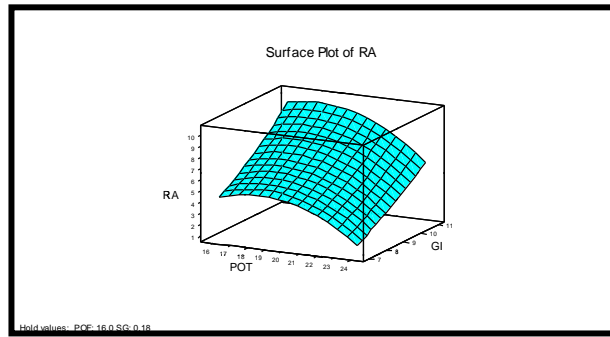


Figure 14. Effects of POT and GI on Ra.

Figure 13 exhibits the effects of POT and POF on Ra. From the surface plot it is evident that Ra initially increases slowly with increase in POT value till 18 and then gradually decreases. Whereas Ra gradually increases with increase in POF. Figure 14 shows the surface plot of MRR for varying POT and GI values. It is evident from the plot that Ra increases slowly with respect to POT up to 19 then gradually decreases. But Ra increases exponentially with respect to GI. It is apparent that GI is having the most significant effect on Ra.

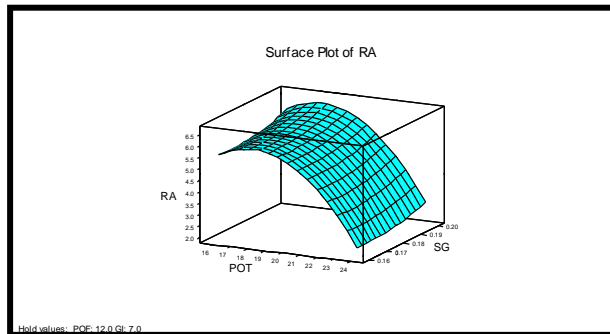


Figure 15. Effects of POT and SG on Ra.

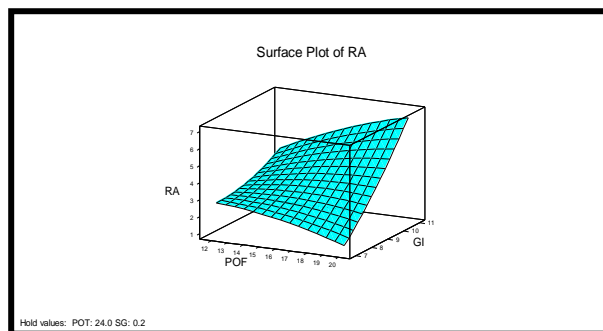


Figure 16. Effects of POF and GI on Ra.

Figure 15 shows the effects of POT and SG on Ra. The surface plot indicates that Ra increases slowly with respect to POT up to 18 and then gradually decreases. Maximum MRR observed at POT value of 18 and minimum MRR is observed at POT value of 24. It is evident that Ra increases almost linearly with increase in SG. Figure 16 illustrates the variation of Ra

against POF and GI respectively. It is evident from the surface plot that Ra decreases gradually with respect to POF whereas it increases significantly with respect to GI. Again GI is the most significant parameter for Ra.

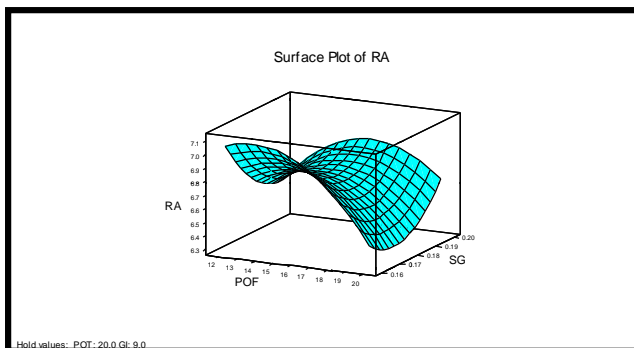


Figure 17. Effects of POF and SG on Ra.

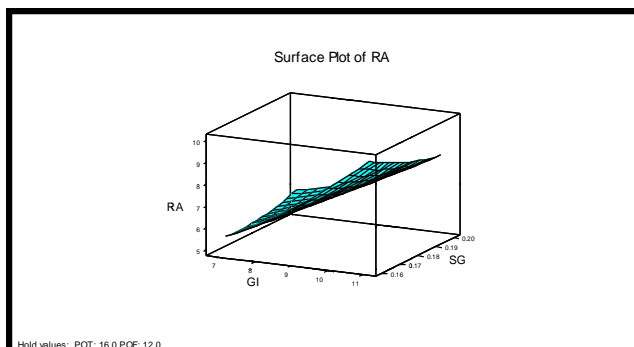


Figure 18. Effects of GI and SG on Ra.

Figure 17 below demonstrates the variation of Ra against POF and SG respectively. Here it is understood from the surface plot that, Ra decreases parabolically with respect to POF, where as Ra initially decreases with increase in SG up to 0.17 then increases significantly. Figure 18 exhibits the effects of GI and SG on Ra. Here it is evident from the surface plot that Ra increases significantly for increase in GI and SG. Apparently it is seen that Ra increases more with respect to GI than SG.

4.4.1. Discussion

It is seen that high levels of the two variables out of four capitulate utmost responses. The GI & SG have the considerable effect on Ra. Since the response is proportional to the variables, there can not have any stationary point as evident from the surface plots. Further, the effect of GI is more pronounced than other three parameters.

4.3. Analysis of Test Results for Overcut (OC)

The empirical model for Ra is shown in equation (9) below:

The estimated regression surface equation for Overcut (OC) is:

$$OC = - 3.12 + 0.084 POT + 0.069 POF + 0.603 GI + 1.3 SG \quad (9)$$

Table 9. Estimated Regression Coefficients for OC

Term	Coef	SE Coef	T	P
Constant	3.775	1.0452	3.612	0.004
POT	0.336	0.5226	0.644	0.532
POF	0.277	0.5226	0.530	0.605
GI	1.206	0.5226	2.308	0.040
SG	0.025	0.5226	0.049	0.962
POT*POT	1.441	0.7839	1.838	0.091
POF*POF	0.761	0.7839	0.971	0.351
GI*GI	0.784	0.7839	1.001	0.337
SG*SG	0.514	0.7839	0.656	0.525
POT*POF	0.214	0.9052	0.236	0.817
POT*GI	-1.098	0.9052	-1.213	0.248
POT*SG	-0.498	0.9052	-0.550	0.593
POF*GI	-0.126	0.9052	-0.139	0.892
POF*SG	0.897	0.9052	0.991	0.341
GI*SG	-0.282	0.9052	-0.312	0.761

Notes: S = 1.810 R-Sq = 51.2% R-Sq(adj) = 0.0%.

The empirical model has R^2 value of 24.5% and it signifies details of the relationship between parameters and responses. The particulars of the regression analysis and subsequent ANOVA details are presented in Table 9 and Table 10 respectively. R-square furnishes a value of 51.2% that implies the model is balanced to explain 51% variability with process variable POT, POF, GI & SG. From the T values of the process variables, it is observed that GI relatively affects the process.

Table 10. ANOVA for OC

Source	DF	Seq SS	Adj SS	Adj MS	F – value	P – value
Regression	14	41.289	41.289	2.9492	0.90	0.580
Linear	4	19.753	19.753	4.9383	1.51	0.262
Square	4	11.940	11.940	2.9850	0.91	0.489
Interaction	6	9.596	9.596	1.5994	0.49	0.805
Residual Error	12	39.330	39.330	3.2775		
Lack-of-Fit	10	37.519	37.519	3.7519	4.14	0.210
Pure Error	2	1.812	1.812	0.9058		
Total	26	80.619				

The normal plot of residuals for OC is shown in Figure 19. It is revealed that the residuals are positioned on a straight line, which signifies that the errors are normally distributed and the non-linear models are moderately healthy fitted with the experimental values.

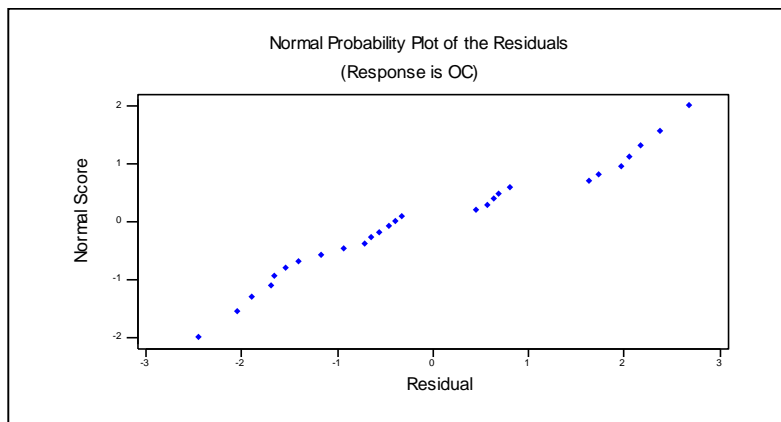


Figure 19. Normal Plot of Residuals for OC.

4.4. Analysis of Response Surface Wireframe Plots for OC

The mathematical model of equation (9) can be used to analyze the OC according to processes parameters, recognized as Response Surface Analysis. The response surface plots of OC with respect to GI, SG, POT and POF are exhibited in the following figures.

Figure 20 demonstrates the variation of OC against POT and POF respectively. It is evident from the surface plot that Overcut decreases significantly with respect to POT up to 22 and then increases. However OC increases significantly with the increase in POF. Figure 21 demonstrates the variation of OC against POT and GI respectively. It is understood from the graph that OC increases significantly with respect to POT. Again OC initially decreases and then increases with increase in GI. But at lower values of both POT and GI, OC seems to have maximum value.

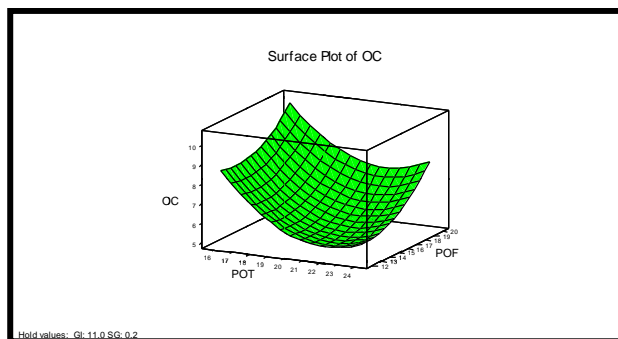


Figure 20. Effects of POF and POF on OC.

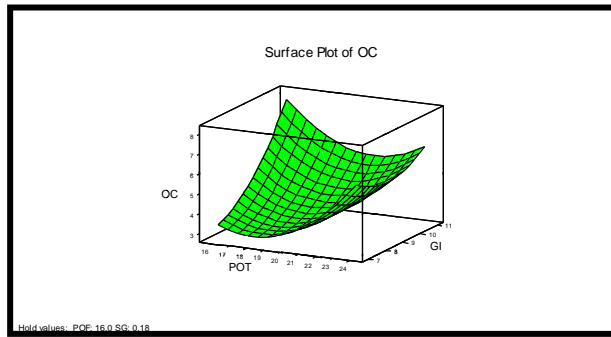


Figure 21. Effects of POT and GI on OC.

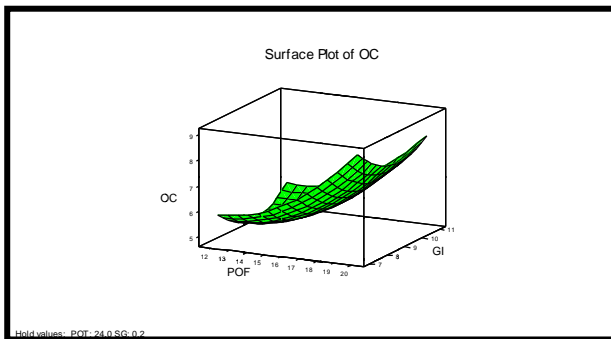


Figure 22. Effects of POF and GI on OC.

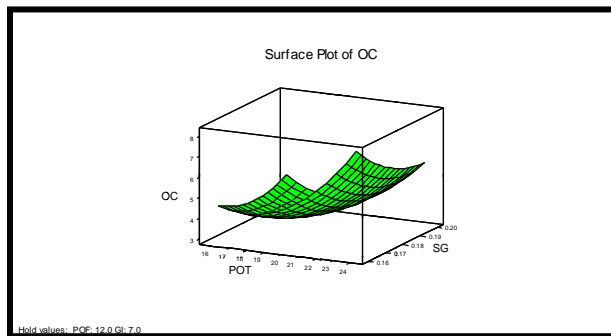


Figure 23. Effects of POT and SG on OC.

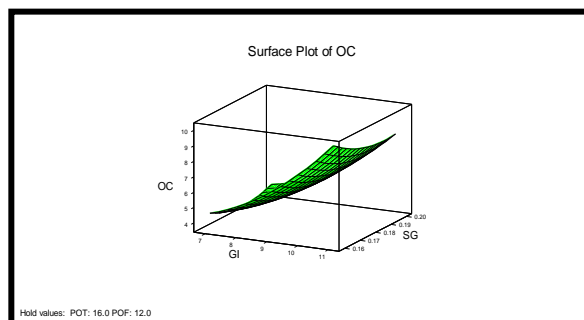


Figure 24. Effects of GI and SG on OC.

Figure 22 shows the consequence of POF and GI on OC. From the wire frame surface plot it is apparent that OC increases gradually with POF. Whereas OC initially decreases with the increase in GI value upto 9 and then increases. Figure 23 illustrates the impact of POT and SG on OC. The trend indicates that OC increases significantly with increase in POT. However incase of SG, OC initially decreases up to 0.17 then increases slowly.

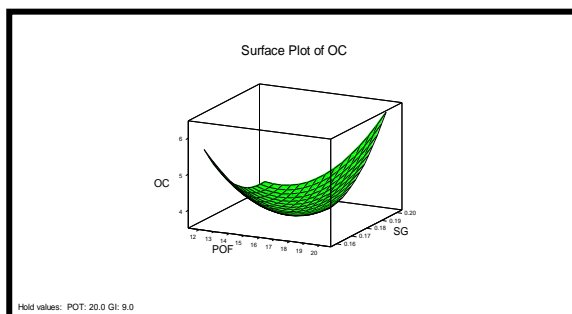


Figure 25. Effects of POF and SG.

Figure 24 demonstrates the variation of OC against GI and SG respectively. It is observed from the Surface plot that OC increases significantly with the increase in GI. However OC gradually decreases with the increase in SG. Figure 25 exhibits the variation of OC against POF and SG respectively. OC initially decreases and then gradually increases with increase in both POF and SG respectively.

4.5. Discussion

The response surface plots of OC with respect to GI, SG, POT and POF are shown. It is witnessed that high levels of the two variables out of four yield maximum responses. As the response is proportional to the variables, there cannot be any stationary point as evident from the surface plots. It is examined that the two variables out of four yield maximum responses. It obvious that the POF and GI are significant parameters for OC.

5. MULTI RESPONSE OPTIMIZATION

5.1. Desirability Functions

Response Optimizer facilitates to recognize the factor settings that optimize a single response or a set of responses. For multiple responses, the necessities for all the responses in the set must be fulfilled. Response optimization is frequently helpful in product development when it is required to find out operating conditions that will result in a product with enviable properties.

Here the goal, lower, target, upper, and weight define the desirability function for each individual response. The importance (Import) parameters resolve how the desirability functions are combined into a single composite desirability.

The optimization procedure chooses numerous starting points from which to begin searching for the optimal factor settings. There are two types of solutions for the search:

- (i) Local solution: For each starting point, there is a local solution. These solutions are the “best” combination of factor settings found beginning from a particular starting point.
- (ii) Global solution: There is only one global solution, which is the best of all the local solutions. The global solution is the “best” combination of factor settings for achieving the desired responses. The predicted responses show the global solution factor levels. The response optimization is shown in Table 11 below.

Table 11. Desirability function results

Parameters	Goal	Lower	Target	Upper	Weight	Import
MRR	Maximum	0.0040	0.2250	0.2880	1	1
Ra	Minimum	2.2170	2.3560	10.7488	1	1
OC	Minimum	1.9083	2.8788	8.8850	1	1
Predicted Responses					Global Solution	
MRR = 0.18365, desirability = 0.81290 (81.29%)					POT = 23.9999	
RA = 4.00257, desirability = 0.80381 (80.38%)					POF = 12.0000	
OC= 5.70377, desirability = 0.52966 (52.966%)					GI = 11.0000	
Composite Desirability = 0.70209 (79.209%)					SG = 0.2000	

The individual desirability for each predicted responses are calculated. The individual desirability values are then combined into the composite desirability. These desirability values can facilitate to understand how close the predicted responses are to the given target requirements.

Desirability is measured on a 0 to 1 scale. Here MRR has an intermediate desirability score of 0.81290 because the predicted response for MRR of 0.18365 is approximately two-thirds of the way between the target of 0.228 and the lower bound of 0.004. The goal for MRR is to maximize; therefore higher values are more desirable. Similarly Ra has a desirability score of 0.80381 because the predicted response of 4 is nearer to the target of 2.356.

The experiment seems to be less successful optimizing Overcut than MRR and Ra respectively. The composite desirability of 0.70209 places greater emphasis on MRR (importance = 2) than on Ra and Overcut (importance = 1).

5.2. The Optimization Plot

Figure 26 represents the optimization plot of the responses (MRR, Ra and OC) with the process variables. It shows how the factors affect the predicted responses and allows to modify the factor settings interactively. The figure shows the goal for the response, the predicted response, y , at the current factor settings, and the individual desirability score. The composite desirability, D , is displayed in the upper left corner of the graph. The label above the composite desirability refers to the current setting. When the optimization plot is created, the label is Optimal. The vertical red lines on the graph represent the current factor settings. The horizontal blue lines represent the current response values.

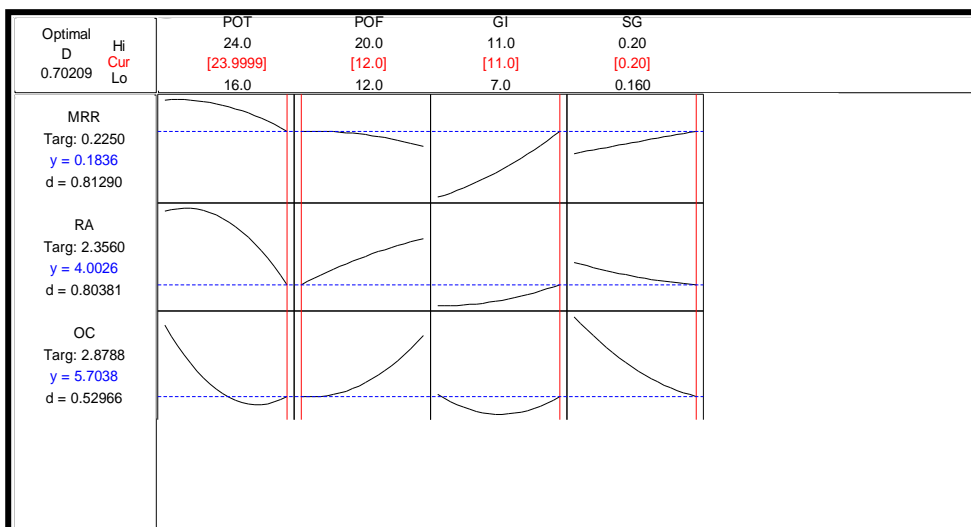


Figure 26. Plot showing responses (MRR and Ra) v/s process variables.

5.3. Overlaid Contour Plots

On an overlaid contour plot, the contours for each response are placed on top of each other in a single graph. Each set of contours defines the boundaries of acceptable response values. The solid contour is the lower bound and the dotted contour is the upper bound. The contours of each response are displayed in a different color. The white area in the graph is the feasible region.

The feasible region is the area formed by the two factors, given the hold values of any other factors, such that the acceptable values for each response are between their respective contours. High MRR, low Ra and low OC are the major attributes of EDM machining process. These responses are conflicting in nature and hence achieving the both simultaneously by a set of optimum variables combination is difficult. In this section the multi response optimization is conceded out so that two conflicting goals are fulfilled concurrently.

Here overlay contour plots are created which are comparatively simple to review the levels of operating parameters that satisfy two constrained objectives. It is considered that Ra

in the range of $2.217 \mu\text{m}$ to $3.824 \mu\text{m}$ found to be reasonably good and acceptable for most of the applications. MRR has been set between a lower bound of $0.004 \text{ mm}^3/\text{min}$ and upper bound of $0.288 \text{ mm}^3/\text{min}$. Similarly OC is set between a lower bound 4.416 mm^2 to an upper bound of 8.88 mm^2 .

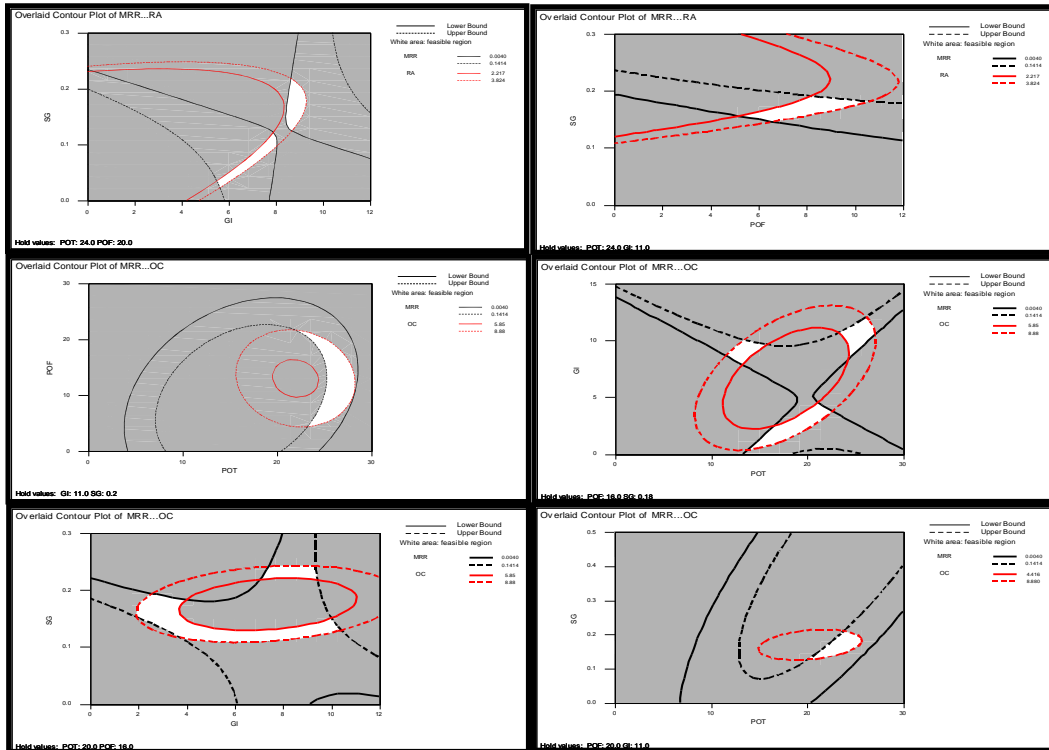


Figure 27. Overlaid Contour plot for MRR, Ra and OC.

CONCLUSION

The experimental study indicates that while machining AISI P - 20 tool steel using die sinking EDM process the responses are dependent on Pulse on time, Pulse off time, Gap current and Spark gap. The ANOVA is a simple method to ascertain implication of several input parameters that administers multiple responses of the process. For higher MRR, GI is the most significant parameter and having F-value of 84.58%. MRR increases with respect to increase of GI. Maximum MRR is obtained at the following parametric combination: POT – $20 \mu\text{Sec}$, POF – $12 \mu\text{Sec}$, GI – 11 amps and SG – 0.2 mm. In case of lower Ra, the GI is having the most significant effect and contributes F – value of 15.64 followed by POT having F – value of 10.14. Ra decreases with the increase of POT and however Ra increases with increase of GI. Minimum Ra is obtained at the following parametric combination: POT – $24 \mu\text{Sec}$, POF – $20 \mu\text{Sec}$, GI – 07 amps and SG – 0.18 mm. For smaller overcut, GI is the significant parameter. The F value of GI assumes a value of approximately 4.

The present work is carried out with a view to optimize MRR (maximize), Ra (minimize) OC (minimize) concurrently by employing a near optimal set of process variables. This

optimization is carried out by RSM that is promised to tender near optimal solution with modest effort. The regression models are established to be creditable to express input-output relationship with a very high degree of predictability. The inferences drawn from the regression analysis is accentuated with the desirability functions. Gap current is found to be the most significant in comparison to the responses. The near optimal combinations of process variables are high POT, POF and low GI and SG to satisfy both the responses (MRR and Ra) simultaneously. This set of inputs can be used to further optimize other functions like machining cost and can form the backbone of adaptive control strategies (adaptive control with optimization and geometric adaptive control). The overlaid contour plot is a good visual aid to identify the feasible region in regard to a set of input variables.

The individual desirability for each predicted responses are calculated. The individual desirability values are then combined into the composite desirability. The closer the predicted responses are to your target requirements, the closer the desirability will be to 1. The composite desirability combines the individual desirability into an overall value, and reflects the relative importance of the responses. The higher the desirability the closer it will be to 1. Here MRR has an intermediate desirability score of 0.81290 because the predicted response for MRR of 0.18365. The goal for MRR is to maximize; therefore higher values are more desirable. Similarly Ra has a desirability score of 0.80381 where as OC has a desirability score of 0.52966. The experiment was less successful optimizing Overcut than MRR and Ra respectively. The composite desirability of 0.70209 places greater emphasis on MRR (importance = 2) than on Ra and Overcut (importance = 1).

The optimization plot of the responses (MRR, Ra and OC) with the process variables is drawn. It illustrates how the factors influence the predicted responses and permit to adapt the factor settings interactively. Finally overlaid contour plots are drawn. The feasible region in white color is formed by the two factors, given the hold values of any other factors, such that the acceptable values for each response are between their respective contours.

The RSM being a powerful tool, its potential can be extended to other areas of machining such as tool life, power and cutting force modeling. The experimental investigation for evaluating the optimal parametric combination and the subsequent effect of the parameters over the responses can act as an efficient & useful guideline for machining and manufacturing various metallic products. The future work in this emerging area can be considered with other parameters and different responses such as cutting force, tool life etc to capture the process in full perspective.

This present research study of P 20 steel will act as a guideline for optimum machining. The present research approach is extremely useful for maximizing the productivity while maintaining high MRR and reasonably low Ra and OC within desired limit. The developed technology setting in the field of electrical discharge machining of P 20 steel will find tremendous potentiality in modern industrial applications for efficient manufacturing of precision jobs.

REFERENCES

- Arikatla, S.P., Krishnaiah, A. and K. Mannan, K. T. (2013), "Optimization of electric discharge machining response variables using design of experiments", *International Journal of Mechanical and Production Engineering*, 2(1), 83-87.
- Ayestaa, I., Izquierdob, B., Sáncheza, J.A., Ramosc, J.M., Plaza, S., Pombod, I., Ortegaa, N., Bravoe, H., Fradejase, R. and Zamakonae, I. (2013), "Influence of EDM parameters on slot machining in C1023 aeronautical alloy", *In the Seventeenth CIRP Conference on Electro Physical and Chemical Machining (ISEM), Procedia CIRP*, 6, 129 – 134.
- Bayramoglu, M. (2005), "Systematic investigation on the use of plate type tools for the production of linear and circular swept surfaces on CNC EDM", *International Journal of Computer Applications in Technology*, 24(3), 165 - 170.
- Bonny, K. , De Baets, P. , Vleugels, J. , Van der Biest, O. , Lauwers, B. and Liu, W. (2009), "EDM machinability and dry sliding friction of WC-Co cemented carbides" , *International Journal of Manufacturing Research*, 4(4), 375 - 394.
- El-Hofy, H., (2005), *Advanced Machining Processes*, McGraw Hill, New York.
- Ghosh, A., & Mallik, A. K., (1991). *Manufacturing Science*, Affiliated East-West Press, New Delhi.
- Jana, T. K., Bose ,G. K., Sarkar, B. and Saha, J. (2011), "Multi objective decision making in single pass turning using response surface methodology", *International Journal of Computational Materials Science and Surface Engineering*, 4(1), 87 -108.
- Kapoor, J., Khamba, J.S. and Singh, S. (2012), "The effect of machining parameters on surface roughness and material removal rate with cryogenic treated wire in WEDM", *International Journal of Machining and Machinability of Materials*, 12(1/2),126 - 141.
- Kumar, A., Kumar V., and Kumar, J. (2012), "Prediction of Surface Roughness in Wire Electric Discharge Machining (WEDM) Process based on Response Surface Methodology", *International Journal of Engineering and Technology*, 2(4), 708-719.
- Lauwers, B., Liu, W., Kruith, J. P., Vleugels, J., Jiang, D. and Van der Biest, O. (2005), "Wire EDM Machining of Si₃N₄, ZrO₂ and Al₂O₃ based ceramics", *International Journal of Electrical Machining*, 10, 33-37.
- Mohantya, C. P., Sahub, J., Mahapatraa, S. S. (2013), "Thermal-structural analysis of Electrical Discharge Machining Process", *In 3rd Nirma University International Conference on Engineering (NUiCONE 2012), Procedia Engineering*, 51, 508 – 513.
- Montgomery, D.C. (2000), *Design and Analysis of Experiments*, 5th ed., John Wiley, New York.
- Ojha, K., Garg, R.K., and Singh, K.K. (2012), "An investigation into the effect of nickel micro powder suspended dielectric and varying triangular shape electrodes on EDM performance measures of EN-19 steel", *International Journal of Mechatronics and Manufacturing Systems*, 5(1),66 - 92.
- Park, S.H. (1996), *Robust Design and Analysis for Quality Engineering*, 1st ed., Chapman & Hall, London, U.K.
- Salem, S. B., Tebni, W., and Bayraktar, E. (2011), "Prediction of surface roughness by experimental design methodology in Electrical Discharge Machining (EDM)", *Journal of Achievements in Materials and Manufacturing Engineering*, 49(2), 150-157.

- Selvakumar, G., Sarkar, S., and Mitra, S. (2013), "An experimental analysis of single pass cutting of aluminium 5083 alloy in different corner angles through WEDM", *International Journal of Machining and Machinability of Materials*, 13(2/3), 262 - 275.
- Singh, K. and Kalra, C. S. (2013). "An Experimental Investigation: Machining of OHNS Steel by EDM", *Journal of Engineering Computers & Applied Sciences*, **2(6)**, 39-42.
- Singh, H. and Singh, A. (2012), "Examination of Surface Roughness Using Different Machining Parameter in EDM", *International Journal of Modern Engineering Research*, 2(6), 4478-4479.
- Suzuki, K., Iwai, M., Sharma, A., Sano, S., and Uematsu T. (2006), " Low-wear diamond electrode for micro-EDM of die-steel", *International Journal of Manufacturing Technology and Management*, 9(1/2), 94 - 108.
- Syed, K. H. and Palaniyandi, K. (2012), "Performance of electrical discharge machining using Aluminium powder suspended distilled water", *Turkish Journal of Engineering Environmental Science*, 36,195 – 207.
- Zolotykh, B.N., (1959), "The mechanism of electrical erosion of metals in liquid dielectric media", *Soviet Physics-Technical Physics*, 12, 1370-1373.

Chapter 10

**YTTERBIUM FIBER LASER
MACHINING OF AA6061 MATRIX
AND Al/Al₂O₃-MMC**

*Alakesh Manna**

Department of Mechanical Engineering,
PEC University of Technology
(Formerly: Punjab Engineering College),
Chandigarh, India

ABSTRACT

This chapter presents some specific investigated results acquired during Ytterbium fiber laser machining of AA6061-Matrix and Al/Al₂O₃-MMC. Some important features of laser beam machining process are also explained in the chapter. The effects of the Ytterbium fiber laser machining parameters such as laser power, modulation frequency, gas pressure, wait time, pulse width on the machining performance criteria e.g., metal removal rate and tapering phenomena have been analyzed through various graphs and reported in the chapter. From machining of AA6061-Matrix results, it is clear that the material removal rate (MRR) increases radically with increase in laser power specifically ranges from 300 to 400 watts. MRR also increases with increase in modulation frequency ranges from 500 to 800 Hz. But during machining of Al/Al₂O₃-MMC, it is found that the MRR increases with increase in laser power ranges from 400 to 1000 watts. Drilled hole deviation and taper increase with increase in modulation frequency ranges from 600 to 1000 Hz. However, optimization of Ytterbium fiber laser machining parameters can be effectively minimized the taper.

Keywords: Ytterbium fiber laser machining, metal removal rate, hole deviation and taper

* Professor & Head, Department of Mechanical Engineering, PEC University of Technology, Chandigarh, India.
Phone: +91-172-275-3551, Fax: +91-172-274-5175; e-mail: kgpmanna@rediffmail.com.

INTRODUCTION

Laser beam machining (LBM) is an unconventional *machining* process in which a *laser* is directed towards the workpiece for machining. Since the rays of a laser beam are monochromatic and parallel it can be focused to a very small diameter and can produce energy as high as 100 MW of energy for a square millimeter of area. Laser machining can be replace mechanical material removal methods in many industrial application, particularly in the processing of difficult to machine materials such as hardened metals, ceramics and composites. Material processing like heat treatment, alloying, cladding, sheet metal bending etc. are also done by utilizing coherent photon or laser beam, which is mostly converted into thermal energy upon interaction with material. In industry, laser beam machining is used for sheet metal cutting, welding, curing of metal deposition, micro and macro drilling of various materials etc.

Laser beam can be focused very easily using optical lenses as their wavelength ranges from half micron to around 70 microns. Focused laser beam has capability to discharge a power density of 1 MW/mm^2 and above. As laser interacts with the material, the energy of the photon is absorbed by the work material leading to rapid substantial rise in local temperature. As a result, melting and vaporization of the workpiece material takes place.

Lasers convert electrical energy into a high energy density beam of light through stimulation and amplification as explained by Corfe (1983). Stimulation occurs when electrons in the lasing medium are excited by an external source such as an electrical arc or flash lamp, resulting in emission of photons. The energy required to raise an electron from one energy state to another is provided by an excitation process or pumping. This is achieved by the lasing medium's absorption of energy from mechanical, chemical, electrical or light sources as explained by George Chryssolouris (1991). The rate of power input to the excitation process must exceed the output power of the laser, since there are many losses associated with the lasing process. The lasing medium typically contains ions, atoms or molecules whose electrons are conducive to changes in energy level. According to the quantum mechanics, atoms or molecules in the lasing medium have discrete electron energy levels. Laser light is created by the transition from a higher to a lower energy level and the wave length produced is a characteristic of the lasing medium. At the beginning of the lasing process, photon emissions are random in nature.

As each photon stimulates other excited electrons to emit photons, however the new photons will have similar wavelength, direction and phase characteristics as the initial photon. Eventually a stream of photons with identical wave length, direction and phase will be produced. The amplification of light in a laser is accomplished by an optical resonator, which is composed of a cavity with the lasing medium set between two high precision, aligned mirrors as explained by Chryssolouris (1991). One mirror is fully reflective and the other is partially transmissive to allow for the beam output. The mirrors channel the light back into the lasing medium, as the photons pass back and forth through the lasing medium; they stimulate more and more emissions. Photons that are not aligned with the resonator are not redirected by the mirrors to stimulate more emissions, so that the cavity will only amplify those photons with the proper orientation and a coherent beam develops quickly.

Population inversion is another necessary condition for the lasing process. When the lasing medium or lasant is in equilibrium, the population of electrons at any energy state is

determined by the Boltzman equation. For a medium with two energy states, the relationship between energy and electron population is

$$\frac{N_2}{N_1} = \exp\left(-\frac{E_2 - E_1}{kT}\right) \quad (\text{Eq.1})$$

where, N_1 and N_2 are the number of electrons at energy states 1 and 2 respectively, E_1 and E_2 are the energy values for state 1 and 2, T is the absolute temperature of the medium and k is Boltzmann's constant. Theoretically only a slight population inversion is required to achieve lasing; however with other energy losses also occurring, there must often be several excited electron states for every equilibrium state electron as explained by Chryssolouris (1991).

Laser can be categorized most easily according to their lasing mediums, which are divided into three basic categories as defined by the state of the lasing material: gas, liquid or solid. Furthermore, all laser types operate in one of two temporal modes: continuous wave (CW) and pulsed modes. In CW mode, the laser beam is emitted without interruption. But in case of pulsed mode, the laser beam is emitted periodically.

Gas Lasers

Gas lasers are further divided into three subgroups based on the composition of the lasing medium such as neutral atom, ion and molecular laser. The He-Ne laser is a typical neutral atom gas laser and is the most popular visible light laser; it can be tuned from infrared to various visible frequencies, with the most common being red at a wave length of 0.6328 μ m as explained by Chryssolouris (1991). The actual lasing occurs during an electron transition in the Ne atom, but the presence of He is essential since it is excited first by an electrical discharge and then its energy is transferred to the Ne atom through kinetic interactions. Excitation is provided by D.C. electrical discharge in a low pressure discharge tube. Ion lasers use an ionized gas such as Ar, Kr and Xe as a lasing medium to produce laser beams with wave lengths ranging from 0.5 to 1.0 μ m. Excitation are initiated by an electrical discharge, caused by ionization of gases and electrons are excited for laser. Molecular lasers use gas molecules as the lasing medium. In this case molecules are excited and through vibrational modes produce photons from CO, HF and CO₂ and produced laser that can be used for machining operations. The pumping is done by A.C. or D.C. electrical discharge.

Liquid Laser

In liquid lasers organic dye molecules used as the lasing medium. The dyes can be absorbed radiation from a wide range of frequencies and have hundreds of overlapping spectral lines from which they can be lased. These lasers are designed so that the frequency at which they lased can be varied.

Solid State Laser

In solid lasers use ions suspended in a crystalline matrix to produce laser. The ions provide the electrons for excitation, while the crystalline matrix propagates the energy between ions. The two main classes of ions in the laser medium are Cr^{3+} for ruby lasers and Nd^{3+} for Nd:YAG and Nd:glass lasers. Ruby laser has low achievable beam power as well as low energy efficiency which barricades its applications. The Nd:YAG and Nd:glass lasers have similar structure and lasing action. They can be widely applied in industry. Excitation is achieved by krypton or xenon flash lamps. Laser machining can replace mechanical material removal methods in many industrial applications, particularly in the processing of difficult to machine materials such as manganese and other hardened metals, ceramics and composites. The laser beam has unique characteristics can be applied for different industrial applications such as material removal, material deposition by therapeutic and curing etc.

Advantages of Laser Machining Process

The laser beam machining has different advantages. Some of the advantages are discussed in brief and listed as follows.

(i) Laser Machining Is a Thermal Process

The effectiveness of laser machining depends upon the thermal properties and to a certain extent, the optical properties rather than the mechanical properties of the material to be machined. The laser beam machining is most suitable for machining of materials having a high degree of brittleness and favorite thermal properties like low thermal diffusivity and conductivity.

(ii) Laser Machining Is a Non-Contact Process

The laser beam machining is a non contact process as here energy is transfer between the laser and the material occurs through irradiation, no cutting forces are generated by the laser, rather absence of the direct contact of cutting tool and materials, mechanically-induced material damage, tool wear and machine vibration. In this process, there is no constrains like cutting forces, tool wear, built up layer and built-up-edges, mechanical tool failure and chattering etc. Hence, the removal of material rate in laser machining is not limited.

(iii) Laser Machining Is a Flexible Process

The laser beam machining can be applicable to all major processes such as drilling, cutting, grooving, welding, material deposition, therapeutic and curing, heat treatment and cladding processes, resistor trimming, substrate scribing, semiconductor annealing, marking, printing etc. For flexible applications of laser beam, required a multi axis work-piece holding and positioning system. A single laser beam machining centre is capable enough for complying all above processes. The laser beam machining can be effectively applicable for generation of higher precision and smaller kerf widths cut and hole diameters as compared to any other well known conventional machining techniques.

Limitations in Laser Beam Machining Process

The laser beam machining is a primarily thermal process; it has a few limitations which are explained as follows

(i) *Low Energy Efficiency*

In laser machining, the removal of material occurs by melting or vaporizing the entire volume of material to be removed. Thus material phase changes during machining, this change may occur on an atom-by-atom basis from the surface of the work-piece material to be removed. In laser machining required higher energy inputs and a minimum processing times, which some where depends on the material characteristics. Hence, laser beam has low energy efficiency as compared to the equivalent mechanical processes.

(ii) *Material Damage*

During laser machining, high power densities of laser beams are required to be introduced on the surface of the work-piece in order to raise the sufficient temperature to melt and vaporize the metal from the point of interest. Hence, created a heat affected zone in the vicinity of the striking of laser beams and erosion point. During laser beam machining of some specific materials, it is also observed that the decomposition of materials occurred by breakdown of molecules, which ultimately converts into some by-products because of generated high temperature and thereby damages material surfaces.

IMPORTANCE AND REVIEW OF LITERATURE

With the rapid technological acceptance of Al/Al₂O₃-MMC in industrial applications, the machining of Al/Al₂O₃-MMC has been very important for manufacturing engineers and applied researchers working in this area. Various non traditional machining processes such as AWJM, ECM, EDM, WEDM, AFF etc. have shown their scope of applications towards the machining of Al/Al₂O₃-MMC but these processes have also their own limitations and still remain machining problems like low material removal rate, high surface roughness and poor dimensional accuracy etc. Manufacturing of miniature and micro dimensional part made of Al/Al₂O₃-MMC with satisfactory tolerance by any well known machining processes is still very difficult as explained by Ghosal and Manna (2013). As laser machining has tremendous potential on account of the versatility of its applications and it is expected that it will be successfully and commercially utilized in modern industries. The better quality of product can be produced by laser beam machining (LBM) through proper optimization and combinational control of various process parameters.

The basic material removal mechanism in laser drilling is based on the absorption of laser energy from a series of laser pulses at the same spot; material is melted and ejected to the form of hole as explained by various authors such as Meijer J. (2004), Tiwari et al. (2005), Biswas et al. (2010), and Ghosal et al.(2013). Tsai and Chen (2003) proposed an explanation for why the focused Nd:YAG laser is used to scribe a groove-crack on the surface of substrate and the defocused CO₂ laser is used to introduce thermal stress. An excimer laser was used to study the basic mechanism roughening the surface of silicon carbide by Tonshoff and Kappel

(1998). The quality of under water laser drilling on LCD glass and alumina substrates are much better as compared to drilling in air as stated by Tsai and Li (2009). A three dimensional thermal model was developed for a laser assisted machining process and validated the developed model by comparing predicted surface temperature histories with measurements made using a focused laser pyrometer by Rozzi et al. (2000). A localized thermal shock is produced due to the incidence of the cold cutting gas-jet during laser cutting and this caused the formation of cracks whose advance was limited by the cooling of melted material which experienced visco-plastic fluency as explained by Pascual Cosp et al. (2002). Samant and Dahotre (2009) studied the Nd:YAG laser machining of MgO and concluded that the multiple reflections and energy losses associated with MgO dissociation affected the total amount of laser energy absorbed. Authors also stated that the evaporation of ceramic was responsible for material removal and vapour pressure ensured the formation of a clean cavity. Li et al. (2007) studied for identifying the optimal laser parameter for cutting quad flat no-lead (QFN) packages by using a diode pumped solid state laser system and concluded that the best cutting quality can be achieved with optimal parameters 2 kHz frequency, 2 mm/s cutting speed, and 29A driving current. The non uniform melts and ejection of material from the groove walls and laser power reduction are the causes of variation in taper angle as explained by Lallemanda (2000), and Dhupal et al. (2008). The structural modifications was observed on the cut surface produced with CO₂ laser cutting of commercial tiles of calcitic marble and limestone as stated by Miranda (2004).

In the research, an attempted has been made to machine Al-matrix and Al/Al₂O₃-MMC by Ytterbium fiber laser and try to conquer the machining problems over Al/Al₂O₃-MMC. Keeping in view, some of the results obtained during experimental investigation on Ytterbium fiber laser machining of Al-matrix and Al/Al₂O₃-MMC are reported in the chapter.

EXPERIMENTAL PLANNING

An Ytterbium laser machine YLR 1000 with CNC system RP 3015 was used for experimental investigation. The stir cast technique was used for fabrication of Al/Al₂O₃-MMC work-piece samples. In the laser machining, laser head produces laser beam, which is used for machining of Al/Al₂O₃-MMC work piece. A laser source has multiple diodes which consists of ytterbium coated fiber that sent the laser light through optical fiber to the laser head, from which the laser beam is focused on the work piece. A cooling unit is used to cool the entire laser machining system during machining.

The movement of the work piece in 'X' and 'Y' directions are controlled through a computer programmable controller. The CNC 'Z' axis controller unit controls the Z-axis movement of lens. Figure 1 shows a schematic block diagram of CNC and Ytterbium laser machining system. A fixture is designed and fabricated to hold the work-piece properly. Table 1 represents the detail specification of Ytterbium fiber laser machine YLR 1000 used for experimentation.

The specific numbers of experiments have been carried out with different combinational values of process variables to investigate the effects of various parameters on machining response characteristics.

Table 1. Detail specification of Ytterbium Laser machine YLR 1000

particulars	parameters	unit	YLR-1000
CW power	i)Operation mode		CW/QCW
	ii)nominal output power	kW	1
beam	i)Emission wave length	nm	1070-1080
	ii)Output fiber core diameter of the feeding fiber	μm	150
	iii)Fiber length	m	10
	iv)polarization		random
gas			No Laser gas
electrical	i)Operating voltage 3-phase	VAC	400-460
	ii)Power frequency	Hz	50-60
	iii)Power consumption	kw	4
cooling	i)Laser cooling water temperature range	⁰ C	22-24
	ii)Laser cooling water flow rate	l/min	5
Environment	i)Operating Ambient air temperature range	⁰ C	10-50
	ii) Humidity with built in conditioner	%	95
	iii)Storage temperature	⁰ C	-40 to 75
dimensions	W x D x H	mm	856x806 x 1186
weight		kg	330

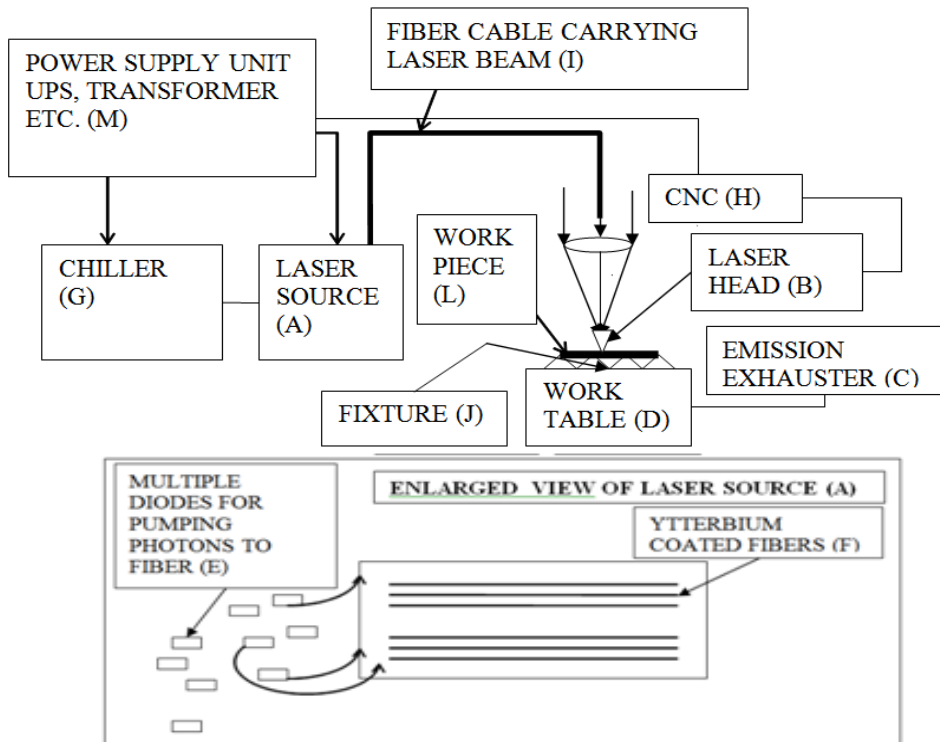


Figure 1. Schematic block diagram of Ytterbium Fiber Laser machining system.

The material removal rate and tapering phenomenon considered as output machining criteria. The machining is carried out for a fixed time interval. Figure 2 shows an Ytterbium fiber laser machining setup used for drilling of Al/Al₂O₃-MMC work-piece. Sartorius Master Series Electronic Balance of least count 0.001g is used to weight the work-pieces before and after each run. The material removal is determined from the difference in weight of the work-piece before and after machining. The top and bottom hole conditions of each micro and macro hole are investigated through SEM taken utilizing JEOL JSM6510LV a Scanning Electron microscope.

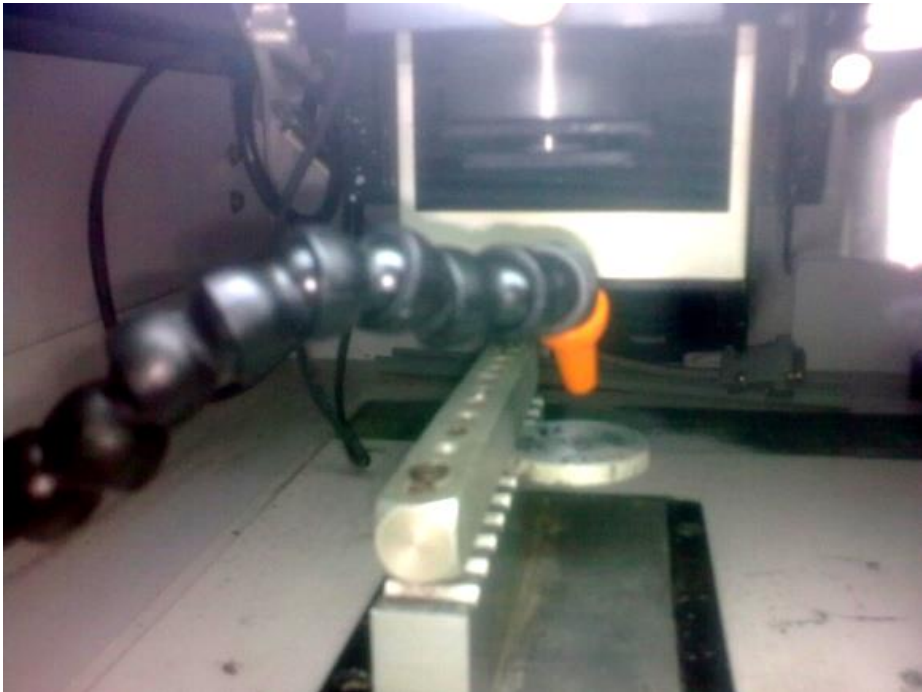


Figure 2. Ytterbium fiber laser drilling on Al/Al₂O₃ MMC.

The taper per unit length of the machined hole was determined by utilizing the relation as given below.

$$\text{Taper} = \frac{(\text{Measured diameter at entrance of hole}) - (\text{Measured diameter at exit of hole})}{2 \times (\text{Thickness of the work-piece})}$$

$$\text{Taper} = \frac{(D - d)}{2.t} \quad (\text{Eq. 2})$$

The taper on hole depth (rad) of the machined hole was determined by utilizing the relation as given below.

$$Taper, \text{radian} = \left[\tan^{-1} \frac{(D-d)}{2t} \right] \cdot \frac{\pi}{180} \quad (\text{Eq. 3})$$

where, D = Measured diameter at top of the machined hole, mm; d = Measured diameter at bottom of the machined hole, mm; t = Thickness of the work-piece, mm

In the present set of analysis, the laser power (x_1), modulation frequency (x_2), gas pressure (x_3), wait time (x_4) and pulse width (x_5) are considered as the controllable variables and their effects on material removal rate (MRR) and tapering phenomena are investigated through a set of planned experiments.

RESULTS AND DISCUSSION

Parametric Effect on Response Characteristics During Machining of AA6061-Matrix

Selecting all important parameters such as Laser power (Watt), Modulation frequency (Hz), Gas pressure (bar), Pulse width (% of duty cycle), Wait time(s) of Ytterbium fiber laser machining process (identified during preliminary test), the different sets of experiments have been carried out to investigate the effects of each individual parameters on machining response characteristics. The effects of variation in setting of parameters as mentioned above have been studied on the response characteristics during Ytterbium fiber laser machining of aluminum alloy matrix (AA6061) and Al/Al₂O₃-MMC, and explained the effects through various graphs.

Figure 3(a), Figure3(b), Figure3(c) and Figure3(d) show the effect of the variation in material removal rate (g/s) with that of (a) laser power (watt) (b) modulation frequency (Hz), (c) N₂-gas pressure (bar), and (d) pulse width (% of duty cycle) during Ytterbium fiber laser machining of aluminum alloy (AA6061)-matrix respectively. From Figure3(a), it is clear that the material removal rate increases radically with increase in laser power specifically ranges from 300 to 400 watts. The MRR also marginally increases with increase in laser power ranges from 400 to 900 watts. From Figure 3(a), it is also clear that the material removal rate again increases moderately with increase in laser power ranges from 900 to 1000 watts. However, during machining it is observed that the material removal is negligible while machining operations are performed with varying laser power ranges from 100 to 300 watts keeping other parameters remains constant i.e., 800 Hz modulation frequency, 17 bar N₂-gas pressure, 0.2 s wait time and 80 % pulse width. This is may be due to the discharge of insufficient laser power which has not enough to scatter and vaporize the materials at the point of incident laser beam as aluminium has higher conductivity. From Figure 3 (b), it is clear that the material removal rate increases radically with increase in modulation frequency specifically ranges from 500 to 800 Hz. The MRR also marginally decreases with increase in modulation frequency ranges from 800 to 900 Hz. However, from Figure 3(b), it is also clear that the material removal rate again increases moderately with increase in modulation frequency from 900 Hz to 1000 Hz. During machining it is observed that the material removal is negligible while machining operations are performed with varying modulation frequency

ranges from 100 to 500 Hz keeping other parameters remains constant i.e., 700 Watts laser power, 17 bar N₂-gas pressure, 0.2 s wait time and 80 % pulse width.

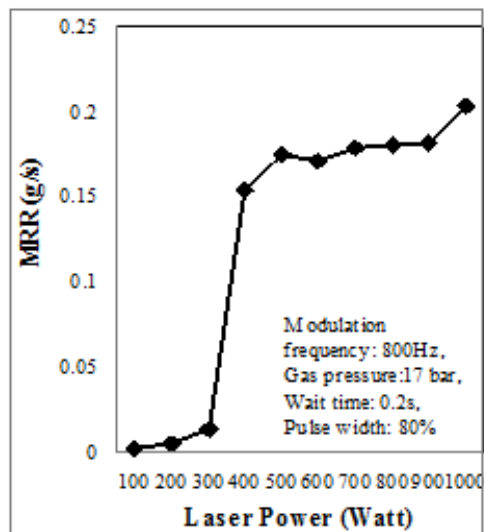


Figure 3(a). Effect of laser power on MRR

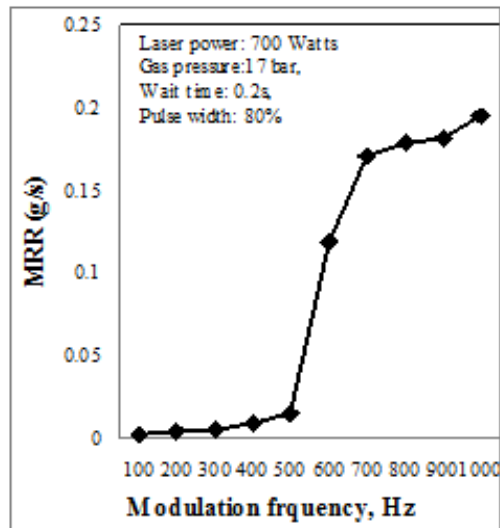


Figure 3(b). Effect of modulation frequency on MRR.

This may be due to the high strength, ductility and conductivity of aluminium alloy matrix and hence lower range of supply frequency not enough to separate the molecules from the incident laser beam spot during machining.

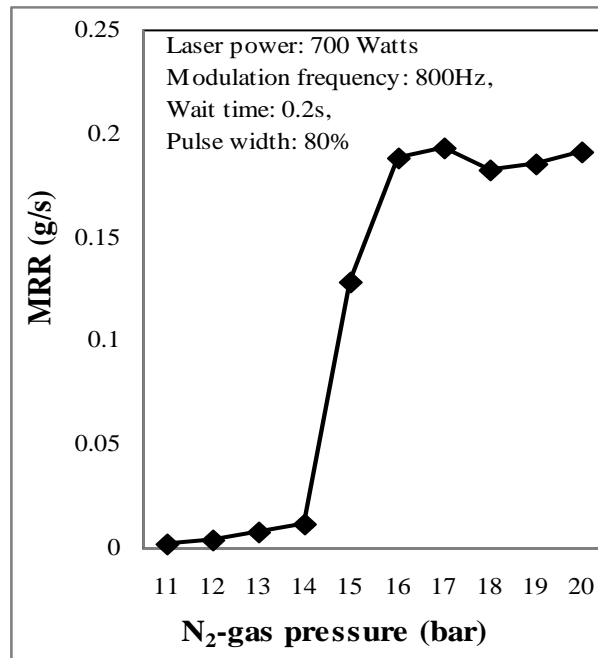


Figure 3(c). Effect of N₂-gas pressure on MRR.

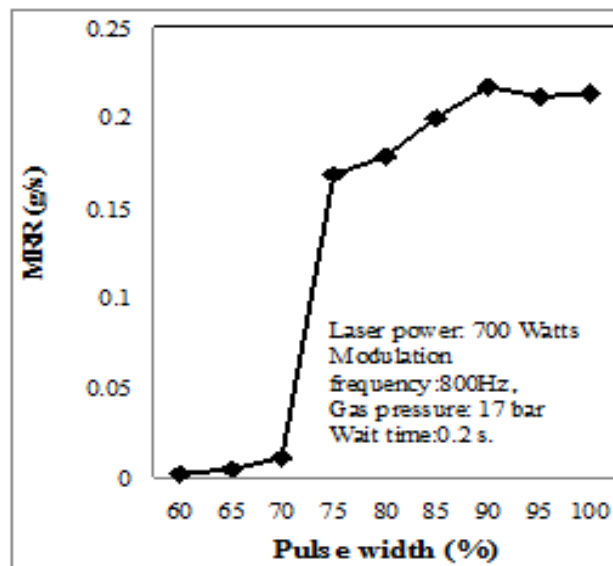


Figure 3 (d). Effect of pulse width (%) on MRR.

Figure 3(c) shows the variation in material removal rates (g/s) with that of N₂-gas pressure (bar) during machining of aluminum alloy (AA6061). From Figure 3(c), it is clear that the N₂-gas pressure ranges from 16 to 17 bars the material removal rate is quite higher as compared to any other value of gas pressure considered for experimentation. It may be due to the high jet of N₂ gas remove molten and metallic debris which are generated during laser

drilling. Figure 3(d) shows the variation in material removal rates (g/s) with that of pulse width (%) during machining of aluminum alloy (AA6061). From Figure 3(d), it is clear that the pulse width ranges between 75 to 90 % of duty cycle the material removal rate is higher. It is because of high energy discharge from the laser beam which was directly stricken to the work-piece surface and material gets vaporized.

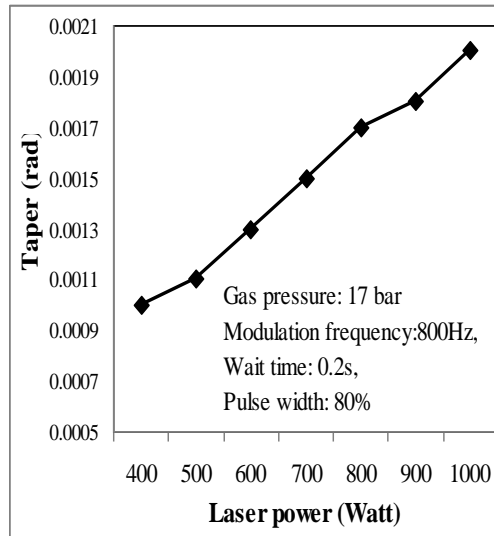


Figure 4 (a). Effect of laser power on taper.

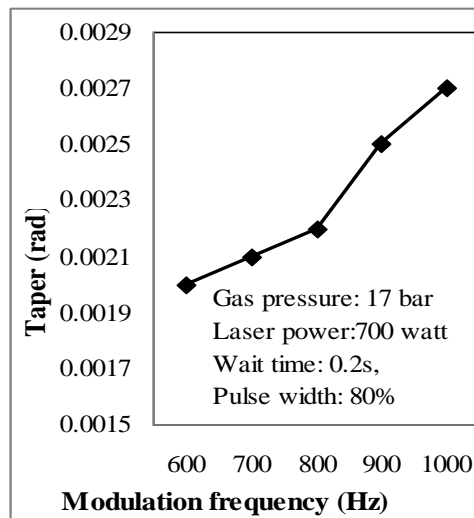


Figure 4 (b). Effect of modulation frequency on taper.

Figure 4(a), Figure4(b), Figure4(c) and Figure4 (d) show the effect of the variation in taper (rad) with that of (a) laser power (watt) (b) modulation frequency (Hz), (c) N2-gas pressure (bar), and (d) pulse width (% of duty cycle) during Ytterbium fiber laser machining of aluminum alloy (AA6061) respectively. From Figure 4(a), it is clear that the taper (rad)

increases radically with increase in laser power ranges from 400 to 1000 watts. This may be due to the discharge of higher energy at higher laser power, which has enough to scatter and vaporize the materials at the point of incident laser beam striking on aluminium material and thereby increases taper. From Figure 4 (b), it is clear that the material removal rate increases radically with increase in modulation frequency ranges from 800 Hz to 1000 Hz. This may be due to the insufficient or not enough to separate the molecules from the incident laser beam spot during machining when machining is done at lower range of supply frequency (i.e., below 600 Hz).

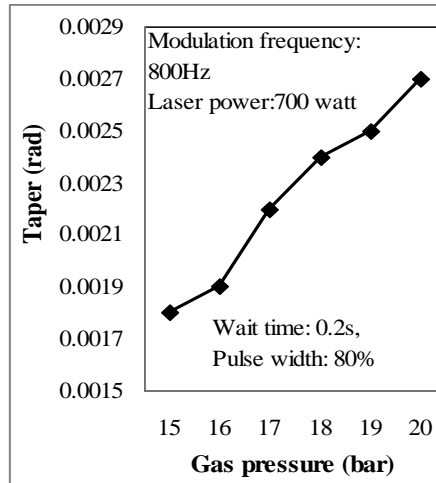


Figure 4(c). Effect of gas pressure on taper.

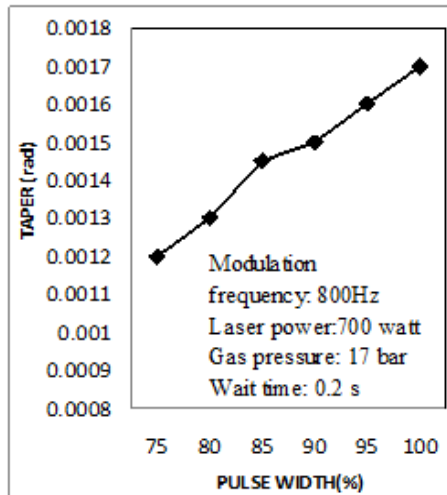


Figure 4(d). Effect of pulse width (%) on taper.

From Figure 4(c), it is clear that the N₂-gas pressure ranges from 17 to 20 bars the taper (rad) is quite higher as compared to any other value of gas pressure considered for experimentation. It may be due to high material removal by discharging of high jet of N₂ gas.

The high jet of N_2 gas pressure removes molten and metallic debris generated during laser drilling. Figure 4(d) shows the variation in taper (rad) with that of pulse width (%) during machining of aluminum alloy (AA6061). From Figure 4(d), it is clear that the pulse width ranges from 75 to 90 % of duty cycle the taper (rad) is higher. It is because of high energy discharge from the laser beam at higher pulse width, which is directly stricken to the work-piece surface and material gets vaporized.

Parametric Effect on Response Characteristics During Machining of Al/ Al_2O_3 -MMC

Figure5(a), Figure5(b), Figure5(c) and 5(d) show the effect of the variation in material removal rate (g/s) with that of (a) laser power (watt), (b) modulation frequency (Hz), (c) N_2 -gas pressure (bar), and (d) pulse width (% of duty cycle) during Ytterbium fiber laser machining of Al/5wt% Al_2O_3 -MMC respectively. From Figure 5(a), it is clear that the material removal rate increases with increase in laser power ranges from 400 to 1000 watts. This may be due to the discharge of sufficient laser power at higher laser power setting and has got enough energy to scatter and vaporize the Al/5wt% Al_2O_3 -MMC material at the point of incident laser beam striking during machining, hence MRR increases with increase in laser power.

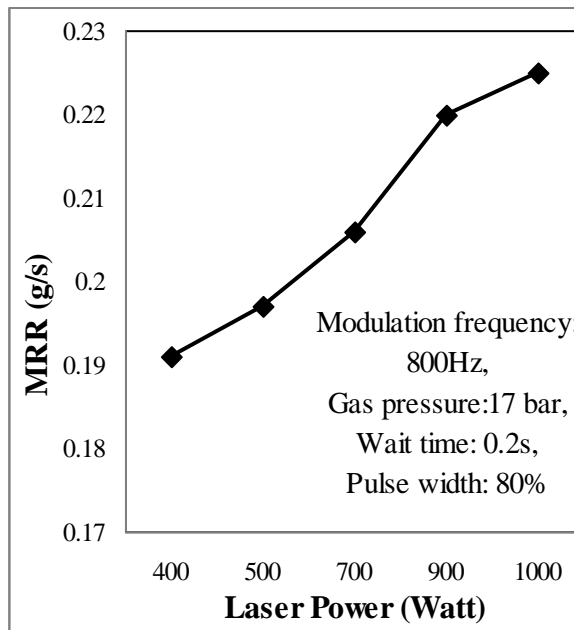


Figure 5(a). Effect of laser power on MRR Figure.

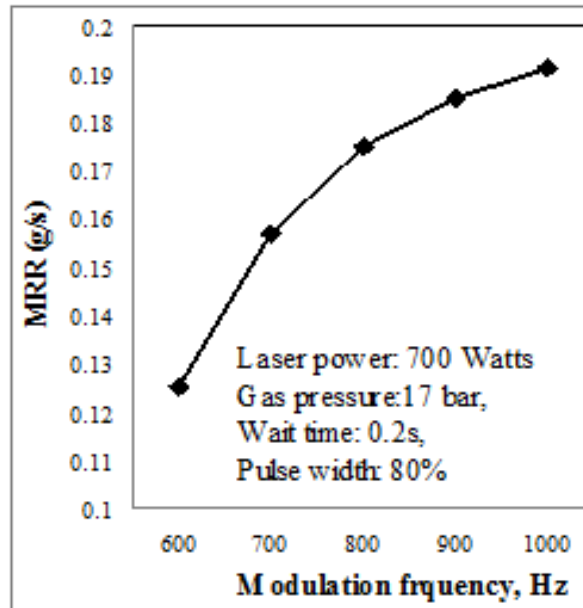


Figure 5(b). Effect of modulation frequency on MRR.

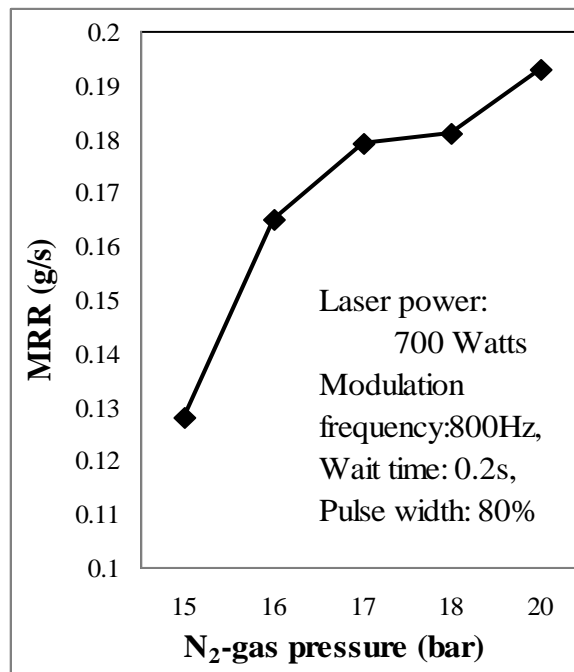


Figure 5(c). Effect of gas pressure on MRR.

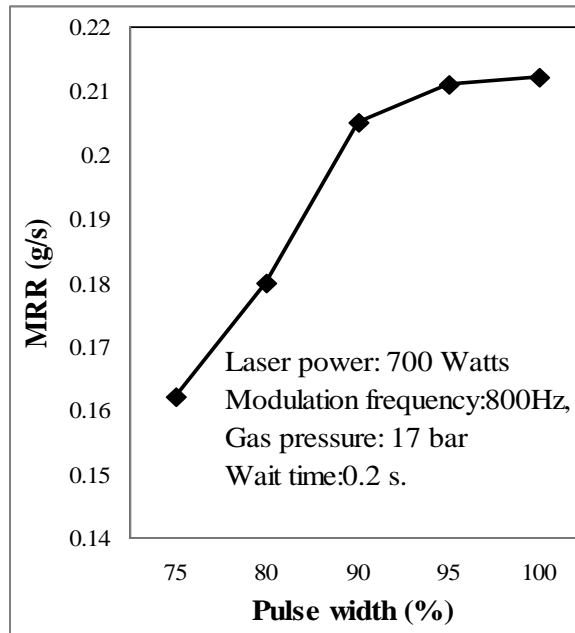


Figure 5(d). Effect of pulse width on MRR.

From Figure 5(b), it is clear that the material removal rate increases with increase in modulation frequency ranges from 600 to 1000 Hz. This may be due to lower range of supply frequency not enough to melt and vaporize as well as separate the molecules by the incident laser beam at spot during machining. Figure 5(c) shows the variation in material removal rates (g/s) with that of N_2 -gas pressure (bar) during machining of Al/5wt% Al_2O_3 -MMC. From Figure 5(c), it is clear that the N_2 -gas pressure ranges from 15 to 20 bars the material removal rate is gradually increased. It may be due to the increase of N_2 gas velocity which removes molten and metallic debris usually generated during laser drilling. Figure 5(d) shows the variation in material removal rates (g/s) with that of pulse width (%) during machining of Al/5wt% Al_2O_3 -MMC. From Figure 5(d), it is clear that the pulse width ranges between 75 to 95 % of duty cycle the material removal rate is gradually increased. It is because of high energy discharge from the laser beam which is directly stricken to the work-piece surface and material gets vaporized, hence increased material removal.

Figure 6(a), 6(b), 6(c) and Figure 6(d) show the effect of the variation in taper (rad) with that of (a) laser power (watt) (b) modulation frequency (Hz), (c) N_2 -gas pressure (bar), and (d) pulse width (% of duty cycle) during Ytterbium fiber laser machining of Al/5wt% Al_2O_3 -MMC respectively. From Figure 6(a), it is clear that the taper (rad) increases with increase in laser power ranges from 400 to 900 watts. The increase of taper may be due to setting of higher laser power which has capable to discharge enough energy to scatter and vaporize the materials at the point of micro drilling where laser beams are striking. Figure 6(b) shows the variation in taper (rad) with that of modulation frequency (Hz) during Ytterbium fiber laser machining of Al/5wt% Al_2O_3 -MMC. From Figure 6(b), it is clear that the taper increases with increase in modulation frequency ranges from 600 to 1000 Hz. This may be due to the higher removal of material at higher modulation frequency. The lower range of supply frequency

e.g., up to 500 Hz are not enough to vaporize the molecules of Al/Al₂O₃-MMC by the incident laser beam on blemish during machining.

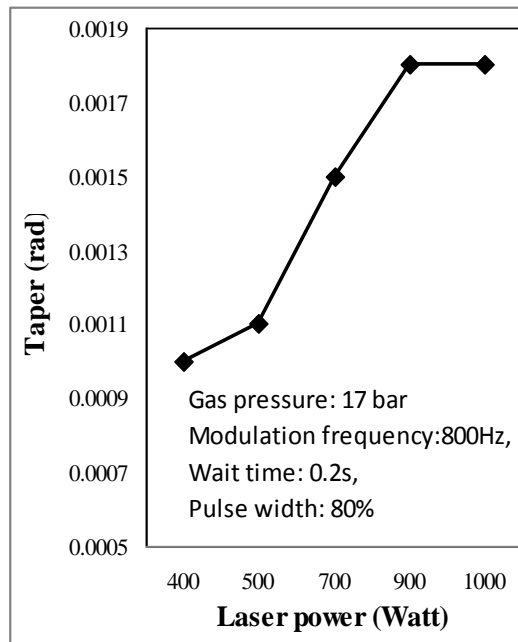


Figure 6(a). Effect of laser power on taper.

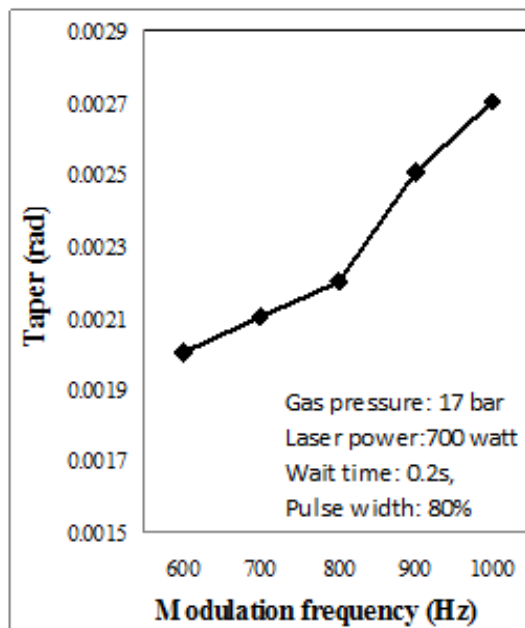


Figure 6 (b). Effect of modulation frequency on taper.

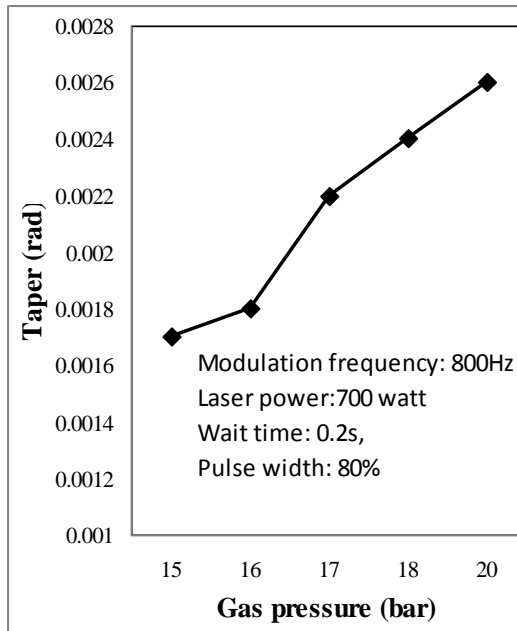


Figure 6(c). Effect of gas pressure on taper.

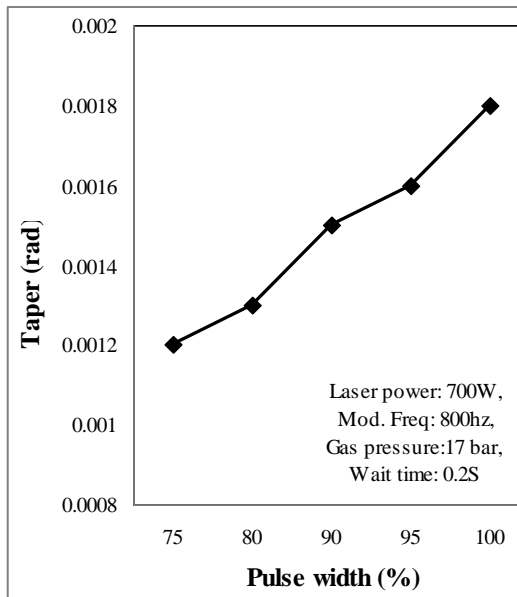


Figure 6(d). Effect of pulse width on taper.

Figure 6(c) shows the variation in taper (rad) with that of N_2 -gas pressure (bar) during machining of Al/5wt% Al_2O_3 -MMC. From Figure 6(c), it is clear that the N_2 -gas pressure ranges from 15 to 20 bars the taper (rad) is gradually increased. It may be due to high material removal by discharging of high velocity N_2 gas which removes molten and metallic debris including Al_2O_3 -reinforced particles during laser drilling. Figure 6(d) shows the variation in

taper (rad) with that of pulse width (%) during machining of Al/5wt%Al₂O₃-MMC. From Figure 6 (d), it is clear that the pulse width ranges from 75 to 100 % of duty cycle the taper (rad) is higher. It is because of high material removal rate as high energy discharge from the laser beam which is directly striking to the work-piece surface and material gets vaporized. This vaporized material is easily removed while machining operation is performed at high velocity N₂ gas with low wait time.

SEM PHOTOS OF MACHINED HOLE BY YTTERBIUM FIBER LASER

Figure 7 shows SEM photograph of a drilled hole produced by Ytterbium fiber laser on Al/5wt%Al₂O₃MMC work-piece. This micro hole is generated with parameters setting at 900 watt laser power, 700 Hz modulation frequency, 16 bar N₂ gas pressure, 0.15 s wait time and 95 % pulse width (i.e., 95 % of duty cycle). Here the shape of the hole is elliptical and debris are found along the periphery of the hole. From Figure7, it is clear that the maximum diameter of the generated hole is 971.94 μm and minimum hole diameter is 599.33 μm. There is a large difference between the maximum and minimum diameter of the generated hole. The generated hole is irregular and elliptical. The Al/Al₂O₃MMCs have heterogeneous in structure and Al₂O₃ reinforced particles has higher melting point as compared to matrix that's why at above parametric setting Al-matrix completely vaporized and removed before Al₂O₃ particles vaporized from the area of the drilled hole during Ytterbium fiber laser machining. Hence, the shape of the drilled hole is elliptical and debris is found along the drilled hole area. Thus, machining with parameters setting at 900 watt laser power, 700 Hz modulation frequency, 16 bar N₂ gas pressure, 0.15 s wait time and 95 % pulse width (i.e., 95 % of duty cycle) is not suitable for drilling of a good quality of hole by Ytterbium fiber laser machine.

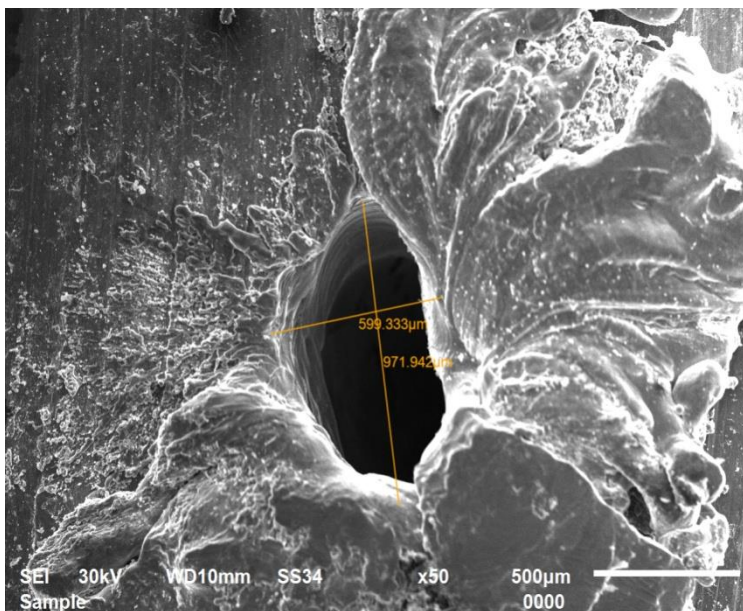


Figure7. SEM photography of a drilled hole on Al/5wt%Al₂O₃MMC work piece.

Figure 8 shows SEM photography of a drilled hole produced by Ytterbium Fiber Laser Machining on Al/10wt%Al₂O₃MMC work-piece. It is one of the experimental results of the experiments performed during preliminary experimentation with random setting and selection of parameters. This micro hole is generated with parameters setting at 500 watt laser power, 700 Hz modulation frequency, 16 bar N₂ gas pressure, 0.15 s wait time and 95 % pulse width (i.e., 95 % of duty cycle). The shape of the generated hole is elliptical and derbies are found along the periphery of the hole. From Figure 8, it is clear that the maximum diameter of the generated hole is 848 μ m and minimum hole diameter is 275 μ m. Here difference between the maximum and minimum length of the hole at the opening is high. The reason is, in this parametric condition the low laser power (i.e., 500 watt) is not sufficient to vaporized and remove the material at equal rate from the drilled hole area. Hence, the above parametric combination i.e., at 500 watt laser power, 700 Hz modulation frequency, 16 bar N₂ gas pressure, 0.15 s wait time and 95 % pulse width (i.e., 95% of duty cycle) is not recommended for generation of the good quality of drill hole by Ytterbium fiber laser machining of Al/10wt%Al₂O₃MMC.

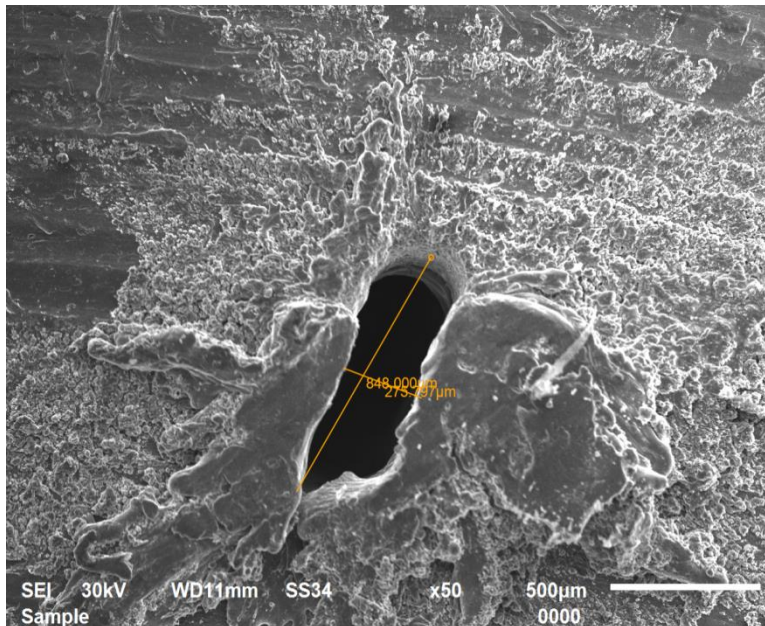


Figure 8. SEM photography of a drilled hole on Al/10wt%Al₂O₃MMC work-piece.

Figure 9 shows SEM photograph of a drilled hole produced by Ytterbium fiber laser machining of Al/15wt%Al₂O₃MMC work-piece. This SEM taken from the experiment with parameters setting at 900 watt laser power, 700 Hz modulation frequency, 16 bar N₂ gas pressure, 0.25 s wait time and 95 % pulse width (i.e., 95 % of duty cycle). The shape of the generated hole is almost round and derbies are found along the periphery as well as inside the wall of the generated hole. From Figure 9, it is clear that the difference between the maximum and minimum average diameter of the hole at the opening is very low. The vaporized material is overflow at the drilling spot it is due to supply of high laser power. From Fig 9, it is clear that the maximum diameter of the hole is 1.008 mm and minimum hole diameter is 1.003 mm. This hole is perfect round hole as only 5 μ m deviation is observed on diameter.

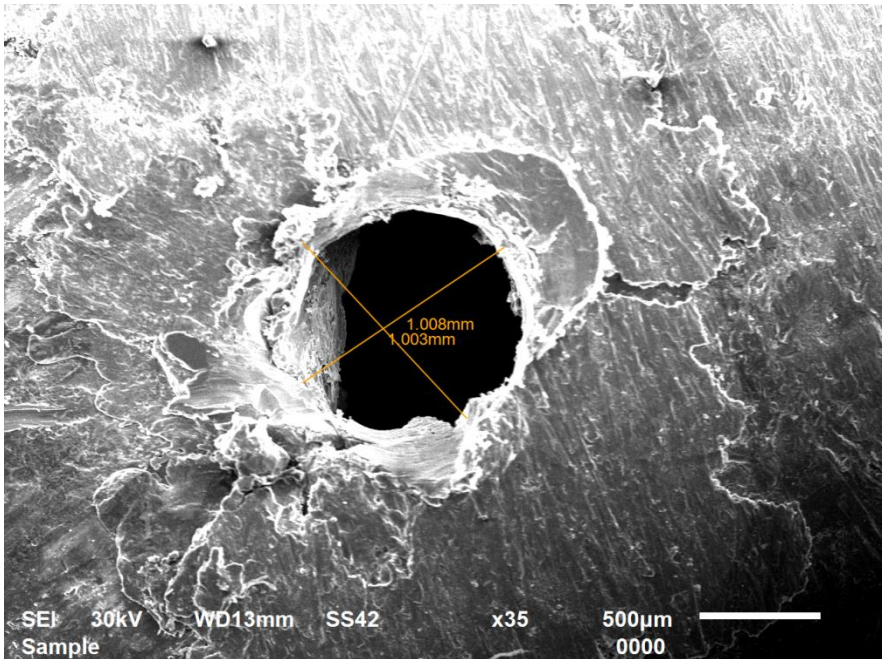


Figure 9. SEM photograph of a drilled hole on Al/15wt% Al₂O₃ MMC work-piece.

CONCLUSION

The Ytterbium fiber laser has a capability to generate the quality hole on Al/Al₂O₃-MMC. The Ytterbium fiber laser process parameter can be possibly controlled for effective drilling of Al/Al₂O₃-MMC. Based on the investigation during machining of Al-matrix and Al/Al₂O₃-MMC by Ytterbium fiber laser the following conclusions are listed below:

- a. The material removal rate increases with increase of laser power. During machining of Al-matrix, the rate of increase of material removal is observed in the incremental range of laser power from 400 to 475 Watts.
- b. The taper (rad) increases with increase in laser power specifically ranges from 400 to 900 watts. The minimum taper angle on machined hole is observed at parametric setting range from 18 to 20 bar gas (Nitrogen) pressure and 600 to 680 Hz modulation frequency.

Ytterbium fiber laser machining can be effectively used even for generation of micro dimensional hole on Al/Al₂O₃ MMC material but before that optimization of parameters and corresponding parametric setting is essential. As an evidence, a perfect round hole with only 5 µm deviation on diameter (i.e., difference between entry and exit diameter) is generated when machining operation is performed at optimal parameters setting e.g., at 900 watt laser power, 700 Hz modulation frequency, 16 bar N₂ gas pressure, 0.25 s wait time and 95 % pulse width (i.e., 95 % of duty cycle).

REFERENCES

- Biswas R., Kuar A.S., Sarkar S., and Mitra S. (2010), A parametric study of pulsed Nd:YAG laser micro-drilling of gamma-titanium aluminide, *Optics and Laser Technology*, 42, 23-31.
- Corfe, A.G. (1983), "Laser Drilling of Aero Engine Components" Proceedings, First International Conference on Laser in Manufacturing, 31-40.
- Chrystolouris, G. (1991), "Laser Machining: Theory and Practice, Mechanical Engineering Series, Springer-Verlag, New York.
- Dhupal D., Doloi B., Bhattacharyya B. (2008), Parametric analysis and optimization of Nd:YAG laser micro-grooving of aluminum titanate (Al_2TiO_5) ceramics, *International Journal of Advanced Manufacturing Technology*, 36, 883-893.
- Ghosal Arindam and Manna Alakesh (2013), "Response surface method based optimization of Ytterbium fiber laser parameter during machining of Al/Al₂O₃-MMC" *Optics & Laser Technology*, 46, 67-76.
- Ghosal Arindam, Manna Alakesh, and Lall k. Arun (2013), "Experimental investigation for optimization of Ytterbium fiber laser parameter during machining of Al/5wt% Al₂O₃-MMC" *Int. J. of Surface Engineering and Interdisciplinary Material Science*, 1(2), 22-34.
- Kacer K.; Muthe M., AKman E.; Demir A., Candan L., Canel T., Gunay V., and Sinmazcelek T.(2009), "Characterization of drilling Alumina ceramic using Nd:YAG pulsed laser", *Journal of Materials Processing Technology*, 209 (4), 2008-2014.
- Li Chen-Hao, Tsai Meng-Jong, Yang Ciann-Dong,(2007), Study of optical laser parameters for cutting QFN packages by Taguchi,s matrix method; *Optics and Laser Technology*, 39, 786-795.
- Lallemanda G.(2000), Grooving by Nd:YAG laser treatment, *Journal of Materials Processing Technology*, 99, 32-37.
- Meijer J.(2004), Laser beam machining state of the art and new opportunities, *Journal of Materials Processing Technology*, 149, 2-17.
- Miranda, R M. (2004), Structural analysis of heat affected zone of marble and lime stone tiles cut by CO₂ laser, *Materials Characterization*, 53, 411-417.
- Pascual-Cosp J., Valle A.J. Ramirezdel, Garcia-Fortea J., Sanchez-Soto P.J. (2002), Laser cutting of high vitrified ceramic materials: development of a method using a Nd:YAG laser to avoid catastrophic breakdown; *Materials Letters*; 55, 274-280.
- Rozzi Jay C., Pfeifferkorn Frank E., Incropera Frank P., Shin Yung C.(2000), Transient three dimensional heat transfer model for laser assisted machining of silicon Nitride: I. Comparison of prediction with measured surface temperature historic; *International Journal of Heat and Mass Transfer*, 41, 1409-1424,
- Samant Anoop N., and Dahotre Narendra B. (2009), An integrated computational approach to single dimensional laser machining of magnesia; *Optics and Lasers in Engineering*; 47, 570-577.
- Tiwari G., Sarin Sundar J.K., Sundarajan G., Joshi S.V. (2005), Influence of process parameters during pulsed Nd:YAG laser cutting of nickel-base superalloys, *Journal of Materials Processing Technology*, 170, 229-239.
- Tsai, Chwan Huei., and Chen Hong-Wen, (2003), Laser cutting of thick ceramic substrates by controlled technique, *Journal of Materials Processing Technology*, 136, 166-173,

- Tonshoff (1) H.K., and Kappel H. (1998), Surface modification of ceramics by laser machining; *Ann of CIRP*, 47(1), 471-474.
- Tsai, Chwan Huei, and Li Chang-Cheng (2009); Investigation of underwater laser drilling for brittle substrate, *Journal of Materials Processing Technology*, 209, 2838-2846,

Chapter 11

LASER TRANSFORMATION HARDENING OF STEEL

Karpuudaiyar Ramaraj Balasubramanian^{1*},
*Purushothaman Dinesh Babu*²
*and Gengusamynaidu Buvanashakaran*³

¹Department of Mechanical Engineering
National Institute of Technology, Tiruchirappalli, Tamilnadu, India

²School of Mechanical Engineering
SASTRA University, Thanjavur, Tamilnadu, India

³Laser Materials Processing Division,
Welding Research Institute, BHEL, Tiruchirappalli, India

ABSTRACT

Lasers have been used in several ways to transform the properties of surfaces, particularly the surfaces of metals. Most often, the intention of the processing is to harden the surface to provide a better wear resistance and fatigue life. This process is termed as transformation hardening, is applicable to certain types of steel and cast iron. Steels and cast irons are particularly good candidates for transformation hardening. Laser surface transformation hardening, commonly known as heat treating, makes use of the rapid heating and cooling rates produced on metal surfaces exposed to scanning laser beams. The process has unique advantages, particularly when used to enhance surface properties in local areas without affecting other areas of the component surface. Surface mechanical properties (hardness, abrasion, resistance, etc.) and chemical properties, (corrosion resistance, etc.) can often be greatly enhanced through the metallurgical reactions produced during these heating and cooling cycles. This chapter will describe the use of lasers and laser parameters to harden the surface of steels through rapid heating and quenching of a surface layer and the change take place in surface properties after hardening.

Keywords: Laser transformation hardening, Hardness, Microstructure, Residual stress, Wear

* Corresponding Author address: Department of Mechanical Engineering, National Institute of Technology, Tiruchirappalli - 620 015, Tamilnadu, India. Fax: +91-431-2500133. Email: krbala@nitt.edu.

INTRODUCTION

Laser transformation hardening is a metal surface treatment process, which is a complementary method to the conventional induction and flame hardening processes. Laser, a narrow beam of light, can be used to perform a variety of processes, e.g., high speed cutting, joining, surface treatment, machining of hard and brittle materials, etc. The primary physical principle in laser transformation hardening is the use of high energy laser beam to heat the metal, in order to change its microstructure for hardening the material surface. The process is at the forefront of new technological development. Laser hardening process enhances the hardness of the material and ensures better process control and quality compared to the conventional hardening processes.

The extreme hardness of the martensitic microstructure will provide improved mechanical properties such as wear resistance and strength. This will result in the wider use of laser hardening of the industrial components for improving the performance and service life. Although laser transformation hardening was one of the first methods of laser based materials processing to be industrialised, the process has not been exploited to its fullest potential.

The reasons are due to lack of knowledge concerning the process, the large number of familiar conventional surface hardening processes that are commercially available and the high instrumental cost. Faster heating and cooling rates make this process as an alternative to conventional processes. Recent developments in the laser technology, optics and software enable the process to be adopted more favourably against the competing processes.

In conventional methods of heat treatment the component is heated to the required temperature and then quenched in oil or water to achieve the desired hardness at the surface. In most industrial applications, wear occurs only in selected areas of the component; hence, it is sufficient to harden these areas to enhance the performance of the component. The advantages of using laser for surface processing results from its highly directional nature and the ability to deliver controlled amounts of energy to desired regions. The energy input is dependent on the absorptivity of the material. Only a fraction of the laser energy is absorbed by the material and the remaining portion is reflected from the surface. The absorption of a polished metal surface depends strongly on the wavelength of irradiation (Dinesh, et al. 2011).

TYPES OF INDUSTRIAL LASER FOR HARDENING

The laser light is set to be coherent, highly monochromatic, and parallel. The parallelism or low divergence makes material processing possible using laser. The parallel beam can be focused to a small spot which provides high power density.

These unique characteristics of laser make it, capable of application it in various engineering fields. The fundamental nature of the stimulated emission process was described theoretically by Einstein in 1917.

Much additional preliminary work on optical spectroscopy was done in the 1930s. By 1940 energy levels and optical materials development have taken place. In 1954, a device

called the maser (microwave amplification by stimulated emission of radiation) was developed by Charles Townes and his co-workers.

The first operating laser was the ruby laser, which was developed in 1960 by Theodore Maiman. From 1962 to 1968, much of the basic developments in lasers have taken place. Almost all types of lasers which includes semiconductor lasers, Neodymium-doped-Yttrium-Aluminum-Garnet (Nd: YAG) laser, Carbon-dioxide (CO₂) gas lasers, dye lasers and other gas lasers were invented during this era (Dutta and Manna, 2003).

During the 1980s and early 1990s, the laser was explored for surface engineering related applications such as heat treatment, cladding, and alloying, glazing and thin film deposition. The laser technology in the future will continue to grow and develop both in the capabilities of the lasers themselves and in other applications. There will be many exciting and important challenges for the laser technology in the future.

Among the available lasers, only a few are used for materials processing. Lasers are commonly classified according to the state or the physical properties of the active medium. The lasers which are used for surface hardening are (i) CO₂ laser (ii) Nd:YAG laser and (iii) Diode laser.

CO₂ Laser

CO₂ laser offers the highest average power for materials processing with average power capacity of 50 kW. But most of the systems in the industrial use are under 15 kW, with the majority under 3 kW. Excitation of CO₂ lasers results from an electric discharge maintained in a gas mixture of carbon dioxide, nitrogen, and helium. The electrical excitation can take place via alternating or direct current (DC).

The DC excitation is realized with two electrodes inside the laser gas mixture. The pumping is carried out over the vibrational excitation of nitrogen molecules, which transfers their energy to the carbon dioxide. During the transition from a higher energy level to the lower energy level, CO₂ molecules emit the radiation with a wavelength of 10.6 μm. Finally the helium atoms lead the CO₂ molecules back to their energy level. At this higher wavelength, the fibre optic cable cannot be used to transfer the laser energy as it absorbs the laser beam energy, which will melt and burn, hence a rigid lens and mirror delivery system is used in CO₂ laser.

Based on the type of gas flow the laser system is classified as axial flow and transverse flow system. In transverse flow lasers, the gas flow, electrical discharge or current flow, and resonator axis are mutually perpendicular to one another. Here the heat generated within the discharge tube can be more efficiently extracted by flowing the gas at a rate of about 60 m/s. This results in a reduced operating temperature and higher operating pressure. The output power for CO₂ laser increases with the pressure.

Transverse flow lasers have asymmetrical modes because the gain characteristics of the discharge vary across the beam; hence it is hard to pulse as it is operated at high discharge currents.

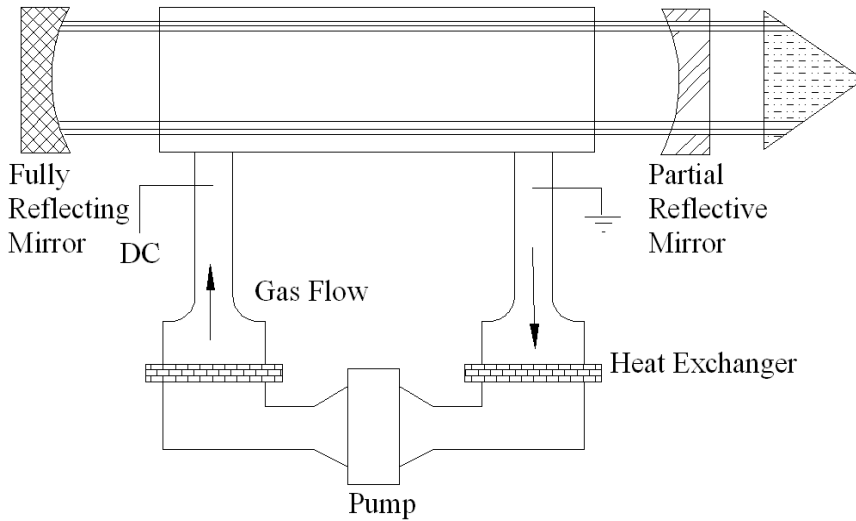


Figure 1. Fast axial flow CO₂ laser system.

Axial flow lasers are small in size, powerful and a better beam quality is achieved with gas flow parallel to the optical axis (refer Figure 1). Fast axial flow CO₂ laser are available from several hundred Watts to 30 kW. In comparison, transverse flow lasers can be made easily and enabling designs can be scaled to higher outputs. The capital cost per kW is lower and the gas usage is lower than the axial flow laser. High power transverse flow lasers are commonly used for material processing operations such as thick section welding and surface treatment.

Nd:YAG Laser

The Nd: YAG laser is one of the high power solid state lasers used for transformation hardening and other industrial applications. Its lasing action is developed by the Nd³⁺ (Neodymium) ion. It is based on a four-level system of electron energy changes within the ion. Figure 2 shows the energy levels and laser transitions.

In the laser pumping cavity, Nd:YAG crystals are excited by absorbing light from a krypton flash lamp. This causes the molecules in the crystal to excite to the E4 pump band from ground state as shown in Figure 2. The molecules radiate heat in the E3 to E2 transition zone. Nd:YAG laser operates in either pulsed or continuous wave (CW) modes. Pulsed Nd:YAG, consists of flash lamps, while CW Nd:YAG laser uses continuous arc lamps. This laser emits in the near infrared light at 1.064 μm wavelength.

Subsequently the heat has to be removed by cooling the crystal rod. A typical solid state laser usually consists of a gain medium, a pumping cavity, an optical resonator, a cooling system and a power supply, as shown in Figure 3. The light emitted by the lamp is coupled into the rod by the cavity. The optical resonator consists of two mirrors mounted separately from the lasing medium. The lamps must be water cooled to remove the heat produced by the lamps using deionized water. In material processing, the Nd:YAG laser is used for welding, drilling, cutting and surface treatment.

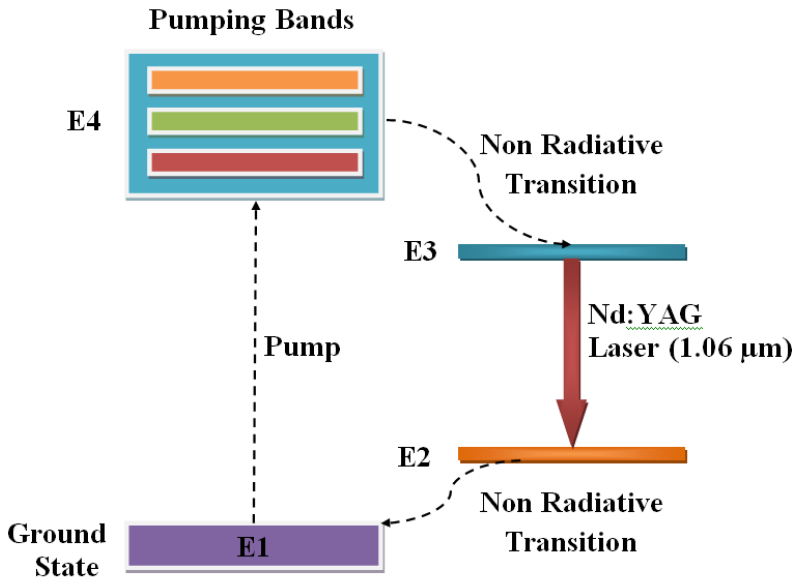


Figure 2. Energy level diagram of an Nd:YAG four level laser.

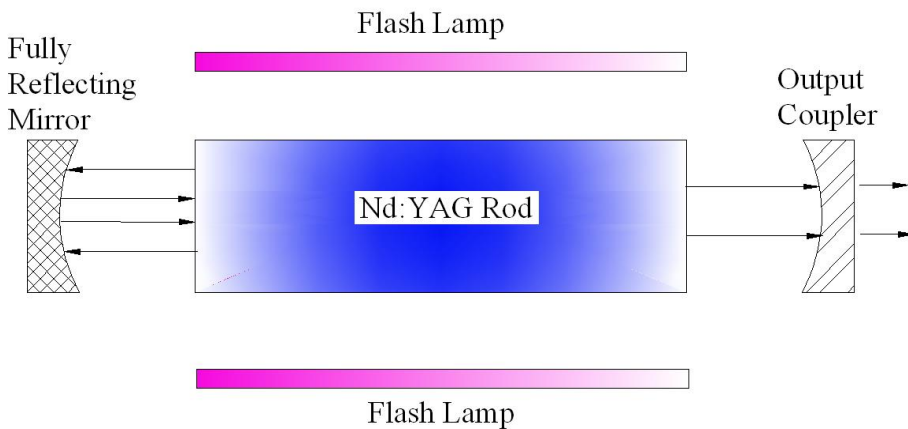


Figure 3. Basic construction of Nd:YAG laser.

One of the most important elements in solid state lasers is the pumping cavity. It provides better coupling between the pumping source and the absorbing active material. It is also responsible for the pump density distribution in the laser element which influences the uniformity, divergence and optical distortion of the output beam.

The laser material is shaped into cylindrical rods whose ends are round and polished to be plane parallel. When the rod is placed between two mirrors facing each other, which are strongly irradiated by an intense light source around it, the laser will be emitted. To minimize cooling problems, YAG rods with smaller diameter are usually used. The rod ends are usually anti-reflection coated. The lower wavelength gives better absorption by metals and allows the use of an optical fibre to carry the beam up to several meters from the source.

Diode Laser

A semiconductor laser is an edge emitting device with a Fabry–Perot optical cavity, as illustrated in Figure 4. The front and rear facets of the cavity are normally coated to act as mirrors, and the sides are roughened to reduce reflection back into the laser. The beam may also be extracted from the top surface by creating an appropriate cavity. Excitation is by electrical means, which results in direct injection of electrons into the active medium. Small (100 μm long) emitters are arranged in a bar about 1 cm in length.

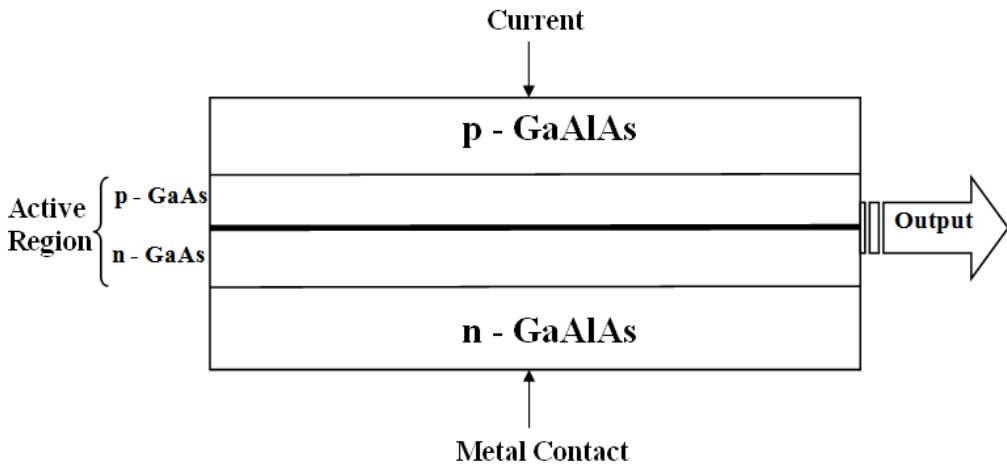


Figure 4. Layout of diode laser system.

Many tens of Watts of power can be extracted from a single bar. Laser output therefore comprises beams from a large number of individual sources, which creates a high beam divergence (because of diffraction effects) and a relatively poor beam quality in comparison with the solid state laser output. Very stable output in CW or pulsed mode can be achieved from Gallium Aluminum Arsenide (GaAlAs) diode lasers. The CW output in the range of 750-850 nm can be produced from a single unit. Multi-kilowatt power levels can be extracted from diode laser arrays.

The raw beam is suitable for surface treatment, but must be manipulated for penetration processing. A variety of cooling geometries have been designed, including backplane cooling of many laser diode bars by a single heat sink, or the use of individual heat sinks attached to each diode bar. Output may be delivered directly to the work-piece, or via a fibre optic cable. The diode lasers are characterized by their mechanical robustness, higher efficiency and compact design.

CHOICE OF SUITABLE LASER FOR HARDENING

The advantage of using laser for surface hardening results from its highly directional nature and the ability to deliver a controlled amount of energy to the desired location. The energy input is dependent on the absorptivity of the material. Only a fraction of the laser

energy is absorbed by the material and the remaining portion is reflected from the surface. The absorption on the polished metal surface depends strongly on the wavelength of irradiation. In the case of steels, the absorptivity increases when the wavelength is short.

The wave length of Nd:YAG and diode laser beam is 1.064 μm and 750 nm respectively, whereas the wavelength of CO₂ laser beam is 10.6 μm . Due to higher wavelength, CO₂ laser offers a low coupling interaction with the metallic substrates. Prior to CO₂ laser hardening, painting or coating has to be applied on the metal surface to increase the absorption rate. The used paint or coating causes pollution and hazardous effects to the environment. In contrast, Nd:YAG laser is emerging as a competitive tool in surface hardening due to the shorter wavelength and high absorbing rate of the materials and coating of base material is not needed which is advantageous as compared to CO₂ laser. The laser energy generated from Nd:YAG and diode laser can be transferred via fibre optic cable to the workplace which is not possible with CO₂ laser. Therefore Nd:YAG and diode lasers are a better choice for transformation hardening applications due to its lower wavelength..

LASER MATERIAL PROCESSING

A high power laser source provides a high energy output for heating the materials, which can be accurately controlled. The development and industrial application of lasers in materials processing such as drilling, cutting and welding have progressed rapidly. With the continuous laser of high output, surface treatment technology is rapidly growing with the identification of new and improved processing methods.

Nowadays, surface treatment is a subject of interest because it offers the chance to save the strategic materials or to allow the improved components with the idealized surface and bulk properties. The privilege of concentrating the power has enhanced the laser beam application in various production processes such as cutting, drilling, welding and soldering, as well as heat treatment of the surface layers (refer Figure 5).

Among the conventional methods, Nd:YAG, CO₂ and diode lasers are becoming more popular for the laser surface treatment of engineering materials, because of the recent development. The Nd:YAG laser is a remarkably versatile surface hardening tool with a number of advantages over conventional methods. The temperature rise at the surface is very rapid and heat is transferred into the bulk material depending on the thermal conductivity. The temperature distribution in the material is determined by its conductivity as well as by the power distribution of the beam over the surface, a consequence of the focusing technique and beam shape, and the rate at which the beam moves over the material.

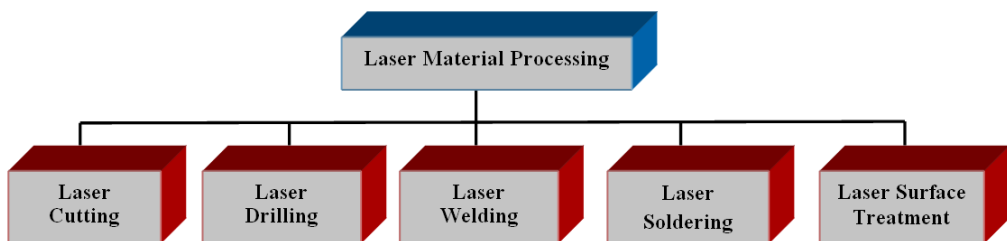


Figure 5. Laser materials processing technologies.

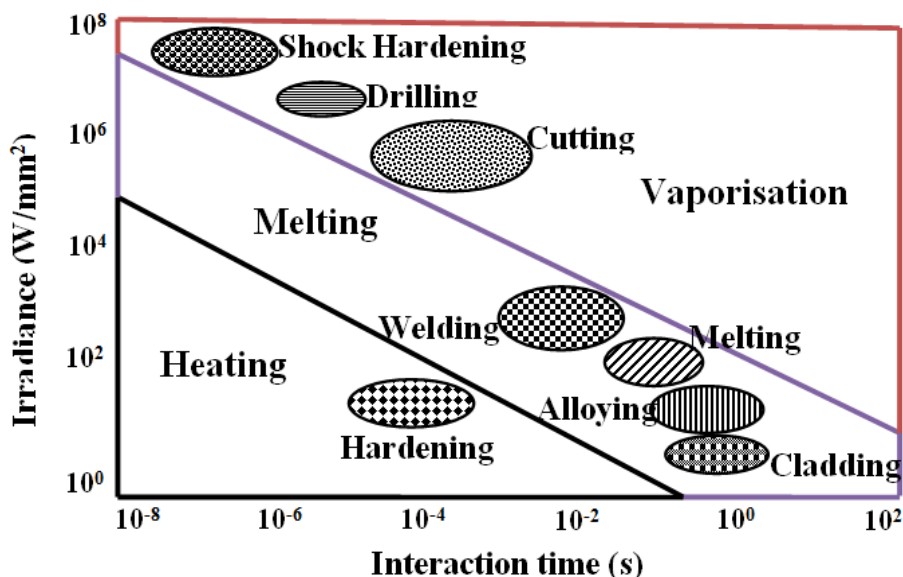


Figure 6. Operating regimes for various methods of laser material processing .

The depth and width of the hardened zone are determined by the harden-ability and the microstructure of the material for the particular temperature distribution resulting from the process parameters. The ability to achieve power densities up to 10^8 W/mm² enables high power lasers to be applied in a variety of industrial applications. In Figure 6, the beam parameters are combined to form power density and beam interaction time, so that the practical operating regimes for various types of laser processing can be defined. Based on the interaction time and irradiance, the laser can be used for heating, melting and vaporization.

LASER SURFACE TREATMENT

The basic physics of laser surface treatment is the interaction of laser energy with the surface of an absorbing material, heat generation and subsequent cooling either by heat conduction into the interior, or by thermal radiation at high temperatures from the surface of the material. It belongs to the group of short time hardening processes which are characterized by the rapid heating and cooling. Laser surface treatments can be subdivided into those which make modification via heating the surface without melting and those melting the surface of the materials. Further classification of laser surface treatments is shown in Figure 7.

Laser Surface Melting

Laser surface melting comprises a family of processes that includes alloying and particle injection, in which the material surface is melted, but not intentionally vaporized, by a scanning distributed laser beam. Surface melting, and subsequent rapid resolidification, is a

means of producing a refined or metastable microstructure in localized areas on a component, which have improved service properties such as resistance to wear, corrosion and oxidation, particularly at high temperatures (Steen, 1991).

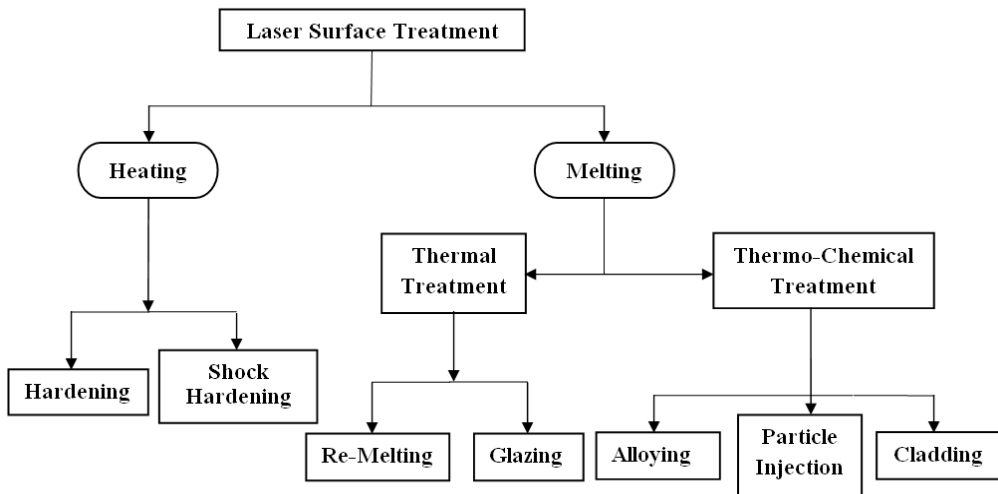


Figure 7. Classifications of laser surface treatments.

There are two reasons why laser surface melting is not widely used in industry:

- If surface melting is required then surface alloying is almost the same process and offers the possibility of vastly improved hardness, wear or corrosion resistance properties.
- The very high hardness achieved with cast irons and tool steels by laser surface melting are associated with some surface movement and hence may require some further surface finishing after treatment. This is not so easy to effect with the high hardness obtained.

Laser Surface Alloying

Surface alloying with a laser is similar to laser surface melting except that another material is injected into the melt pool. Laser surface alloying is also similar to surface cladding, in that if the cladding process is performed with excess power then surface alloying would result. It is therefore one extreme of surface cladding. The main characteristics of the surface alloying process are as follows:

The alloyed region shows a fine microstructure with nearly homogeneous mixing throughout the melt region. In homogeneities are only seen in very fast melt tracks (~ 0.5 m/s). Most materials can be alloyed into most substrates. The high quench rate ensures that segregation is minimal. Some surface alloys can only be prepared via a rapid surface quench, e.g., Fe-Cr-C-Mn. The thickness of the treated zone can be from 1-2000 μm . Very thin, very fast quenched alloy regions can be made using Q-switched Nd:YAG lasers.

Laser Cladding

The aim of most cladding operations is to overlay one metal with another to form a sound interfacial bond or weld without diluting the cladding metal with substrate material. In this situation dilution is generally considered to be contamination of the cladding which degrades its mechanical or corrosion resistant properties. Thick section cladding (> 0.25 mm) is frequently carried out by welding methods. The substantial melting of the substrate is produced and therefore dilution can be a major problem. Dilution is observed in tungsten inert gas, oxy-acetylene flame or plasma surface welding processes in which the melt pool is well stirred by electromagnetic, Marangoni and convective forces. This dilution necessitates laying down thicker clad layers to achieve the required clad property, but does have the advantage of a good interfacial bond.

The two most common methods of supplying the cladding material are

- Preplacement of cladding material powder on the substrate.
- Inert gas propulsion of material powder into a laser generated molten pool.

In both laser alloying and laser cladding another material or powder is needed to change the surface properties at that time of laser treatment it may produce smoke and pollute environment and also it is needed to control the amount of added material in order to attain the required surface properties. These difficulties can be overcome by the laser transformation hardening method, it is not required any additional material, there is no melting occurred in the surface and it is not required any post processing after treatment.

Laser Transformation Hardening

In laser transformation hardening, the laser beam energy is applied to harden the surface with the rest of the component acting as a heat sink avoiding surface melting. Laser hardening is similar to other conventional hardening processes such as flame hardening, induction hardening and electron beam hardening, but it selectively heat treats the surface of the steel to reach austenitization temperature to the required depth and then is quenched very rapidly to obtain the martensitic structure. The high energy density laser beam heats the surface much faster and reduces the time for conducting the heat into the bulk of the component. The hardening mechanism involves the formation of austenite during heating cycle and transformation to martensite structure during the cooling cycle. The laser transformation hardening process is usually applicable to harden localized area and not required to harden an entire part. The reason is that the wear or high stress is localized, hence only well defined small area needs to be hardened. Also it is advantageous to have most of the remaining component keeps its toughness and ductility.

The hardening of steel occurs by the temperature dependent transformation of the crystal structure of iron and changes in carbon solubility. In surface hardening, the heating period and the holding of the process cycle is much shorter than those of bulk hardening. This is particularly true for laser transformation hardening where heating to the austenitization

temperature occurs within seconds or even fractions of a second. Laser transformation hardening competes with many other established methods of surface treatment.

Table 1. Comparison of laser transformation hardening with competing methods of hardening

Parameter \ Type	Laser Hardening	Induction Hardening	Carburizing	Flame Hardening	Electron beam
Hardened depth (mm)	1.5	5	3	10	1
Distortion	Very low	Medium	Medium	High	Very low
Flexibility	High	Low	Medium	High	Medium
Precision	High	Medium	Medium	Low	High
Operator skill	Medium	Medium	Medium	High	Medium
Environmental impact	Low	Low	High	Medium	Low
Quenchant required	No	Mostly	Yes	Yes	No
Material flexibility	High	Medium	Low	Medium	High

Table 1 summarizes the principal features of laser hardening and its competing techniques. The advantages and drawbacks of laser hardening are summarized by comparison with the competing techniques (Ion, 2002). From the table it is observed that the electron beam hardening process has similar properties like laser beam hardening but the flexibility is low compared to laser hardening process.

The important criteria for laser transformation hardening are:

- The temperature of the zone being hardened must reach well into austenitization zone.
- Between the heating and cooling cycle, the substrate should be maintained at the austenitization temperature long enough for carbon diffusion.
- There should be enough mass ratios between the treated layer and the bulk so that the cooling rate by self quenching is such that it could satisfy the critical quenching rate requirement.
- The surface of the work-piece heated by laser beam should not reach the melting temperature.
- The phase transformation induced by laser hardening for steels take the following steps:
 - Formation of austenite from pearlite-ferrite (hypo-eutectoid steels) or pearlite-cementite (hyper-eutectoid steels) aggregate structure.
 - Martensite transformation from austenite.

Austenite Formation Mechanism

In general, the structure of steel consists of the transforming product from austenite. Depending on the parameters (rate of cooling, carbon percentage), the transformed products from austenite may be pearlite, bainite or martensite. The basic reaction taking place during

laser hardening is the phase transformation of the body centered cubic α -solid solution to face centered cubic γ -solid solution. This occurs by nucleation and growth of the new phase in the matrix of the initial phase. Before heating, microstructure of steel consists of ferrite, pearlite and carbides in widely different amounts depending upon the carbon content and alloying elements in the steel. The steels with carbon content less than 0.77 % are called hypo-eutectoid steels and those above 0.77 % C are called hyper-eutectoid steels.

During heating of steel the initial structural change begins when its temperature reaches lower critical temperature, A_{C1} (723 °C). At this temperature pearlite changes into austenite. The phase transformation occurs by nucleation of austenite phase at the interfaces between the ferrite and carbide (cementite) crystals. The rate of nucleation increases with increase in the ferrite and cementite interfacial area. As the temperature increases, more and more ferrite, cementites are dissolved in austenite and the structure becomes completely austenitic after reaching the upper critical temperature, A_{C3} . However, some undissolved carbides are still present and formation of homogeneous austenite occurs after holding the steel at this temperature. The formation of austenite is dependent upon the time and temperature of heating. The vertical line indicated in the austenization diagram shows the time required for forming austenite during laser hardening.

Martensite Formation Mechanism

After the formation of homogeneous austenite, the steel is allowed to cool. Depending upon the rate of cooling, austenite is made to transform, to different phases. Ferrite, pearlite and cementite are obtained during slow cooling, while bainite is formed in the moderate cooling and martensite is formed when the steel is cooled rapidly.

In eutectoid steels containing 0.8 % carbon, transformation of austenite to pearlite occurs when austenite reaches the lower critical temperature during slow cooling. The transformation begins with the nucleation and growth of alternate plates of cementite and ferrite at several points along the austenite grain boundaries. This forms pearlite colonies, which grow until the entire austenite grain has been consumed and has become a pearlite nodule.

When hypo-eutectoid and hyper-eutectoid steels are cooled from austenite region, precipitation of ferrite and cementite takes place between the upper and lower critical temperature. Ferrite or cementite is formed at the grain boundaries of austenite, if sufficient time is allowed for the diffusion to take place. The pro-eutectoid phase forms at the grain boundaries while the pearlite occupies the centre of the grains, thus forming a network structure. Transformation of austenite to pro-eutectoid ferrite and cementite, and eutectoid pearlite can be avoided by cooling the steel at a faster rate. When austenite is cooled at a rate greater than the critical cooling rate, it transforms instantly to a new phase called martensite. Martensitic transformation is a diffusionless $\gamma \rightarrow \alpha$ transformation which results in single phase martensite. The carbon atoms solved in the γ -austenite cannot precipitate, and remain in the transforming lattice, which results in an oversaturated solid solution. It also leads to significant deformation of the lattice. This distorts the lattice of martensite to a tetragonal lattice. The greater lattice deformation caused by the excess carbon atoms in the martensite lattice results in the high hardness of the martensitic microstructure. This lattice distortion leads to high lattice stresses, providing the theoretical background for martensitic hardening, which results in the greatest hardness of the steels. High hardness and strength are obtained

due to the formation of martensite. In laser transformation hardening the cooling rates obtained from heat conduction into the substrate is generally high enough for martensite transformation even for steels with lower carbon content.

Advantages of Laser Surface Treatment

Advantages of laser surface heat treatment can be categorized from different points of view:

- Limited energy consumption and its consequences:
- Savings in energy compared to conventional surface heat treatment as heating is restricted to only a shallow layer of a small volume, and localised only to the required area.
- Due to minimal energy input, small deformations or dimensional changes of the work-piece after heat treatment.
- No need for or minimal final machining of the parts from grinding.
- Environmental aspects:
- Hardened surface is achieved due to self-quenching of the heated surface layer through heat conduction into the cold bulk of the material which acts as the heat sink.
- Since heat treatment is done without any external agents for quenching, the procedure is a clean one.
- Flexibility and productivity of the process:
- The energy input can be adapted over a wide range by changing the laser source power, and focusing lenses having different focuses.
- Capable of switching the laser beam between various workstations by simple optical devices at atmospheric environment.
- The optical system can be adapted to the shape or complexity of the product by means of suitable shapes of lenses and mirrors.
- It is possible to heat-treat extremely small or large parts with complex shapes including small bores as well as treating inaccessible areas;
- The interaction of the beam over the work-piece surface is controlled with computer support.
- Laser heat treatment is convenient for individual or mass production of parts.
- Reproducibility and reliability of the treated surface layer with accurately controlled depth and width of the layer.
- High level of suitability for production line incorporation and automation of the procedure.

APPLICABILITY OF LASER TRANSFORMATION HARDENING

Today many automotive industries have in house lasers for hardening of different automotive components more efficiently than the use of big furnaces, quenching baths and

post cleaning processes. Significant research has been done to make lasers cost effective and enhance their applicability within the work place.

Selection of suitable material for laser hardening is important to achieve the improved surface properties.

Suitable Materials for Laser Transformation Hardening

Ferrous alloys, such as carbon–manganese steels, low alloy steels, tool steels, and martensitic stainless steels and cast irons are suitable for laser hardening.

(i) Low carbon steels:

During laser transformation hardening of low carbon steels, very rapid quenching is required to obtain martensite. A shallow case depth of up to 0.5 mm can be achieved. The maximum hardness which can be reached is dependent upon the carbon content percentage in the steel.

(ii) Medium and high carbon steels:

Medium and high carbon steels are better choices than low carbon steel because, the higher the carbon content is, the higher will be the martensitic hardness. The maximum case depth achievable is around 1.0 mm.

(iii) Alloy steels:

Alloy steels are the most desirable type of steel for laser transformation hardening. The alloying elements such as, manganese, molybdenum, nickel, boron, vanadium and chromium are aided in hardenability. These steels can be heat treated up to a case depth of 2 mm and the maximum hardness, which can be achieved, is dependent upon the carbon content.

(iv) Tool steels:

These can also be treated easily by the laser hardening process. During laser hardening, the carbon, chromium and molybdenum atoms enrich austenite grains in the structure of the steel. After laser hardening, there is a large amount of molybdenum carbides formed, that contributes to the excellent wear resistance. Laser hardened tool steels are generally used for cold working operations such as stamping and forming.

(v) Martensitic stainless steel:

Martensitic stainless steels offer excellent cavitation erosion resistance followed by austenitic and ferritic stainless steels. However, the occurrence of erosion is severe due to higher operational pressures and speeds of hydraulic systems to cope up with the increasing energy requirements. The laser surface hardening is an effective and feasible method to increase the cavitation erosion resistance. These steels are characterized by high contents of

alloying elements and laser beam process parameters have to be chosen considering their chemical, physical and optical properties, which are completely different with respect to the medium carbon steels (Mahmoudi, et al. 2011). Table 2 summarizes the hardness value of various steels after laser transformation hardening.

Table 2. Surface hardness of laser transformation hardened steels

Steel Type	Grade	Carbon Content (weight %)	Vicker's Hardness (HV)	Reference
Hypo eutectoid C-Mn steel	AISI 1045	0.45	700	(Ion and Anisdahl, 1997)
	EN8	0.36	680	(Rakesh, et al. 2005)
	C 45	0.46	700	(Bach, et al. 1990)
	C60	0.62	875	(Bach, et al. 1990)
	SM45C	0.45	700	(KIM, et al. 2009)
Low alloy steels	49MnVS3	0.47	750	(Ion, et al. 1992)
	15CrNi6	0.15	500	(Katsamas and Haidemenopoulos, 1999)
	EN25	0.31	780	(Dinesh, et al. 2013a)
Medium alloy steels	42CrMo4	0.40	664	(Ion and Anisdahl, 1997)
	AISI 4130	0.28	880	(Doong, et al. 1989)
	AISI 4340	0.40	690	(Shiue and Chen, 1992)
	AISI 5135	0.40	910	(Senthil, et al. 1999)
	X100CrMoV51	1.00	750	(Ion and Anisdahl, 1997)
	AISI5150H	0.50	800	(Patwa and Shin, 2007)
High alloy steels	X155CrVMo121	1.55	850	(Bach, et al. 1990)
	X210Cr 12	2.09	950	(Bach, et al. 1990)
Martensitic Stainless steels	AISI 440	0.61	585	(Ion, et al. 1991)
	AISI 420	0.18	490	(Mahmoudi, et al. 2010)
Tool Steel	AISI 01	0.90	780	(Jiaren, et al. 2011)
	AISI H13	0.41	500	(Lee, et al. 2009)
	DF2	0.90	770	(SeDao, et al. 2009)

(vi) Cast iron:

All cast irons with pearlitic structures can be hardened by the laser. The amount of the pearlite present in cast irons determines their response to laser hardening. The greater the amount of pearlite presence higher will be the hardenability. Typical hardness values of various cast iron grades after laser hardening are given in Table 3.

Variations in composition and thermal conductivity affect the hardness of cast irons after laser transformation hardening. A high thermal conductivity means that the surface temperature remains relatively low, and surface melting is less likely. In contrast, high carbon content lowers the melting temperature, which limits the depth of hardening that can be achieved before surface melting occurs.

Table 3. Surface hardness of transformation hardened cast iron

Cast Iron Type	Grade	Hardness (HV)	Reference
Pearlitic grey	ASTM 40	1000	(Molian, 1986)
	Grade 17 Meehanite GC	850	(Trafford, et al. 1983)
Austenitic grey	GGL 25	530	(Wiesner and Eckstein, 1987)
Pearlitic nodular	GGG 60	950	(Amende, 1985)
	GGG 40	650	(Amende, 1985)
Ferritic pearlitic (nodular)	ASTM 80-55-06	960	(Molian and Mathur, 1986)
Blackheart malleable	ASTM A47	700	(Miller and Wineman, 1977)
Alloyed	Cr-Mo Alloyed	900	(Amende, 1985)

LASER HARDENING PARAMETERS

Laser transformation hardening is a rapid and efficient process for hardening various materials such as, medium-carbon steel, low alloy steel, tool steel and die steel. Selection of process parameters such as laser power, beam diameter, beam shape, travel speed, focusing conditions and the shielding gas flow rate, environmental conditions, as well as the material properties are important to obtain the desired performance (Yan, et al. 1990).

The effect of hardening zones strongly depends on the selection of process parameters as well as the thermo-physical properties of the material (Shercliff and Ashby, 1991). The operating process parameters play a significant role in the quality of hardened zone obtained during transformation hardening.

The major input process parameters are laser power, travel speed, focal length, beam spot size and the absorptivity of the material. In this, laser power and travel speed are closely related to the geometry of the hardened zone. The important output parameters are hardness, microstructure, wear resistance and geometry of the heat-affected zone (hardened width, hardened depth and hardened area). As these process parameters are nonlinear and interrelated, the selection of suitable process parameters is important to obtain the desired output (Dinesh, et al. 2013a).

In laser transformation hardening process, the main goal is to harden the surface with minimum hardened depth and maximum hardened width (Badkar, et al. 2012). One can choose a set of parameters by conducting a number of experiments by varying one parameter at a time by trial and error method.

The results obtained may not be the optimal one, and the number of experiments will be more which will lead to more manpower, time and cost. These difficulties can be overcome, if a suitable statistical and mathematical model is formulated. To predict the optimal input parameters without consuming time, materials and labour effort, there are various methods available to obtain the desired output values through model development.

ENHANCEMENT OF SURFACE PROPERTIES BY LASER HARDENING

Improvement in the performance of work-pieces, so as to increase the safe life and efficiency of engines and mechanisms, is the main goal of laser transformation hardening. In order to accomplish this, it is not only important to improve a particular performance characteristic, but to be able to achieve reproducible results with acceptable accuracy. In accordance with this, and also for the systematic accumulation of the information that is needed to create systems to control the laser surface treatment processes, it is best to examine the performance characteristics.

The performance characteristics of the work-pieces are directly dependent upon the condition and properties of the work-piece surface layer. These properties can be directly changed by organizing the corresponding physical-chemical processes (heat, thermo-deformation, oxidation, and others), determined by four main variables - temperature, time, heating time, cooling time. The needed combination of these variables, resulting from the progress of the necessary physical-chemical process, can be received by registering and changing some of the factors connected with the laser beam, the irradiation conditions, and the treated workpiece. At the same time, there is a definite connection between the parameters of the process and the performance properties of the surface.

Hardness and its Distribution

The hardness of the surface layer of alloys, and its distribution along the surface and depth has a great influence on the performance characteristics of materials. Under the conditions of laser irradiation, it is determined by the chemical composition and original structure-phase condition of the alloy and by the parameters of the thermal cycle, i.e., the "heating-cooling" cycle.

Table 4. Hardness along depth at various travel speed for the laser power of 750 W (Purushothaman, et al. 2012)

Laser Power (W)	Travel Speed (mm/min)	Hardness (HV _{0.5}) at different depths from top surface (μm)										
		100	200	300	400	500	600	700	800	900	1000	1100
750	500	780	790	792	781	778	775	778	648	365	369	372
750	750	775	777	780	778	760	769	631	362	360	370	378
750	1000	765	768	770	775	777	609	369	370	365	367	364

Table 4 shows the effect of travel speed on hardness along the depth direction for low alloy steel (EN25). For the lower travel speed of 500 mm/min in the laser power of 750 W, the average hardness (782 HV_{0.5}) is almost uniform up to a depth of 0.7 mm and after that a small transition zone of 0.1 mm is formed with the hardness of around 648 HV_{0.5}. Below 0.8 mm depth, the base material hardness (360-380 HV_{0.5}) is maintained with the same properties and without being affected by the laser heat. It is observed that the average hardness in the

hardened zone is almost the same for the different travel speed of 500-1000 mm/min, but hardened depth is more (0.7 mm) for the lower travel speed of 500 mm/min.

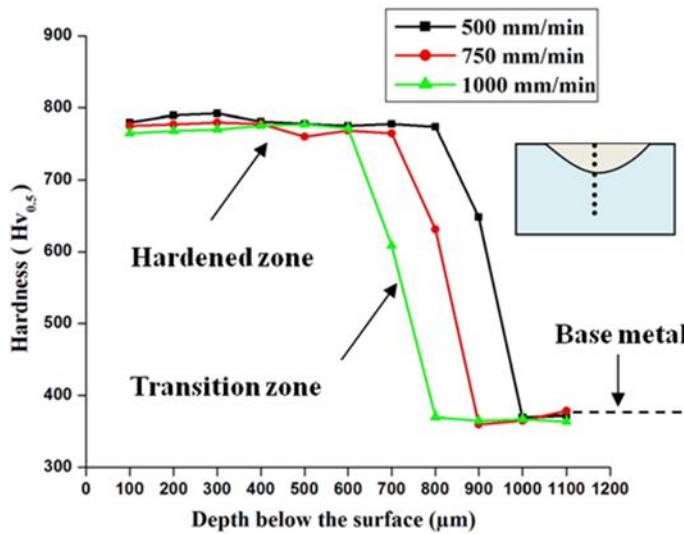


Figure 8. Effect of travel speed on hardness along depth for the laser power of 750 W (Purushothaman, et al. 2012).

Figure 8 shows the effect of travel speed on hardness profile beneath the surface for the low alloy steel (EN25) for the laser power of 750 W. It is clear that, as the travel speed increases, the average hardness in depth direction decreases. The average hardness in the hardened zone are 782, 773, 771 HV_{0.5} for the travel speed of 500, 750, 1000 mm/min respectively. The average hardness in the transition zone for 500, 750, 1000 mm/min speeds are around 648, 631, 609 HV_{0.5} respectively. Below the transition zone the base metal hardness is maintained at the same level of 360-380 HV_{0.5} without any change.

The microstructure in Figure 9 shows the indentation in the cross section region of the laser hardened sample. Figure 9 (b) clearly reveals the indentation of two different sizes observed in the microstructure, which differentiate the hardness variation in hardened zone and base metal zone.

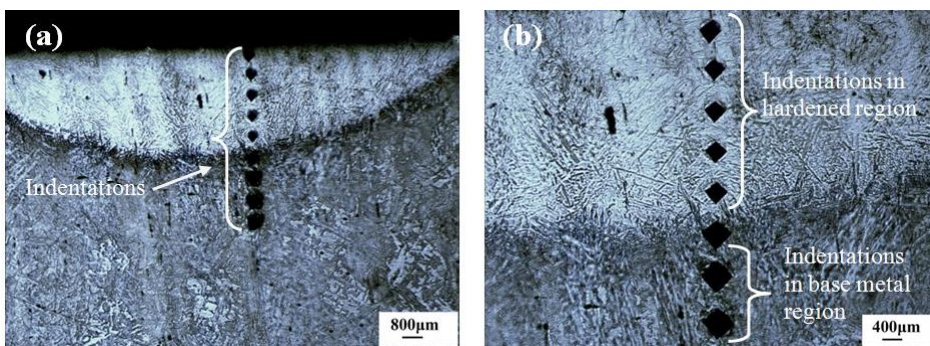


Figure 9. Microstructure of the laser hardened sample after hardness test (a) the indentations in hardened and base metal region (b) view of indentations in higher magnification.

Microstructure

The microstructures of laser hardened materials are examined using a metallurgical optical microscope with image analyser software, to study the micro-structural changes in different process parameters. The micro-structural evaluation is required to obtain a more informative and quantitative result.

Figure 10 shows the microstructure of the base metal (low alloy EN25 steel) which contains ferrite (white region), fine pearlite (dark region), and sheaves of bainite. The moderate cooling during the normalizing process allows the austenite phase to transform into bainite phase. This bainitic structure gives strength and toughness to the steel with moderate hardness. After laser hardening, different zones are occurred on the surface of the specimens. The cross-sectional micro-structural view of the three zones obtained after laser hardening is presented in Figure 11.

Top layer represents the laser hardened zone, middle layer of the thin transition zone below the laser hardened zone and the remaining bulk being the base metal where no change in structure occurs.

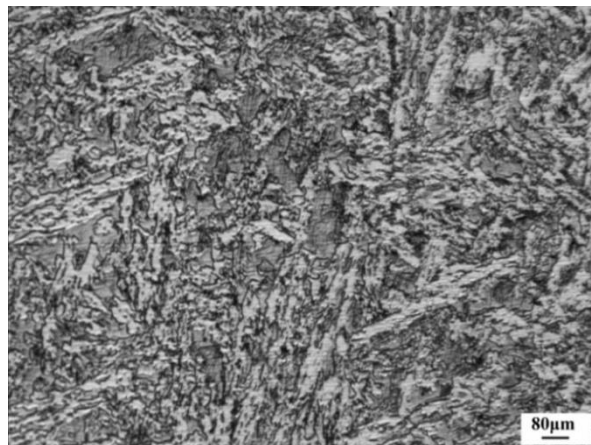


Figure 10. Microstructure of base metal (EN25 steel) (Dinesh, et al. 2013b).

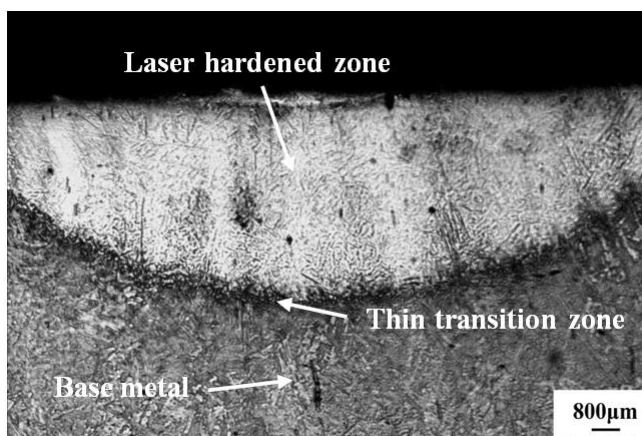


Figure 11. Microstructure of different zones after laser hardening (Dinesh, et al. 2013b).

Figure 12 evidences the lath martensite structure obtained in the laser hardened zone of low alloy steel. It can be seen from the figure that the initial bainite structure is mostly transformed to martensite, with small amount of retained austenite after the rapid cooling which occurs due to the self quenching of the laser hardening process and the resultant microstructure gives a uniform maximum hardness to the surface of the material.

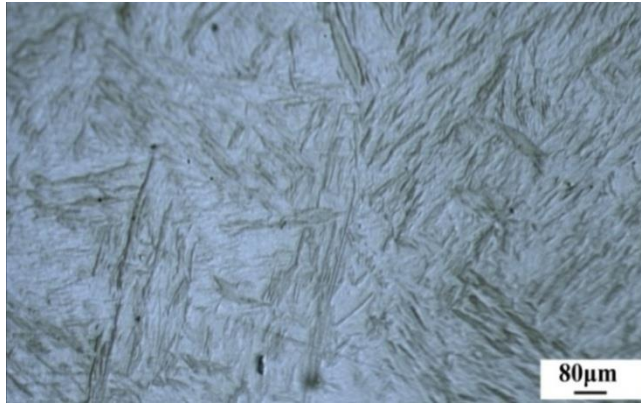


Figure 12. Microstructure of laser hardened zone (EN25 steel) (Dinesh, et al. 2013b).

Residual Stress

Residual stresses formed in the laser-treated surfaces due to rapid heating and constrained cooling and due to the clamping of the work-pieces. The nature and magnitude of these stresses on the surfaces formed during laser processing depend on the type of processing, temperature gradients, and phase-change kinetics. This in turn may or may not give rise to cracking tendency after processing depending on the level of stress, the distribution and nature of the type of stress distribution, and the mechanical strength of the phases present in the laser-treated microstructures. Residual compressive stresses are beneficial to enhance the fatigue resistance because they will help to retard the crack growth. On the other hand, residual tensile stresses are deleterious for the fatigue resistance due to the enhancement of crack propagation rates. Hence it is generally recommended that a simple post-processing step such as annealing or a pretreatment step such as preheating of the base material before laser processing be carried out to minimize the chances of cracking tendency.

Both destructive and nondestructive techniques are useful in the experimental measurement of residual stresses. The nondestructive measurement techniques include X-ray or neutron diffraction method. In general, X-ray methods involve $\sin^2\psi$ technique (ψ being the angle between the normal to the surface and the reflecting plane) and chemical etching rather than mechanical methods to avoid the problem of spurious stresses introduced into the surface (Fletcher, 1989). The thermal processes taking place in the local bulk of the workpiece during laser hardening, and also the structural phase changes connected with them, determine the stress state of the work-piece surface layers. Because the pure thermal processes (heating-cooling) determine the forming of stretched thermal structures, while structural phase transformations (martensitic) affect residual stress structures, the resulting stress state will be determined by their relationship. The size, sign, and distribution

characteristics of the residual stresses depend upon the irradiation mode and the disposition of the hardened zones of the treated surface.

From Figure 13 and 14, it is observed that phase transformation has a significant effect on the final stress state. Thermal residual stresses are essentially tensile, while stresses due to martensite and bainite transformations are compressive. During heating of the workpiece, austenite transformation is accompanied by a slight volume contraction, while during cooling, martensite or bainite is accompanied by a large volume expansion.

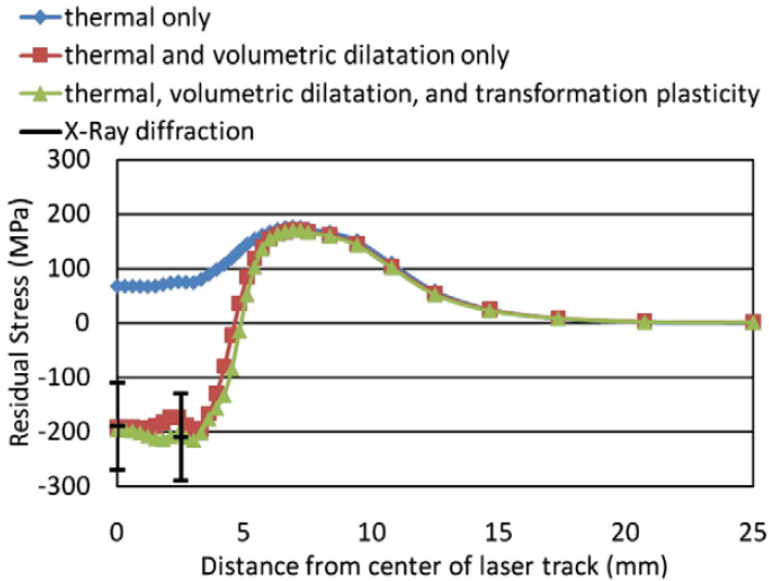


Figure 13. Residual stresses perpendicular to the laser travel along the surface of the Material (AISI 4140 steel) (Bailey, et al. 2009).

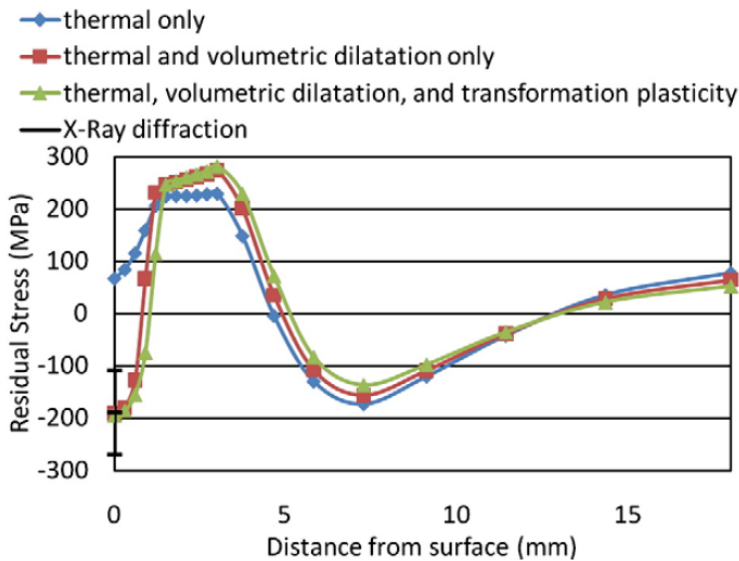


Figure 14. Residual stresses perpendicular to the laser travel into the depth of the material (AISI 4140 steel) (Bailey, et al. 2009).

Thus, depending on whether thermal strains or phase transformation strains are dominant, the residual stress field in a laser hardened track can be either predominantly tensile or compressive. Austenite-to-martensite transformation leads to a high compressive stress region of about 300 MPa in the transverse direction (perpendicular to laser travel), near the center of the laser track. Volumetric dilatation is the major contributor in phase transformation stresses. Stresses across the surface, as well as stresses into the workpiece depth, show a strong compressive stress zone, then a small tensile stress region, followed by a weak compressive stress region. Compressive stresses are favourable towards higher fatigue strength and resistance to corrosion and wear.

Wear Resistance

Wear is one of the major industrial problems, where the cost of replacing the worn out parts is highly expensive. Among all failures, the failure due to wear accounts for almost 60 % to 80 %, where the material is removed from one or both of the two solid surfaces which is in solid state contact (Rabinowicz, 1983). Wear is positively influenced by increased hardness due to higher resistance against abrasion and adhesion (Pellizzari, et al. 2005). For many metals and alloys, there is a transition temperature over which the wear rates are much lesser than the wear rates at lower temperatures due to the establishment of continuous and compact oxide layers, known as glazes that afford decreased resistance to sliding and protect from wear (Stott, et al. 1985).

Oxides will form on the surface of the metals under atmospheric conditions due to their thermo-dynamical instability. Oxidation is accelerated during sliding contact and tribo-oxides will reduce the metal-metal contact, protecting steels against wear. Depending on the temperature created at the metal contacts and alloying elements the amount of the oxidation will differ (Wei, et al. 2011). The transition occurrence from the mild oxidative wear to the cruel delamination wear can be determined by the working parameters such as load, sliding speed, temperature and test duration (Straffelini, et al. 2011).

Laser transformation hardening produces good wear resistant and hardened layer compared to conventional hardening methods. Tribological studies of laser hardened materials have been mostly focused on room temperature dry sliding wear test by varying load, sliding distance and speed. But the laser hardened steels (low alloy) are also used in many elevated temperature applications such as gear shaft, connecting rod, hot forging die and piercing tool etc.,. Therefore it is necessary to evaluating the effect of oxide layer formation in the elevated temperature sliding wear of the laser hardened steels in different process conditions.

The surface damage (removal of material) occurs when one or both of the two solid surfaces are in a sliding motion relative to one another. Wear arises by mechanical and chemical means and steps up by frictional heating. The types of wear mechanisms are adhesive and abrasive. Mostly, the wear begins with one wear mechanism and it may continue by other wear mechanism which complicates the failure. Adhesive wear occurs when two nominally flat solid bodies are in sliding contact and it occurs when the asperity contacts the interface, these contacts are sheared by sliding, which may result in detachment of a fragment from one surface and attachment to the other surface. As the sliding continues, the transferred fragments may come off from the surface and get transferred back to the

original surface. Abrasive wear occurs when asperities of a rough, hard surface slide on a softer surface and damage the interface by plastic deformation or fracture.

There are two general situations for abrasive wear. In the first case, the hard surface is the harder of the two rubbing surfaces (two body abrasion) and in the second case, the hard surface is a third body, generally a small particle of abrasive, caught between the two surfaces and it is able to abrade either one or both of the mating surfaces and is called a three body abrasion (Bharat, 2002). During sliding frictional heating increases the contact temperature, which induces oxidation on the sliding surface and this process is called oxidative wear mechanism. In steels, this type of wear usually takes place when the flash temperature is about 400 °C (Straffellini, et al. 2001).

At room temperature, when the pin material slides over the disc, metal to metal contact takes place. Due to surface interaction and due to unevenness of the surface (asperities) plastic deformation takes place due to which unwanted metal displacement occurs which is known as adhesion. On further sliding the detached metal particles which deposit on the disc (wear debris) will enhance the material removal or wear rate which is known as abrasive wear. This is due to the metal to metal contact. When the temperature increases gradually from room temperature, the wear rate will increase and a metal oxide layer will form which acts as a lubricant and reduces the friction. On further increase in temperature (< 550 °C) the oxide layer will break and will leads to more wear rate, and volume loss.

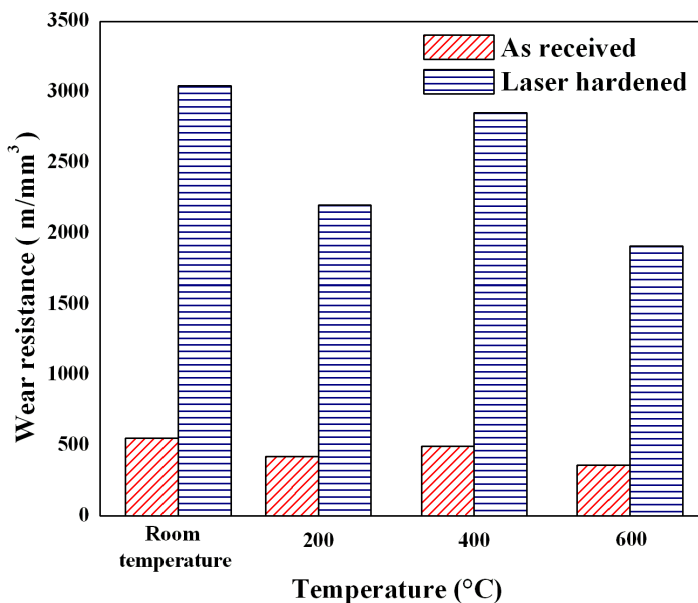


Figure 15. Wear resistance of as-received and laser hardened samples (EN25 steel) at a constant load of 40 N for 3000 m sliding distance at room and elevated temperatures (Dinesh, et al. 2013b).

The comparison of wear resistance of as-received (base material), laser hardened samples at room temperature and at different elevated temperatures are given in Figure 15. It is observed that the laser hardened samples exhibit a relatively higher wear resistance than the as-received samples in all the tested elevated temperatures. At the room temperature for the load of 40 N the wear resistance of a laser hardened sample is 3042 m/mm³ which is fivefold

more than the wear resistance of as-received steel (552 m/mm^3). At the elevated temperature of 200°C in the same case, the wear resistance (2200 m/mm^3) is reduced in the hardened sample, which is due to the increase in friction between the contact surfaces. At this lower temperature of 200°C , almost no oxide layer is formed on the surface in both as received and laser hardened samples. At a temperature of 400°C , the oxide layer on the steel surface reduces the friction and considerably improves the wear resistance of as-received sample to 493 m/mm^3 and laser hardened sample to 2854 m/mm^3 . With further increasing temperature, the protective thick oxide layer fractured under wear stress. Failure to protect the oxide layer causes severe adhesion and abrasive wear, resulting in a less wear resistance of 1910 m/mm^3 in the laser hardened sample at 600°C .

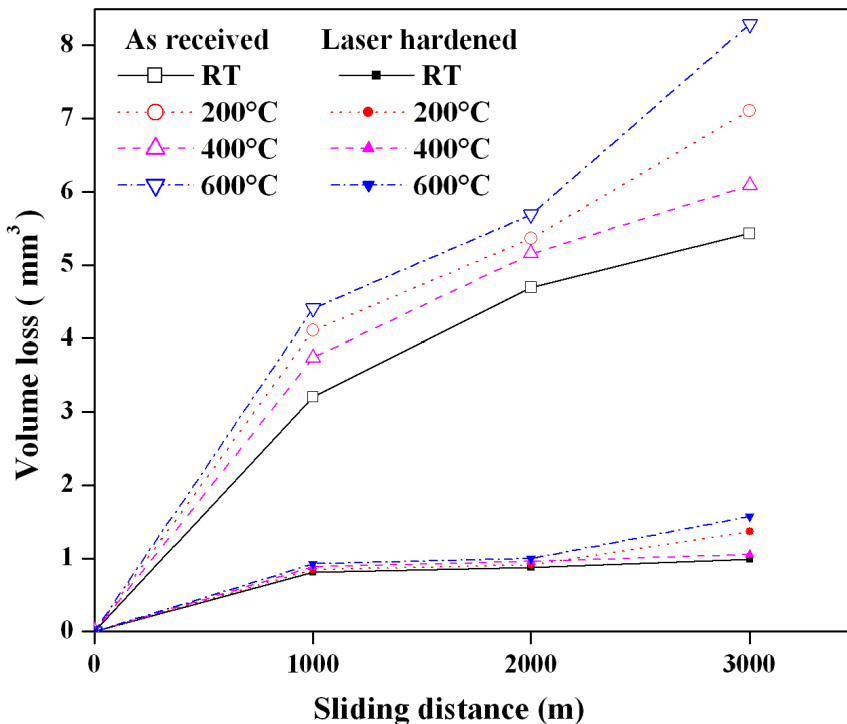


Figure 16 .Comparison of volume loss of as-received, laser hardened EN25 steel samples at a given temperature with sliding distance at a load of 40 N and a sliding speed of 0.15 m/s (Dinesh, et al. 2013b).

Figure 16 presents the volume loss of as-received and laser hardened EN25 steel at room temperature and various elevated temperatures with different sliding distances. Under a given temperature condition, the steady-state volume loss of the steel increased linearly with sliding distance for the both as-received and laser hardened samples. A drastic reduction in volume loss is observed in the laser hardened samples as compared to the as-received samples. In laser hardened samples, other than the oxide layer formation, the newly formed martensite structure with compressive residual stresses and high hardness in the surface may provide higher mechanical stability during sliding wear at elevated temperatures and it may increase the wear resistance.

SUMMARY AND CONCLUSION

Lasers have been used in a number of ways to modify the properties of surfaces, especially the surfaces of steels. Most often, the objective of the processing is to harden the surface in order to provide increased wear resistance and corrosion resistance. The most common competing technique for surface hardening of metals is heating in an induction furnace. Induction heating can produce hardened layers with thickness up to a few millimeters. For applications in which the depth of hardening does not have to be great and where the part geometry is uneven, so that induction processing is not very suitable, laser hardening provides a good alternative. Laser hardening can provide more selective hardening than induction heating, and it yields somewhat higher values of hardness because of the more rapid quenching. Laser hardening also produces a substantial increase in surface hardness at a reasonably high rate with minimum distortion of the part. However, equipment for laser hardening is more expensive, especially because it usually requires a multi-kilowatt laser. Thus, it has not replaced induction hardening except for selected applications.

Several methods are nowadays being tried for providing hardened surfaces through laser processing, which includes glazing, alloying, and cladding. These methods are all less well developed than transformation hardening, but they appear to offer promise for future exploitation. Laser transformation hardening was one of the first laser-based processes to be industrialized. However, because the technical and economic benefits of the process could not immediately be appreciated, and there were already a large number of familiar hardening processes available, its potential was not realized as quickly as many had anticipated. The principles of laser transformation hardening are similar to those of conventional autogenous hardening processes, the main distinction being that laser-induced thermal cycles are an order of magnitude shorter. Transformation temperatures are eminent on heating, and the time available for the microstructure to be homogenized (necessary for an evenly hardened surface) is limited, but cooling occurs rapidly by self-quenching. Ferrous materials with a fine microstructure and carbon content between about 0.25 and 0.5wt% are particularly suitable for laser hardening. Well-defined hardened regions are produced in materials of high hardenability, notably those designed for hardening through austenitising and quenching in air. Laser transformation hardening is particularly suitable for high volume production of small, discrete hardened regions on large parts, or those of irregular section that would distort during conventional heat treatment. Parts with widely varying shapes and sizes may be treated with a single laser beam, through software control, and parts may be hardened in their final machined condition. Analytical equations describing temperature fields and phase transformations, combined with empirical hardness formulae, provide sufficient accuracy to be used for constructing laser hardening diagrams, which aid in developing preliminary processing procedures. Laser transformation hardening should be achieved at low cost by reducing the laser power and minimum processing time by increasing the travel speed, which will maximize the production rate. The effects of process variables on the laser hardened profile parameters are important. The main advantages of laser hardening originate from the highly controllable application of low amounts of optical energy, which reduce distortion, eliminate post-treatment finishing, and provide a high degree of processing flexibility. The process can be used as a simple substitute for an existing hardening technique, but the most profitable applications are those that add significant value to a product, or enable it to be

made more quickly and cheaply through the use of new materials and component designs. The major drawbacks are the high capital cost of equipment, a continuing lack of familiarity in comparison with established hardening techniques, and the lack of quality assurance codes. These factors are being addressed through the application of more efficient laser sources, flexible optics, computer aided design and control programs, which can be integrated into turnkey systems, thus increasing the scope of potential application.

REFERENCES

- Amende, W., (1985). Hardening of materials and machine components with a high power laser. Dusseldorf, VDI Verlag, German.
- Bach, J., Damascheck, R., Geissler, E., Bergmann H. W., (1990). Laser transformation hardening of different steels. *Proceedings of 3rd European Conference on Laser Treatment of Materials*. Coburg, Sprechsaal Publishing Group, 265–282.
- Badkar, D.S., Pandey, K.S., Buvanashakaran, G., (2012). Application of the central composite design in optimization of laser transformation hardening parameters of commercially pure titanium using Nd:YAG laser. *Int. J. Adv. Manuf. Tech.* 59, 169-92.
- Bailey, N.S., Wenda Tan, Yung, C., Shin, (2009). Predictive modeling and experimental results for residual stresses in laser hardening of AISI 4140 steel by a high power diode laser. *Surf. Coat. Tech.* 203, 2003-12.
- Bharat Bhushan, (2002). Introduction to tribology. *John Wiley & sons*, New York.
- Dinesh Babu, P., Balasubramanian, K.R., Buvanashakaran, G., (2011). Laser surface hardening: a review. *Int. J. Surf. Sci. Engg.* 5(2), 131-51.
- Dinesh Babu, P., Buvanashakaran, G., Balasubramanian, K.R., (2013a). Experimental investigation of laser transformation hardening of low alloy steel using response surface methodology. *Int. J. Adv. Manuf. Tech.* 67(5-8), 1883-97.
- Dinesh Babu, P., Buvanashakaran, G., Balasubramanian, K.R., (2013b). Dry sliding wear resistance of laser hardened low alloy steel at room and elevated temperatures. The final, definitive version of this paper has been published in *Proc. Inst. Mech. Eng. Part J J. Engg. Trib.* 227 (10), 1138-49, by SAGE Publications Ltd. <http://pij.sagepub.com/content/227/10/1138>.
- Doong, J.L., Chen, T.J., Tan, Y.H., (1989). Effect of laser surface hardening on fatigue crack growth rate in AISI-4130 steel. *Eng. Fract. Mech.* 33(3), 483–491.
- Dutta Majumdar, J., Manna, I., (2003). Laser processing of materials. *Sadhana*. 28, 495-562.
- Fletcher, A.J., (1989). Thermal stress and strain generation in heat treatment. *Elsevier Applied Science Publishers*. New York, 1-203.
- Ion, J.C., (2002) Review- laser transformation hardening. *J. Surf. Engg.* 18(1), 14-31.
- Ion, J.C., Anisdahl L.M., (1997). A PC-based system for procedure development in laser transformation hardening. *J. Mater. Process. Technol.* 65, 261–7.
- Ion, J.C., Moisiso, T. J.L., Paju, M., Johansson, J., (1992). Laser transformation hardening of low alloy hypoeutectoid steel. *Mater. Sci. Technol.* 8, 799–803.
- Ion, J. C., Moisiso, T., Pedersen, T. F., Sorensen, B., Hansson, C.M., (1991). Laser surface modification of a 13.5% Cr, 0.6% C steel. *J. Mater. Sci.*, 26, 43–48.

- Jiaren Jiang, Lijue Xue, Shaodong Wang, (2011). Discrete laser spot transformation hardening of AISI O1 tool steel using pulsed Nd:YAG laser. *Surf. Coat. Tech.*, 205, 5156-64.
- Katsamas, A.I., Haidemenopoulos, G.N., (1999). Surface hardening of low alloy 15CrNi6 steel by CO₂ laser beam. *Surf. Coat. Tech.* 115, 249–55.
- Kim, J.D., Lee, M.H., Lee, S.J., Kang, W.J., (2009). Laser transformation hardening on rod-shaped carbon steel by gaussian beam. *Transac. Nonfer. Metals Soc. China.* 19, 941-5.
- Mahmoudi, B., Torkamany, M.J., Sabour Rouh Aghdam, A.R., Sabbaghzade, J., (2010). Laser surface hardening of AISI 420 stainless steel treated by pulsed Nd:YAG laser. *Mater. Des.* 31, 2553-60.
- Mahmoudi, B., Torkamany, M.J., Sabour Rouh Aghdam, A.R., Sabbaghzade, J., (2011) Effect of laser surface hardening on the hydrogen embrittlement of AISI 420: Martensitic stainless steel. *Mater. Des.* 32, 2621-27.
- Miller, J.E., Wineman, J.A., (1977). Laser hardening at Saginaw Steering Gear. *Met. Prog.* 111(5), 38–43.
- Molian, P.A., (1986). Engineering applications and analysis of *hardened* data for laserheat treated ferrous alloys. *Surf. Eng.* 2(1), 19–28.
- Molian, P.A., Mathur, A.K., (1986). Laser Heat Treatment of Cast Irons—Optimization of Process Variables. Part II. *J. Eng. Mater. Technol.* 108, 233–9.
- Pellizzari, M., Molinari, A., Straffelini, G., (2005). Tribological behaviour of hot rolling rolls. *Wear.* 259, 1281-9.
- Purushothaman Dinesh Babu, Gengusamynaidu Buvanashakaran, Karupuudaiyar Balasubramanian R., (2012). Experimental studies on the microstructure and hardness of laser transformation hardening of low alloy steel. *Transac. Canadian Soc. Mech. Engg.* 36(3), 241-57.
- Rabinowicz, (1983). *Wear of materials. Proceedings Int. Conf. Wear Mater.* Reston, Virginia, USA, 12-7.
- SeDao, Hua, M., Shao, T.M., Tam, H.Y., (2009). Surface modification of DF-2 tool steel under the scan of a YAG laser in continuously moving mode. *J. Mater. Proces. Tech.* 209, 4689–97
- Senthil Selvan, J., Subramanian, K. Nath, A.K., (1999). Effect of laser surface hardening on En18 (AISI 5135) steel. *J. Mater. Proces. Tech.* 91, 29–36.
- Shercliff, Ashby, M.F., (1991). The prediction of case depth in laser transformation hardening. *Metall. Transac. A.* 22A, 2459-66.
- Shiue, R.K., Chen, C., (1992). Laser transformation hardening of tempered 4340 steel. *Metall. Transac.* 23A, 163–70.
- Steen, W.M., (1991). *Laser material processing.* Springer-Verlag, London Limited.
- Stott, F.H., Glascott, J., Wood, G.C., (1985). The sliding wear of commercial Fe–12%Cr alloys at high temperature. *Wear.* 101, 311–24.
- Straffelini, G., Trabucco, D. Molinari, A. (2001). Oxidative wear of heat treated steels. *Wear.* 250, 485-91.
- Straffelini, G., Pellizzari, M., Maines, L., (2011). Effect of sliding speed and contact pressure on the oxidative wear of austempered ductile iron. *Wear.* 270, 714-9.
- Trafford, D.N.H., Bell, T., Megaw, J.H.P.C., Bransden, A.D., (1983). Laser treatment of grey iron, *Metals Tech.* 2, 69–77.

- Wei, M.X., Wang, S.Q., Chen, K.M., Cui, X.H., (2011). Relations between oxidative wear and Cr content of steels. *Wear*. 272, 110-121.
- Wiesner, P., Eckstein, M., (1987). Laser hardening of steel and cast iron, *Weld. Int.* 1, 986-9.
- Yang, L.J., Jana, S., Tam, S.C., (1990). Laser transformation hardening of tool steel specimens, *J. Mater. Proces. Tech.*, vol. 21, 119-30.

Chapter 12

MATERIAL JOINING PROCESS OF NON-FERROUS METALS

N. Muthukrishnan^{1} and V. Gurusamy²*

¹Department of Mechanical Engineering

Department of Marine Engineering and Convener, Welding Research Cell

²Sri Venkateswara College of Engineering, Tamil Nadu, India

ABSTRACT

Nonferrous metals are non-iron-based metals such as aluminum and aluminum alloys, copper and copper alloys, nickel and nickel alloys, titanium and titanium alloys, and magnesium and magnesium alloys. Today, nonferrous metals are used in various welding constructions for various industrial applications. However, their weld ability is fairly different from that of steel, due to specific physical and metallurgical characteristics. Therefore, the welding procedure for nonferrous metals should be systematically examined taking into account the intrinsic characteristics of the particular nonferrous metal to be welded, in order to obtain sound weldments. The main requirement for safe commercial joining processes, particularly in the light-gauge area or low melting point materials or non-ferrous metals like Magnesium, Aluminum, Nickel, titanium etc., requires welding processes with maximum process stability and adjustable, reduced heat input. The problem associated with the non-ferrous materials are low melting point, low vaporization point, distortion during welding, spatter problems etc., However, new applications in particular require a high deposition rate and precise deposition of the wire electrode. Unsurprisingly, the requirement for minimal spatter has now become a demand for virtually no spatter. Arc welding now meets these requirements, even in the lower power end, to an extent that has never been seen before. There is a requirement of new approach, which incorporates welding current polarity changing and reversal of the wire movement into process control, that must offers a greater degree of freedom, with the result that these demands can be met in full. This chapter focuses on the welding of aluminum, aluminum alloys, copper, copper alloys, nickel, magnesium and magnesium alloys, nickel alloys that are used more extensively for industrial applications.

* Corresponding author : E-mail Address: mk@svce.ac.in.

Keywords: Non-ferrous alloys, Metal Inert Gas Welding, Gas Tungsten Arc welding, Weldability and filler wire

1. INTRODUCTION

Recently, the literature regarding welding process of non-ferrous alloys has increased rapidly, mainly focusing on arc welding, laser beam welding, electron beam welding, diffusion welding and friction stir welding. However, since the vaporization point of non-ferrous alloys are low, there is always some sag on the top surface of weld bead and loss of alloying agents in the fusion zone. Gas tungsten arc filler welding of AZ31B is studied, and it is a remedy for the lost agents.¹⁰ Metal inert gas (MIG) welding not only has a better gap bridging ability but can also make up for the lost alloying agents. Metal inert gas welding is simpler to operate and full of efficiency compared with other methods. Except those advantages, MIG welding is fit for welding thick plates compared with tungsten inert gas welding and gas tungsten arc filler welding. Owing to low melting point (650uC) and low vaporisation point (1100uC), difficulties (particularly spattering) frequently arise during MIG welding. A crucial factor in MIG welding is the energy input into the filler wire. This energy input must be regulated in such a way that the wire must melt completely but not vaporise. Thus, it is hard to realise a stable MIG welding of magnesium alloys. Only a few reports on MIG welding of magnesium alloys can be found in literature. Wohlfahrt and Rethmeier in Germany got the weld beads of magnesium alloys using a triggered short arc in 2003. The strength of AZ31 weld beads is 81–93% that of the base metal. The fatigue strength is 50–75% of the base metal.^{11–13} Ueyama and Nakata in Japan also got the weld beads of the magnesium alloys using pulsed MIG welding in 2004. The tensile strength of the welds is about 91% that of the base metal.¹⁴ However, spattering and welding stability are still the important problems to MIG welding of magnesium alloy. In this article, pulsed MIG welding of AZ31B are studied in detail. Continuous butt joints with different filler wires (AZ31 and AZ61) are obtained by improving the welding process. The effects of parameters on weld formation and the drop transition of pulsed MIG welding are studied. The microstructure and mechanical properties of welding joints are investigated comprehensively.

Nowadays, aluminum and aluminum alloys are extensively used for various applications such as household utensils, autos, railroad cars, buildings, bridges, aircrafts, spacecrafts, ships, chemical equipment, water gates, and storage tanks, because of the inherent advantages of high strength-to-weight ratio, high notch toughness at cryogenic temperatures, excellent corrosion resistance, ease in extrusion, and good fabricability. Aluminum and its alloys are readily joined with most of the known joining processes including welding, brazing, soldering, adhesive bonding, and mechanical fastening. Of these joining processes, welding is most widely used. The welding processes used for aluminum and its alloy assemblies are arc welding, stud welding, electron beam welding, laser beam welding, resistance welding, solid-state welding, and oxyfuel gas welding. Of these welding processes, arc welding is most extensively used. The arc welding processes used commonly in the assemblies are gas tungsten arc welding (GTAW) and gas metal arc welding (GMAW). Basically, aluminum and its alloys can successfully be arc welded by using conventional GTAW/GMAW equipment and techniques used for other metals, provided the welding procedure is suitable. However,

occasionally specialized equipment or techniques, or both, are required due to the inherent unique physical and mechanical characteristics of aluminum and its alloys. This section focuses on GTAW and GMAW of aluminum and its alloys and discusses diverse types of such metals and their weldability, suitable welding Equipment, proper filler metals and welding procedures, and provides tips for sound welds.

2. WELDING OF ALUMINUM AND ALUMINUM ALLOYS

2.1. Weldability of Aluminum and Aluminum Alloys

Aluminum and its alloys can readily be arc welded except specific types of aluminum alloys; however, their inherent physical and metallurgical characteristics should sufficiently be understood in order to implement successful arc welding.

Following are typical characteristics of aluminum and its alloys that can be drawbacks in arc welding.

2.1.1. Higher Specific Heat, Latent Heat of Fusion and Thermal Conductivity

Aluminum and its alloys feature lower melting point but higher specific heat, latent heat of fusion and thermal conductivity compared with steel; therefore, a larger amount of heat is needed in a short time to fuse aluminum and its alloys relative to steel.

2.1.2. Stronger Oxide Film

Aluminum and its alloys produce strong oxide films on their surfaces when heated at high temperatures and fused, unless the surface is shielded sufficiently with an inert gas. The oxide film prevents fusion between the base metal and the filler metal.

2.1.3. Larger Distortion

Welding aluminum and its alloys causes much more distortion compared with welding steel because the expansion coefficient of aluminum and its alloys is larger than that of steel.

2.1.4. More Sensitive to Hot Cracking

Hot cracking is the most noticeable type of cracking in welding aluminum and its alloys, which may occur in the welds at temperatures close to the solidus of the base metal and filler metal during the weld cooling cycle, if the welding procedure (including type of base metal, type of filler metal and welding parameters) is inappropriate.

Hot cracking in the welds is caused mainly by the segregation of alloying elements and low-melting-point constituents at the grain boundaries. In general, pure aluminum offers the lowest crack susceptibility among aluminum and its alloys. In contrast, Cu-bearing aluminum alloys exhibit higher crack susceptibility.

For instance, aluminum alloys with high copper content, such as alloy 2024 (Al-4.5%Cu-1.5%Mg), also known as super duralumine, and 7075 (Al-1.6%Cu-2.5%Mg-5.5%Zn), also known as extra super duralumine, are not acceptable for arc welding. The amounts of other alloying elements such as Mg, Zn and Si affect crack sensitivity.

2.1.5. More Likely to Cause Porosity

The arc welding of aluminum and its alloys is more likely to cause porosity in weld metals, relative to welding other metals. It is reported that the main cause of porosity is hydrogen in the weld metal.

2.2 Filler Metal Selection

Varieties of filler metals are available for GTAW and GMAW. The filler metals are selected by the following factors.

- Al: 99.70% min for 1070; Al: 99.00 min for 1100; Al: 99.00 min for 1200.

The rough center of the JIS-specified range of each main alloying element. The remainders are other minor alloying elements and balancing Al.

- In the as-welded condition

In selecting an appropriate filler metal, crack susceptibility, joint tensile strength, ductility, corrosion resistibility and weld metal-to-base metal color matching after anodic oxidation treatment should be taken into account. A guide to the selection of filler metals for general purpose welding of various aluminum and aluminum alloy combinations, including castings, is presented in Table 2.3. Among these various filler metals, alloys 4043 and 5356 are major filler metals. The following paragraphs discuss key notes for better selection of the filler metal. (1) Alloy 4043 offers excellent resistibility against hot cracking, which is suitable for 6XXX series and aluminum alloy castings. However, it has such drawbacks that the weld metal exhibits low ductility and toughness, and due to a high Si content, poor color matching to 5XXX and 6XXX series base metal after anodic oxidation treatment. In addition, it is not suitable for welding high magnesium (3% or more Mg) 5XXX series alloys because intermetallic compound of Mg₂Si developed excessively in the weld metal decreases the ductility and increases the crack sensitivity of the weld metal.

(2) Alloy 5356 is widely used for 5XXX series alloys (e.g., 5083) and 6XXX series alloys (e.g., 6061), and the consumption of this filler metal reaches 60% of the total consumption of aluminum and aluminum alloy filler metals. This filler metal contains a small amount of Ti to provide a fine microstructure and thereby improve mechanical properties of the weld metal. Where a good color match after anodic oxidation treatment is needed (e.g., ornamental or architectural applications) in welding 5XXX and 6XXX series alloys, alloy 5356 filler metal is a good choice.

3. WELDING PROCESSES AND PROCEDURES

Gas tungsten arc welding (GTAW) and gas metal arc welding (GMAW) are most widely used for welding aluminum and its alloys. The individual principles of the GTAW and GMAW processes for welding aluminum and its alloys are similar respectively to those for

welding other metals. However, aluminum and its alloys use specific welding procedures different from those used in welding ordinary steels to create sound welds. This section discusses essential techniques needed specifically for welding aluminum and its alloys, excluding the principles and techniques of GTAW and GMAW common to all kinds of metals.

4. COPPER AND COPPER ALLOYS

4.1. Introduction

Copper and copper alloys possess distinctive electrical and thermal conductivity, corrosion resistance, metal-to-metal wear resistance, and aesthetic appearance. Copper offers high electrical and thermal conductivity; therefore, it is widely used for electrical conductors and other electrical equipment. Copper exhibits excellent corrosion resistance against atmosphere, seawater, chemicals, and foods. This is why copper is also used for various applications such as water supply tubes and tanks, chemical containers, brewing equipment, food-processing equipment, and components of ships. Copper alloys possess the electrical and thermal conductivity inferior to copper and their corrosion resistance varies depending on their chemical compositions. However, they offer higher strength over copper and therefore they are used for structural components such as water tubing, valves, fittings, heat exchangers, chemical equipment, and bearings.

Copper and its alloys can be joined by welding, brazing, and soldering. The welding processes used for joining copper materials are arc welding, oxyfuel gas welding, laser welding, electron beam welding, ultrasonic welding, resistance welding, flash welding, friction welding, and pressure welding. Among arc welding processes, gas tungsten arc welding (GTAW) and gas metal arc welding (GMAW) are most extensively used due to better performances, although shielded metal arc welding (SMAW) can be used for many non-critical applications.

4.2. Filler Metals and Welding Procedures

Copper and its alloys listed in the aforementioned tables are arc weldable at good or fair degree; however, the inherent physical and metallurgical characteristics of such metals and suitable filler metals should be sufficiently understood in order to obtain successful welding results.

4.2.1. Types and Characteristics of Filler Metals

Covered electrodes, bare electrode wires and rods are available for welding copper and its alloys to themselves and to other metals. These filler metals are included in JIS Z 3231, Copper and Copper Alloy Covered Electrodes; JIS Z 3341, Copper and Copper Alloy Rods and Wires for Inert Gas Shielded Arc Welding; AWS A5.6, Copper and Copper-Alloy Electrodes for Shielded Metal Arc Welding, and AWS A5.7, Copper and Copper Alloy Bare Welding Rods and Electrodes. Table 2.1 shows nominal chemical compositions of and

mechanical property requirements for covered electrodes for SMAW, as per AWS A5.6. Table 2.2 shows nominal chemical compositions of bare electrode wires and rods for GMAW and GTAW, in accordance with AWS A5.7.

4.3. Weldability and Welding Procedures

Most copper and copper alloys are arc weldable but at a lower degree than in steel. The difficulties in arc welding copper and its alloys can be attributed to the following reasons. First, high thermal conductivity tends to cause insufficient fusion. Second, high thermal expansion is apt to cause distortion and cracking. Third, low melting point can cause slag inclusions in SMAW because the melting temperature of the slag can be higher than that of the weld metal. Forth, the coarse crystal grains of weld metal degrade the mechanical properties. Fifth, added elements such as Pb, Sn, Bi, and P can cause cracking and embrittlement, and Zn vapors can cause insufficient fusion. Copper features extremely high heat conductivity (eight times that of steel); therefore, the heat of arc can rapidly be spread from the weld through the base metal. Consequently, sufficient penetration can hardly be obtained and, in turn, insufficient fusion can occur.

The arc welding of strictly-restrained thick work of oxygen-free copper and deoxidized copper tends to cause hot cracking. Blowholes can also occur in copper weld metals, caused by hydrogen dissolved during welding. Electrolytic tough pitch copper that contains a high amount of oxygen has inferior weldability than low-oxygen copper metals because it is more likely to cause hot cracking and blowholes than low-oxygen coppers. GTAW, GMAW and SMAW can be applied by using the matching filler metals of ERCu and ECu, respectively. Copper alloy type filler metals such as ERCuSi-A, ERCuSn-A, ECuSi, ECuSn-A and ECuSn-C are also used where good electrical or thermal conductivity is not a major requirement. Such copper alloy filler metals, unlike the copper type, possess lower heat conductivity and therefore better fusion can be obtained with a lower preheating temperature. However, the electrical resistivity of the silicon- and phosphor-bronze weld metals is higher than that of the copper base metal. GTAW and GMAW can establish higher heat concentration over SMAW, thereby obtaining better fusion and penetration. In GTAW and GMAW, argon gas is generally used for shielding. The use of helium gas can decrease the minimum preheating temperature. In general, GTAW is suitable for thin metals up to 6 mm, while GMAW is used for thicker metals over 6 mm. The high thermal conductivity of copper requires preheating to achieve complete fusion and adequate joint penetration. Preheat requirements depend on material thickness, the welding process, and the shielding gas.

4.3.1. Copper-Zinc Alloys (Brass)

Since zinc vaporizes from molten brass, zinc fuming is the major problem when welding brasses and is worse for the high-zinc brasses. The zinc vaporization degrades workability and weldability, causing incomplete fusion and blowholes. From these reasons, low zinc brasses have good weldability, and high-zinc brasses only fair weldability. Recommended welding processes are GTAW and GMAW due to better performance over SMAW. To minimize zinc fuming, GTAW is better than GMAW due to shallower penetration. A compositionally matching filler metal is not available because of the poor workability resulted from the zinc vaporization. Phosphorous bronze filler metals, ERCuSn-A, ECuSn-A and

ECuSn-C, provide a good color match with some brasses. Silicon bronze filler metals, ERCuSi-A and ECuSi, feature lower thermal conductivity and thus can use lower preheating temperatures, and have better fluidity. Aluminum bronze filler metals, ERCuAl-A2 and ECuAl-A2, provide good joint strength for high-zinc brasses. In GTAW and GMAW, argon shielding is normally used. The weldability of brasses with SMAW is not as good as with GTAW and GMAW, and relatively large groove angles are needed for good joint penetration and avoidance of slag entrapment. Proper preheating temperature depends on the welding process, plate thickness, and the zinc content of the base metal (the preheat temperature can be lowered for the high-zinc brasses), which range from approximately 100 to 350°C. The arc should be directed on the molten weld pool to minimize penetration and thus zinc fuming.

4.3.2. Copper-Aluminium Alloys (Aluminium bronze)

Single-phase (alpha phase) aluminum bronzes containing 7 percent or lower aluminum are hot-short and, therefore, weldments in these alloys may crack in the HAZ. Two-phase (alpha-beta phase) copper-aluminum alloys containing more than 8 percent aluminum are better weldable because of fine crystal grains of lower crack susceptibility. In welding copper-aluminum alloys, aluminum oxides (Al₂O₃) tend to cover the joint surfaces and molten weld metal, thereby causing insufficient fusion and slag inclusions. GMAW with DC-EP that provides oxide-cleaning action is best suited for welding aluminum bronzes, in which argon shielding is used in most applications.

In GTAW, AC current with argon shielding is usually used due to possible oxide-cleaning action. In SMAW, use of a short arc length and stringer beads are recommended, and each bead must be thoroughly cleaned of slag before the next bead is applied to prevent slag inclusions.

SMAW, however, should only be used where GMAW or GTAW is inconvenient. Filler metals suitable for aluminium bronzes are ERCuAl-A1, ERCuAl-A2, ERCuAl-A3, ECuAl-A2, and ECuAl-B for GMAW, GTAW and SMAW, respectively. Preheat and interpass temperature depends on the thickness of the work and the welding process, which ranges from 100-250°C. Where the thickness of the work is less than 20 mm, preheat may be unnecessary.

4.4. Dissimilar Metal Combinations

Copper and copper alloy welding joints often consist of dissimilar metals in various constructions such as oil refinery, chemical synthetic and power generation equipment from the standpoint of design requirements including strength, corrosion resistance, and material cost.

Dissimilar metal welding is involved in overlaying of copper or copper alloy weld metals on carbon steel substrates, joining copper or copper alloy and either carbon steel, stainless steel, or nickel-based alloy, and joining clad steels. In such dissimilar metal welding, specific considerations in terms of metallurgy are necessary to get successful results for specific dissimilar metal combinations. The following paragraphs discuss such metallurgy considerations for three categories of base metals to be welded with copper or copper alloys: carbon steel, stainless steel and nickel-based alloy, and clad steel.

- Carbon steel

The melting point of copper and copper alloys ranges from approximately 900 to 1200°C depending on the type of copper and copper alloy, while that of carbon steel is approximately 1500°C. Such a considerable difference in melting point can cause very little penetration in the carbon steel base metal when welding with a copper alloy filler metal.

- Stainless steel and nickel-based alloy

In addition to the problems of insufficient fusion and copper infiltration like the case of carbon steel, the copper or copper alloy weld metal increases chromium content due to the dilution from the base metal of stainless steel or nickel-based alloy (e.g., Inconel containing nominally 76%Ni, 16%Cr, and 8%Fe), thereby increasing its susceptibility to cracking. To overcome this problem, buttering the base metal with a nickel (ENi-1, ERNi-1) or nickel-based alloy filler metal (ENiCu-7, ERNiCu-7) is generally used prior to the filling pass welding with a copper or copper alloy filler metal.

- Clad steel

A variety of carbon or low-alloy steel forms can be clad with copper or copper alloy to protect them in harsh environments, usually to provide better corrosion or erosion resistance. Copper or copper alloy clad steels are produced mainly by explosion cladding and roll cladding [Ref. 7]. Because of the benefits of good electric conductivity and corrosion resistance, copper clad (deoxidized copper, and oxygen-free copper) steels are used for electric field linear accelerators, alcohol production tanks, and food processing equipment. Copper alloy clad (90/10 cupronickel, 70/30 cupronickel, aluminum bronze, and naval brass) steels are used for end plates of seawater heat exchangers, equipment for seawater desalination plants, and chemical synthetic equipment, due to excellent resistance to seawater corrosion and erosion.

5. NICKEL AND NICKEL ALLOYS

5.1. Introduction

Nickel and nickel alloys possess superior corrosion resistance and excellent low and high-temperature mechanical properties, the applications of which can be seen in various chemical process equipment and high-temperature service machinery that are operated in severe environments where stainless steels may be damaged. Uses of commercial purity nickel are relatively limited; however, an enormous range of nickel alloys is available. The typical applications of nickel alloys include various components of gas turbines, jet aircraft engines, organic and inorganic chemical equipment, oil refineries, ethylene plants, hydrogen production plants, and hydrogen chlorides removal equipment for coal and oil-fired power plants. Nickel and its alloys can be joined by welding, brazing, and soldering. The welding processes used generally for joining nickel and its alloys are arc welding, electron beam

welding, and resistance welding. Among arc welding processes, the gas tungsten arc welding (GTAW) process is most extensively used due to better performances, although shielded metal arc welding (SMAW), gas metal arc welding (GMAW) and submerged arc welding (SAW) are also used for many non-critical applications.

5.2. Types and Characteristics of Nickel and Nickel Alloys

Nickel and nickel alloys (specific superalloys that contain Ni as one of the main elements are also included) offer excellent ductility, formability, resistance to oxidation and corrosion, and high temperature strength, which find applications in various chemical equipment and high temperature service machinery. High purity nickels are more resistant to chemicals such as caustic soda, while nickel-based alloys are superior in tensile strength and corrosion resistance in the high temperature and severe corrosive environments where stainless steels cannot withstand. Nickel and its alloys are available in various forms such as plates, sheets, strips, pipes, tubes, bars, and castings. This section discusses characteristics of various types of nickel and its alloys that are weldable at good or fair degrees.

5.3. Filler Metals and Welding Procedures

Solid-solution nickel and nickel alloys used for welding constructions have comparatively good weldability, and most of the alloys use gas tungsten arc welding (GTAW), shielded metal arc welding (SMAW), and gas metal arc welding (GMAW) with solid or flux-cored wires. However, some alloys use only GTAW to prevent hot cracking. To obtain successful welding results, choice of filler metal and control of welding procedure are essential.

5.3.1. Weldability and Welding Procedures

Nickel and nickel alloys can be arc welded commonly by SMAW, GTAW and GMAW with suitable filler metals, though some alloys use only GTAW to overcome a lesser degree of weldability. The weldability can be affected by several factors; i.e., wrought alloys surpass castings, fine grain alloys are superior to coarse grain alloys, and annealed alloys are better than age- or work-hardened alloyed. The suitable filler metal normally has the chemical composition similar to the base metal, but some base metal uses a specific filler metal to prevent hot cracking in the weld metal and to improve corrosion resistance to a specific environment. Nickel and its alloys, like austenitic stainless steel, have an austenitic face centered cubic (fcc) crystal structure and exhibit no structural transformation in the solidification process, thereby causing high susceptibility to hot cracking in arc welding. The Ni-Cr-Fe and Ni-Fe-Cr alloys, like some austenitic stainless steels, can exhibit carbide precipitation in the weld heat-affected zone, though in most environments such sensitization does not impair corrosion resistance in nickel-based alloys as it does in the austenitic stainless steel. This is because many alloys have an addition of titanium or niobium to stabilize carbon. Porosity in the weld metal may be a problem, which can generally occur associated with oxidation of carbon and dissolved nitrogen in arc welding. Virtually all filler metals for nickel

and nickel alloys contain such elements as Mn, Al, Ti and Nb to deoxidize and denitrify the weld metal to avoid porosity. However, excessive amounts of oxygen and nitrogen entrapped in the weld metal can cause blowholes.

Precipitation-hardenable alloys generally contain higher amounts of Al and Ti to improve the elevated temperature strength. With this type of alloy, SMAW can result in degraded weld metal mechanical properties and inter-bead slag adhesion, while high-heat-input GMAW can cause strain-age cracking in the heat-affected zone of the base metal.

Therefore, GTAW is generally used in the annealed (solid solution treated) condition, and the completed fabrication is age-hardened with postweld heat treatment.

Such complicated welding procedures including preweld annealing and postweld age-hardening should be conducted by consulting the suppliers of the base metal and filler metal to be used.

The following sections discuss the weldability of widely used solid solution alloys and the proper welding procedures for general applications by the type of alloy.

5.3.2. Nickel

Pure nickel metals, typically Nickel 200 (UNS N0200) and Nickel 201 (UNS 0201), feature comparatively low susceptibility to hot cracking and can be welded with similar filler metals, typically ENi-1 and ERNi-1, modified with Al and Ti to avoid porosity. GTAW is common due to better weldability.

5.3.3. Nickel-Copper Alloys

Nickel copper alloys, typically Monel 400 (UNS 04400) are readily joined by arc welding.

Filler metals, usually ENiCu-7 and ERNiCu-7, differ somewhat from the base metal in the chemical composition, containing Al and Ti to improve strength and to eliminate porosity in the weld metal. To prevent hot cracking, heat input and interpass temperature should be kept lower. GTAW and SMAW are common.

5.3.4. Nickel-Chromium Alloys

Examples of nickel-chromium alloys are Inconel 600 (UNS N06600), 601 (UNS N06601), 617 (UNS N06617), and 690 (UNS N06690), all of which possess outstanding weldability by SMAW, GTAW and GMAW in the use of matching filler metals. ENiCrFe-1, ENiCrFe-2, ENiCrFe-3, ERNiCr-3, ENiCr3T, and ERNiCrFe-5 are all suitable for alloy 600. ENiCrFe-11 is used for alloy 601. ENiCrCoMo-1 and ERNiCrCoMo-1 are matching filler metals for alloy 617. ENiCrFe-7 and ERNiCrFe-7 are suited for alloy 690. However, the weld crater tends to contain hot cracks, and thick sections are likely to contain microcracks; therefore, heat input and interpass temperature should be kept lower.

5.3.5. Nickel-Iron-Chromium Alloys

Incoloy 800 (UNS N08800), 800H (UNS N08810), 800HT (UNS N08811) and 825 (UNS N08825) are well known proprietary alloys. Inconel type filler metals such as ENiCrFe-2 and ERNiCr-3 are commonly used for alloys 800, 800H and 800HT. For alloy 825, a matching filler metal of ERNiFeCr-1 is available but ENiCrMo-3 and ERNiCrMo-3,

and ENiCrMo3T are usually used. Heat input and interpass temperature should be kept lower to prevent hot cracking.

5.4. Dissimilar Metal Combinations

Nickel and nickel alloys offer excellent corrosion resistance against various acids and alkaline solutions, but they are very expensive materials. Therefore, they are often used by overlaying, cladding and lining onto carbon steel, low-alloy steel and stainless steel, where corrosion resistance is the essential requirement. In this case, dissimilar metal welding is involved in overlaying nickel and nickel alloy weld metals on the base metal, joining clad steels, and affixing liners onto the substrate. In such dissimilar metal welding, specific considerations in terms of metallurgy are necessary to get successful results.

5.5. Tips for Successful Welding and Safe Practices

Most of the solid-solution nickel and nickel alloys, except high-silicon castings, can be arc welded by SMAW, GTAW and GMAW. GTAW is the most widely used process due to better weldability. However, specific considerations based on the characteristics of nickel and nickel alloys must be taken to obtain successful results, as discussed in the following.

- Joint preparation

The most significant characteristic of nickel and its alloys is the sluggish nature of molten weld metal, which does not spread easily, requiring accurate metal placement by the welder within the welding groove. This is why wider groove angles are used. Secondly, the force of arc is weaker, resulting in the less depth of fusion in nickel-based alloys than in carbon steels. The smaller depth of fusion makes it necessary to use a narrower root face. Based on these specific characteristics, the various joint designs. The backing bar (usually copper) is to assist in bead shape on the root side. In addition to such dimensional requirements, the weld surfaces must be prepared clean without oil, grease, paint, and other sulfur- and lead-bearing substances to prevent hot cracking of the weld metal. Cleaning should be by vapor or solvent degreasing and by brushing with stainless steel — not mild steel — brushes.

- SMAW techniques

Most of the covered electrodes for nickel and nickel alloys are recommended to use with direct current electrode positive (DCEP) electrical characteristics for better performance, although some proprietary electrodes can also be used with alternating current. Nickel and nickel-alloy molten weld metals are sluggish with lower fluidity. Therefore, the welder may need to weave the electrode so that the weld pool wets the groove sidewalls to prevent incomplete fusion, but the weaving should not be wider than, as per Ref. 2, three times (1.5 times for Ni-Mo alloys) the electrode core diameter to reduce the risk of hot cracking and porosity in the weld. When the welder is ready to break the arc the weld crater should be

treated to form a smaller, slightly convex contour to prevent crater cracking (solidification cracking). When restarting the arc to join the preceding bead, use the back step technique to prevent the starting porosity. All starts and craters should be strictly inspected and, if necessary, they should be grounded to sound weld. Complete slag removal from all welds is recommended because the slag can accelerate corrosion both in aqueous and high temperature environments.

- GTAW techniques

Power supplies equipped with high frequency start, pre-purge and post-purge, and upslope and down-slope controls are recommended. The common polarity is direct current electrode negative (DCEN). In manual GTAW welds, the shielding gas is usually high purity argon for the torch shielding and back purging. For the tungsten electrode, 2% thoriated electrode is used due to longer life. Arc stability is best when the tungsten electrode is ground to a flattened point. As shown for the point geometry recommended in Figure 2.4, cone angles of 30 to 60 degrees with a small flat apex are generally used. The point geometry, however, should be designed for the particular application, varying from sharp to flat. The shape of the electrode tip has an effect on the depth of fusion and bead width, with all other welding conditions being equal. The welding torch should be held essentially perpendicular to the work piece for better shielding effect; if it is inclined too much, air may be drawn into the shielding gas and cause porosity in the weld metal with some nickel alloys. To ensure better shielding effect and minimize heat input, stringer technique is usually employed. During welding, the tip of the welding filler wire should always be held under the shielding gas to prevent oxidation of the hot welding filler wire. In the manual GTAW process, the amount of filler metal added — thus conversely the amount of base metal melted — may vary considerably depending on welder technique. For this reason, welder training and qualification is very important in terms of the dilution control.

- GMAW techniques

GMAW uses solid wires or flux-cored wires for filler metal. The recommended polarity is DCEP with, normally, constant-potential power sources. With a solid wire, the dominant mode of metal transfer is spray transfer, but short circuiting and pulsed spray welding are also widely employed depending on the welding position and joint thickness. For shielding the weld zone, solid wires normally use argon or argon mixed with helium. The addition of helium is believed to be beneficial for obtaining wider and flatter beads and less depth of fusion. The optimum shielding gas will vary with, primarily, the type of metal transfer used for better performance, as shown in Table 2.6. In contrast, gas shielded flux-cored wires normally use 75-80% Ar/Balance CO₂. Still, some proprietary filler metals may use shielding gases with specific compositions.

In manipulating the welding torch, the torch should be kept virtually perpendicular to the joint for better shielding effect. Some slight inclination is permissible to allow the visibility for manual welding; however, excessive displacement can result in aspiration of the surrounding atmosphere into the shielding gas, thereby causing porosity or heavily oxidized welds.

- Heat input control

High heat input during welding reduces the cooling speed of the weld, thereby causing some degree of annealing and grain growth in the heat-affected zone (HAZ) of nickel and its alloys. High heat input may result in excessive constitutional liquation and carbide precipitation. The liquation of the interface between weld metal crystals can be opened — thus cracked — by the contraction stresses induced by solidification of the weld metal, which is referred to as the solidification cracking that is often observed in the weld metal and its crater. The liquation occurred in the grain boundaries of a solid weld metal or base metal can be opened or cracked by the restraint stresses of the weldment, which is called the reheat cracking that is often recognized in the heat-affected zone of the base metal. Both cracks are also referred to as hot cracking. Low-melting-point chemical compounds (e.g., Ni_2S_2 : 645°C; Ni_2P : 880°C; FeS : 988°C; Fe_2P : 1050°C; FeSi : 1200°C — Ref. [7]) and metals (e.g., Pb, Bi and their alloys) are believed to be the principal causes of the inter-crystal and inter-granular liquation. On the other hand, the carbide precipitation, which can occur in the grain boundaries heated in the 500-850°C range [Ref. 6], can be a detrimental effect on the corrosion resistance of the weld. In order to minimize heat input, the welding current should be lower, the arc length shorter, and the weaving width smaller.

- Preheat and inter pass temperature control

Preheat is not usually required or recommended in arc welding of nickel and its alloys. However, if the base metal is cold, heating to about 16°C or above [Ref. 2] avoids condensed moisture that could cause weld porosity. However, excessive preheat can cause grain growth if cold-worked base metal is brought above its recrystallization temperature. In addition, to reduce the risk of hot cracking and minimize the carbide precipitation, the weld should be cooled faster by controlling preheat and interpass temperatures. A preheat and inter pass temperature of 150°C max is widely used, although 90°C max [Ref. 2] is recommended for some corrosion-resistant alloys.

- Porosity considerations

Porosity is one of the problems encountered in welding nickel and its alloys. To prevent the occurrence of porosity in the weld metal, (1) shielding gas must possess sufficient qualities with low amounts of impurity, (2) welding technique must be correct to protect the weld pool from the atmosphere, and (3) GTAW and GMAW equipment must be maintained free from shielding gas contamination and turbulence.

Porosity can be caused by hydrogen, oxygen and nitrogen in the weld metal. Nickel and nickel alloys can dissolve a high amount of hydrogen in molten state, and even in solid state, they can dissolve a high amount of hydrogen about three times that in low carbon steel. Therefore, hydrogen alone seldom causes porosity. On the other hand, molten nickel can dissolve a high amount of oxygen (1.18% at 1720°C) but the solubility reduces to 1/20 (0.06% at 1470°C) when it solidifies. Such an excessive amount of oxygen oxidizes the molten nickel to produce NiO. Then NiO can react with hydrogen ($\text{NiO} + \text{H}_2 \rightarrow \text{Ni} + \text{H}_2\text{O}$) in the nickel to produce water vapors, thereby causing porosity. Oxygen can also combine with

carbon in the molten nickel to produce CO, which causes porosity. On the other hand, nitrogen cannot produce stable nitrides with nickel; therefore, it causes porosity. To prevent porosity, the use of correct filler metal and welding procedure is essential.

7. WELDING OF MAGNESIUM ALLOYS

Magnesium is the lightest structural metal. It is approximately two-thirds as heavy as aluminum and one-fourth as heavy as steel. Magnesium alloys containing small amounts of aluminum, manganese, zinc, zirconium, etc., have strengths equalling that of mild steels. They can be rolled into plate, shapes, and strip. Magnesium can be cast, forged, fabricated, and machined. As a structural metal it is used in aircraft. It is used by the materials-moving industry for parts of machinery and for hand-power tools due to its strength to weight ratio.

Magnesium can be welded by many of the arc and resistance welding processes, as well as by the oxy-fuel gas welding process, and it can be brazed. Magnesium possesses properties that make welding it different than the welding of steels. Many of these are the same as for aluminum. These are:

1. Magnesium oxide surface coating
2. High thermal conductivity
3. Relatively high thermal expansion coefficient
4. Relatively low melting temperature
5. The absence of color change as temperature approaches the melting point.

The normal metallurgical factors that apply to other metals apply to magnesium as well. Magnesium is a very active metal and the rate of oxidation increases as the temperature is increased. The melting point of magnesium is very close to that of aluminum, but the melting point of the oxide is very high. In view of this, the oxide coating must be removed. Magnesium has high thermal heat conductivity and a high coefficient of thermal expansion. The thermal conductivity is not as high as aluminum but the coefficient of thermal expansion is very nearly the same. The absence of color change is not too important with respect to the arc welding processes.

CONCLUSION

General overview comprising basics of welding aluminium, copper, magnesium and nickel based alloys were elaborated in this chapter. And also general weldability, properties of alloys that influence on weldability, welding processes, and possible complications that may appear during processes, were dealt in detail in this chapter.

The following are the some of the conclusions related to welding of non-ferrous alloys

- Aluminum is different to weld from steels is that it does not exhibit color as it approaches its melting temperature.

- All of the copper alloys derive their strength from cold working. The heat of welding will anneal the copper in the heat-affected area adjacent to the weld and reduce the strength provided by cold working. This must be considered when welding high-strength joints.
- There is one other problem associated with the copper alloys that contain zinc. Zinc has a relatively low boiling temperature, and under the heat of an arc will tend to vaporize and escape from the weld. For this reason the arc processes are not recommended for the alloys containing zinc.
- Magnesium has high thermal heat conductivity and a high coefficient of thermal expansion. The thermal conductivity is not as high as aluminum but the coefficient of thermal expansion is very nearly the same. The absence of color change is not too important with respect to the arc welding processes.
- In the case of welding of nickel alloys, with respect to the minimum penetration, it is necessary to increase the opening of groove angles and to provide adequate root openings when full-penetration welds are used. The bevel or groove angles should be increased to approximately 40% over those used for carbon.
- Almost all the welding processes can be used for welding the nickel alloys. In addition, they can be joined by brazing and soldering.

REFERENCES

- [1] Kamio (1999), *The New Era of Aluminum*, Kogyo Chosakai Publishing Co., Ltd.
- [2] Kobe Steel Ltd (1964), *Welding Electrodes Handbook*,
- [3] M. Mizuno, et. al., (1979), *Welding of Aluminum and Aluminum Alloys*, Sanpo Publications Inc.,
- [4] *Exposition of Welding Terms* (1999), Shinko Welding Service Co., Ltd.
- [5] Tachibana (2001), Materials and Procedures for Aluminum MIG Welding, *Journal of the Japan Welding Society*, Vol. 70.
- [6] The American Welding Society (1991), *Welding Handbook*, 8th Edition.
- [7] Kobe Steel, Ltd., (1998), *Technical Guide*, No. 344.
- [8] Kobe Steel, Ltd. (1969) *Welding of Nonferrous Metals and Supper Alloys*,
- [9] The American Welding Society (1996), *Welding Handbook, 8th Edition*, Vol. 3,
- [10] The American Welding Society (1998), *Welding Handbook, 8th Edition*, Vol. 4,
- [11] Kobe Steel, Ltd (1983), *Technical Guide*, No. 156.
- [12] Kobe Steel, Ltd. (1979), *Technical Guide*, No. 105, January.
- [13] Kobe Steel, Ltd. (1980), *Technical Guide*, No. 119, March.
- [14] High Pressure Institute of Japan (1992), *Welding Practices in Cladded Steels*. Sanpo Publishing Company.
- [15] CASTI Metals Red Book (2003) *Nonferrous Metals*, 4th Edition. CASTI Publishing Inc.
- [16] M. Sugiyama (1997), *Nonferrous Metallic Materials*. Corona Publishing Co.
- [17] High Pressure Institute of Japan (1992), *Welding Practices in Cladded Steels*. Sanpo Pub.,

- [18] CASTI Metals Red Book (2003), *Nonferrous Metals*, 4th Edition. CASTI Publishing Inc.,
- [19] CASTI Metals Blue Book (2000), *Welding Filler Metals*, 3rd Edition. CASTI Publishing Inc.,
- [20] S. Natsume (2001), Welding of Ni and Ni alloys, *Welding Technique*. Sanpo Publications Inc.

INDEX

A

acetone, 29
acid, 25
acoustic techniques, x, 23
adhesion, x, 64, 234, 235, 236, 250
adsorption, 26
advancements, 8
aerospace, ix, 11, 12, 13, 15, 21, 24, 34, 54, 58, 64, 73, 80, 164
aesthetic(s), 14, 245
aggregation, 100, 101, 102
air temperature, 195
AISI P -20 tool steel, 163, 166
Al₂O₃ particles, 150, 207
alcohol production, 248
algorithm, x, 35, 91, 92, 105, 110, 114, 126, 134, 135, 137, 139, 153, 155, 162
alternative energy, ix
aluminium, 35, 53, 58, 64, 67, 150, 151, 165, 188, 197, 201, 247, 254
aluminum oxide, 247
amine group, 25
amines, 25
amplitude, 55, 66, 67, 84, 93, 140, 153
analysis of variance, 139
annealing, 192, 232, 250, 253
ANOVA, xi, 136, 137, 138, 139, 145, 146, 147, 148, 163, 164, 165, 166, 168, 169, 170, 171, 172, 175, 176, 179, 186
APC, 49
apex, 252
argon, 246, 247, 252
arrest, 13
artificial intelligence, 55
aspiration, 252
Assembly Jig, 11, 14, 17, 19, 20
asymmetry, 14

atmosphere, 245, 252, 253
atmospheric pressure, 32
atoms, 190, 215, 224, 226
automation, 13, 21, 155, 225

B

base, xi, 29, 30, 91, 96, 99, 111, 113, 114, 115, 119, 120, 126, 143, 155, 210, 219, 229, 230, 231, 232, 235, 242, 243, 244, 246, 247, 248, 249, 250, 251, 252, 253
baths, 225
beams, xii, 30, 191, 193, 204, 213, 218
benchmarks, 92
bending, 144, 190
benefits, 4, 5, 13, 21, 64, 66, 67, 237, 248
benzene, 26, 29
biocompatibility, 53
bleaching, 30
bonding, x, 23, 25, 30, 32, 242
boundary value problem, 44
brass, 135, 140, 164, 246, 248
Brazil, 51, 159
breakdown, 14, 65, 193, 210
breeding, 105
BRICS, ix
brittleness, 192
bromine, 25
burn, 215
burr, 57, 58, 62, 66, 67, 70, 75
by-products, 193

C

CAD, 13, 21, 78, 134, 153, 155
calibration, 22
CAM, x, 21, 77, 78, 80, 81, 134, 153, 155

- CAM software, x, 77, 78, 80
 candidates, xii, 213
 carbides, 61, 64, 67, 187, 224, 226
 carbon, 24, 25, 29, 30, 31, 32, 35, 47, 48, 53, 58, 70, 71, 73, 154, 215, 222, 223, 224, 226, 227, 228, 237, 239, 247, 248, 249, 251, 253, 255
 carbon atoms, 24, 25, 224
 carbon dioxide (CO₂), 191, 193, 210, 215, 216, 219, 239, 252
 carbon nanotubes, 31, 32
 carboxyl, 25
 carboxylic groups, 25
 case study(s), ix, 2, 3, 11, 21
 cationic surfactants, 26
 C-C, 69
 ceramic(s), 24, 25, 52, 62, 65, 71, 72, 73, 93, 134, 144, 147, 151, 194, 210
 ceramic materials, 52, 144, 210
 challenges, 34, 78, 215
 chaotic behavior, 108
 chemical(s), xii, 24, 25, 34, 190, 213, 227, 229, 232, 234, 242, 245, 247, 248, 249, 250, 253
 chemical etching, 232
 chemical properties, xii, 213
 chemical vapour deposition, 24
 Chicago, 49
 China, 165, 239
 chlorine, 25
 chromium, 24, 67, 68, 143, 166, 226, 248, 250
 chromosome, 105, 106, 108, 109
 circulation, 166
 cladding, 190, 192, 215, 221, 222, 237, 248, 251
 classes, 98, 192
 classical logic, 98
 classification, 220
 cleaning, 226, 247
 clustering, 142, 156
 clusters, 142
 CNC milling machine, 78, 80
 coal, 248
 coatings, 65, 69
 cobalt, 150, 152, 160
 coding, 106
 color, 108, 184, 186, 244, 247, 254, 255
 complexity, 106, 121, 123, 153, 225
 composites, ix, xi, 23, 24, 25, 26, 27, 28, 29, 30, 31, 32, 47, 48, 50, 51, 52, 58, 60, 67, 71, 72, 129, 134, 147, 150, 151, 155, 156, 159, 160, 161, 162, 190, 192
 composition, 61, 100, 102, 191, 227, 229, 249, 250
 compounds, 25, 26, 253
 compression, 28, 29, 34
 computer, 12, 92, 127, 130, 135, 153, 194, 225, 238
 computing, 7, 92, 126, 160
 conceptualization, 14
 conduction, 220, 225
 conductivity, 31, 67, 134, 192, 197, 198, 219, 227, 243, 245, 246, 247, 254, 255
 conductors, 155, 245
 configuration, 13, 15, 18, 19, 47, 78, 84, 95, 96
 constant load, 235
 constituents, 34, 51, 243
 construction, 19, 114, 217
 consulting, 250
 consumption, 195, 244
 containers, 245
 contamination, 222, 253
 contour, xi, 90, 135, 142, 153, 163, 165, 184, 186, 252
 convergence, 83, 107, 109, 114
 convergence criteria, 109
 cooling, xii, 55, 56, 63, 194, 195, 213, 214, 216, 217, 218, 220, 222, 223, 224, 229, 231, 232, 233, 237, 243, 253
 copper, xii, 64, 71, 140, 144, 145, 241, 243, 245, 246, 247, 248, 250, 251, 254, 255
 correlation, 8, 55
 correlation coefficient, 55
 corrosion, xii, 34, 51, 53, 54, 80, 144, 152, 159, 213, 221, 222, 234, 237, 242, 244, 245, 247, 248, 249, 251, 252, 253
 cost, x, 3, 4, 6, 12, 13, 14, 15, 19, 21, 30, 40, 41, 43, 51, 64, 109, 130, 131, 144, 164, 166, 186, 214, 216, 226, 228, 234, 237, 247
 covalent bonding, 25
 cracks, 54, 59, 67, 131, 150, 194, 250, 253
 critical value, 35, 142
 crystal structure, 222, 249
 crystalline, 56, 192
 crystals, 216, 224, 253
 cubic boron nitride, 61, 73
 cutting force, 53, 54, 55, 62, 63, 64, 66, 67, 68, 70, 73, 78, 84, 127, 152, 186, 192
 CVD, 53, 164
 cycles, xii, 213, 237

D

- damages, 144, 193
 damping, 35, 36
 data set, 54, 116
 decoding, 105
 decomposition, 99, 102, 114, 193
 defect site, 25
 defects, 6, 8, 25, 56, 73
 deformation, 56, 108, 224, 229

degradation, 59
 delamination, x, 33, 34, 35, 37, 40, 46, 47, 48, 49,
 59, 60, 71, 72, 74, 234
 deposition, xii, 29, 190, 192, 215, 241
 deposition rate, xii, 241
 depth, 53, 54, 55, 56, 57, 58, 62, 63, 64, 65, 66, 67,
 68, 70, 80, 81, 82, 83, 84, 85, 93, 132, 133, 137,
 146, 148, 152, 160, 165, 196, 220, 222, 223, 225,
 226, 227, 228, 229, 230, 233, 234, 237, 239, 251,
 252
 derivatives, 26, 116
 Design for Assembly (DFA), 11, 14
 detachment, 234
 detection, 135, 142, 154, 156
 deviation, xii, 12, 54, 82, 83, 127, 142, 155, 189,
 208, 209
 diffraction, 218, 232
 diffusion, 223, 224, 242
 diffusivity, 151, 192
 diode laser, 218, 219, 238
 diodes, 194
 direct measure, 55
 discharges, 130, 133, 140, 142, 153, 154, 164
 dispersion, ix, 23, 24, 25, 26, 27, 28, 29, 30, 31, 32
 displacement, 66, 235, 252
 disposition, 233
 dissociation, 194
 distilled water, 30, 165, 188
 distributed load, 35
 distribution, 79, 141, 142, 144, 147, 152, 153, 157,
 159, 217, 219, 220, 229, 232
 divergence, 214, 217, 218
 diversity, 34
 DMF, 29
 drilling, x, 33, 34, 35, 36, 37, 38, 40, 46, 47, 48, 49,
 50, 58, 59, 60, 67, 71, 72, 74, 190, 192, 193, 196,
 200, 202, 204, 206, 207, 208, 209, 210, 211, 216,
 219
 ductility, 198, 222, 244, 249
 dyes, 191

E

ECM, 193
 economics, 54
 elastic deformation, 54
 elastic fracture, 35
 electric conductivity, 248
 electric(al) conductivity, 140, 248
 electrical discharge machining, xi, 129, 140, 150,
 152, 153, 157, 159, 160, 161, 162, 164, 165, 187,
 188
 electrical properties, 24, 25, 32

electrical resistance, 152
 electricity, 130
 electrodes, 71, 130, 133, 140, 155, 158, 161, 164,
 188, 215, 245, 251
 electromagnetic, 222
 electron(s), 132, 190, 191, 192, 216, 218, 222, 223,
 242, 245, 248
 electron state, 191
 emission, 190, 214, 215
 emitters, 218
 energy, 26, 65, 66, 68, 130, 131, 132, 133, 134, 135,
 140, 141, 142, 143, 150, 153, 158, 159, 164, 190,
 191, 192, 193, 200, 201, 202, 204, 207, 214, 215,
 216, 218, 219, 220, 222, 225, 226, 237, 242
 energy consumption, 225
 energy density, 26, 141, 190, 222
 energy efficiency, 141, 192, 193
 energy input, 193, 214, 218, 225, 242
 engineering, ix, 23, 24, 31, 50, 54, 109, 154, 214,
 215, 219
 England, 127
 entrapment, 247
 entropy, 152
 environment(s), 3, 4, 55, 105, 219, 222, 225, 248,
 249, 252
 environmental aspects, 6
 environmental conditions, 228
 environmental effects, 3
 equilibrium, 190, 191
 equipment, ix, 30, 64, 237, 238, 242, 245, 247, 248,
 249, 253
 erosion, xi, 129, 131, 136, 141, 153, 154, 156, 159,
 161, 163, 164, 188, 193, 226, 248
 ester, 27, 32
 ethanol, 29
 ethylene, 28, 248
 evacuation, 133
 evaporation, 194
 evolution, 64, 65, 105, 156
 excitation, 190, 192, 215
 execution, 80
 experimental design, 138, 165, 188
 exploitation, 237
 external influences, 108
 extrusion, 29, 30, 130, 152, 242

F

fabrication, 61, 77, 130, 194, 250
 fatigue endurance, 53
 fault diagnosis, 135, 158
 FEM, 56, 67, 68
 ferrite, 55, 223, 224, 231

ferromagnetic, 152, 161
 fiber, x, xi, 32, 33, 34, 35, 36, 47, 48, 49, 71, 189,
 194, 195, 196, 197, 200, 202, 204, 207, 208, 209,
 210
 fiber reinforced plastics (FRPs), x, 33, 35, 36, 47, 48,
 71
 filament, 29, 34, 52
 filler(s), ix, x, 23, 24, 25, 26, 27, 28, 29, 30, 31, 242,
 243, 244, 245, 246, 248, 249, 250, 252, 254
 filler particles, x, 23, 25, 30
 filler surface, 25
 filler wire, 242, 252
 films, 243
 finite element method, 153
 fisheries, 3
 fishing, 9
 fitness, 105, 106, 107, 109, 110, 111, 115, 118, 123
 flame, 214, 222
 flank, 52, 53, 56, 62, 64, 72, 78
 flatness, 137, 143, 154, 155
 flexibility, 2, 9, 34, 223, 237
 flight(s), ix, 11, 12, 13, 18, 24
 fluctuations, 136
 fluid, 130, 133, 149, 165
 fluorine, 25
 food, 245, 248
 force(s), x, 24, 27, 33, 35, 36, 37, 38, 40, 41, 46, 47,
 48, 49, 50, 52, 53, 54, 55, 56, 60, 61, 62, 64, 66,
 67, 68, 70, 73, 75, 78, 84, 88, 127, 133, 136, 144,
 152, 187, 192, 222, 251
 formamide, 29
 formation, 5, 53, 54, 56, 57, 59, 63, 64, 68, 69, 70,
 73, 74, 75, 92, 126, 142, 194, 222, 224, 225, 234,
 236, 242
 formula, 134
 fracture toughness, 31, 54
 fragments, 234
 freedom, xii, 13, 16, 135, 241
 friction, 35, 53, 60, 75, 187, 235, 236, 242, 245
 function values, 98, 111
 functionalization, 23, 25, 26, 32
 fusion, 242, 243, 246, 247, 248, 251, 252
 fuzzy logic, x, xi, 2, 4, 9, 10, 36, 37, 91, 92, 98, 111,
 112, 113, 126, 127, 155
 fuzzy membership, 96
 fuzzy set theory, 93
 fuzzy sets, 94, 95, 97, 98, 101, 111

G

gas tungsten arc welding, 242, 245, 249
 genes, 108
 genetic algorithm, x, 91, 92, 110, 114, 126, 137, 155

genetic information, 108
 genetics, 105
 geometrical parameters, ix, 11, 12
 geometry, 12, 13, 15, 18, 19, 35, 48, 54, 56, 57, 61,
 63, 65, 66, 70, 71, 78, 92, 128, 133, 151, 152,
 153, 155, 228, 237, 252
 Germany, 64, 127, 242
 grades, 70, 94, 136, 227
 grain boundaries, 224, 243, 253
 grain size, 55, 56, 57, 62, 70
 granules, 26, 27
 graphene sheet, 26
 graphite, 24, 26, 49
 GRAS, 72
 gravity, 104
 growth, 224, 232, 238, 253
 growth rate, 238
 guidelines, 14

H

Hamiltonian, 41, 42, 43
 hardener, 29
 hardening process, 214, 220, 222, 223, 226, 228,
 232, 237
 hardness, xii, 53, 54, 55, 61, 62, 64, 66, 67, 70, 166,
 213, 214, 221, 224, 226, 227, 228, 229, 230, 231,
 232, 234, 236, 237, 239
 heat conductivity, 246, 254, 255
 heat transfer, 141, 153, 154, 156, 210
 height, 29, 57, 62, 79, 80, 94, 101, 109, 133
 helium, 215, 246, 252
 hemp, 24
 high strength, xi, 24, 28, 34, 53, 58, 72, 80, 163, 164,
 198, 242
 hole deviation and taper, xii, 189
 House, 1, 4, 6, 9, 159
 hybrid, 68, 71, 144, 154
 hybridization, 155
 hydrogen, 25, 30, 239, 244, 246, 248, 253
 hydrogen chloride, 248
 hydrogen peroxide, 25, 30
 hydroxyl groups, 25

I

image, 47, 59, 92, 231
 image analysis, 47
 impact strength, 30
 indentation, 230
 India, 1, 11, 23, 33, 50, 129, 163, 189, 213, 241
 induction, 214, 222, 237

industrialized countries, ix
 industry(s), ix, x, 11, 14, 33, 34, 51, 52, 53, 54, 62,
 64, 68, 78, 80, 93, 130, 154, 164, 190, 192, 193,
 221, 225, 254
 inferences, 102, 103, 186
 insertion, 14
 integration, 13, 21, 153, 155
 integrity, 51, 54, 62, 64, 67, 69, 71, 74, 75, 134, 144,
 164
 interaction effect(s), 136
 interdependence, 3
 interface, 15, 16, 19, 20, 32, 53, 234, 253
 interfacial adhesion, x, 23
 interference, 17, 111, 138
 inversion, 191
 investments, 64
 ionization, 132, 191
 ions, 190, 192
 iron, xii, 35, 53, 57, 62, 68, 70, 71, 72, 74, 89, 143,
 159, 213, 222, 227, 228, 239, 240, 241
 irradiation, 192, 214, 219, 229, 233
 Italy, 48, 49
 iteration, 109, 111, 115

J

Japan, 242, 255
 jigless, 13, 14, 15, 17, 19, 21
 Jigless Assembly, ix, 11, 12, 13, 14, 17, 19, 21, 22
 jigless manufacturing, 17, 21
 joints, 242, 247, 255

K

kinetics, 232
 krypton, 192, 216

L

lamination, 35
 laser ablation, 24
 laser beam welding, 242
 laser transformation hardening, 214, 222, 223, 225,
 226, 227, 228, 229, 237, 238, 239
 lasers, xii, 191, 192, 213, 215, 216, 217, 219, 220,
 221, 225
 latency, 13
 lead, 2, 12, 13, 14, 19, 21, 28, 64, 78, 83, 107, 141,
 144, 153, 194, 215, 228, 251
 learning, 55, 92, 120, 138, 139, 148
 lens, 194, 215
 life cycle, 3

light, xii, 34, 64, 190, 191, 194, 214, 216, 217, 241
 limestone, 194
 linear function, 37, 113, 118, 126
 linear model, 172, 176, 180
 linguistic rule, 98, 99
 lithium, 25
 locus, 36
 logic rules, 111, 127
 low temperatures, 52
 Luo, 141, 159

M

machinability, 51, 52, 53, 64, 68, 69, 70, 72, 74, 92,
 127, 143, 151, 156, 158, 159, 165, 187
 machinery, 248, 249, 254
 machining efficiency, 78, 141, 143
 magnesium, xii, 241, 242, 244, 254
 magnesium alloys, xii, 241, 242
 magnet, 27
 magnitude, 55, 232, 237
 manganese, 192, 226, 254
 manufacturing, ix, x, xi, 1, 2, 3, 4, 6, 8, 9, 10, 11, 12,
 13, 14, 16, 17, 18, 21, 22, 23, 24, 25, 34, 54, 57,
 64, 71, 74, 78, 80, 89, 92, 126, 130, 135, 140,
 142, 153, 154, 155, 159, 163, 164, 187, 193
 manufacturing companies, 64
 manufacturing engineering, ix
 manufacturing systems, ix, 1, 2, 8
 mapping, 6, 9, 105
 mass, 223, 225
 material removal rate, xi, 67, 133, 134, 136, 137,
 140, 143, 144, 150, 151, 159, 161, 164, 165, 187,
 189, 193, 196, 197, 199, 201, 202, 204, 207, 209
 material surface, 193, 214, 220
 matrix, ix, xi, 2, 4, 5, 6, 7, 8, 23, 24, 25, 26, 27, 28,
 29, 30, 31, 32, 34, 38, 40, 41, 44, 45, 46, 48, 59,
 60, 61, 67, 72, 117, 129, 134, 135, 139, 150, 151,
 155, 156, 158, 159, 160, 192, 194, 197, 198, 207,
 209, 210, 224
 measurement(s), 13, 53, 69, 70, 71, 72, 75, 81, 83,
 88, 101, 102, 111, 194, 232
 mechanical properties, xii, 24, 31, 34, 48, 55, 192,
 213, 214, 242, 244, 246, 248, 250
 media, 19, 188
 medical, 34
 melt(s), 28, 134, 164, 193, 194, 204, 215, 221, 222,
 242
 melting, xii, 27, 130, 151, 153, 190, 193, 207, 220,
 221, 222, 223, 227, 241, 242, 243, 246, 248, 253,
 254
 melting temperature, 223, 227, 246, 254

membership, 93, 94, 95, 96, 98, 99, 100, 104, 111, 112, 113, 114, 115
 metal removal rate, xi, 54, 137, 143, 147, 150, 189
 metallurgy, 54, 247, 251
 metals, ix, xii, 23, 24, 30, 50, 130, 188, 190, 192, 213, 217, 234, 237, 241, 242, 244, 245, 246, 247, 249, 250, 251, 252, 253, 254
 meter, 133
 methanol, 29
 methodology, 3, 4, 9, 12, 13, 15, 16, 19, 21, 92, 127, 135, 137, 139, 142, 143, 146, 151, 152, 153, 154, 155, 160, 161, 163, 165, 187, 188, 238
 microhardness, 54
 microscope, 166, 196, 231
 microstructure(s), 54, 55, 67, 147, 150, 151, 214, 220, 221, 224, 228, 230, 231, 232, 237, 239, 242, 244
 miniature, 154, 155, 193
 Ministry of Education, 69
 Missouri, 91
 mixing, 26, 27, 29, 221
 MMCs, 151, 207
 modeling, x, xi, 33, 49, 70, 74, 91, 127, 128, 129, 138, 141, 153, 157, 161, 186, 238
 modelling, 21, 47, 55, 89, 160
 models, x, xi, 21, 33, 35, 37, 55, 69, 90, 91, 92, 118, 120, 121, 123, 126, 127, 128, 137, 138, 139, 140, 141, 142, 148, 154, 155, 160
 modifications, 2, 17, 19
 modules, 111, 113
 moisture, 253
 mold(s), 62, 71, 72, 74, 89, 166
 molecules, 190, 191, 193, 198, 201, 204, 205, 215, 216
 molybdenum, 226
 monomers, 28
 Morocco, 77
 morphology, 153
 moulding, 28, 29
 multiple regression, xi, 55, 91, 114, 138
 mutation, 108, 111

N

nano composites, ix, 23, 24, 25, 26, 27, 28, 30, 31, 32
 nanostructures, 32
 nanotechnology, 32
 nanotube, 31, 32
 natural fibres, x, 23, 24, 30
 natural selection, 105
 Nd, 154, 192, 193, 210, 215, 216, 217, 219, 221, 238, 239

neural network(s), 35, 36, 37, 48, 49, 92, 137, 138, 143, 144, 153, 155, 157, 160
 next generation, 12, 107
 nickel, xii, 52, 57, 64, 74, 143, 152, 166, 188, 210, 226, 241, 247, 248, 249, 250, 251, 252, 253, 254, 255
 niobium, 143, 249
 nitrides, 254
 nitrogen, 65, 75, 215, 249, 253
 nodes, 92
 non-ferrous alloys, 242, 254
 nucleation, 224

O

oil, 53, 165, 214, 247, 248, 251
 operating costs, 2
 operations, 2, 13, 52, 53, 57, 61, 67, 72, 92, 94, 97, 98, 126, 127, 128, 144, 146, 153, 154, 155, 160, 191, 197, 216, 222, 226
 optical fiber, 194
 optical properties, 192, 227
 optimization method, 137, 138
 overcut, xi, 152, 163, 165, 186
 overlay, 184, 222
 overproduction, 6
 overtime, 136
 oxidation, 61, 221, 229, 234, 235, 244, 249, 252, 254
 oxygen, 246, 248, 250, 253
 ozone, 25

P

parallel, 21, 78, 79, 81, 87, 88, 190, 214, 216, 217
 parallelism, 133, 214
 Pareto, 139, 164
 Pareto optimal, 164
 percolation, 31
 permit, 155, 186
 phase transformation, 56, 71, 223, 224, 232, 233, 234, 237
 photons, 190, 191
 physical and mechanical properties, 31
 physical properties, 149, 151, 215, 228
 physics, 220
 pitch, 18, 246
 plasma current, 136
 plastic deformation, 55, 56, 235
 plasticity, 56
 plastics, x, 28, 33, 35, 36, 47, 48, 71
 platelets, 26
 point load, 35

polarity, xii, 132, 165, 241, 252
 polarization, 195
 pollution, 219
 polymer(s), 24, 25, 26, 27, 28, 29, 30, 31, 32
 polymer composites, 30, 31
 polymer materials, 24
 polymer matrix, 25, 26, 27, 28
 polymer molecule, 26, 29
 polymerization, x, 23, 29, 31
 population, 105, 106, 107, 109, 110, 111, 114, 190, 191
 Population inversion, 190
 population size, 109, 111
 porosity, 244, 250, 251, 252, 253
 Portugal, 51
 potassium, 25
 power generation, 247
 power plants, 248
 precipitation, 224, 249, 253
 predictability, 186
 preparation, 29, 251
 prevention, 131, 141, 156, 158
 principles, 8, 237, 244
 probability, 94, 107, 108, 111, 118, 120, 123
 probability density function, 94
 process control, xii, 61, 136, 214, 241
 process planning, x, 77, 78
 product design, 3, 9, 14
 profilometer, 166
 programming, 134
 propagation, 135, 138, 144, 146, 157, 232
 proposition, 93, 97, 98
 propylene, 28
 prototype, 4, 130
 pulse discharge, 140, 153
 pultrusion, 29, 32, 34
 purity, 248, 249, 252
 P-value, 168, 169

Q

quality assurance, 238
 quality improvement, 73
 quantum mechanics, 190
 quartz, 67

R

radiation, 73, 191, 215, 220
 radius, 53, 57, 62, 75, 135, 136, 158
 random numbers, 106
 ratio analysis, 167, 168

raw materials, 34
 reactions, xii, 213
 reagents, 25
 real numbers, 39
 real time, 2, 13, 36, 142, 154, 155, 162
 recombination, 108
 recovery, 1, 2
 recrystallization, 68, 253
 regression, xi, 91, 92, 114, 115, 126, 136, 138, 139, 140, 143, 144, 145, 146, 157, 162, 171, 175, 179, 186
 regression analysis, 92, 143, 145, 171, 175, 179, 186
 regression method, 138
 regression model, 136, 138, 139, 144, 146, 186
 reinforcement, x, 23, 24, 30, 34, 147, 150, 151, 155
 rejection, 34, 135
 reliability, 12, 13, 54, 225
 remanufacturing system, ix, 1, 2, 5, 6, 7, 8
 reproduction, 107, 108, 110, 118, 120, 123
 requirements, x, xii, 2, 3, 4, 6, 9, 12, 13, 15, 16, 19, 33, 34, 41, 148, 183, 186, 226, 241, 246, 247, 251
 researchers, x, 4, 23, 34, 56, 63, 68, 92, 164, 193
 residual stress, 54, 55, 56, 57, 62, 65, 66, 70, 72, 73, 165, 232, 233, 234, 236, 238
 residuals, 172, 176, 180
 resins, 27, 31
 resistance, xii, 34, 52, 53, 68, 80, 137, 140, 213, 214, 221, 226, 228, 232, 234, 235, 236, 237, 238, 242, 245, 247, 248, 249, 251, 253, 254
 resonator, 190, 215, 216
 resources, 4, 89
 response, xi, 40, 73, 137, 138, 142, 143, 146, 152, 153, 154, 157, 159, 160, 161, 163, 165, 170, 171, 172, 174, 176, 178, 180, 182, 183, 184, 186, 187, 194, 197, 227, 238
 response surface methodology, 143, 152, 153, 160, 161, 165, 187, 238
 risk(s), x, 51, 142, 251, 253
 robust design, 137, 143, 154, 160
 rods, 217, 245
 room temperature, 30, 234, 235, 236
 root, 36, 93, 251, 255
 root-mean-square, 93
 roughness measurements, 87
 rubber, 31
 rules, 36, 99, 100, 101, 102, 111, 113, 114, 115, 118, 119, 120, 121, 123, 136, 142

S

safety, 54, 80
 SAXS, 26
 scaling, 139, 140

- scanning electron microscopy, 26
scatter, 197, 201, 202, 204
scattering, 26
scope, xi, 129, 141, 144, 154, 193, 238
search space, 106, 108
segregation, 221, 243
semiconductor, 192, 215, 218
semiconductor lasers, 215
sensitivity, 243, 244
sensitization, 249
set theory, 93
shape, 12, 28, 52, 75, 112, 113, 133, 140, 142, 153, 188, 207, 208, 219, 225, 228, 251, 252
shear, 27, 57
shock, 194
showing, 31, 64, 168, 169, 184
 Si_3N_4 , 67, 74, 144, 164, 187
signals, 74
silica, 24
silicon, 150, 151, 152, 193, 210, 246, 251
simulation, 16, 47, 73, 92, 144
SKD, 147
skin, 15, 18, 152, 161
slag, 246, 247, 250, 252
sodium, 30
sodium hydroxide, 30
solid state, 194, 216, 217, 218, 234, 253
solid surfaces, 234
solidification, 249, 252, 253
solubility, 25, 222, 253
solution, 30, 38, 39, 44, 49, 50, 54, 105, 106, 107, 108, 109, 111, 117, 140, 142, 145, 153, 183, 186, 224, 249, 250, 251
solvents, 25, 26, 29
specific gravity, 165
specific heat, 243
specifications, 78
spectroscopy, 215
spindle, 35, 60, 62, 136
stability, xii, 25, 63, 66, 83, 236, 241, 242, 252
standard error, 82
state(s), x, 4, 33, 38, 39, 40, 41, 42, 43, 44, 45, 46, 54, 62, 142, 168, 169, 190, 191, 210, 215, 216, 232, 233, 236, 242, 253
storage, 12, 242
strategy use, 88
stress, 52, 54, 55, 56, 62, 65, 144, 193, 214, 222, 232, 233, 234, 236, 238
structural assemblies, ix, 11, 21, 22
structural changes, 231
structural modifications, 194
structure, ix, 11, 12, 13, 15, 17, 18, 19, 25, 54, 55, 61, 109, 112, 192, 207, 222, 223, 224, 226, 229, 231, 232, 236
subgroups, 191
substrate(s), 65, 192, 194, 193, 210, 211, 219, 221, 222, 223, 225, 247, 251
sulfur, 251
Sun, 9
supplier(s), 4, 9, 250
surface alloys, 221
surface area, 25, 29
surface hardness, 237
surface integrity, 54, 62, 64, 67, 69, 71, 74, 75, 134, 144, 164
surface layer, xii, 59, 213, 219, 225, 229, 232
surface modification, 238
surface properties, xii, 213, 222, 226
surface tension, 26
surface treatment, 214, 216, 218, 219, 220, 221, 223, 229
surfactant(s), x, 23, 26, 32
survival, 105, 106
susceptibility, 243, 244, 247, 248, 249, 250
sustainability, 3, 4, 10
symmetry, 87, 88
symptoms, 142
synthesis, 24, 30, 127
- T**
- tanks, 29, 242, 245, 248
target, 182, 183, 186
team members, 2, 5
techniques, x, 4, 8, 10, 22, 23, 24, 25, 27, 29, 30, 36, 37, 50, 51, 52, 55, 69, 71, 92, 99, 100, 138, 144, 153, 154, 155, 164, 192, 223, 232, 238, 242, 245, 251, 252
technological developments, 12
technology(s), ix, 11, 12, 13, 17, 22, 61, 130, 161, 164, 187, 214, 215, 219
tensile strength, 35, 49, 242, 244
tension(s), 133, 137, 140, 141, 142, 143, 145, 147, 150, 151, 153, 154, 162, 164
test data, 121
testing, 120, 138, 150
tetragonal lattice, 224
texture, 79, 89
thermal energy, 130, 190
thermal expansion, 24, 63, 151, 246, 254, 255
thermal properties, ix, 23, 152, 192
thermal stability, 31
thermoplastics, 26, 28
thermosets, 48

titanate, 210
 titanium, xii, 24, 48, 53, 57, 64, 65, 67, 68, 69, 71,
 72, 74, 75, 143, 154, 160, 165, 210, 238, 241, 249
 tooling design, ix, 11
 tools, ix, x, xi, 1, 2, 3, 4, 5, 6, 7, 8, 9, 13, 14, 19, 29,
 51, 53, 54, 60, 61, 62, 63, 64, 65, 66, 69, 70, 71,
 72, 74, 78, 79, 126, 129, 162, 164, 187, 254
 tooth, 58, 62, 89
 torsion, 15
 total product, 144
 tracks, 40, 221
 training, 8, 117, 118, 252
 trajectory, 36, 37, 46, 78, 135
 transactions, 158
 transducer, 26
 transformation(s), xii, 55, 56, 135, 213, 214, 216,
 219, 222, 223, 224, 226, 227, 228, 229, 233, 234,
 237, 238, 239, 240, 249
 transition temperature, 234
 transmission, 26
 transmission electron microscopy (TEM), 26
 treatment, x, 23, 25, 30, 32, 146, 155, 190, 192, 210,
 214, 215, 219, 221, 222, 225, 237, 238, 239, 244,
 250
 tribology, 238
 tungsten, 28, 53, 64, 69, 71, 144, 150, 151, 158, 160,
 222, 242, 244, 252
 tungsten carbide, 28, 53, 69, 144, 150, 151, 158, 160
 turbulence, 133, 253
 turning, x, xi, 52, 53, 54, 55, 56, 57, 61, 62, 63, 64,
 65, 66, 67, 68, 69, 70, 71, 72, 73, 74, 91, 92, 118,
 120, 124, 126, 127, 128, 135, 157, 159, 165, 187

U

UK, 22
 ultrasonic vibrations, 66, 73
 USA, 49, 64, 89, 127, 239

V

validation, 2, 56, 121
 vanadium, 226
 vapor, 251
 variables, xi, 73, 94, 101, 103, 104, 106, 109, 110,
 111, 112, 113, 114, 115, 118, 123, 126, 138, 148,
 152, 163, 165, 166, 167, 168, 169, 170, 171, 172,
 174, 176, 178, 179, 182, 184, 186, 187, 194, 197,
 229, 237
 variations, 50, 56, 83, 120, 164, 168, 170
 varieties, 164

vector, 1, 2, 7, 8, 38, 40, 41, 44, 45, 57
 vehicles, 12
 velocity, 27, 57, 66, 89, 122, 124, 125, 136, 137,
 141, 142, 145, 153, 204, 206
 versatility, 193
 vessels, x, 23
 vibration, 53, 55, 60, 63, 66, 67, 68, 70, 72, 74, 75,
 83, 92, 136, 140, 141, 142, 144, 153, 155, 157,
 160, 192
 viscosity, 26, 28
 vision, 47, 73, 92, 127

W

Washington, 49
 waste, 3, 4, 8
 water, 25, 26, 28, 29, 30, 130, 131, 143, 144, 152,
 164, 194, 195, 214, 216, 242, 245, 253
 water vapor, 253
 water-soluble polymers, 26
 wear, xii, 52, 53, 56, 62, 64, 65, 67, 69, 70, 72, 74,
 137, 143, 145, 148, 152, 156, 164, 165, 188, 192,
 213, 214, 221, 222, 226, 228, 234, 235, 236, 237,
 238, 239, 240, 245
 weight ratio, 24, 30, 34, 58, 242, 254
 weldability, 246, 247, 249, 250
 welding, ix, xii, 11, 190, 192, 216, 219, 222, 241,
 242, 243, 244, 245, 246, 247, 248, 249, 250, 251,
 252, 253, 254, 255
 wettability, 31
 wires, 152, 242, 245, 249, 252
 workflow, 80
 workforce, 6, 8

X

xenon, 192
 XRD, 55

Y

yield, 174, 182
 Ytterbium fiber laser machining, xi, 189, 194, 196,
 197, 200, 202, 204, 207, 208, 209

Z

zinc, 140, 144, 246, 254, 255
 zirconium, 254